MODEL UPDATING IN REAL-TIME OPTIMIZATION

By

Wai San Yip, B. Eng., M. Phil.

A Thesis

Submitted to the School of Graduate Studies

in Partial Fulfillment of the Requirements

for the Degree of Doctor of Philosophy

McMaster University

MODEL UPDATING IN REAL-TIME OPTIMIZATION

Doctor of Philosophy (2002)
(Chemical Engineering)

McMaster University
Hamilton, Ontario

TITLE: Model Updating in Real-Time Optimization

AUTHOR: Wai San Yip, B. Eng. (University of Hong Kong)
M. Phil. (Hong Kong University of Science and Technology)

SUPERVISOR: Professor T.E. Marlin

NUMBER OF PAGES: xix, 242

ABSTRACT

A model-based real-time optimization (RTO) system can improve the operating profit of the plant by tracking the changing optimum responding to disturbances. Naturally, the RTO tracking capability relies on the accuracy of the model and the estimated parameters. This thesis develops the technologies to enhance RTO performance by acquiring better data sets for updating and investigates the effect of model fidelity on RTO performance.

The main contribution of this thesis is to improve updating through the use of multiple data sets (current and recent past data sets), including the possibility of judiciously designed plant experiments. A moving window approach is used to keep a record of current and historical data sets for updating. When plant variation exists in the data sets, extra parameters, which require plant variation for accurate estimation, can be updated to reduce the plant/model mismatch. The updater diagnostic tests are implemented to identify the maximum number of parameters that can be estimated from the available data sets. The parameter estimation problem is formulated by incorporating prior knowledge of disturbance frequency to track the disturbances with different dynamics. Accurate estimation of some of the adjustable parameters requires plant variation which can be generated by disturbances. When the data sets do not have sufficient plant variation for updating, limited plant perturbation can improve updating. A new expected profit approach for designing plant experiments is developed and integrated with the RTO system. Experiments are designed to maximize the overall expected profit to trade off the benefits achieved by improved model and cost of experimentation.

The effect of model fidelity on RTO performance is investigated using several case studies including an industrial boiler case study. A model-free direct search method

and model-based methods using a fundamental model and an empirical efficiency curve model are implemented in the boiler network optimization. The tradeoff between model complexity and plant experimentation is investigated in this case study. The RTO system using a fundamental model can track the changing optimum closely without plant experimentation. Using an empirical efficiency curve model, experimentation is required to track the changing optimum responding to the disturbances in fuel composition and heat exchanger fouling. There is a loss in boiler efficiency during experimentation which is not desirable for tracking fast disturbances. The model-free direct search method takes a lot of steps to reach the optimum, and a significant loss in boiler efficiency is observed during transient.

ACKNOWLEDGEMENTS

I would like to acknowledge the people who made this thesis possible.

I would like to express my gratitude to my supervisor, Dr. T. E. Marlin, for his supervision throughout this thesis. His support and encouragement have made my life being a graduate student enjoyable.

I would also like to thank my supervisory committee members, Drs. J. F. MacGregor and M. Elbestawi, for their comments and suggestions which enhanced the quality of this thesis.

I am grateful to the steam and utility group in Dofasco for supplying the boiler drawings and operating data for the model development and validation in my boiler case study. Special thank is given to Tom Lumley for helping me understand the operation of Dofasco's boiler.

I would also like to thank the colleagues from my research group for their support and friendship throughout the thesis work. Special thanks go to Adam, Chunliang Danielle, Honglu, Ivan, Laura, Manish, Niki, Seongkyu, Tong and Yongsong for their research advice and encouragement.

I would like to thank Kitty for her encouragement in my thesis work. Her patience and willingness in listening to my problems and difficulties encountered in my research work are greatly appreciated.

Last but not least, I would like to thank my family for the support throughout my thesis work. Without their encouragement and understanding, I would never publish this thesis.

TABLE OF CONTENTS

LIST OF FIGURES

LIST OF TABLES

1. INTRODUCTION

On-line operations optimization of chemical processes has received considerable attention in the past few decades, and it has become increasingly important in achieving a competitive advantage in industries [Culter and Perry, 1983; Darby and White, 1988; Marlin and Hrymak, 1997]. Typically, operations optimization methods are grouped into two categories: direct search [Garcia and Morari, 1981] and model-based [Roberts, 1979] approaches. This thesis focuses on the model-based real-time optimization (RTO) of steady-state chemical plants.

Chemical plants that can receive benefits from real-time operations optimization should satisfy the following criteria [Marlin and Hrymak, 1997]: 1) there are extra manipulated variables for optimization after the higher priority safety, production rate and product quality objectives have been satisfied; 2) there is a significant improvement in profit when the operation variables are optimized; and 3) plant optimum varies with time due to disturbances in external variables and to changes in plant performance, demand and economics. Operating profit can be increased by implementation of real-time optimization to track the changing optimum responding to these non-stationary disturbances.

Numerous successful applications of real-time optimization in industrial practice have been reported [Hardin et al., 1995; Pedersen et al., 1995; Yoon et al., 1995]. Economic benefits can be achieved by increased productivity, improved product quality and reduced energy requirements. Typical industrial processes in which operating profit can be improved by real-time optimization include refinery crude unit, hydrocracker and ethylene plant.

In model-based real-time optimization, process model is updated from plant measurements to correct for disturbances and modelling errors. Therefore, information content in the data sets for model updating is crucial in reducing the mismatch between the plant and the model for better tracking of the operating profit. The objective of this thesis is to investigate the effects of plant data and model fidelity on real-time optimization performance and to develop methods for acquiring needed data for model updating to improve real-time optimization performance.

Major portion of this chapter is devoted to reviewing the technologies in operations optimization. The first section presents the process control hierarchy in chemical plants. Direct search and model-based approaches in operations optimization are then discussed. The final two sections provide the overview of the thesis contents and summaries of the terms and conventions used throughout this thesis.

1.1 Process Control Hierarchy

Typical process control hierarchy [Marlin and Hrymak, 1997; McCaw, 1995; White, 1997] is broken down into scheduling, real-time optimization and process control shown in Figure 1.1. The cascade design in process control hierarchy enables the decisions to be made at different frequency in each layer.

The upper scheduling layer deals with long term economic goals. Decisions such as allocation of materials, production policies and inventory targets are made in this layer. Operating conditions of the plant are not modelled in the scheduling layer in sufficient detail to allow direct implementation. Typically, the execution period of scheduling calculation is in the order of days to weeks and considers a horizon of weeks to months.

Real-time optimization layer, in which the economics are considered explicitly, determines the best operating policy by maximizing the operating profit or minimizing

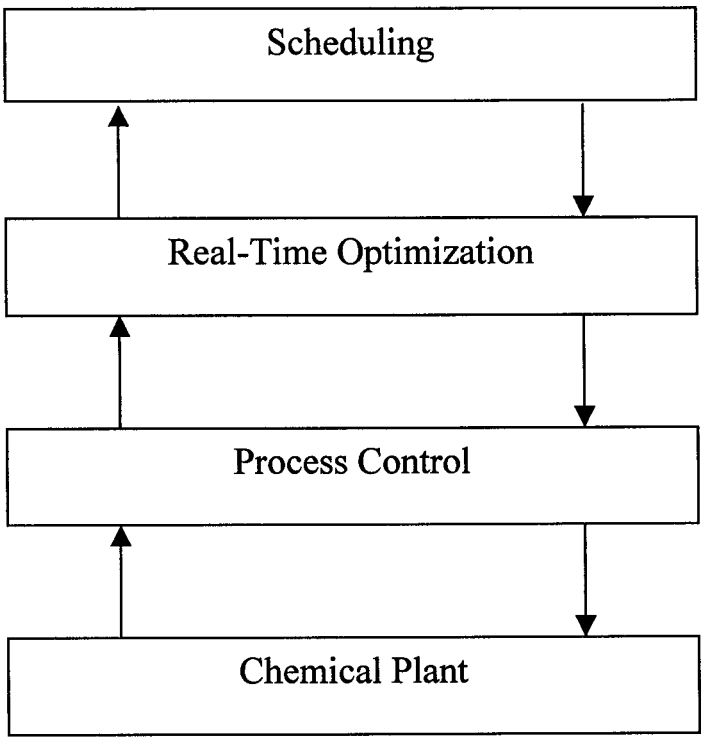

Figure 1.1 Process control hierarchy

the operating cost. This layer rejects the disturbances with frequencies higher than those considered in the scheduling layer, which could be catalyst deactivation, heat exchanger fouling and changes in feed composition. The real-time optimization layer is executed every few hours or minutes, depending on the dynamics of the processes. The optimizer results are implemented in the plant as controller setpoints in the process control layer.

The lower process control layer rejects high frequency disturbances to maintain the controlled variables at the setpoints. The control systems include regulatory control and advanced process control. The control calculation is performed at a frequency of minutes or seconds. The manipulated variables in the plant are adjusted to achieve high priority control objectives such as safety, product quality and production targets, as well as tracking of the economic optimum determined by the real-time optimization layer.

The main focus of this thesis is the real-time optimization layer for operations optimization. The following section presents the overview of operations optimization and discusses the direct search and model-based approaches in operations optimization.

1.2 Overview of Operations Optimization

Operations optimization determines the operating conditions to maximize the operating profit or minimize the operating cost of a chemical plant. There are two approaches in optimizing the economic performance of a plant: direct search and mode-based approaches. In direct search methods, economic optimum is determined from the response surface of the plant. Model-based methods utilize a fundamental model to captures the plant behavior and an objective function to measure the profitability. The objective function is optimized subject to the plant model to determine the optimum operating conditions.

1.2.1 Direct Search Methods

Direct search methods explore the process response surface to locate the optimum from a series of plant experiments. A classical direct search approach, Evolutionary Operation (EVOP), was introduced by Box (1957), and Box and Draper (1969). In EVOP, a set of plant experiments at steady state is performed around the current operating point. The plant performances at the experimental points are compared with the performance at the current operating point. If there is an improvement in plant performance statistically, the plant is moved in the direction that shows the greatest improvement, and the experimentation process is repeated again.

An empirical model, which relates the plant performance and the optimization variables, can be used to determine the search direction in direct search methods. Usually, a simple linear or quadratic function is sufficient to describe the plant performance. The

parameters in the empirical model are updated periodically from the experimental points. The search direction can be determined from the derivatives of the plant performance with respect to the optimization variables from the empirical model.

Direct search methods using steady-state experiments can take a long time to reach the optimum when the process dynamics are slow. Direct search methods have been extended to incorporate dynamic models for operations optimizations [Bamberger and Isermann, 1978; Garcia and Morari, 1981; Hamber and Richenberg, 1988; Lee and Lee, 1985]. Two main steps in this method are: 1) identification of the dynamic model using measurements from the transient, and 2) determination of the direction of plant performance improvement. In the identification phase, the plant is persistently excited by an input signal. Parameters in the dynamic model are estimated using recursive least squares methods. The steady-state gain from the estimated dynamic model is used to calculate the derivatives, and hence the search direction, of the plant performance. The plant is then moved along the direction of improving plant performance.

The main advantage of direct search methods for operations optimization is the ease of implementation. It is particularly useful when there is limited knowledge about the process. In direct search methods, operating conditions are calculated from the plant data at each iteration and the calculated setpoints are implemented to the plant. The calculation of the controller setpoints does not require extensive computation, and therefore, direct search methods are easy to maintain.

There are certain disadvantages in direct search methods which limit the applications in industrial processes. Direct search methods require online measurement of plant performance which may not be possible in some chemical plants. Plant experiments are required to generate gradient information of the plant performance. Extensive plant perturbation is undesirable, especially when there are a large number of variables, since plant experiments are expensive to perform. Most importantly, the number of

experiments is proportional to the number of optimization (manipulated) variables, and each experiment has a duration of the time for the plant to reach steady state. For example, a plant with 20 optimization variables and 4 hours to return to steady state would require 80 hours for one gradient evaluation! This approach would only be appropriate when disturbances occur very slowly, perhaps in the order of once per month or less frequently.

1.2.2 Model-Based Methods

In model-based methods, the optimum is determined by solving a mathematical programming problem. The mathematical models for optimization are usually developed based on fundamental theories such as conservations of mass, energy and momentum. Constitutive equations such as thermodynamics relationship, rate expressions and equipment modelling are also included in the models. A typical model-based real-time optimization system has two main components: model updating using plant measurements and an economic optimization using the updated model.

The models used in economic optimization can be steady-state or dynamic. Steady-state models are simpler to solve and require less computation effort. However, steady-state optimization is applicable to continuous processes with disturbance frequency slower than the dynamics of the feedback system. Optimization using dynamic models requires either integration of the differential equations [Jang et al., 1987] or discretization of the differential equations by collocation methods [Cuthrell and Biegler, 1987]. Integration of the differential equations models can dramatically increase the computational requirement for optimization. Discretization of the differential equations models increases the dimension of the optimization problem compared to steady-state optimization. In this thesis, operations optimization using steady-state models is considered, in which the disturbance frequency is slower than the execution frequency of the real-time optimization systems.

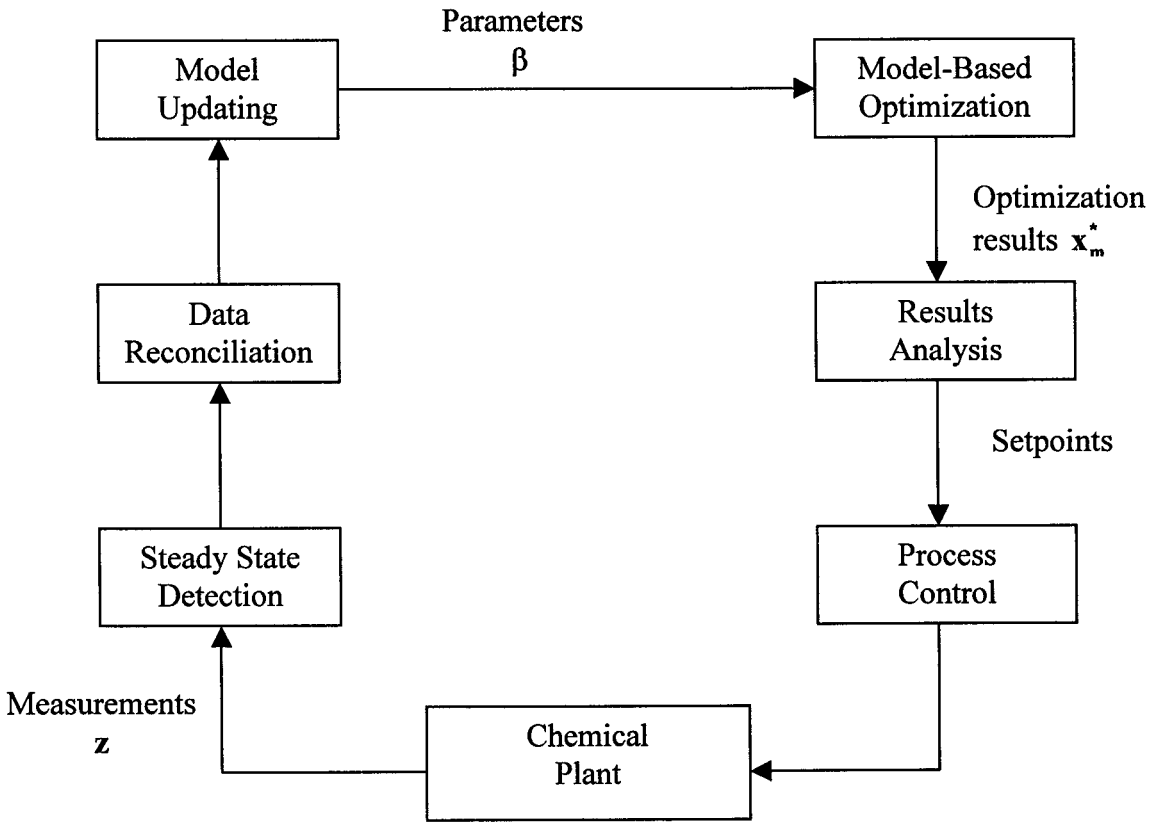

Figure 1.2 Real-time optimization loop structure

Typical structure of a closed-loop real-time operations optimization system [Koninckx, 1988] is shown in Figure 1.2. Measurements are taken from the plant and checked if the process has reached steady state. Steady-state data is then passed to data reconciliation module to identify if there are gross errors in the measurements. After eliminating the gross errors, steady-state measurements are then used to estimate the parameters in model updater. The updated model is optimized to determine the economic optimum in model-based optimizer. The optimization results are analyzed before transmitted to process controllers for implementation. The details of the individual element in this closed-loop real-time optimization system are discussed in Chapter 2.

The capability of a closed-loop real-time optimization system to track the optimum closely relies on the accuracy of the model. In real-time optimization system, simplified model is often used to reduce the computation effort. Accuracy of the simplified model is ensured by periodic updating using the process measurements to reduce the modelling errors. This thesis concentrates on developing methods to generate better data sets for model updating to improve profit tracking in real-time optimization system.

1.3 Thesis Objectives and Scope

The objective of this thesis is to develop methods to enhance real-time optimization performance through model updating. The accuracy of the prediction of the optimum is influenced by the model uncertainty. In a closed-loop real-time optimization system, the model parameters are updated using plant measurements to reduce the modelling errors and correct for disturbances. Therefore, good data sets taken from the plant can improve the quality of the parameters estimates and hence, improve the performance of real-time optimization systems.

In this thesis, the following assumptions are made to focus the investigation in model updating:

1) steady state has been reached and detected, and the data sets used in model updating are the steady-state measurements from the plant,
2) gross errors in the data sets have been identified and eliminated through redundant measurements, and the data sets for model updating do not have identifiable gross errors,
3) an adequate control system is implemented in the process control layer to maintain the plant at the optimum determined in the real-time optimization layer.

Realism is retained by investigating challenging scenarios. These scenarios include measurement errors, unmeasured disturbances, and model errors. Details of each scenario are presented when the results are reported.

The thesis is organized as follows. In Chapter 2, research work that has been done in real-time optimization systems is reviewed. The improvements in the real-time optimization performance from the methods developed in this thesis are compared with current best technology presented in Chapter 2, which provides a base case for the investigations. Multiple data sets for modeling updating is presented in Chapter 3. In this approach, several sequential sets of steady-state data are used in model updating to update more parameters for correcting modelling errors and reduce the effect of stationary noise. Chapter 4 presents the experimental design strategy in obtaining better data sets for model updating. The main contribution of this work is the development of a new experimental design criterion based on profit to maximize profit when experimentation and subsequent improvements are considered. In Chapter 5, the effect of model fidelity on real-time optimization performance in an industrial boiler case study and the tradeoff of model complexity and plant experimentation are investigated. The experimental design strategy developed in Chapter 4 is demonstrated in a realistic industrial boiler system in Chapter 5. The real-time optimization systems using the direct search methods and model-based methods with a fundamental model and an empirical model are implemented in the simulated boiler case study. This case study can provide some guidelines on selection of the model structure and measurements for real-time operations optimization of a boiler network for various commonly encountered disturbances.

1.4 Thesis Conventions

Throughout this thesis, **real-time optimization (RTO)**, **RTO system**, and **online optimization** are used to describe the steady-state operations optimization system shown

in Figure 1.2. **Model updater** and **model updating** are used describe the parameter estimation problem in a closed-loop real-time optimization system to estimate the parameters in the model from plant data. **Optimizer** and **economic optimization system** refer to the optimization problem to determine the optimum operating conditions.

The process variables are classified into **independent variables** and **dependent variables**. Independent variables are the variables that can be independently adjusted in the plant to improve the plant performance. Dependent variables are the variables that are determined once the values of the independent variables are fixed. The **reduced space** is the space of the independent variables once the dependent variables are eliminated from the optimization problem.

This thesis deals with plant and model behavior with respect to optimization. The terms **plant** and **true plant** are used to describe the chemical plant in which the operating conditions are to be optimized. In this thesis, results are generated from simulation. Therefore, plant and true plant refer to the system of equations to simulate the chemical plant shown in Figure 1.2. The terms **model** and **plant model** refer to the system of simplified equations used in the RTO system to approximate the plant, which are the equations used in model updating and model-based optimization in Figure 1.2. **True plant optimum** and **plant optimum** refer to the optimal operations of the plant, while **model optimum** and **predicted optimum** refer to the optimum predicted by the optimizer in the RTO system. **Experiments** refer to changes in the setpoints of the simulated plant when plant experimentation is performed.

Throughout the thesis, whenever a term or convention is introduced for the first time, explanation is given.

2. STRUCTURE OF A CLOSED-LOOP REAL-TIME OPTIMIZATION SYSTEM

2.1 Introduction

The typical structure of a closed-loop RTO system has been introduced in Chapter 1. This chapter focuses on the detailed descriptions of the elements in an RTO loop and discussions of the research work that has been done on the design and implementation issues of the RTO systems. The technology described in this chapter provides the basis for the research in later chapters. Thus, the research results are compared with the "best available" technology described here.

Economic performance of an RTO system is influenced by the accuracy of the model optimum prediction. The accuracy can be characterized by two terms, 1) offset between the true plant optimum and noise-free predicted optimum, and 2) variability of the predicted optimum. Offset is caused by mismatch between the plant and the model due to errors in the model structure and parameter values. Variability of the predicted optimum is caused by high frequency stationary disturbances propagating in the feedback RTO loop. Offset and variability can have significant impact on the operating profit, which is illustrated in Figure 2.1. Previous research work concentrated on reducing the offset and variability to improve profit tracking through proper RTO design and implementation.

Naturally, design decisions strongly affect the closed-loop RTO performance. Key design decisions are the selection of a model for RTO application, and selection of parameters, measurements and updating formulation for model updating to yield an RTO system which can track the operating profit closely.

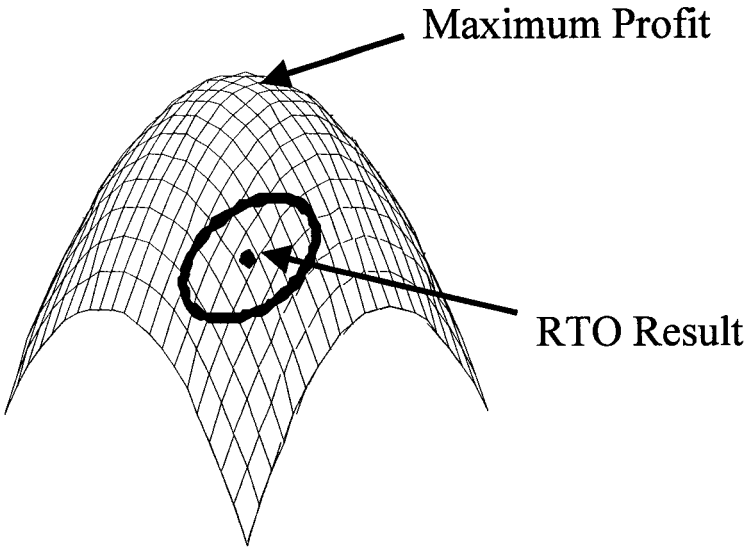

Figure 2.1 RTO performance measured by offset and variability

Plant operation can also affect the RTO performance. A well-designed RTO system may encounter performance degradation due to real-time issues such as noisy data and sensor failure. Implementations of real-time results analysis and updater diagnosis are essential in achieving good profit tracking in the changing situations encountered in the system during plant operation.

This chapter reviews the current best technologies in design and implementation of the RTO system for profit tracking which provide the base case technology in this thesis. Although all the components in the RTO loop in Figure 1.2 are discussed in the following sections, the research work in this thesis focuses on model updater, model-based optimizer and results analysis.

2.2 Steady State Detection

Most of the industrial applications of RTO system consider steady-state optimization in which the disturbance frequency is slower than the feedback dynamics.

Therefore, measurements taken from the plant for model updating should represent the steady-state plant behavior. Steady state detection module avoids passing the dynamic data for steady-state model updating, which can deteriorate the RTO performance [Koninckx, 1988].

Steady state can be detected by various statistical methods. Control charts in statistical process control, such as Shewart chart [Contino, 1987], can be used to monitor the process variables. If the variations of the process variables are within the control limits, the process is considered at steady state. Steady state can also be detected by hypothesis test [Narasimhan et al., 1986; Narasimhan et al., 1987]. A certain number of successive sets of measurements are taken in two consecutive periods. The sample means and variances of the process variables are estimated from the measurements in these periods. A Hotelling T^2 test is then performed to test the equality of the sample means in these two consecutive periods. If the sample means are statistically equal, the process is considered at steady state.

2.3 Data Reconciliation and Gross Error Detection

Steady-state measurements are reconciled and detected for gross errors before being used in model updating. Process measurements are inevitably corrupted by errors during measurement, processing and signal transmission. Measurement errors are categorized into random error (noise) and systematic or gross error (bias). Because of these measurement errors, material and energy balances are not exactly satisfied. Process data is reconciled to estimate the true values of the process variables based on steady-state material and energy balances, and gross errors are identified and eliminated using statistics before passing the data sets to model updater. Detailed review on data reconciliation and gross error detection can be found in Narasimhan and Jordache (2000).

In data reconciliation, the true values of the process variables are estimated by minimizing the measurement adjustments subject to the material and energy balance constraints. The general nonlinear steady-state data reconciliation is stated in (2.1) [Kim et al., 1997],

$$\begin{aligned} &\underset{\hat{\mathbf{z}}}{\text{minimize}} && (\mathbf{z}-\hat{\mathbf{z}})^{\mathrm{T}}\mathbf{V}^{-1}(\mathbf{z}-\hat{\mathbf{z}}) \\ &\text{subject to} && \mathbf{h}(\hat{\mathbf{z}})=\mathbf{0} \end{aligned} \tag{2.1}$$

where $\hat{\mathbf{z}}$ is the estimated values of the process variables with measured values $\mathbf{z}$, $\mathbf{V}$ is the covariance matrix of the measurements, and $\mathbf{h}$ is the steady-state material and energy balance equations. The linear data reconciliation using overall balances [Crowe et al., 1983] and bilinear data reconciliation using component balances [Crowe, 1986] are the special cases of (2.1). In the above formulation, it is assumed that measurements are subject to random errors only. The data reconciliation problem can be solved by existing optimization algorithms [Edgar et al. (2001); Gill et al. (1981)].

Gross errors can be detected using statistical tests on the measurement adjustments, $\mathbf{a}=\mathbf{z}-\hat{\mathbf{z}}$, estimated from the solution of (2.1). Univariate [Crowe et al., 1983], Chi-square [Crowe et al., 1983] and maximum power tests [Crowe, 1989; Mah and Tamhane, 1982] on $\mathbf{a}$ can be performed to detect the gross errors in the measurements. Similar tests on the residuals of the constraints can also be used. These tests do not consider the correlation between the estimated measurement adjustments, and their performance is not always satisfactory. Tong and Crowe (1995) proposed the principal component analysis (PCA) to reliably detect gross errors when the variables are highly correlated so that univariate and maximum power tests fail.

Identification of gross errors in the measurements from the solution of (2.1) requires iteration. When a gross error is detected, the suspect measurement that

corresponds to the maximum test statistic exceeding the test criterion is removed. The procedures of solving (2.1) and statistical tests on detecting gross errors are repeated until no more gross error is detected. The reason for identifying gross errors using iterative process is that the assumption of random errors in the measurements may bias the results of data reconciliation when the measurements have gross errors. Tjoa and Biegler (1991) proposed a bivariate distribution function to replace the objective function in (2.1), which takes the random and systematic errors into account, to simultaneously reconcile the data and detect the gross errors without iteration. Johnston and Kramer (1995) developed the bivariate distribution function from Bayes' theorem and extended it to incorporate historical plant data to determine an a priori probability distribution to improve the performance of data reconciliation and gross errors detection.

2.4 Model Updater

Model is updated from plant measurements in model updater to correct model errors and disturbances. In most RTO applications, model updating is usually restricted to parameter estimation without changing the model structure. Major design decisions in designing a closed-loop RTO system are the selection of a model for online application and selection of parameters and measurements for updating. The main focus of this thesis is to improve the RTO performance through model updating. Therefore, previous research work on model updating is discussed in details in this section. In this section, the issues in model selection addressed by Forbes (1994) are first discussed. Research work on parameters and measurements selection is then reviewed. Various formulations for parameter estimation are presented. Finally, research work on diagnosing updater results is discussed.

2.4.1. Selection of Process Model

Using a suitable process model is the key to the success of RTO applications. Fundamental models developed from first principle are always recommended for online applications. However, solving detailed fundamental models require extensive computation which may not be suitable for online calculation. Forbes (1994) addressed the issues of model structure selection for RTO systems by developing a set of design criteria, which include model adequacy tests and stability criterion, for achieving good RTO performance. These criteria provide the guidelines for excluding the models, which are not capable of achieving good RTO performance, from different alternatives.

A point-wise model adequacy test was developed [Forbes, 1994; Forbes et al., 1994; Jewell, 1996] to exclude the models that are not adequate for process optimization. Point-wise model adequacy is defined as the ability of a model to predict the values of the manipulated variables, which coincide with the values of the plant optimum, by adjusting the values of a set of parameters in the model. This idea is illustrated in Figure 2.2. A set of mathematical criteria was developed from the Karush-Kuhn-Tucker (KKT) conditions [Edgar et al., (2001); Gill et al., (1981)] to test the point-wise model adequacy which examined the curvature of the profit function of the model at the optimum in reduced space. The testing criteria consist of the followings: 1) the reduced gradient of the model at the plant optimum is zero, and 2) the reduced Hessian matrix of the model at the plant optimum is positive (negative) definite for minimization (maximization) in the economic optimization.

The point-wise adequacy test is a minimum requirement to investigate the suitability of a model for process optimization. A point-wise adequate model can by itself predict the plant optimum. There is no indication of how the model will perform in a closed-loop RTO system. The augmented model adequacy test [Forbes, 1994; Forbes and Marlin, 1996] was developed to investigate whether the model is able to predict the plant

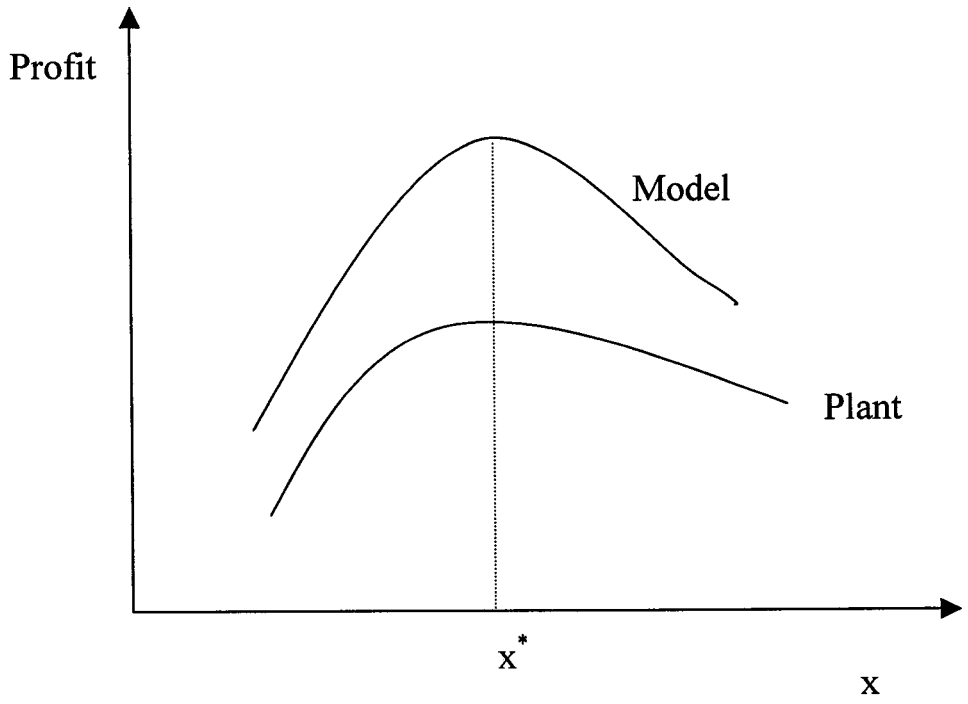

Figure 2.2 Point-wise model adequacy

optimum when integrated with model updater in an RTO loop. The augmented model adequacy test ensures that the parameter values should satisfy the point-wise adequacy test and the corresponding KKT conditions of the model updating problem simultaneously. Therefore, a model is able to predict the plant optimum if there exists a set of adjustable parameters which satisfies the following conditions: 1) the point-wise adequacy criteria, 2) the reduced gradient of the objective function in model updater is zero, and 3) the reduced Hessian matrix of the objective function in model updater is positive definite. If such values of model parameters exist, the plant optimum is an equilibrium solution of the model-based optimization problem.

The augmented model adequacy test does not address the stability of a closed-loop RTO system. The point-wise stability criterion [Forbes, 1994; Forbes and Marlin, 1996] was developed to evaluate if the perturbations from the optimum would be

amplified or settled out in an RTO loop. The testing criterion requires the derivatives of the model updater, optimizer and plant estimated from linear sensitivity analysis. This criterion is valid only for small perturbations from the optimum. It is not guaranteed that the RTO loop converges to the optimum for any finite distance from the optimum.

The design criteria of point-wise adequacy test, augmented adequacy test and point-wise stability test provide sequential tests with increasing computational effort for screening the bad design from different alternatives. This sequential approach reduces the computation effort by eliminating the undesirable design alternatives earlier in the testing process.

The main requirement of these tests is the knowledge of the plant optimum and plant derivatives. Plant optimum and its derivative can be estimated from a rigorous model which is too complicated for online application. Plant optimum can also be estimated from process knowledge or plant experimentation.

2.4.2 Selection of Parameters for Updating

Parameters which strongly affect the accuracy of the optimum prediction require frequent and accurate estimation. Krishnan et al. (1992) suggested selecting the parameters which significantly affect the profit and/or alter the active set of the constraints for updating. The effect of the parameters on profit and active set of constraints can be evaluated by perturbing the parameters and re-optimizing the model. However, parameters which change the profit significantly may not have any effect on the gradient of profit which determines the optimum operating conditions. Forbes and Marlin (1996), and Zhang and Forbes (2000) proposed the design cost criterion for selecting the parameters for updating to minimize the performance loss due to offset and variability. Loeblein and Perkins (1998) extended the RTO performance measure to include the performance loss due to the backoff from the active constraints for ensuring

feasible operation in the presence of uncertainty and suggested selecting the parameters for updating to reduce the performance loss. Evaluation of the RTO performance requires knowledge of the true plant optimum which can be estimated using a detailed model not suitable for RTO application or from plant experience.

2.4.3 Selection of Measurements for Updating

Proper choice of measurements for updating can improve the accuracy of the estimated parameter and hence the optimum prediction in the model-based optimizer. Measurement selection for parameter estimation has been addressed by Kage and Joseph (1990), Krishnan et al. (1992) and Zhang (1998); they proposed selecting measurements yielding parameter estimation with a small uncertainty in the estimates. These methods do not consider the effect of the measurements on the RTO performance. Fraleigh (1999), and Loeblein and Perkins (1998) proposed selecting measurements for updating which can improve the profit tracking in a closed-loop RTO system.

2.4.4 Formulation of Parameter Estimation Problem

Selected model parameters are updated using plant measurements to reduce (but not eliminate) model mismatch using an appropriate formulation of parameter estimation problem. The parameter estimation problem has the following features: nonlinearity, noise in all variables and no distinction between dependent and independent variables. The model can be expressed in terms of the process variables, $\mathbf{x}$, fixed parameters, $\boldsymbol{\alpha}$, and adjustable parameters, $\boldsymbol{\beta}$, given in (2.2).

$$\mathbf{f}(\mathbf{x}, \boldsymbol{\alpha}, \boldsymbol{\beta}) = \mathbf{0} \tag{2.2}$$

Two commonly used parameter estimation formulations suitable for RTO applications are the improved parameter estimation [Bard, 1974; Box, 1970; Sutton and MacGregor,

1977a] and simultaneous data reconciliation and parameter estimation (DRPE) [Bard, 1974; Kim et al., 1990; Kim et al., 1991; MacDonald and Howat, 1998; Zhang, 1998]. The DRPE formulation is commonly used in RTO research, and its application in industrial RTO system has also been reported [Hardin et al., 1995]. Therefore, this formulation is selected for model updating in this thesis, although it is computationally more expensive than the improved parameter estimation. The algorithms (SQP and MINOS) for solving the parameter estimation problem in this thesis are described in Appendix A.

In simultaneous data reconciliation and parameter estimation (DRPE), parameters are estimated by minimizing the difference between the sensor and calculated values of the measured variables in a least squares sense. The vector of process variables, $\mathbf{x}$, is partitioned into measured and unmeasured variables, $\mathbf{x}^m$ and $\mathbf{x}^u$, respectively. The difference between the sensor and calculated values is signified by a variable, $\mathbf{a}$, with $\mathbf{x}^m = \mathbf{z} + \mathbf{a}$. The parameters, $\boldsymbol{\beta}$, the measurement adjustments, $\mathbf{a}$, and the values of the unmeasured variables, $\mathbf{x}^u$, are evaluated so that the objective function is minimized and the equality constraints in (2.2) are satisfied exactly. The problem formulation is given in (2.3).

$$\begin{aligned} &\underset{\boldsymbol{\beta},\mathbf{x}^u,\mathbf{a}}{\text{minimize}} && \mathbf{a}^T\mathbf{V}^{-1}\mathbf{a} \\ &\text{subject to} && \mathbf{f}(\mathbf{z}+\mathbf{a},\mathbf{x}^u,\boldsymbol{\alpha},\boldsymbol{\beta}) = \mathbf{0} \end{aligned} \tag{2.3}$$

Parameters estimated by (2.3) are uncertain due to the presence of the measurement noise. The covariance matrix of the parameters can be estimated by linear sensitivity analysis of (2.3) and is given in (2.4).

$$\mathbf{Q}_\beta = \left(\frac{d\boldsymbol{\beta}}{d\mathbf{z}}\right)\mathbf{V}\left(\frac{d\boldsymbol{\beta}}{d\mathbf{z}}\right)^T \tag{2.4}$$

Estimation of the sensitivity matrix at the solution is discussed in Appendix B.

2.4.5 Updater Diagnosis

The measurements and parameters in (2.3) are selected to give a well-conditioned calculation. However, the calculation can become ill-conditioned because of real-time issues like missing measurements or changing operating conditions. When the estimates of the parameters are very uncertain in an ill-conditioned problem, prediction of the optimum using those uncertain parameters can be poor resulting to poor profit tracking. Updater diagnosis [Miletic and Marlin, 1998a] has been developed to detect ill-conditioning in the model updater to avoid amplifying the uncertainty in the RTO loop.

Ill-conditioning in parameter estimation problem can be detected from the covariance matrix of the parameters, $\mathbf{Q}_\beta$. The shape of the joint confidence region of the estimated parameters is characterized by the condition number of $\mathbf{Q}_\beta$. A large condition number indicates that the joint confidence region is elongated in one direction. A well-known example is to estimate the frequency factor and activation energy in an Arrhenius rate expression from the data with small variation in temperature which results to poor estimates of the parameters and a large condition number of $\mathbf{Q}_\beta$.

The causes of ill-conditioning can be diagnosed from singular value decomposition of $\mathbf{Q}_\beta'$, which is the scaled version of $\mathbf{Q}_\beta$, obtained by pre and post multiplication of $\mathbf{Q}_\beta$ by the reciprocals of the parameter estimates. If the condition number of $\mathbf{Q}_\beta'$ is larger than its upper control limit (UCL), the estimation is deemed ill-conditioned. The upper control limit can be tuned for an operating region based on the plant experience.

Recovery strategy has to be implemented to avoid passing the variability to the setpoints once ill-conditioning has been detected in the updater. Miletic and Marlin (1998a) suggested re-defining the structure of the parameter estimation problem for recovering from ill-conditioning. The parameter which contributes the most to ill-conditioning is identified from the eigenvalues of $\mathbf{Q}_{\beta}^{'}$. That parameter is fixed at the previous estimated value, and other parameters are re-estimated. These procedures are repeated until the parameter estimation problem becomes well-conditioned. Parameters estimated from a well-conditioned parameter estimation problem are then sent to model-based optimizer for predicting the plant optimum.

2.5 Model-Based Optimizer

The optimum operating policy is determined in the optimizer based on the updated model and an economic objective function. The economic optimization problem used for RTO can be stated in (2.5).

$$\begin{aligned} \underset{\mathbf{x}}{\text{minimize}} \quad & P(\mathbf{x}, \boldsymbol{\alpha}, \boldsymbol{\beta}) \\ \text{subject to} \quad & \mathbf{f}(\mathbf{x}, \boldsymbol{\alpha}, \boldsymbol{\beta}) = \mathbf{0} \\ & \mathbf{g}(\mathbf{x}, \boldsymbol{\alpha}, \boldsymbol{\beta}) \geq \mathbf{0} \end{aligned} \tag{2.5}$$

P is the economic objective function, and $\boldsymbol{\alpha}$ is the vector of fixed parameters which remain constant. The vector, $\boldsymbol{\beta}$, contains the parameters that are updated by solving (2.3). The vector, $\mathbf{x}$, of optimization variables includes dependent variables, $\mathbf{x}_D$, and independent variables, $\mathbf{x}_I$, i.e., those that can be manipulated for optimization. The optimum values of $\mathbf{x}$ are determined by maximizing the operating profit or minimizing the operating cost of the model such that the equality constraints, $\mathbf{f}$, and the inequality constraints, $\mathbf{g}$, are satisfied.

The equality and inequality constraints approximate the plant behavior mathematically. The equality constraints contain material and energy balances, thermodynamic and kinetic information, and constitutive equations for plant equipment. The inequality constraints specify the safety requirement and equipment limitations.

The optimum cannot be exactly predicted by solving (2.5) because of the uncertainty in the parameters, $\boldsymbol{\beta}$. The variability of the predicted optimum is characterized by its covariance matrix, $\mathbf{Q}_{x_m^*}$. The covariance matrix of the predicted optimum can be estimated from the sensitivity matrix obtained by linear approximation, and $\mathbf{Q}_{\beta}$, as shown in (2.6).

$$\mathbf{Q}_{x_m^*} = \left(\frac{d\mathbf{x}_m^*}{d\boldsymbol{\beta}}\right)\mathbf{Q}_{\beta}\left(\frac{d\mathbf{x}_m^*}{d\boldsymbol{\beta}}\right)^T \tag{2.6}$$

Estimation of the sensitivity matrix of the optimizer evaluated at the solution is discussed in Appendix B. These optimizer results are then analyzed in results analysis before implementation.

2.6 Results Analysis

The results of the optimization are influenced by high frequency stationary variation and therefore should be evaluated with respect to the likely "common cause" effects of this variation. In this thesis, the results analysis method of Miletic (1995), and Miletic and Marlin (1998b) is used. The goal of results analysis is to reduce unnecessary changes in the independent variables, $\mathbf{x}_I$, due to high frequency disturbances. This approach involves evaluation of optimization results using a statistical test before the values are applied in the plant. Only the statistically significant changes from the current operation are implemented in the plant.

Predicted optima from successive RTO executions are tested to determine if they are statistically different using Hotelling T^2 test. This test can be formulated as the following hypothesis test in the reduced space of the independent optimization variables.

$$\begin{aligned} H_0 &: \quad \mathbf{x}_{I,1} = \mathbf{x}_{I,2} \\ H_1 &: \quad \mathbf{x}_{I,1} \neq \mathbf{x}_{I,2} \end{aligned} \tag{2.7}$$

The Hotelling T^2 statistic is given by (2.8).

$$T^2 = (\bar{\mathbf{x}}_{I,1} - \bar{\mathbf{x}}_{I,2})^T \left(\frac{\mathbf{Q}_{\bar{x}_{I,1}}}{N_1} + \frac{\mathbf{Q}_{\bar{x}_{I,2}}}{N_2} \right)^{-1} (\bar{\mathbf{x}}_{I,1} - \bar{\mathbf{x}}_{I,2}) \tag{2.8}$$

In (2.8), $\mathbf{Q}_{x_{I,i}}$ is the covariance matrix at the optimum, $\mathbf{x}_{I,i}$. Miletic and Marlin (1998b) found that the performance of results analysis could be improved by averaging several RTO results; therefore, N_i is the number of optimization points used to calculate $\bar{\mathbf{x}}_{I,i}$.

The new (average) setpoint vector is implemented (i.e., H_1 is accepted) if T^2 exceeds its upper control limit (UCL). The UCL represents the distinction between common cause variation due to high frequency variation and significant changes in plant behavior due to disturbances. The UCL should be evaluated using plant data near the expected operating condition. A large UCL reduces the frequency of unnecessary plant movement but slows down the tracking of non-stationary disturbances. On the other hand, a small UCL increases the variability of the setpoints but tracks the changing optimum quickly. Therefore, UCL affects the tradeoff between tracking and variability.

The hypothesis test in results analysis has been extended to the situation when a trust region is defined to limit the plant movement [Zhang et al., 2001]. Results analysis proposed by Miletic and Marlin (1998b) does not consider inequality constraints. Zhang et al. (2001) incorporated the hypothesis test on the Lagrange multipliers of the active

inequality constraints of the trust region to identify if the insignificant changes in optimization variables are due to the presence of the trust region or common cause variation.

Recently, a new move moderation technique [Ronholm, 2000] was developed to reduce the magnitudes of the plant movement after a significantly different operating point has been identified in the results analysis. In RTO applications, frequent large moves may be undesirable because they can reduce the plant profit due to off-specification product during the transition. The move moderation technique determines the setpoint by trading off the change in profit and the size of the change of the operating variables while ensuring that the plant movement is still statistically significant. This method can make the transition between operating points more gradual.

2.7 Process Control

Successful tracking of the plant optimum relies on a well-designed control system for keeping the process at the optimum closely without violation of the constraints in the presence of disturbances and uncertainty. The optimum determined in the RTO layer provides an upper bound on profit. The plant is actually moving inside a region around the steady-state optimum because of the closed-loop control system responding to high frequency disturbances entering the plant. The actual profit achieved is therefore lower than the best attainable profit determined by the RTO layer. There is an additional loss in profit from the backoff of the steady-state optimum from the active inequality constraints to ensure feasible operation for the anticipated disturbances entering the plant. A good control system should reduce the impact of high frequency disturbances on the economic performance. This can be achieved by proper selection of control structure and implementation of well-tuned controllers.

Control structure selection based on economics has been addressed by Health et al., (2000) and Narraway and Perkins (1993). They proposed selecting the controlled and manipulated variables by minimizing the profit loss due to backoff for the anticipated disturbance magnitudes and frequencies. The problem is formulated as a mixed integer linear programming (MILP) in which linearized profit loss from the steady-state optimum and linearized dynamic model are used in the objective function and constraints respectively. Narraway and Perkins (1993) simplified the problem by assuming perfect control to avoid the need of tuning the controllers in solving the control structure selection problem. Health et al. (2000) relaxed this assumption to extend the MILP approach in control structure selection to include decentralized PI controllers in the problem formulation. This formulation simultaneously selects the controlled and manipulated variables, loop pairing and PI controller tuning.

Evaluation of the effect of control structure on operating profit can be performed by incorporating steady-state effect of controller models in optimization [Contreras-Dordelly and Marlin, 2000]. The steady-state effect of the controllers can be formulated as an optimization problem which is solved simultaneously with steady-state optimization [Kassidas et al., 2000; Marlin and Young, 1998]. The optimization problem in the controller models is replaced by the stationarity conditions and converted to a set of algebraic equations. With the controller models in steady-state optimization, Contreras-Dordelly and Marlin (2000) found that controlling the active set of constraints could further improve the operating profit compared to backing off the optimum from the active set of constraints in the presence of disturbances and model errors.

Structural design of integrated online process optimization and regulatory control systems based on economics has been addressed by Loeblein and Perkins (1999a). In this approach, the RTO performance evaluated by the backoff developed by Loeblein and Perkins (1998) was extended to include the regulatory backoff estimated from the covariance matrix of the controlled variables for a given disturbance model. The

proposed approach was applied to a simulated fluid catalytic cracker (FCC) unit to select the optimal structure for online optimization [Loeblein and Perkins, 1999b].

2.8 Summary

This chapter has provided the outline of the structure of an RTO loop. Design and implementation issues addressed in the previous research work have been discussed. The common goal of the previous work done by different researchers is to develop an RTO system to track the optimum closely by minimizing the performance loss as indicated in Figure 2.1. This can be achieved by using a proper model, selecting appropriate parameters and measurements for updating, and implementing a well-designed regulatory control system.

Details of the problem definitions of model updating and updater diagnosis have been discussed in this chapter. This research investigates the use of more and better data sets for model updating to improve the RTO performance. The current state of the art on model updating and updater diagnosis provide the basis on which the multiple data sets for model updating and experimental design can be built. These new technologies are developed in the following chapters.

The RTO system under consideration in the following chapters is shown in Figure 2.3. As discussed in the assumptions in Chapter 1, this thesis focuses on model updating, model-based optimization and results analysis. The DRPE in (2.3) is selected for the model updating formulation. The formulation of the model-based optimization in (2.5) includes the inequality constraints. In this thesis, it is further assumed that the set of active inequality constraints remains unchanged. Therefore, the optimization results can be analyzed in an unchanging reduced space in the results analysis in (2.7) and (2.8).

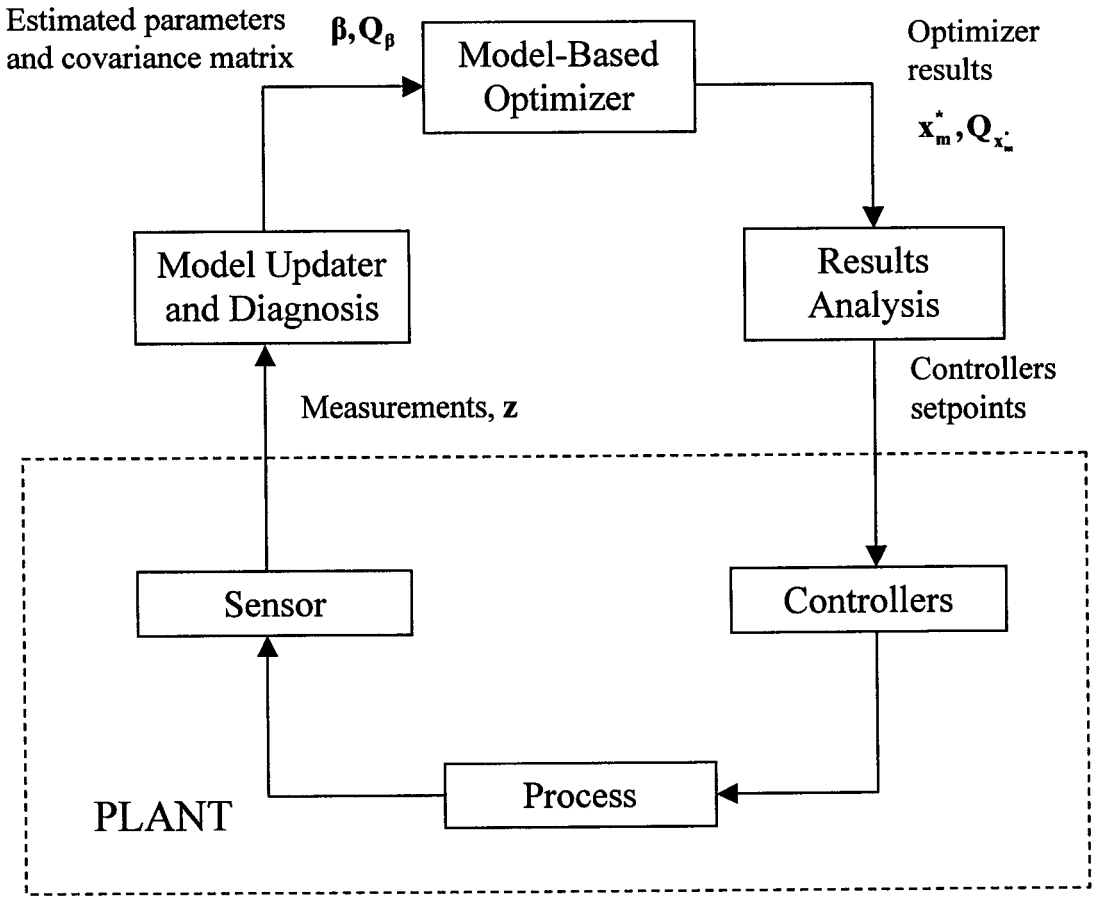

Figure 2.3 Structure of the closed-loop RTO system under consideration

3. MULTIPLE DATA SETS FOR MODEL UPDATING IN REAL-TIME OPERATIONS OPTIMIZATION

3.1 Introduction

The technologies reviewed in Chapter 2 were developed based on a single data set for model updating. A single data set for model updating is the current practice in industrial applications and academic studies. In this chapter, the current best technologies are extended to include the most recent historical data sets (multiple data sets) for model updating to further improve the RTO performance. As discussed in the assumptions in Chapter 1, this chapter focuses on model updating, model-based optimization and results analysis, and the RTO system under consideration is shown in Figure 2.3.

Multiple data sets for model updating involves keeping the most recent historical steady-state data sets for model updating. The expected advantages of using multiple data sets are an increase in the number of parameters estimated and a reduction in the effects of high frequency stationary disturbances. A single data set for model updating restricts the parameters to be updated to those observable from one set of data; for example, in a temperature dependent rate constant, either the frequency factor or activation energy can be estimated using one reactor data set. With temperature variation in the data sets, both the frequency factor and activation energy can be updated to correct for modelling errors. In addition, the variability of setpoints due to high frequency stationary disturbances with respect to RTO execution frequency can be reduced by the filtering effects of using several data sets for estimation.

The major drawbacks of using multiple data sets for updating are slower tracking of the changing optimum and an increase in computation effort for parameter estimation and sensitivity analysis in model updater. Slower tracking of the changing optimum

results from the memory effect from the past data sets. Keeping more historical data sets takes a longer time to forget the past data sets which slows down the adaptation of the change in parameter values and hence the changing optimum due to disturbances. When more historical data sets are included for updating, the problem size for parameter estimation increases, and more extensive computation is required for solving a larger estimation problem. In addition, for DRPE formulation, a larger number of perturbations is required for estimating the second derivatives in sensitivity analysis. The second derivatives are estimated by perturbing the variables in the reduced space as discussed in Appendix B. The dimension of the reduced space increases with the number of data sets for DRPE formulation because there are more measurement adjustments to be solved, and therefore, extensive computation for numerical differentiation is required.

In multiple data sets for model updating, a moving window with a fixed size is used to keep a record of the current and historical data sets. The strategy involves identifying the parameters that can be estimated reliably using the data sets in the moving window and incorporating prior knowledge of disturbance frequency to categorize the parameters as fast or slow changing in parameter estimation formulation. Previous work on updater diagnosis discussed in Chapter 2 is extended to identify the maximum number of parameters that can be estimated reliably using the current data; this number changes due to differences in variability in operating condition and sensor availability. The use of prior knowledge of disturbance frequency in parameter estimation formulation considers the tradeoff between tracking and variability, and enables the RTO system to track the changing optimum closely responding to fast disturbances.

This chapter is organized as follows. The strategy of using multiple data sets for model updating is first presented. The performance of the proposed approach is demonstrated on a Williams-Otto reactor case study. Finally, the case study results are presented to compare the RTO performance using a single data set and multiple data sets for model updating.

3.2 Strategy of Multiple Data Sets for Model Updating

The model updating method proposed here uses multiple data sets in a moving window manner as shown in Figure 3.1. This moving window keeps N_{data} successive data sets for model updating, in which Set 1 is the current data set. Using multiple data sets for model updating, the parameter estimation problem in (2.3) can be modified as stated in (3.1).

$$\begin{aligned} &\text{minimize} && \sum_{i=1}^{N_{data}} \mathbf{a}_i^T \mathbf{V}_i^{-1} \mathbf{a}_i \\ &\boldsymbol{\beta}\,,\ \mathbf{a}_i,\ \mathbf{x}_i^u \\ &\text{subject to} && \mathbf{f}(\mathbf{z}_i+\mathbf{a}_i,\ \mathbf{x}_i^u, \boldsymbol{\alpha}\,,\ \boldsymbol{\beta}\,) = \mathbf{0} \qquad \text{for } i = 1, 2, \ldots, N_{data} \end{aligned} \tag{3.1}$$

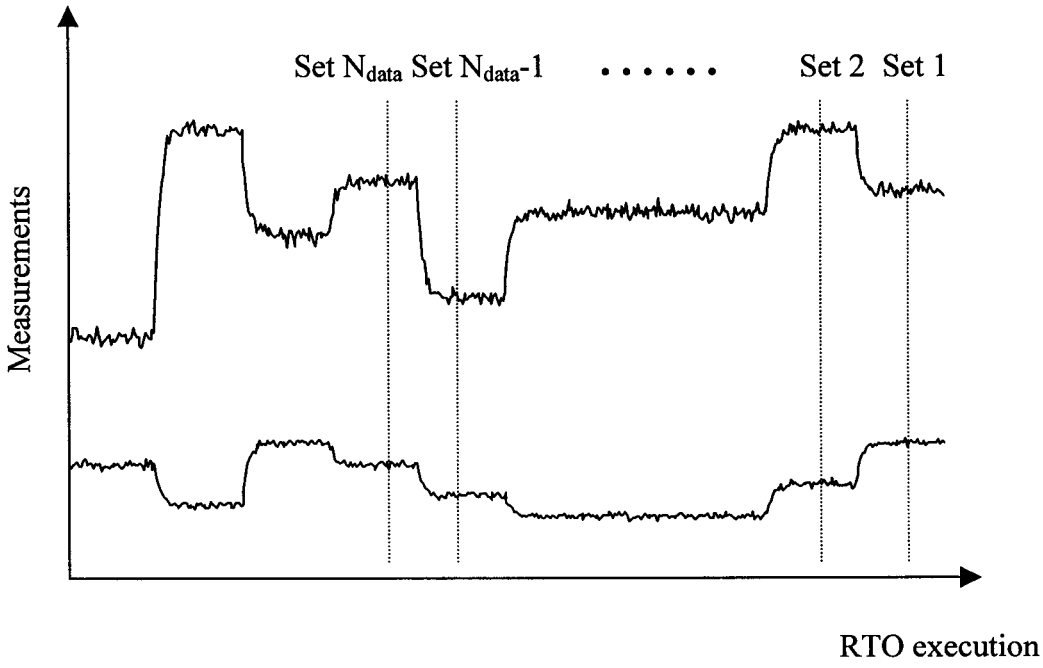

Figure 3.1 Moving window approach for model updating using multiple data sets (variation in data sets could be due to disturbances or implemented optimizer results)

The number of steady-state data sets in the moving window, N_{data}, is a design parameter. Increasing N_{data} can reduce the variability of the estimated parameters and the predicted optimum, but this will slow down the tracking of the changing optimum because it will take longer time to forget the past data sets. Therefore, the window size, N_{data}, is chosen to trade off variability against tracking and computation time [Robertson et. al, 1996; Vos et al., 1997].

Parameter estimation is formulated by taking advantage of a priori knowledge of disturbance frequencies. The vector of adjustable parameters, $\boldsymbol{\beta}$, is partitioned into $\boldsymbol{\beta}_1$, $\boldsymbol{\beta}_2$ and $\boldsymbol{\beta}_3$ as shown in (3.2) and Table 3.1.

$$\boldsymbol{\beta} = \begin{bmatrix} \boldsymbol{\beta}_1 \\ \boldsymbol{\beta}_2 \\ \boldsymbol{\beta}_3 \end{bmatrix} \tag{3.2}$$

The parameters in $\boldsymbol{\beta}_1$ and $\boldsymbol{\beta}_2$ change slowly with respect to the window size, while those in $\boldsymbol{\beta}_3$ change quickly. For example, $\boldsymbol{\beta}_1$ and $\boldsymbol{\beta}_2$ could contain catalyst activities and heat transfer coefficients which decay slowly with time. In contrast, $\boldsymbol{\beta}_3$ could contain an unmeasured feed impurity that can change rapidly. Since $\boldsymbol{\beta}_1$ and $\boldsymbol{\beta}_2$ change slowly with time, they can be assumed to be constant within the updating window. The parameters in $\boldsymbol{\beta}_3$ are allowed to have different values for each data set in the window to track this fast changing parameter. The categorization of the parameters based on process knowledge enables the RTO system to track the changing optimum due to fast disturbances ($\boldsymbol{\beta}_3$) quickly while achieving the reduction in variability by filtering.

Table 3.1 Partitioning of the vector of adjustable parameters

Parameter	Dynamics with respect to window size	Evaluated values in window	Data sets required for estimation
β_1	Slow	Constant	Single
β_2	Slow	Constant	Multiple
β_3	Fast	Varying	Single

The modified parameter updating formulation, which uses the information on parameter changes, can be expressed mathematically in Problem 3.1.

$$\text{Problem 3.1} \quad \underset{\beta_1,\beta_2,\beta_{3i},a_i,x_i^u}{\text{minimize}} \quad \sum_{i=1}^{N_{data}} a_i^T V_i^{-1} a_i \tag{3.3}$$

$$\text{subject to} \quad f(z_i+a_i, x_i^u, \alpha, \beta_1,\beta_2,\beta_{3i}) = 0 \quad \text{for } i = 1, 2, \ldots N_{data}$$

Further, knowledge about the observability of the updated parameters can be included into the updating strategy using multiple data sets. As indicated in Table 3.1, the parameters in β_1 and β_{3i} can be estimated well using a single data set; an example of such a parameter is the intercept of a linear relationship (e.g. frequency factor). In contrast, accurate estimation of the parameters in β_2 requires multiple data sets with plant variation; an example of such a parameter is the slope of a straight line (e.g. activation energy). β_2 is the vector of *additional parameters* which can only be updated from multiple data sets with sufficient plant variation. When sufficient plant variation exists, the data sets are said to have *sufficient information content*. Naturally, other situations are possible, but this will demonstrate the performance of the proposed method.

The data sets may not have sufficient information to estimate all the parameters in β accurately, and Problem 3.1 may be poorly-conditioned. Even a well-designed system can become ill-conditioned because of changes in plant data, e.g. loss of a sensor or lack

of variability in the input variables, Problem 3.1 is especially susceptible because it requires variability in plant operation. Therefore, updater diagnosis is implemented to ensure the parameter estimation is well-conditioned. The diagnosis used is essentially the method presented by Miletic and Marlin (1998a) applied to Problem 3.1.

The proposed strategy of parameter estimation using multiple data sets for model updating is shown in Figure 3.2, which replaces the model updater and updater diagnosis in Figure 2.3. The strategy consists of two updater diagnoses (UD1 and UD2). The first updater diagnosis (UD1) determines if the data sets have sufficient information to estimate all of the parameters in Problem 3.1, $\boldsymbol{\beta}_1$, $\boldsymbol{\beta}_2$ and $\boldsymbol{\beta}_{3i}$, by post-solution analysis. If the information content is insufficient, the difficulty is likely with the parameters in $\boldsymbol{\beta}_2$, which requires variation in plant operation, because plant data might not have this variation. In response to insufficient information in estimating all of the parameters, $\boldsymbol{\beta}_2$ is fixed at its previous value, and $\boldsymbol{\beta}_1$ and $\boldsymbol{\beta}_{3i}$ are re-estimated. This recovery strategy is shown as Problem 3.2 in Figure 3.2, and the formulation is stated in (3.4).

$$\text{Problem 3.2} \quad \underset{\boldsymbol{\beta}_1,\boldsymbol{\beta}_{3i},\mathbf{a}_i,\mathbf{x}_i^u}{\text{minimize}} \quad \sum_{i=1}^{N_{data}} \mathbf{a}_i^T \mathbf{V}_i^{-1} \mathbf{a}_i \qquad (3.4)$$

$$\text{subject to} \quad \mathbf{f}(\mathbf{z}_i+\mathbf{a}_i, \mathbf{x}_i^u, \boldsymbol{\alpha}, \boldsymbol{\beta}_1, \boldsymbol{\beta}_{3i}) = \mathbf{0} \quad \text{for } i = 1, 2, \ldots N_{data}$$

Under typical operating conditions (i.e., with all sensors functioning), Problem 3.2 is well-conditioned even though the data sets are from the same steady state, because these parameters can be estimated well using a single data set. However, it is possible to have ill-conditioning in the estimation of $\boldsymbol{\beta}_1$ and $\boldsymbol{\beta}_{3i}$ due to sensor failures. Therefore, another updater diagnosis (UD2) is also implemented after Problem 3.2 to ensure that the estimation of $\boldsymbol{\beta}_1$ and $\boldsymbol{\beta}_{3i}$ is well-conditioned. If ill-conditioning occurs in updating $\boldsymbol{\beta}_1$ and $\boldsymbol{\beta}_{3i}$, a further recovery strategy is required. Initially, some of the parameters in $\boldsymbol{\beta}_1$ are

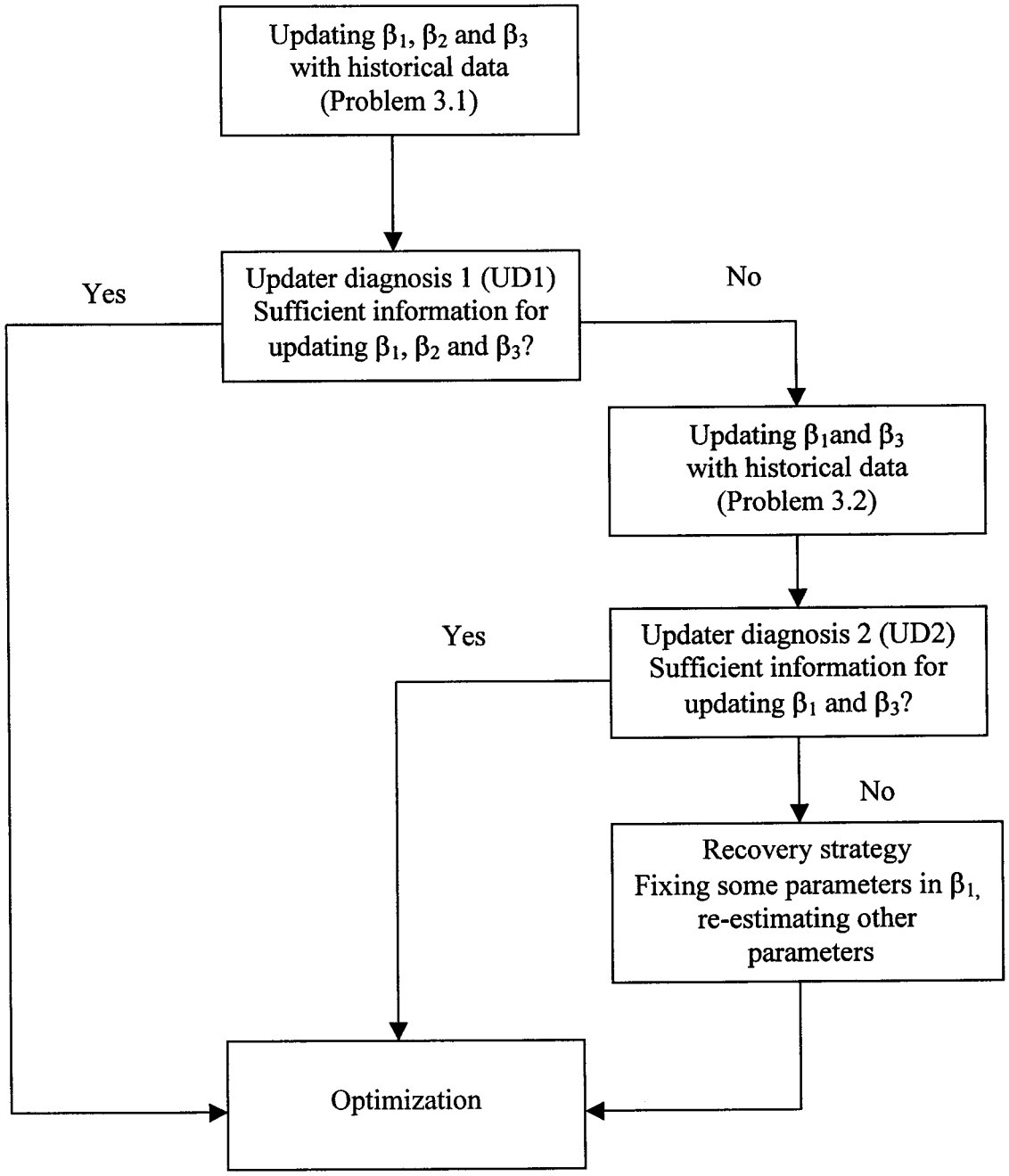

Figure 3.2 Parameter estimation strategy for model updating using multiple data sets

eliminated from the estimation. The reason for fixing some parameters in $\boldsymbol{\beta}_1$ instead of $\boldsymbol{\beta}_{3i}$ is that the parameters that change slowly with time (i.e., require many RTO executions to change significantly) are grouped in $\boldsymbol{\beta}_1$, and it is more reasonable to assume $\boldsymbol{\beta}_1$ to be equal to its last estimate.

The above strategy of deciding which parameters to be fixed at the previous values when poorly-conditioned parameter estimation is encountered is developed based on the assumptions on the dynamics of the parameter change in Table 3.1. Miletic and Marlin (1998a) developed online results diagnosis to determine which parameter contributes the most to the ill-conditioning of the parameter estimation problem via singular value decomposition of the covariance matrix of the parameters. The parameter that contributes the most to the ill-conditioning is eliminated for model updating.

Tuning of the upper control limits in the updater diagnoses (UD1 and UD2) for Problems 3.1 and 3.2 is required to achieve good closed-loop RTO performance. Ill-conditioning in parameter estimation problems can be determined from the scaled covariance matrix of the parameters, $\mathbf{Q}_\beta'$, which will have a large condition number and/or large determinant. In this thesis, both the condition number and the determinant of $\mathbf{Q}_\beta'$ are monitored to ensure the parameters are estimated with good quality. In the updater diagnoses (UD1 and UD2), parameter estimations in Problems 3.1 and 3.2 are considered to be well-conditioned if the condition number and determinant of $\mathbf{Q}_\beta'$ are both below their upper control limits, denoted by $UCL_{UD,1}$ and $UCL_{UD,2}$ respectively, as shown in (3.5) and (3.6), and the parameters are updated by the calculated values if both (3.5) and (3.6) are satisfied.

$$\text{cond}(\mathbf{Q}_\beta') < UCL_{UD,1} \tag{3.5}$$

$$|\mathbf{Q}_\beta'| < UCL_{UD,2} \tag{3.6}$$

Plant experience is required to define the upper control limits ($UCL_{UD,1}$ and $UCL_{UD,2}$) for the updater diagnoses to clearly distinguish between variability due to noise and significantly different data in the data sets. In industrial practice, control limits can be defined from the past good operation data [Kourti et al., 1996]. In this study, simulation data was used for tuning.

In summary, multiple data sets for model updating in RTO systems involves using the current and recent past data sets to accurately estimate the parameters. Before the parameters are used for profit optimization, the estimation calculation is diagnosed. If an estimation problem is determined to be ill-conditioned, a recovery strategy is implemented which reduces the number of parameters being estimated. Therefore, the RTO system should be able to continue closed-loop operation, albeit at reduced capacity, when some data is not available.

3.3 Williams-Otto Reactor Case Study

The proposed model updating approach is applied to a simulated chemical reactor developed by Williams and Otto (1960). In this case study, the simplified process of the continuous-stirred tank reactor (CSTR) [Forbes et al., 1994] is considered. The RTO systems shown in Figures 2.3 and 3.2 are applied to the simulated Williams-Otto reactor system to compare the RTO performance of a single data set and multiple data sets for model updating. They are compared based on two performance measures; profit attained and variability of the predicted optimum.

The simplified configuration of the Williams-Otto reactor is shown in Figure 3.3. Two feed streams containing pure components A and B enter the reactor with mass flow rate F_a and F_b, respectively. Three irreversible elementary reactions take place in the reactor to produce products C, P, E, and G. The elementary reactions are shown in (3.7).

$$
\begin{aligned}
A + B &\rightarrow C & k_1 &= A_1 e^{-\frac{B_1}{T_r}} \\
C + B &\rightarrow P + E & k_2 &= A_2 e^{-\frac{B_2}{T_r}} \\
P + C &\rightarrow G & k_3 &= A_3 e^{-\frac{B_3}{T_r}}
\end{aligned}
\tag{3.7}
$$

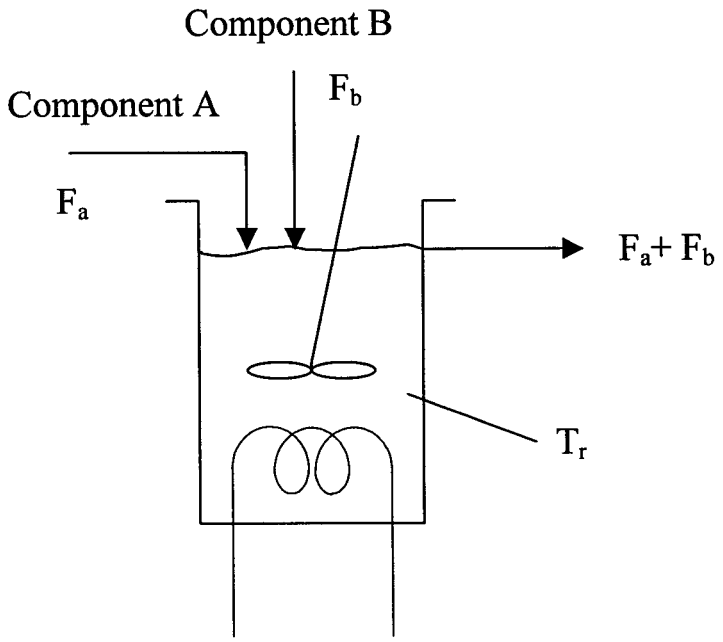

Figure 3.3 Schematic of the Williams-Otto reactor

Components P and E are desirable products. The by-products, C and G, have no sale values and are waste. The profit is given by (3.8),

$$P(\mathbf{x}, \mathbf{u}) = 70000.3(F_a + F_b)X_p + 1586.9(F_a + F_b)X_e - 4667.0F_a - 7000.2F_b \tag{3.8}$$

where X_i is the mass fraction of component, i. The steady-state model of the reactor system consists of the steady-state material balances of the components. In this case study, inequality constraints are not considered. The constraints are therefore given by (3.9).

$$
\begin{aligned}
&F_a - (F_a + F_b)X_a - V_r X_a X_b A_1 e^{-B_1/T_r} = 0 \\
&F_b - (F_a + F_b)X_b - V_r (X_a X_b A_1 e^{-B_1/T_r} + X_b X_c A_2 e^{-B_2/T_r}) = 0 \\
&-(F_a + F_b)X_c - V_r (2X_a X_b A_1 e^{-B_1/T_r} - 2X_b X_c A_2 e^{-B_2/T_r} \\
&\qquad + X_c X_p A_3 e^{-B_3/T_r}) = 0 \qquad (3.9) \\
&-(F_a + F_b)X_e + 2V_r X_b X_c A_2 e^{-B_2/T_r} = 0 \\
&-(F_a + F_b)X_p - V_r (X_b X_c A_2 e^{-B_2/T_r} - 0.5 X_p X_c A_3 e^{-B_3/T_r}) = 0 \\
&-(F_a + F_b)X_g + 1.5 V_r X_p X_c A_3 e^{-B_3/T_r} = 0
\end{aligned}
$$

In this case study, it is assumed that there is no structural mismatch between the model in the optimizer and the true plant model in (3.9). The mismatch considered in this case study is the parametric mismatch caused by the disturbances. While this is never true in practice, it enables us to concentrate on the performance of various parameter estimation formulations.

The flow rate of B (F_b) and the reactor temperature (T_r) are the independent optimization variables, i.e. $\mathbf{x}_I = [F_b \; T_r]^T$. In the simulated case studies, the inlet flow rate of component A (F_a) and the reactor volume (V_r) are not manipulated, and their noise-free nominal values are equal to 0.145×10^5 lb/h and 0.0464×10^5 lb respectively. All the component compositions in the reactor effluent are the dependent variables. The reactor temperature can be attained by adjusting the flow rates of the heating and cooling mediums with negligible cost.

The RTO system uses values supplied by plant sensors to estimate the parameters in the model. The measurements are the flow rates F_a and F_b, reactor volume, reactor temperature, and all effluent compositions. The measurements have zero mean white noise added to the true plant values, and the measurement noise on each of the individual process variable is uncorrelated. The standard deviations for the measurement noise are

3.3 R for temperature, 1.0 % for flow rates, 2.0 % for reactor volume and 3.0 % for compositions. In this case study, it is assumed that gross errors in the measurements do not occur or have been identified and eliminated through redundant measurements [e.g., Narasimhan and Jordache, 2000; Tong and Crowe, 1995].

The parameters to be updated are the frequency factors, A_1, A_2 and A_3, for the reactions and the activation energy for the second reaction, B_2. The parameter vector is partitioned as follows:

$$\boldsymbol{\beta}_1 = \begin{bmatrix} A_1 \\ A_2 \end{bmatrix} \qquad \boldsymbol{\beta}_2 = B_2 \qquad \boldsymbol{\beta}_3 = A_3 \tag{3.10}$$

Recall that the frequency factors, $\boldsymbol{\beta}_1$, and $\boldsymbol{\beta}_3$, can be estimated under normal operating conditions using a single data set. Updating $\boldsymbol{\beta}_1$, $\boldsymbol{\beta}_2$ and $\boldsymbol{\beta}_3$ requires multiple data sets with variation in temperature in the data sets. Also, $\boldsymbol{\beta}_1$ and $\boldsymbol{\beta}_2$ change slowly but $\boldsymbol{\beta}_3$ changes rapidly.

An updating window size of five data sets was chosen by considering the size and frequency of the disturbances in the case studies. This window size achieved an appropriate tradeoff between fast tracking and filtering to reduce variability.

The RTO performance is evaluated based on total profit attained and variability. Total profit attained is expressed in percentage of maximum profit available; the maximum profit is calculated by using a perfect plant model with error-free sensors and exact measures of disturbances (not actually measured in the plant). This maximum profit is not realistically achievable, but it is a useful basis for comparison, especially since the maximum profit is different for each scenario. Variability is measured by the norm of the plant movement between successive RTO executions as stated in (3.11).

$$\text{Variability} = \sum_{N=1}^{M} \left\| \mathbf{S}\mathbf{x}_{\mathbf{m}}^{*}(N) - \mathbf{S}\mathbf{x}_{\mathbf{m}}^{*}(N-1) \right\|_2 \tag{3.11}$$

Here, N is the RTO execution, M is the total number of RTO executions, and $\mathbf{x}_{\mathbf{m}}^{*}$ is the RTO model optimum. Since the independent variables have different units, the variables are scaled by the scaling matrix, **S**. The scaling matrix is a diagonal matrix with the scaling factors in the diagonal elements. The scaling factors are taken to be the reciprocals of the sensor ranges, which are 0.7×10^5 lb/h for F_b and 200 R for T_r.

3.4 Case Study Results and RTO Performance Evaluation

3.4.1 Design of Case Studies

The performances of closed-loop RTO systems with different updating approaches depend critically on the information in the data, and the strongest factors affecting information are the disturbances. Therefore, the cases involve different disturbance variables and time-varying behavior. The disturbance scenarios are described in Table 3.2 and Figure 3.4. The first three cases are disturbances in frequency factors, A_i, including slow disturbance in β_1 and fast disturbance in β_3. These frequency factor parameters can be updated by either a single data set or multiple data sets. The last three cases are the disturbances in the activation energy of the second reaction, B_2. Only model updating using multiple data sets is able to estimate all the frequency factors and this activation energy parameter.

3.4.1.1 Disturbances in Frequency Factors

In Scenarios 1 to 3, changes occur in the frequency factors. In addition, the RTO model has mismatch in the activation energy B_2. The true, initial plant parameter values

Table 3.2 Descriptions of the disturbances scenarios

Disturbance Scenario	Parameter	Description	Number of RTO executions simulated
1	A_1	Decay to 50% of nominal value over 1000 RTO execution	1000
2	A_2	Decay to 80% of nominal value over 1000 RTO execution	1000
3	A_3	Periodic step disturbance varying between +25 % and –50 % of the nominal value	1000
4	B_2	Ramp disturbance from 12000 to 15250 at a rate of 250 per RTO execution	1000
5	B_2	Ramp disturbance from 12000 to 15250 at a rate of 10 per RTO execution	2000
6	B_2	Ramp disturbance from 12000 to 15250 at a rate of 10 per RTO execution with plant experimentation at 500th RTO execution	2000

and optimum operating conditions for the plant before the disturbance changes are given in (3.12). These values and the optimum are not available to the RTO system.

$$\boldsymbol{\beta}_p = \begin{bmatrix} A_1 \\ A_2 \\ B_2 \\ A_3 \end{bmatrix} = \begin{bmatrix} 5.9755\times10^{9} \\ 2.5962\times10^{12} \\ 15250 \\ 9.6283\times10^{15} \end{bmatrix} \qquad \mathbf{x}_p^* = \begin{bmatrix} F_b \\ T_r \end{bmatrix} = \begin{bmatrix} 0.3472 \\ 0.6444 \end{bmatrix} \tag{3.12}$$

The A_i's are in $[(\text{weight fraction})(\text{hour})]^{-1}$; B_2 is in R, F_b is in 10^5 lb/h and T_r is in 10^3 R.

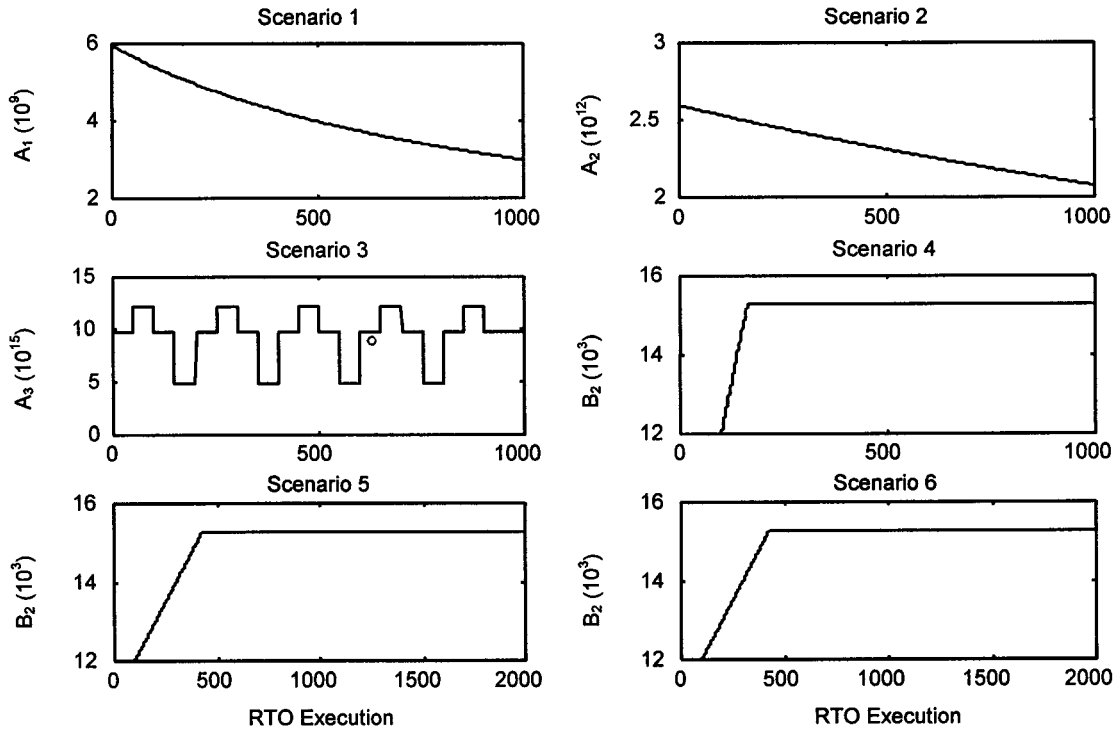

Figure 3.4 Disturbance scenarios in Williams-Otto case study (A_i's are in [(weight fraction)(hour)]$^{-1}$, B_2 is in R)

Since the RTO system uses the erroneous values of A_2 and B_2, the scenarios begin away from the true plant optimum. The starting point for the RTO model is given in (3.13). This represents a stationary point for the *closed-loop* RTO using a single data set for updating with an error in the value of B_2.

$$\boldsymbol{\beta}_m = \begin{bmatrix} A_1 \\ A_2 \\ B_2 \\ A_3 \end{bmatrix} = \begin{bmatrix} 5.9755\times10^{9} \\ 1.4416\times10^{10} \\ 12000 \\ 9.6283\times10^{15} \end{bmatrix} \qquad \mathbf{x}_m^* = \begin{bmatrix} F_b \\ T_r \end{bmatrix} = \begin{bmatrix} 0.2790 \\ 0.6257 \end{bmatrix} \tag{3.13}$$

For Scenarios 1 and 2, the decay of the frequency factors, A_1 and A_2, are simulated by assuming the decay follows a second order kinetics described in Fogler

(1992). The decay equation is given in (3.14) where $A_{0,i}$ is the original value of the frequency factor, λ_i is the decay rate constant and N is the RTO execution (time).

$$\frac{d}{dN}\left(\frac{A_i}{A_{0,i}}\right) = -\lambda_i\left(\frac{A_i}{A_{0,i}}\right)^2 \qquad \text{for } i = 1, 2 \qquad (3.14)$$

$$A_i(N) = \frac{A_{0,i}}{1+\lambda_i N}$$

3.4.1.2 Disturbances in Activation Energy

For Scenarios 4 to 6 with disturbances in activation energy, it is assumed that the initial parameter values are perfectly known. Therefore, the plant is started at the true plant optimum. Changes occur in the activation energy, B_2, and the updater estimates all frequency factors and one activation energy. The initial parameter values and the starting point for the closed-loop RTO system are shown in (3.15).

$$\boldsymbol{\beta} = \begin{bmatrix} A_1 \\ A_2 \\ B_2 \\ A_3 \end{bmatrix} = \begin{bmatrix} 5.9755\times10^{9} \\ 2.5962\times10^{12} \\ 12000 \\ 9.6283\times10^{15} \end{bmatrix} \qquad \mathbf{x} = \begin{bmatrix} F_b \\ T_r \end{bmatrix} = \begin{bmatrix} 0.3895 \\ 0.7487 \end{bmatrix} \qquad (3.15)$$

The RTO model has no mismatch at the initial point, given in (3.15), but it deviates from the true plant thereafter because of the disturbance scenarios.

In addition to disturbances in Scenario 6, design of experiments is introduced to generate better information for updating B_2 and improve the RTO performance. The experiments are designed to minimize the size of the covariance matrix of the estimated parameters, and a single experiment is designed at 500^{th} RTO execution. The design of experiments does not consider the cost of performing the plant experiments; however, the

case study results will evaluate the total profit, including the time when experiments have been performed.

The experimental design problem to minimize the size of the covariance matrix of the estimated parameters is formulated in (3.16).

$$\begin{aligned} &\underset{\mathbf{x}}{\text{minimize}} && |\mathbf{Q}_\beta| \\ &\text{subject to} && \mathbf{f}(\mathbf{x}, \boldsymbol{\beta}) = \mathbf{0} \\ & && \mathbf{x}_{I,l} \le \mathbf{x}_I \le \mathbf{x}_{I,u} \end{aligned} \tag{3.16}$$

where $\mathbf{x}_{I,l}$ and $\mathbf{x}_{I,u}$ are the lower and upper limits for the independent variables which define the experimental window in which the experiments are performed. The bounds of the independent variables in this case study is given in (3.17).

$$\begin{bmatrix} 0.20 \\ 0.60 \end{bmatrix} \le \begin{bmatrix} F_b \\ T_r \end{bmatrix} \le \begin{bmatrix} 0.40 \\ 0.65 \end{bmatrix} \tag{3.17}$$

These bounds are set somewhat arbitrarily. A thorough analysis of the cost of this experiment and the future benefit of an improved model is required which will be discussed in the next chapter.

Keeler and Reilly (1992) developed the expression for $\mathbf{Q}_\beta$, which is given in (3.18).

$$\mathbf{Q}_\beta = \left\{ \left(\frac{\mathbf{df}}{\mathbf{d\beta}}\right)^T \left[\left(\frac{\mathbf{df}}{\mathbf{dz}}\right) \mathbf{V} \left(\frac{\mathbf{df}}{\mathbf{dz}}\right)^T \right]^{-1} \left(\frac{\mathbf{df}}{\mathbf{d\beta}}\right) \right\}^{-1} \tag{3.18}$$

The derivatives are evaluated at the current values of the measurements and parameter estimates when the experiment is designed.

Parameters are scaled to improve the conditioning of the parameter estimation. In this case study, the frequency factor are scaled by reparametrization of the rate expression as shown in (3.19).

$$k = A'e^{-B\left(\frac{1}{T_r}-\frac{1}{T_{ref}}\right)} \tag{3.19}$$

The reference temperature, T_{ref}, is chosen so that the scaled frequency factor, A', and the activation, B, have similar order of magnitude. The unscaled frequency factor is given by (3.20).

$$A = A'e^{\frac{B}{T_{ref}}} \tag{3.20}$$

3.4.2 Tuning the Updater Diagnostics

The performance of the closed-loop RTO system will depend on the tuning of the diagnostic checks. Recall that the tuning parameters are the upper control limits on the statistical tests. Well-conditioned estimates yield parameter covariance matrices with "small" determinants and condition numbers. Upper control limits are tuned to distinguish acceptable from unacceptable parameter updates. Tuning should be performed using plant data; in this study, data was generated using the model with measurement noise and scenarios yielding acceptable updates and unacceptable updates. Since the values of the condition number and determinant of $\mathbf{Q}_\beta'$ do not follow standard distributions (such as normal and student-t distributions), the distributions were obtained empirically from the simulation results. The control limits were determined by selecting the value to give the desired confidence level for the tests.

3.4.2.1 Tuning of Updater Diagnosis (UD1) for Updating β_1, β_2 and β_3

Simulated data was used to define the normal or common cause variation in the updater diagnostic variables, the determinant and condition number of the parameter covariance matrix. Upper control limits were defined from the simulated training set, and the values above those encountered in the training set are considered to be unacceptable. This is the typical manner for determining the control limits in statistical process control.

In this study, the effects of different control limit values on RTO performance will be evaluated. Therefore, two sets of tuning values are evaluated, one for common cause data containing large disturbances and the other for data containing smaller disturbances. The measurement noise is the same for both. Data was generated with the plant beginning at the optimum operation but subject to disturbances; since the RTO system was not in operation, the plant varied about its initial condition. The disturbances have the form of Scenario 3, periodic step disturbance in A_3, with large (+100 % to –75 % of the nominal) and small (nominal value to –75 %) magnitudes. These disturbances generated data sets with sufficient information to update the parameters in updating Problem 3.1 over a wide range of operating region. The control limits for UD1 are reported in Table 3.3.

The smaller disturbances provided the loose tuning, with larger control limits; the larger disturbances provided the tight tuning, with smaller control limits. It is interesting to note that the control limits for the condition number have relatively small values, far from typical values used to define "ill-conditioning". Thus, experience shows that poor parameter estimates (and poor RTO performance) result from updating that is observable, yet propagates noise.

Table 3.3 Tuning values for the updater diagnosis UD1 in Williams-Otto reactor case study

Tuning	UCLs	
	$UCL_{UD1,1}$	$UCL_{UD1,2}$
	$cond(\mathbf{Q}_\beta')$	$\lvert\mathbf{Q}_\beta'\rvert$
1. Loosely tuned	10669	1.69×10^{-16}
2. Tightly tuned	1366	6.09×10^{-18}

3.4.2.2 Tuning of Updater Diagnosis (UD2) for Updating β_1 and β_3

The updater diagnosis (UD2) for Problem 3.2 is used whenever only the frequency factors (β_1 and β_3) are estimated. This updater problem is solved when 1) the single data set updater is used, and 2) the first diagnostic (UD1) in the multiple data sets approach determines that the data is not sufficient for estimating all the parameters. The disturbance scenarios used for evaluating the control limits were 1) no disturbance, 2) decay in A_1 to 75% of its nominal value, 3) decay in A_2 to 75% of its nominal value, 4) 50% increase in A_3, and 5) 25% decrease in A_3.

The tuning values are reported in Tables 3.4 and 3.5 for operation around two different nominal operating points. Since the plant is nonlinear, the tuning values depend on the operating region, and they should be changed when the plant changes its operating point. In the case studies for the disturbance Scenarios 1 to 3, the plant is started at $\mathbf{x}_I = [0.2790\ 0.6257]^T$, and the tuning values in Table 3.4 are used. For the disturbance Scenarios 4 to 6 in which the plant is started at $\mathbf{x}_I = [0.3895\ 0.7487]^T$, the tuning values in Table 3.5 are used.

Table 3.4 Tuning values for the updater diagnosis UD2 in Williams-Otto reactor around the nominal operating point $\mathbf{x}_I = [0.3789\ 0.6531]^T$

Number of Data Sets	UCLs	
	$UCL_{UD2,1}$	$UCL_{UD1,2}$
	$cond(\mathbf{Q}_\beta')$	$\lvert\mathbf{Q}_\beta'\rvert$
1	2059	2.83×10^{-13}
5	266	9.25×10^{-15}

Table 3.5 Tuning values for the updater diagnosis UD2 in Williams-Otto reactor around the nominal operating point $\mathbf{x}_I = [0.3895\ 0.7487]^T$

Number of Data Sets	UCLs	
	$UCL_{UD1,1}$	$UCL_{UD1,2}$
	$cond(\mathbf{Q}_\beta')$	$\lvert\mathbf{Q}_\beta'\rvert$
1	1.24×10^{7}	8.23×10^{-9}
5	5.16×10^{6}	1.10×10^{-9}

3.4.3 Case Study Results

The case studies involve many scenarios, each with many executions. Therefore, the plot of a typical scenario will be presented first; then, tabulations summarizing many cases will be reported. The tracking performance of the closed-loop RTO with a single data set and multiple data sets for updating is shown in Figure 3.5 for the disturbance Scenario 4 (involving a fast ramp disturbance in the activation energy B_2 from 12000 to 15250 R).

A single data set contains insufficient information to update all frequency factors and the activation energy. Therefore, Figure 3.5a shows a significant offset between the true plant optimum and the model prediction after the disturbance change. The conventional, single data set approach involves updating the frequency factors but leaving B_2 at its initial value of 12000 R.

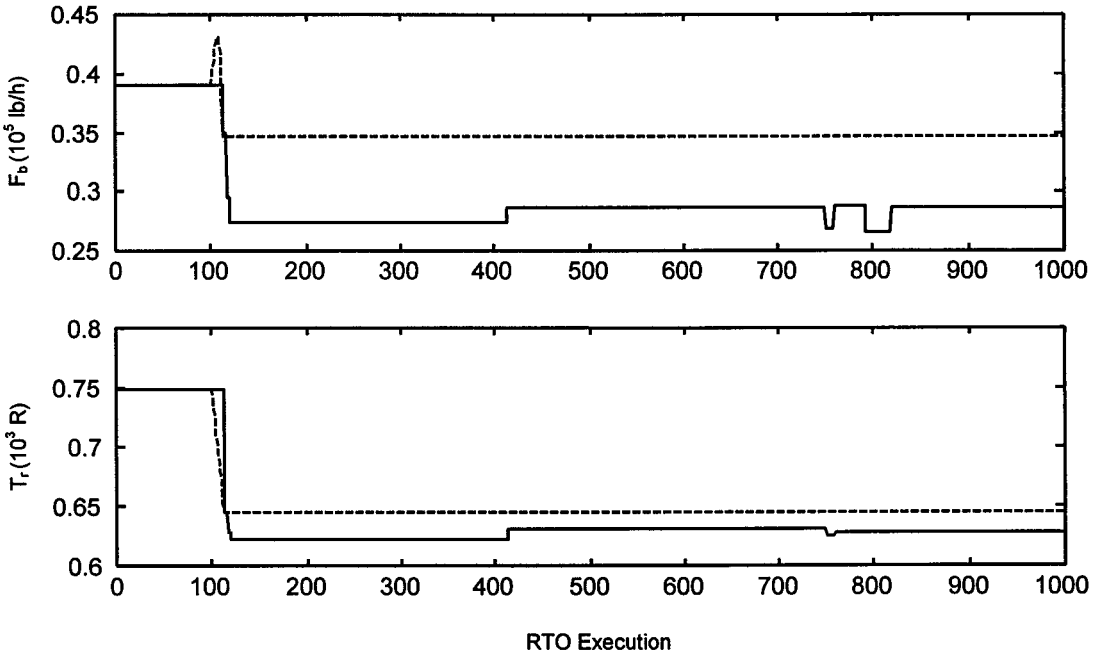

(a)

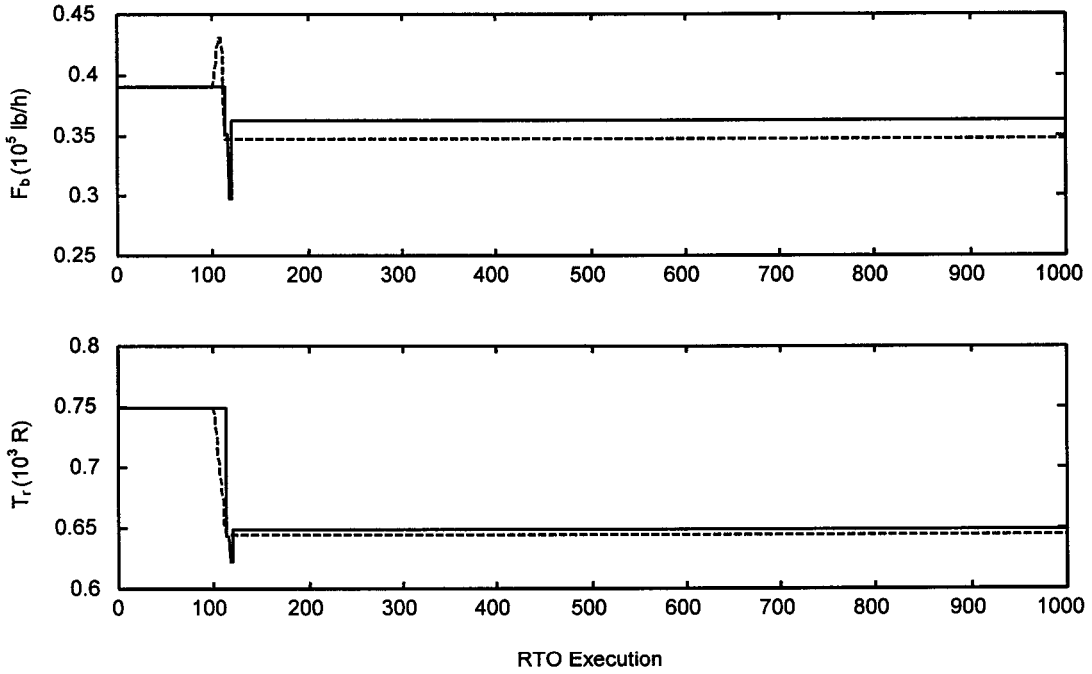

(b)

Figure 3.5 Tracking of the optimum by the RTO system for Scenario 4: (a) single data set (b) five data sets using Tuning 2 in the updater diagnosis, UD1 (Dotted line: True plant optimum; Solid line: Closed-loop RTO prediction)

When little variation exists, the multiple data sets approach is not possible to update all the parameters, but the diagnostic recognizes the limitation and reverts updating to the frequency factors. When variation exists (i.e., when the disturbance occurs), the historical data sets contain sufficient information to enable reliable estimation of both frequency factors and the activation energy. Therefore, the diagnostic tests allow all parameters to be updated. Note that the disturbance itself generates plant movement to obtain data sets at different temperature for updating B_2. Offset is reduced using multiple data sets for updating all parameters, as shown in Figure 3.5b.

The economic performance of the RTO system is reported for several disturbance scenarios in Table 3.6. The profit integrated over the entire time of the scenario is reported as the percent of the maximum profit. Finally, the variability of the closed-loop system is reported as the sum of the norms of the changes implemented by each closed-loop system; see (3.11). Tuning 1 in Table 3.3 (based on smaller disturbances) was selected for the updater diagnosis, UD1.

In all scenarios, the use of multiple data sets for model updating increases the operating profit significantly over the profit achieved using a single data because the offset is reduced. However, these improvements are achieved at the cost of a slightly higher variability. This increase in variability is caused by updating more parameters using multiple data sets. In these results, the increase in profit resulting from the reduced offset is more important than the small decrease in profit due to variability. Some increase in variability improves the information content of the data and improves the ability of tracking changes in the activation energy. However, increased changes in plant operation might involve losses in profit during dynamic transients, which is not evaluated here.

The RTO performance depends on the tuning of the updater diagnostic control limits. The results for the closed-loop RTO using both more and less restrictive control limits (see Table 3.3) are reported in Table 3.7. Recall that Tuning 2 is more restrictive,

Table 3.6 RTO performance for different disturbance scenarios using Tuning 1 in updater diagnosis UD1

Disturbance Scenario	Total profit attained (% max. profit)		Variability $= \sum_{N=1}^{M} \left\| \mathbf{Sx}_m^*(N) - \mathbf{Sx}_m^*(N-1) \right\|_2$	
	1 Data Set	5 Data Sets	1 Data Set	5 Data Sets
1	72.32	92.92	0.2847	2.1771
2	71.47	84.69	0.2813	5.2299
3	82.21	96.10	2.0303	4.5679
4	91.77	95.18	0.8518	2.1323
5	92.48	97.97	1.1853	3.4182
6	91.93	97.17	1.1882	4.5051

i.e., has lower control limits, than Tuning 1 and that multiple data sets are used for all results in this table. One result is very clear. The less restrictive tuning set provides much better tracking for the gradual disturbances in Scenarios 1 and 2; the performance for Scenario 5, with a slower ramp, is also somewhat better, which are shown in Figures 3.6 and 3.7. As expected, this better tracking is achieved at the cost of slightly higher input variability.

Table 3.7 RTO performance using five data sets for updating for different tuning values in updater diagnosis UD1

Disturbance Scenarios	Total profit attained (% max. profit)		Is B_2 Updated?		Variability $= \sum_{N=1}^{M} \left\| \mathbf{Sx}_m^*(N) - \mathbf{Sx}_m^*(N-1) \right\|_2$	
	Tuning 1	Tuning 2	Tuning 1	Tuning 2	Tuning 1	Tuning 2
1	92.92	72.87	Yes	No	2.1771	0.2693
2	84.69	69.73	Yes	No	5.2299	0.3662
3	96.10	96.57	Yes	No	4.5679	2.0876
4	95.18	98.52	Yes	Yes	2.1322	0.8160
5	97.97	93.22	Yes	No	3.4182	1.3810
6	97.17	98.24	Yes	Yes	4.5051	1.5079

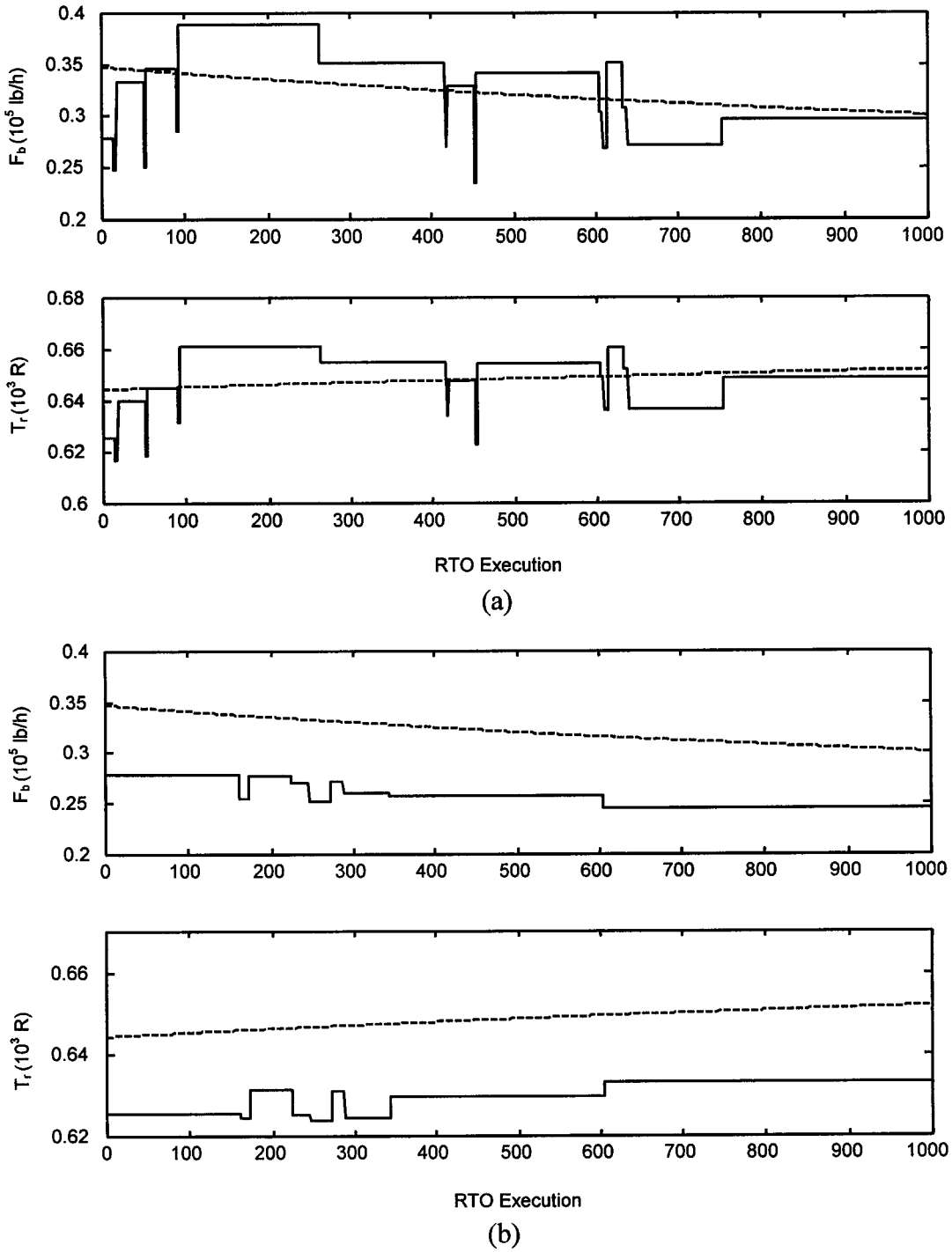

Figure 3.6 Tracking of the optimum by the RTO system with multiple data sets for model updating for Scenario 1 using different tuning values in UD1: (a) Tuning 1 (b) Tuning 2 (Dotted line: True plant optimum; Solid line: Closed-loop RTO prediction)

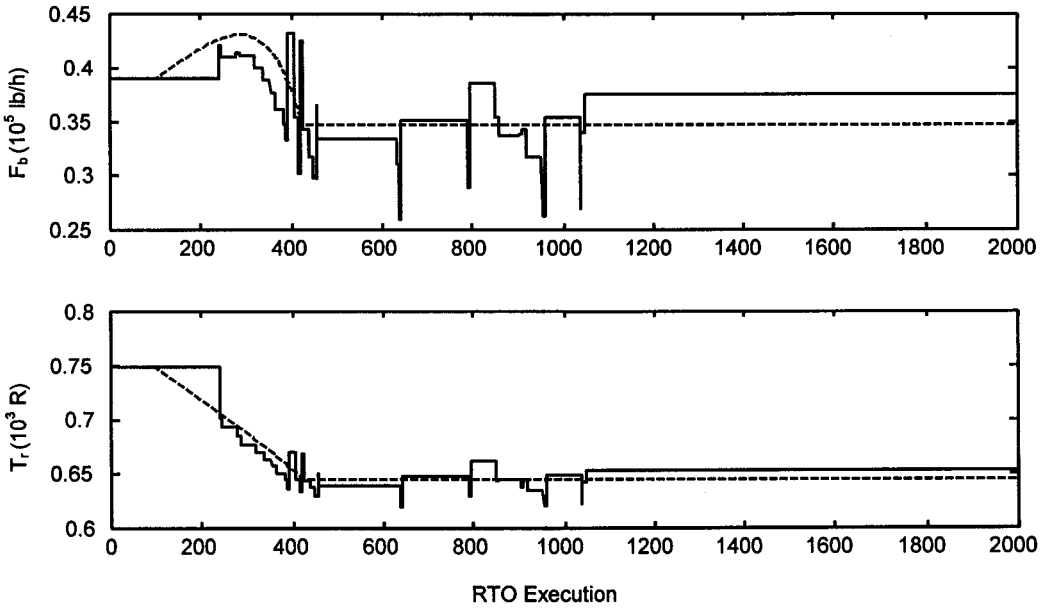

(a)

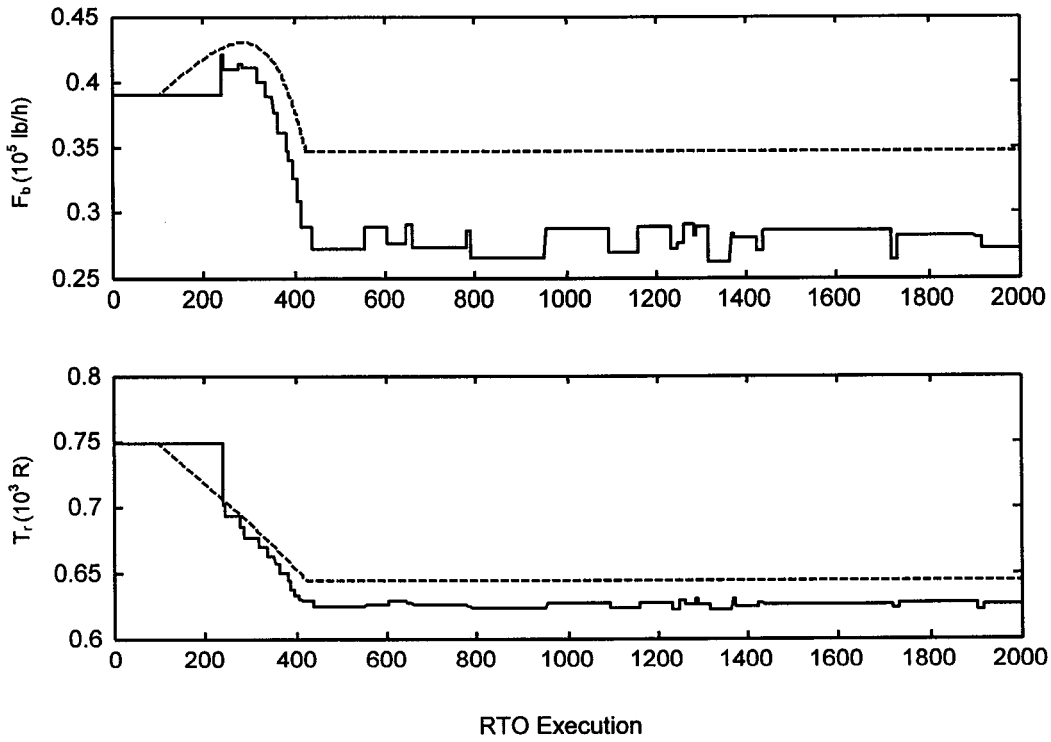

(b)

Figure 3.7 Tracking of the optimum by the RTO system with multiple data sets for model updating for Scenario 5 using different tuning values in UD1: (a) Tuning 1 (b) Tuning 2 (Dotted line: True plant optimum; Solid line: Closed-loop RTO prediction)

For all other scenarios, the difference between the two diagnostic tunings is small. However, the performance of the less restrictive diagnostic gives about the same average profit as the more restrictive for Scenarios 3, 4, and 6. Also, the more restrictive diagnostic scenario seems to perform somewhat better for the scenario with large disturbances. This is expected because of the good information content generated by large plant movement, and a more restrictive updater diagnosis can further reduce the variability to improve the operating profit.

When the information in the data sets is insufficient to update B_2, plant experiments can be implemented to generate better information for model updating. This will be demonstrated by one example. For a slow ramp disturbance in Scenario 5 with a tightly tuned updater diagnosis, updating B_2 is not possible because the information is not sufficient to pass the diagnostic tests. To improve the performance, a single experiment is implemented at 500^{th} RTO execution for disturbance 5. The experiments are documented in Table 3.8.

Table 3.8 Plant experiment designed by minimizing the size of the covariance matrix of the parameters

Independent Variables	1 Date Set	5 Data Sets	
		Tuning 1	Tuning 2
F_b	0.2485	0.2000	0.2485
T_r	0.6500	0.6500	0.6500

The RTO performance is shown as Scenario 6 in Tables 3.6 and 3.7. A single data set for model updating with experimental design does not show any improvement in profit because the additional parameter B_2 cannot be updated using a single data set. When using multiple data sets for model updating, plant experimentation can improve the information content for updating B_2. As a result of the more accurate model, the profit attained from the closed-loop RTO increased from 93.22 % (without experimentation) to

98.24% (with experimentation) for a tightly tuned updater diagnosis. When the updater diagnosis is loosely tuned using the tuning values in Tuning 1, there is an insignificant improvement in RTO performance through experimental design. This result is expected because the less restrictive tuning allows variability from sensor noise and higher frequency disturbances to pass to the setpoints. This variability generates better information for updating without experimentation.

In summary, operating profit can be improved by using multiple data sets for model updating to correct the modelling errors in the parameters. The improvement is especially important when variation occurs and updating must be applied for parameters that cannot be estimated using a single data set. The RTO performance depends on the tuning of the control limits used in the updater diagnosis. Diagnostic tests with large UCLs can pass the variability to the setpoints; large variability is generally undesirable but can improve the information content of the data sets for updating the additional parameters. Variability can be reduced by a tightly tuned updater diagnosis. In this situation, large disturbances or well-designed experiments are required to generate better information for model updating. In tuning the diagnostic test, the designer has to consider the disturbance characteristics to define the values of the control limits properly.

3.5 Conclusions

The ability of a closed-loop RTO system to track the changing optimum depends on the accuracy of the model structure and its estimated parameters. This chapter presents a method for parameter updating using multiple data sets. This approach has two advantages; filtering and parameter observability. The filtering effect reduces the variance caused by high frequency stationary disturbances in estimated parameters due to the multiple data sets. Observability is improved because some parameters cannot be updated using a single data set but can be estimated using multiple data from different operating conditions. Naturally, the greatest advantage for using multiple data sets occurs

when the parameters actually changing in the plant require multiple data sets for accurate estimation. Sufficient information for increased observability can be provided in data with variability from either disturbances or designed experiments.

A method for using multiple data sets in model updating has been presented for improving the RTO performance. The approach includes diagnostic tests to check for sufficient information for updating additional parameters; this is essential because the number of parameters will change based on the data available. The approach also uses prior knowledge of the disturbance frequencies to track the fast and slow disturbances. This approach prevents rapid changing of parameters that cannot change quickly based on physical understanding of the process. Also, the approach provides a basis for simplifying the parameter estimation calculations, i.e., reduced the number of parameters estimated, when limited information is present in the data.

The strategy of multiple data sets for updating increases the computation effort compared to using a single data set for updating. The increase in computation requirement results from solving a larger nonlinear program when compared with the single data set and a reduced dimension estimation problem if the original estimation is deemed unreliable from the diagnostic tests before proceeding to the economic optimization. Computation time can be reduced by exploiting the structure of the Jacobian matrix in parameter estimation problem. The overall sparsity and almost block diagonal structure in the Jacobian matrix can help reduce the memory requirement and computation time in solving parameter estimation problem using the reduced SQP [Cervantes and Biegler, 1998; Cervantes and Biegler, 2000].

In choosing the number of data sets for updating, the designer has to consider the tradeoff between tracking and variability. More data sets for model updating can reduce the variability, but this can slow down the tracking of the changing optimum.

The RTO performance also depends on the tuning of the updater diagnostics. The control limits used in the hypothesis tests can be defined from the past plant experience. Improved profit tracking requires good tuning that allows the estimation of only those parameters that can be reliably determined from the data.

The proposed method has been applied to the Williams-Otto reactor case study. Diagnostic tests, which defined good estimation performance, were tuned from the simulation data. Simulated case studies have shown that multiple data sets for model updating with a well-tuned updater diagnosis can improve the RTO performance. The proposed strategy in model updating using multiple data sets is able to correct the modelling error in frequency factors and activation energy, which cannot be estimated using a single data set. Estimation of all these parameters requires data with variation in temperature.

This variability can exist due to responses of the closed-loop RTO system to disturbances. If such disturbances do not occur, designed experiments are required. Although experimental design techniques are well-developed for laboratory experiments, design procedures for operating plants are needed to complement the results presented in this chapter. The strategies in designing plant experiments for RTO system will be discussed in the next chapter.

4. DESIGNING PLANT EXPERIMENTS FOR REAL-TIME OPERATIONS OPTIMIZATION SYSTEMS

4.1 Introduction

The RTO system with multiple data sets for model updating discussed in Chapter 3 can improve the RTO performance. Sufficient information content in the data sets is required for updating additional parameters to reduce the model mismatch. Sufficient information content in the data sets can be generated by large disturbances. The plant movement determined by the RTO system provides plant variation in the data sets for updating additional parameters. When the plant is not excited by the disturbance and there is little or no plant variation in the data sets, updating the additional parameters accurately is not possible. In this situation, plant perturbation can improve the information content of the data sets for updating which has been illustrated in the case study in Chapter 3.

Plant experiments are expensive to perform, and therefore, minimum perturbations are desired. Classical optimum experimental design approaches [Keeler and Reilly, 1992; Pritchard and Bacon, 1978; Sutton and MacGregor, 1977b] consider the information content of the data sets without considering the cost of performing experiments. In these approaches, the number of experiments and the experimental window in which experiments are performed have to be specified. Usually, the experiments are located close to the boundary of the experimental window, and the plant is perturbed in different directions. This approach is appropriate for laboratory experiments in which the cost of experimentation is negligible. For an industrial plant, the experiments designed by these approaches may be far from the current optimum, and the direction and size of the perturbation may cause a significant loss in profit.

A new criterion for designing plant experiments for model-based RTO system is developed in this chapter. Experiments are designed by maximizing the total expected profit over a future horizon. The objective function for designing plant experiments include the gain in profit after the experiment due to reduced offset and variability and the loss in profit before and during experimentation. Therefore, large plant movement from the current optimum during experimentation and many experiments are penalized by the profit loss term. By solving the experimental design problem, the time to start experimentation, number of experiments and experimental operating conditions are determined by trading off the profit loss before and during experimentation and profit gain after experimentation.

This chapter begins with a discussion of the concepts and formulation of the expected profit approach in designing plant experiments for RTO systems. This new experimental design criterion is then demonstrated in the Williams-Otto reactor case study. Finally, the RTO performances with and without experimentation are compared to investigate if plant experiments designed by this approach can improve the RTO performance.

4.2 Expected Profit Approach in Designing Plant Experiments

Designed experiments in the plant might be costly, and reducing their cost while achieving the benefits of improved models is desirable. The expected profit approach in designing plant experiments finds the best tradeoff between the profit gain due to improved modelling and the profit loss before and during experimentation.

The approach must be tailored to the specific scenario because the strategy of experimentation depends on the characteristics of the disturbances. The scenario considered here is the presence of an unmeasured non-stationary disturbance. Experiments are required to generate data sets with sufficient information to correct for that disturbance to improve the profit tracking. For the common scenario considered in

this chapter, it is assumed that the followings can be estimated: 1) the occurrence of the non-stationary disturbance (e.g., a feed composition change due to a change in feed tank), 2) disturbance dynamics, 3) the time between disturbances (when the next feed change will occur), and 4) the likely profit loss due to the disturbance if experiments are not made. It is also assumed that the active set of inequality constraints remains constant, so that the problem can be analyzed in an unchanging reduced space.

The experiments are designed by maximizing the overall expected profit over the future horizon, N_D, shown in Figure 4.1. An unmeasured disturbance change occurs at execution 0. The RTO system without experimentation will update some parameters and move the plant as shown in the dotted line in Figure 4.1. Recall that although the disturbance is unmeasured, its occurrence can be inferred by, for example, changing feed tanks. It is expected that additional parameters can be estimated by perturbing the plant to improve the information content of the data sets for reducing the model mismatch. Suppose experiments will be performed after N_o RTO execution. The number of experiments to be designed is N_{expt} at the operating points $\mathbf{x}_{expt}$. During experimentation, there will be a loss in profit. After performing experiments, additional parameters are updated, and the profit increases. The goal in experimental design using expected profit approach is to determine N_o, N_{expt} and $\mathbf{x}_{expt}$ by maximizing the overall expected profit.

The experimental design approach will be added to the standard RTO system. The experiments are designed to have sufficient information in the data sets to update the disturbance. Recall that the experiments are designed to maximize the overall expected profit. Therefore, information content in the data sets has to be expressed in term of profit. When there is sufficient information in the data sets, the parameters can be estimated accurately which results in better estimation of the optimum to improve the operating profit.

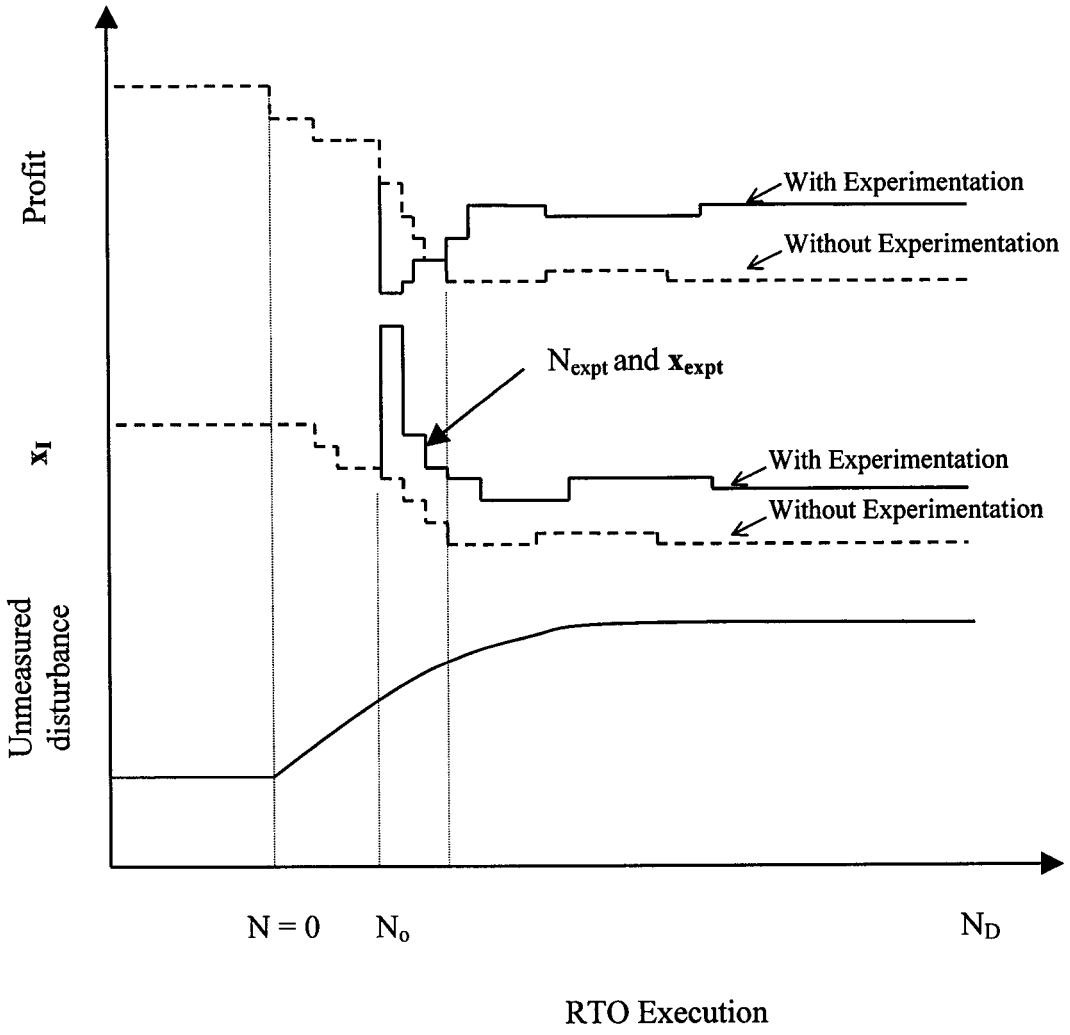

Figure 4.1 Expected profit experimental design approach

The formulation of the expected profit experimental design criterion is given in Problem 4.1, and the derivation is presented in Appendix C.

$$\text{Problem 4.1} \quad \underset{N_o,\, N_{expt},\, \mathbf{x}_{expt}(N)}{\text{maximize}} \quad EP = P_1 + P_2 + P_3 \qquad (4.1)$$

$$\text{subject to} \quad \mathbf{f}(\mathbf{x}_{expt}(N), \boldsymbol{\alpha}, \boldsymbol{\beta}) = \mathbf{0} \quad \text{for } N = N_o+1, \ldots, N_o+N_{expt}$$

P_1, P_2 and P_3 are given by

$$P_1 = \sum_{N=1}^{N_o} R_{\Delta_o}{}^2(N) \frac{\sum_{i=1}^{n} \lambda_i \left(\nabla_r{}^2 P \Big|_{x_{mo}^*} \right)}{n} + \sum_{N=N_o+1}^{N_o+N_{expt}} R_{\Delta_o}{}^2(N) \frac{\sum_{i=1}^{n} \lambda_i \left(\nabla_r{}^2 P \Big|_{x_{mo}^*} \right)}{n} +$$

$$\sum_{N=N_o+N_{expt}+1}^{N_D} R_{\Delta}{}^2(N) \frac{\sum_{i=1}^{n} \lambda_i \left(\nabla_r{}^2 P \Big|_{x_{mo}^*} \right)}{n}$$

$$P_2 = \sum_{N=N_o+1}^{N_o+N_{expt}} (\mathbf{x}_{mo}^* - \mathbf{x}_{expt}(N))^T \nabla_r{}^2 P \Big|_{x_{mo}^*} (\mathbf{x}_{mo}^* - \mathbf{x}_{expt}(N))$$

$$P_3 = \sum_{N=1}^{N_o} \nabla_r{}^2 P \Big|_{x_{mo}^*} \circ \mathbf{Q}_{x_{mo}^*} + \sum_{N=N_o+N_{expt}+1}^{N_D} \nabla_r{}^2 P \Big|_{x_{mo}^*} \circ \mathbf{Q}_{x_m^*(N)}$$

where

N is the RTO execution,

N_D is the future horizon, the estimated disturbance period,

N_o is the time to start experiments after the disturbance change,

N_{expt} is the number of experiments to be performed

$\mathbf{x}_{expt}$ is the experiments to be designed

$\mathbf{f}$ is the plant model with fixed parameters, $\boldsymbol{\alpha}$, and adjustable parameters, $\boldsymbol{\beta}$,

$\mathbf{x}_{mo}^*$ is the current model optimum,

$\nabla_r{}^2 P \Big|_{x_{mo}^*}$ is the reduced Hessian matrix at the current model optimum,

$\lambda(\bullet)$ is the eigenvalue of $\bullet$,

R_{Δ_o} is the Euclidean norm of offset changing with time before experimentation,

R_{Δ} is the Euclidean norm of offset changing with time after experimentation,

$\mathbf{Q}_{x_{mo}^*}$ is the variability of the model optimum before experimentation, and

$\mathbf{Q}_{x_m^*(N)}$ is the variability of the future model optimum after experimentation.

The matrix multiplication operator, $\circ$, is the Hadamard element-by-element product which is defined as follow,

$$\mathbf{X} \circ \mathbf{Y} = \sum_{i=1}^{n} \sum_{j=1}^{m} x_{ij} y_{ij}$$

where x_{ij} and y_{ij} are the ij elements in the n × m matrices **X** and **Y** respectively.

P_1 is the profit change due to the offset caused by the disturbance if the RTO controller were operating and no experiments were performed. While the disturbance occurrence is known, its sign is unknown. The norm of offset (R_{Δ_0} and R_{Δ} before and after experimentation, respectively) is estimated from plant experience without knowing the direction of the current unmeasured disturbance. Therefore, the profit change is estimated by the average eigenvalue of the reduced Hessian matrix of the profit. At the beginning of the disturbance change, the offset may not be too large and the profit loss may not be too high. Experiments are therefore performed after N_o RTO executions to trade off the profit loss before experimentation from N = 1 to N_o and the profit gain after experimentation from $N = N_o + N_{expt} + 1$ to N_D.

P_2 is the profit change caused by experimentation. Many and large plant perturbations are penalized by this term. This profit change is estimated from the information of the current model optimum about the curvature of the model profit contours predicted from the optimizer. Therefore, unlike the estimation of P_1, estimation of the profit loss during experimentation considers the directionality of the plant perturbation because the directionality of the experiments is known. To reduce the cost of experimentation, experimental operating conditions will be designed close to the current optimum or along the direction of low profit sensitivity.

P_3 is the profit change due to variability of the model optimum; this term exists before and after the experimentation. Naturally, experiments are designed to estimate the

additional parameters with a smaller $\mathbf{Q}_{x^*_{m(N)}}$ which is the covariance matrix of the future optimum predicted by using the additional parameters estimated from the experiments. Because of this term, experiments far away from the current operating point increase profit (reduce variability) after the experiments have been performed.

The covariance matrix of the manipulated variables after experimentation, $\mathbf{Q}_{x^*_{m(N)}}$, can be estimated from the linear sensitivity matrix of the optimizer evaluated at the current estimates of $\boldsymbol{\beta}$ and covariance matrix of the parameters, $\mathbf{Q}_{\beta}$, as shown in (4.2).

$$\mathbf{Q}_{x^*_{m(N)}} = \left(\frac{d\mathbf{x}^*_m}{d\boldsymbol{\beta}}\right)^T \mathbf{Q}_{\beta} \left(\frac{d\mathbf{x}^*_m}{d\boldsymbol{\beta}}\right) \tag{4.2}$$

The expression for $\mathbf{Q}_{\beta}$ depends on the formulation of the parameter estimation problem. In this chapter, error-in-variables model is used for model updating. Experimental design for this approach is discussed in Keeler and Reilly (1992) who derived $\mathbf{Q}_{\beta}$ in terms of the historical and experimental data sets, and the covariance matrix of the measurements, **V**, as shown in (4.3),

$$\mathbf{Q}_{\beta} = \left\{ \sum_{i=1}^{N_h} \left(\frac{\partial \mathbf{f}}{\partial \boldsymbol{\beta}}\right)_i^T \left[\left(\frac{\partial \mathbf{f}}{\partial \mathbf{z}}\right)_i \mathbf{V} \left(\frac{\partial \mathbf{f}}{\partial \mathbf{z}}\right)_i^T \right]^{-1} \left(\frac{\partial \mathbf{f}}{\partial \boldsymbol{\beta}}\right)_i + \sum_{i=1}^{N_{expt}} \left(\frac{\partial \mathbf{f}}{\partial \boldsymbol{\beta}}\right)_i^T \left[\left(\frac{\partial \mathbf{f}}{\partial \mathbf{z}}\right)_i \mathbf{V} \left(\frac{\partial \mathbf{f}}{\partial \mathbf{z}}\right)_i^T \right]^{-1} \left(\frac{\partial \mathbf{f}}{\partial \boldsymbol{\beta}}\right)_i \right\}^{-1} \tag{4.3}$$

where N_h is the number of historical data sets. The Jacobian matrices of the model with respect to $\boldsymbol{\beta}$ and measurements, **z**, and the optimizer sensitivity matrix, $\frac{d\mathbf{x}^*_m}{d\boldsymbol{\beta}}$, are evaluated at the current estimates of $\boldsymbol{\beta}$ and model optimum. The first term is a function

of the historical data sets which is not influenced by future experiments. Experimental operating conditions influence the second term in the above expression, and hence the expected profit through $\mathbf{Q}_\beta$.

The strategy of solving the experimental design problem using expected profit approach is summarized in the following.

(1) If no disturbance is observed, execute a normal RTO calculation without experiment and wait until next steady state.
(2) If a disturbance has just occurred, set N = 1 and proceed.
(3) Solve Problem 4.1 using the current model optimum and reduced Hessian matrix. The continuous variables are solved using a SQP and the discrete are enumerated,
(4) If $N < N_o$, update the model and perform a standard RTO calculation, set $N = N + 1$, and go to (3).
(5) If $N = N_o$, perform N_{expt} experiments in the plant starting from next RTO execution, and set $N = N_o + N_{expt} + 1$
(6) Continue solving standard RTO calculation without experimentation until the next disturbance, then go to (1).

4.3 Williams-Otto Reactor Case Study

The Williams-Otto reactor system described in Chapter 3 is used to compare the standard RTO performance with the performance of RTO system with experimental design. In this case study, it is assumed that there is no structural mismatch between the model in the optimizer and the true plant model. The mismatch considered in this chapter is the error in the parameters. The parameters selected for updating are shown in (3.10).

The RTO performance is evaluated based on total profit achieved and steady-state profit achieved after the transient effect from the non-stationary disturbance. The profit

achieved is expressed in percentage of maximum profit available which is calculated by using a perfect plant model with error-free sensors and exact measures of disturbances (not actually measured in the plant). This maximum profit is not realistically achievable, but it is a useful basis for comparing performance, especially since the maximum profit is different for each scenario.

4.4 Case Study Results and RTO Performance Evaluation

4.4.1 Design of Case Studies

The case studies are selected to evaluate if the proposed experimental design technique can improve RTO performance. A disturbance in the activation energy for the second reaction, B_2, is considered in this case study. Updating both the frequency factors and B_2 is not possible if the data sets have no or little variation in temperature; therefore, plant experimentation is expected to improve performance in some circumstances.

The actual disturbance occurring in the plant is the unmeasured non-stationary disturbance in B_2. Different disturbance scenarios shown in Figure 4.2 are considered in this case study. The disturbance scenarios considered have different sizes and dynamics. If these disturbances were perfectly known, the optimum would be determined exactly, and the profit attained would be the best available profit. This best available profit is not achievable because the actual disturbances shown in Figure 4.2 are not measured.

A disturbance model has to be assumed to estimate the loss in profit due to the disturbance when no experiments are performed. For designing experiments, the activation energy, B_2, is assumed to change as a first order system with a time constant of 40 RTO executions and a total steady-state change from 13000 to 15250 R, that is,

$$B_2(N) = 13000 + 2250(1 - e^{-N/40}) \tag{4.4}$$

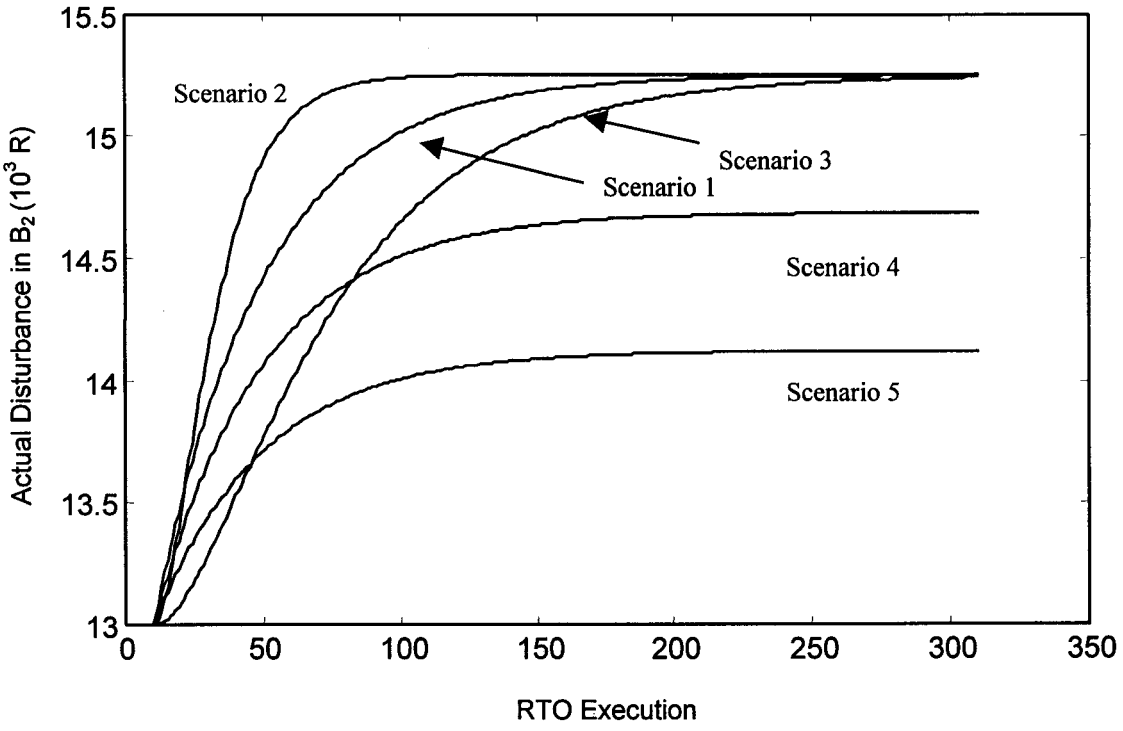

Figure 4.2 Actual disturbance occurring in the plant

This disturbance is *not* the same as the actual disturbance occurring in the plant, and the assumed disturbance in (4.4) is used to estimate the norms of the offset in P_1 term in Problem 4.1.

The profit loss as a function of time has to be estimated to determine the potential benefit for experimentation. Recall that the disturbance is not measured. Therefore, the offset from the optimum without experimentation is characterized by a norm. Without experimentation, the frequency factors are updated to correct for disturbances. For the disturbance considered in B_2, the closed-loop RTO prediction is found to be $\mathbf{x}_m^* = [0.2981\ 0.6307]^T$. If the disturbance were perfectly known, the true plant optimum at steady state would be $\mathbf{x}_m^* = [0.3472\ 0.6444]^T$. Therefore, the Euclidean norm of the offset in $\mathbf{x}_1$ space at steady state is estimated to be 0.051. It is assumed that without experimentation, the

norm of the offset grows from 0 to 0.051 at the same dynamics as B_2 stated in (4.4), but *the direction is unknown.* Therefore,

$$R_{\Delta_2}(N) = 0.051(1 - e^{-N/40}) \tag{4.5}$$

Immediately after experimentation, modelling errors can be reduced by updating the additional parameter, B_2. In the experimental design calculation, it is assumed that the offset can be totally removed after updating B_2. After experimentation, the disturbance continues to occur with the same dynamics, and the offset grows again. Therefore, the offset terms in P_1 in Problem 4.1 are given by

$$\begin{aligned} R_{\Delta_2}(N) &= 0.051(1 - e^{-N/40}) \\ R_{\Delta}(N) &= 0.051(1 - e^{-N/40}) - 0.051(1 - e^{-(N_0+N_{expt})/40}) \end{aligned} \tag{4.6}$$

The assumed disturbance in (4.4) and the estimation of the norm of the offset in (4.6) are not the same as the actual disturbance occurring in the plant. Table 4.1 compares the actual and assumed disturbances for different case study scenarios. In the first scenario, the plant disturbance matches the assumed disturbance exactly. The other case study scenarios are designed to enable the evaluation of RTO performance with experimental design when there are different types of transient and steady-state mismatch between the actual and assumed disturbances.

Table 4.1 Descriptions of the case study scenarios (See Figure 4.2)

Scenario	Plant Disturbance
1	Same as assumed disturbance
2	Faster than assumed disturbance
3	Slower than assumed disturbance
4	Actual size is 75% of the assumed size
5	Actual size is 50% of the assumed size

There are various tuning parameters set by the designer for the RTO system with experimentation. A window size of two is chosen for model updating with a conditioning diagnostic to determine which parameters can be updated for each RTO execution. A disturbance period of 300 RTO executions is used for the future horizon, N_D, for expected profit experimental design problem. The maximum number of experiments to be performed is three; so the design can select 0 to 3 experiments.

4.4.2 Case Study Results

The RTO performances with and without experimentation are compared for cases with different plant operation; measurement noise level, change in operating condition due to the change in production rate, and presence of bias in the measurements. For each situation, all scenarios reported in Table 4.1 are investigated. The Williams-Otto reactor system described in Chapter 3 is selected to be the base case of this case study. The results of the base case will be presented first. Following will be the results for the case study on different situations in plant operation.

The RTO behavior is evaluated based on two measures of economic performances. The *total transient profit* is the sum of the profit attained over the horizon N_D which is defined as follow.

$$\text{Total transient profit} = \sum_{N=1}^{N_D} P(\mathbf{x}_m^*(N)) \tag{4.7}$$

The *steady-state profit* is the sum of profit from the time after the transient to the end of the disturbance change. The time after the transient is taken to be four times the disturbance time constant which is 160 in this case study. Therefore, the steady-state profit is defined as follows.

$$\text{Steady-state profit} = \sum_{N=160}^{N_D} P(\mathbf{x}_m^*(N)) \tag{4.8}$$

These two performance measures are expressed as the percentage of the maximum total transient profit and maximum steady-state profit respectively. The maximum profit is calculated by replacing $P(\mathbf{x}_m^*)$ by the true plant profit, $P(\mathbf{x}_p^*)$, in (4.7) and (4.8), and the true plant profit is determined by true plant model with exact measure of disturbance (see p. 10 in Chapter 1). Each case study is simulated for 10 different seeds of random noise, and the mean and variance of the profits are reported. The following section presents the case study results for different scenarios.

4.4.2.1 Case 1: Base Case

This investigates if the RTO performance with experimentation will improve the operating profit for the base case plant experiencing the scenarios reported in Table 4.1. The RTO performance for tracking the optimum for Scenario 1 is shown in Figure 4.3. By solving the expected profit approach for designing plant experiments, three experiments are designed after the 63rd RTO execution. The RTO system with experimentation tracks the optimum better because the offset between the prediction and the true plant optimum is reduced as shown in Figure 4.3.

The profit term during experimentation (P_2 in Problem 4.1) automatically restricts the size of the perturbation. Since updating frequency factors and activation energy requires variation in temperature in the data sets, it is shown in Figure 4.4 that the experiment at $\mathbf{x}_{expt} = [0.294\ 0.630]^T$ with the historical data at $\mathbf{x} = [0.390\ 0.662]^T$ provide sufficient variation in temperature (about 30 R) for updating. It can also be observed that the profit loss during experimentation is small because the point, $\mathbf{x}_{expt} = [0.294\ 0.630]^T$, is along the ridge of high profit, and the other experiments are close to the model optimum.

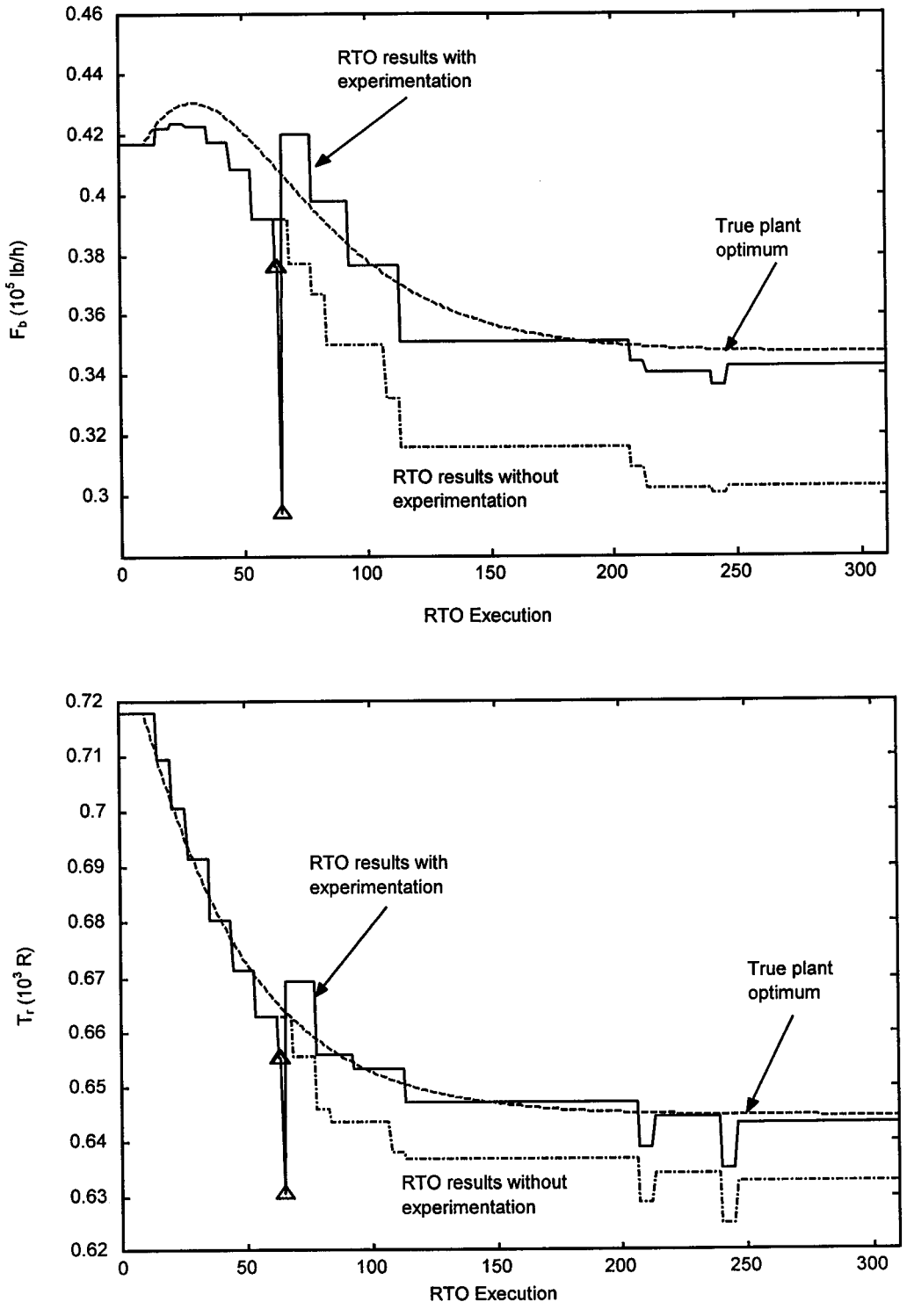

Figure 4.3 Tracking of the optimum by the RTO system with and without experimentation for Scenario 1 in the base case (Δ : experiments)

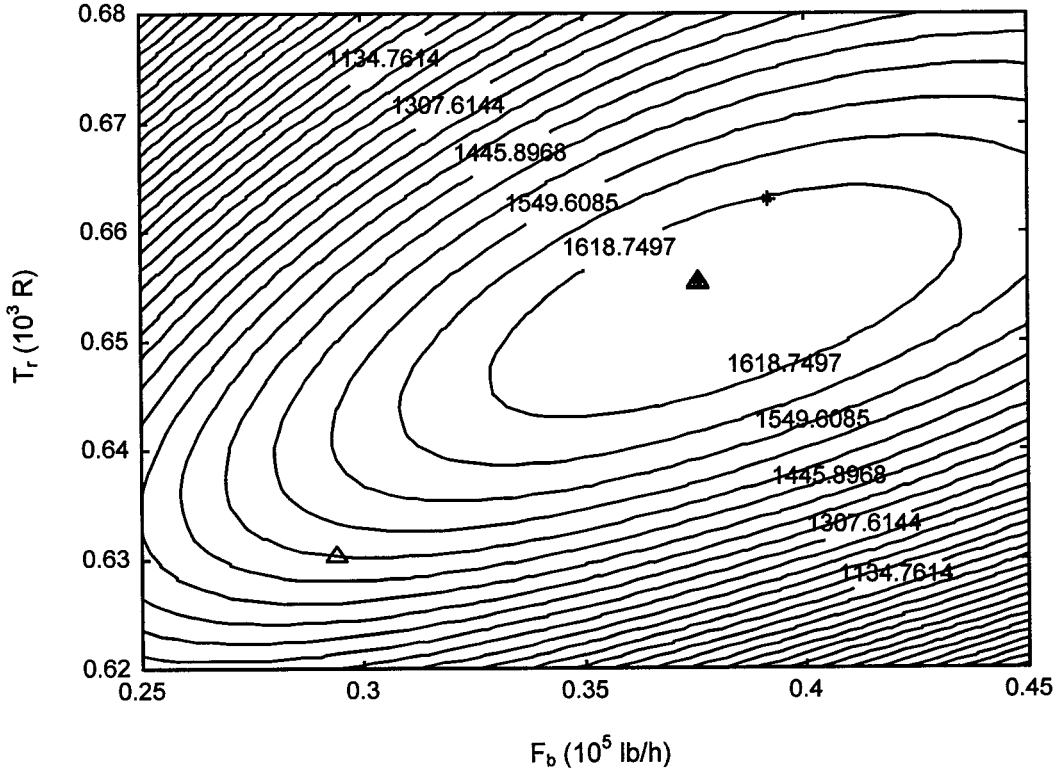

Figure 4.4 Experimental operating conditions for the experiments designed after the 63rd RTO execution for Scenario 1 in the base case (*: historical data, Δ: experiments)

The profit attained for the RTO systems with and without experimentation is shown in Table 4.2. In Scenarios 1 to 3, there is a substantial increase, about 10 % at steady state, in profit when the experimental design is implemented in the RTO system. This good RTO performance with experimentation is not sensitive to the disturbance dynamics. The size of the disturbance can also affect the RTO performance with experimental design. In Scenarios 4 and 5, the disturbance size is too small to cause a significant loss in profit. Without experimentation, the RTO system can achieve nearly 99 % of the profit; therefore, there is no opportunity for improvement when experimental design is implemented.

Table 4.2 RTO performance in terms of profit for the base case plant in case 1 (values in the parentheses are the standard deviation of profit)

Scenario	Total transient profit (% of maximum total transient profit)		Steady-state profit (% of maximum steady-state profit)	
	Without Experimentation	With Experimentation	Without Experimentation	With Experimentation
1	97.38 (0.3350)	99.24 (0. 3947)	90.49 (1.5639)	98.49 (1.284)
2	95.86 (0.7898)	98.98 (0.7434)	88.67 (2.7147)	98.77 (0.9717)
3	98.33 (0.2701)	99.46 (0.2072)	91.98 (1.5829)	99.05 (0.7299)
4	99.30 (0.1387)	99.62 (0.1818)	98.78 (0.3128)	99.60 (0. 2224)
5	99.74 (0.0883)	99.78 (0.08546)	99.62 (0.1836)	99.83 (0.1101)

4.4.2.2 Case 2: Reduction of Noise Level by 50 % in all Measurements

This case study investigates the effect of noise level on the RTO performance. The noise level is reduced by 50 % in both the plant simulation and covariance matrix used in experimental design. The results shown in Table 4.3 are similar to the base case. A significant improvement in profit is achieved for large disturbances (Scenarios 1 to 3), and the improvement in profit is negligible when the disturbance size is small (Scenarios 4 and 5).

The size of perturbation in the designed experiment is influenced by the noise level of the measurements, **V**, in (4.3). Figure 4.5 shows the experimental conditions designed by solving Problem 4.1 for reduced noise. When the noise level in all the measurements is reduced by 50 %, a smaller temperature variation is sufficient to generate sufficient information content in the data sets. A smaller noise level in all the measurements means a smaller profit loss during experimentation.

Table 4.3 RTO performance in terms of profit for the plant with 50 % reduction in noise level in case 2 (values in the parentheses are the standard deviation of profit)

Scenario	Total transient profit (% of maximum total transient profit)		Steady-state profit (% of maximum steady-state profit)	
	Without Experimentation	With Experimentation	Without Experimentation	With Experimentation
1	97.30 (0.1548)	99.31 (0.4265)	90.22 (0.9449)	98.77 (1.1353)
2	95.99 (0.3855)	99.05 (0.7563)	89.19 (1.6309)	98.46 (2.0583)
3	98.44 (0.1081)	99.65 (0.2144)	92.55 (0.5805)	99.56 (0.3760)
4	99.17 (0.0851)	99.78 (0.1359)	98.44 (0.2206)	99.80 (0.1938)
5	99.81 (0.0309)	99.89 (0.0544)	99.71 (0.0673)	99.93 (0.0471)

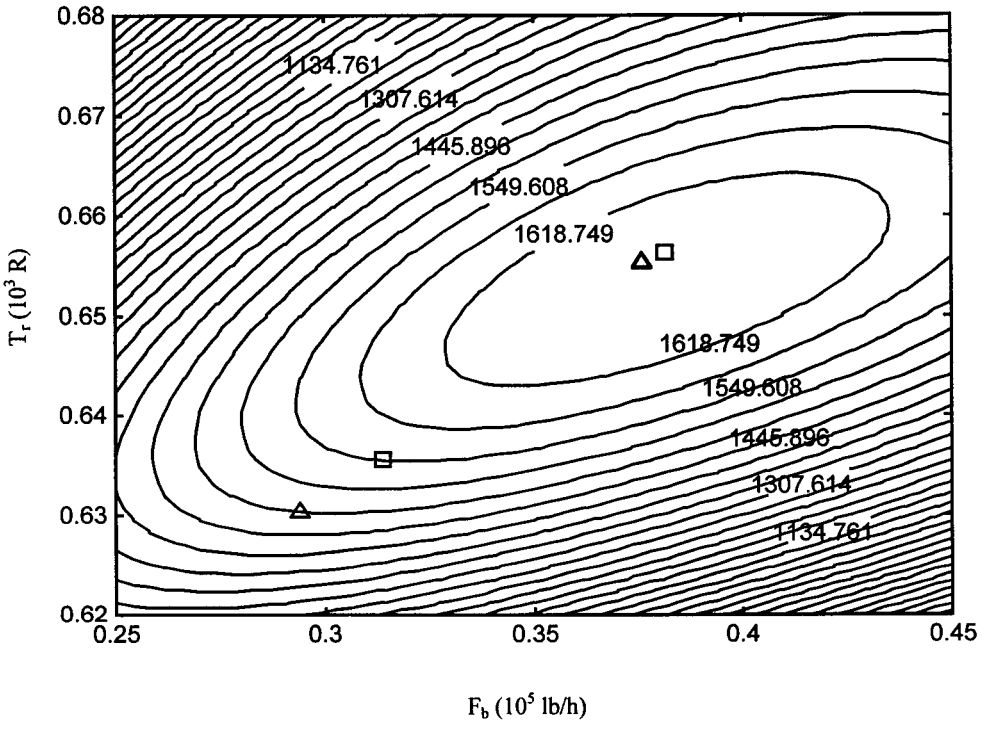

Figure 4.5 Experimental operating conditions for the experiments designed after the 63rd RTO execution for Scenario 1 for different noise level (Δ: base case, □: 50 % reduction in noise level)

4.4.2.3 Case 3: Reduction of F_a by 20 %

This case study investigates the RTO performance with experimentation when there is a change in operating condition due to a change in production rate. The feed flow rate of A is reduced by 20 %. The results presented in Table 4.4 are similar to the base case, where a significant improvement in operating profit is achieved for large disturbances (Scenarios 1 to 3), and there is an insignificant gain in profit when the disturbance size is reduced (Scenarios 4 and 5).

Table 4.4 RTO performance in terms of profit for a change in production rate in case 3 (values in the parentheses are the standard deviation of profit)

Scenario	Total transient profit (% of maximum total transient profit)		Steady-state profit (% of maximum steady-state profit)	
	Without Experimentation	With Experimentation	Without Experimentation	With Experimentation
1	97.59 (0.4951)	99.16 (0.4897)	92.42 (1.8961)	98.68 (1.0269)
2	96.02 (0.8266)	99.25 (0.4671)	90.49 (2.6357)	99.05 (1.2490)
3	98.58 (0.1904)	99.47 (0.1557)	94.25 (0.9788)	99.05 (0.4714)
4	99.19 (0.2072)	99.68 (0.1616)	98.51 (0.4600)	99.75 (0.2083)
5	99.76 (0.0816)	99.79 (0.0594)	99.66 (0.1734)	99.86 (0.0933)

4.4.2.4 Bias in Measurements

Bias in measurements can be caused by miscalibration or physical wear of the sensors or a change in physical properties of the fluids. Gross errors in measurements may not be always identified by gross error detection. This case study investigates the RTO performances with and without experimentation when there is a bias in the

measurements of the optimizer independent variables, T_r and F_b, with various signs and magnitudes.

When there are biases in the measurements of variables under feedback control, the actual process variables in the plant will not be equal to the setpoints. If the controllers have integral modes, so that there are no steady-state offsets between the setpoints and the measured variables, the actual process variable, $\mathbf{x_p}$, and its measured values, $\mathbf{x_p^m}$, are related by (4.9) and (4.10)

$$\mathbf{x_p} = \mathbf{x_{SP}} - \mathbf{b} \tag{4.9}$$

$$\mathbf{x_p^m} = \mathbf{x_p} + \mathbf{b} + \mathbf{n} \tag{4.10}$$

where $\mathbf{x_{SP}}$ is the controller setpoint from the optimizer, **b** is the bias of the measurements and **n** is the zero-mean measurement noise.

This case study investigates whether the RTO system with experimentation will improve the profit tracking when there are biases in the measurements of T_r and F_b. In the T_r measurement, the biases considered are ±5 R and ±10 R and are significantly larger than its noise standard deviation of about 3.3 R. In the F_b measurement, the biases considered are ±1500 lb/h and ±3500 lb/h and are significantly larger than its noise standard deviation of about 380 lb/h.

4.4.2.4.1 Case 4: Bias in Temperature Measurement

Higher profit can be achieved by the RTO system with experimentation compared to the standard RTO system without experimentation, as shown in Tables 4.5 to 4.8, when there is a bias in T_r measurement. For Scenarios 1 to 3, around 10 % improvement in the steady-state profit can be achieved by experimentation. Better information content

Table 4.5 RTO performance in terms of profit when there is a bias of 5 R in T_r measurement in case 4 (values in the parentheses are the standard deviation of profit)

Scenario	Total transient profit (% of maximum total transient profit)		Steady-state profit (% of maximum steady-state profit)	
	Without Experimentation	With Experimentation	Without Experimentation	With Experimentation
1	97.15 (0.4396)	99.19 (0.4579)	89.53 (1.9793)	98.49 (1.1913)
2	95.42 (0.6389)	98.96 (0.7510)	87.45 (2.0552)	98.49 (1.8069)
3	98.25 (0.1247)	99.43 (0.1921)	91.91 (0.8448)	98.64 (0.9120)
4	99.19 (0.1303)	99.62 (0.1474)	98.57 (0.3488)	99.63 (0.1600)
5	99.72 (0.0919)	99.80 (0.1503)	99.59 (0.1961)	99.89 (0.0988)

Table 4.6 RTO performance in terms of profit when there is a bias of 10 R in T_r measurement in case 4 (values in the parentheses are the standard deviation of profit)

Scenario	Total transient profit (% of maximum total transient profit)		Steady-state profit (% of maximum steady-state profit)	
	Without Experimentation	With Experimentation	Without Experimentation	With Experimentation
1	97.31 (0.3940)	99.12 (0.4674)	90.47 (1.9891)	97.99 (1.8247)
2	95.69 (0.4950)	98.88 (0.8144)	88.22 (1.6894)	98.27 (1.8885)
3	98.31 (0.2220)	99.45 (0.1722)	92.28 (1.3610)	98.83 (0.8432)
4	99.17 (0.1485)	99.64 (0.1793)	98.51 (0.4033)	99.67 (0.2558)
5	99.73 (0.0948)	99.80 (0.1078)	99.62 (0.2048)	99.89 (0.1063)

Table 4.7 RTO performance in terms of profit when there is a bias of -5 R in T_r measurement in case 4 (values in the parentheses are the standard deviation of profit)

Scenario	Total transient profit (% of maximum total transient profit)		Steady-state profit (% of maximum steady-state profit)	
	Without Experimentation	With Experimentation	Without Experimentation	With Experimentation
1	97.23 (0.3736)	99.18 (0.4657)	90.03 (1.8568)	98.49 (1.2215)
2	95.45 (0.6536)	98.96 (0.7510)	87.68 (2.0150)	98.49 (1.8069)
3	98.28 (0.1172)	99.44 (0.1819)	91.99 (0.7560)	98.68 (0.9454)
4	99.18 (0.1729)	99.65 (0.1441)	98.52 (0.4226)	99.67 (0.2178)
5	99.72 (0.0910)	99.79 (0.0934)	99.60 (0.2004)	99.86 (0.0951)

Table 4.8 RTO performance in terms of profit when there is a bias of -10 R in T_r measurement in case 4 (values in the parentheses are the standard deviation of profit)

Scenario	Total transient profit (% of maximum total transient profit)		Steady-state profit (% of maximum steady-state profit)	
	Without Experimentation	With Experimentation	Without Experimentation	With Experimentation
1	97.22 (0.3746)	99.04 (0.4402)	89.98 (1.8514)	97.89 (1.2434)
2	95.47 (0.6651)	98.88 (0.8144)	87.69 (2.0099)	98.27 (1.8885)
3	98.30 (0.1243)	99.42 (0.2324)	92.06 (0.7581)	98.67 (0.9812)
4	99.19 (0.1791)	99.65 (0.1488)	98.54 (0.3956)	99.68 (0.2309)
5	99.69 (0.1073)	99.78 (0.0895)	99.54 (0.2303)	99.84 (0.0837)

generated by the experiments can correct the modelling errors from the disturbance in B_2 and measurement bias. In Scenarios 4 and 5, improvement in operating profit is insignificant because the disturbance sizes are too small to cause a significant loss in profit.

The RTO performances are not degraded by the bias in T_r measurement. This is illustrated by the case study results in Scenario 1 reported in Table 4.9 for different sign and magnitude of the bias in T_r measurement. About 90 % and 98 % of the maximum profit can be achieved by the RTO system with and without experimentation, respectively, regardless the size and sign of the bias. Presumably, updating frequency factors (and activation energy) can compensate the modelling error from bias in T_r measurement. For an Arrhenius rate expression shown in (4.11),

$$k = Ae^{-\frac{B}{T_r}} \tag{4.11}$$

the derivative of the rate constant with respect to the temperature is given in (4.12).

$$\frac{dk}{dT_r} = \frac{AB}{T_r^2} e^{-\frac{B}{T_r}} \tag{4.12}$$

Table 4.9 RTO performance for Scenario 1 when there are biases in T_r measurement in case 4 (values in the parentheses are the standard deviation of profit)

Bias in T_r measurement (R)	**Steady-state profit without experimentation** (% of maximum steady-state profit)	**Steady-state profit with experimentation** (% of maximum steady-state profit)
No bias (base case)	90.49 (1.5639)	98.49 (1.2840)
-5	90.03 (1.8568)	98.49 (1.2215)
5	89.53 (1.9793)	98.49 (1.1913)
-10	89.98 (1.8514)	97.89 (1.2434)
10	90.47 (1.9891)	97.99 (1.8247)

Therefore, when there is a bias in the temperature measurement, the error in the gradient of the plant, which determines the location of the optimum, can be corrected by adjusting the frequency factor or activation energy to compensate for the bias. Figure 4.6 shows the effect of the bias in the T_r measurement on the trajectory of the actual process variables without experimentation, and it is clearly shown that the bias does not influence the trajectory and hence the profit achieved. The contours shown in Figure 4.6 are the true plant profit contours at the end of the simulation. The plant reaches the similar steady states regardless the sign of the bias, and therefore the steady-state profits reported in Table 4.9 are similar for different sign and magnitude of the bias.

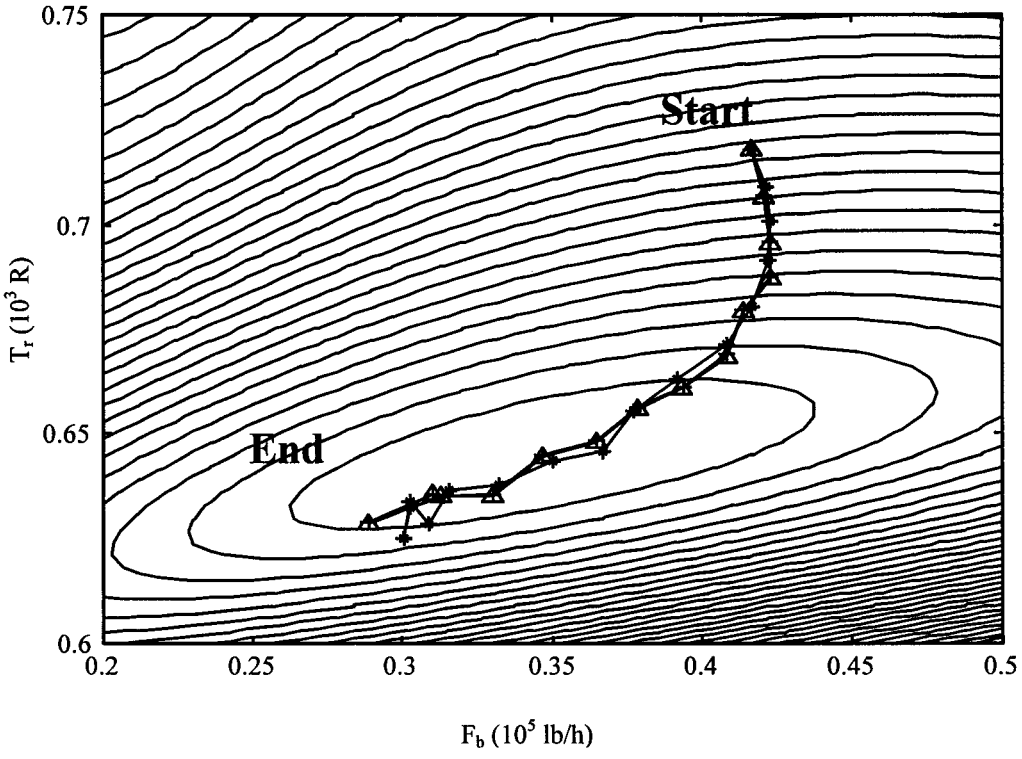

Figure 4.6 The trajectory of the actual process variables for different bias in the T_r measurement for Scenario 1 without experimentation (* : No bias; + : -10 R; Δ : +10 R)

4.4.2.4.2 Case 5: Bias in Flow Measurement

The RTO system with experimentation can improve the operating profit compared to the profit achieved by the RTO system without experimentation when there is a bias in F_b measurement. Tables 4.10 to 4.13 report the performances of the RTO system with and without experimentation for this case study. For Scenarios 1 to 3 in which the disturbances are large, significant improvement in operating profit can be achieved when experiments are performed. A 5 % to more than 10 % improvement in the steady-state profit is obtained, depending on the magnitude and sign of the bias. Similar to the base case, there is no significant improvement in profit for small disturbances in Scenarios 4 and 5.

Unlike the bias in T_r measurement, the RTO performances are influenced by the magnitude and sign of the bias. Table 4.14 compares the effect of the bias sign and magnitude on the RTO performances based on steady-state profit for Scenario 1. A small bias of ±1500 lb/h does not cause a significant decrease in operating profit. When the bias is large, the sign of the bias can have an impact on the RTO performances. Without experimentation, there is about 3 % drop in steady-state profit when the bias is –3500 lb/h, but a 15 % drop in steady-state profit is observed for a bias of 3500 lb/h. At the end of the simulation, different steady-state operating points are reached for different sign of bias in the measurement. When the bias is 3500 lb/h, after the disturbance change, the plant reaches a steady-state operating point with a lower operating profit. This is illustrated in the plot of the trajectory of the process variables shown in Figure 4.7. Updating the frequency factor or activation energy cannot remove the mismatch due to the bias in F_b measurement because these adjustable parameters do not appear in the plant gradient with respect to F_b. It is shown in the last column in Table 4.14 that although designed experiments provide substantial improvement in operating profit, the RTO performance is still degraded compared to the base case where there is no bias in the

Table 4.10 RTO performance in terms of profit when there is a bias of 1500 lb/h in F_b measurement in case 5 (values in the parentheses are the standard deviation of profit)

Scenario	Total transient profit (% of maximum total transient profit)		Steady-state profit (% of maximum steady-state profit)	
	Without Experimentation	With Experimentation	Without Experimentation	With Experimentation
1	96.08 (0.3816)	98.97 (0.2182)	86.13 (1.9034)	97.80 (1.1609)
2	94.22 (0.6114)	98.60 (0.1911)	84.66 (1.6775)	97.70 (0.7241)
3	97.62 (0.2420)	99.16 (0.1651)	89.54 (1.5022)	97.72 (1.1292)
4	98.77 (0.1529)	99.43 (0.1654)	97.96 (0.3864)	99.32 (0.3217)
5	99.50 (0.0838)	99.59 (0.1230)	99.36 (0.1728)	99.62 (0.2129)

Table 4.11 RTO performance in terms of profit when there is a bias of 3500 lb/h in F_b measurement in case 5 (values in the parentheses are the standard deviation of profit)

Scenario	Total transient profit (% of maximum total transient profit)		Steady-state profit (% of maximum steady-state profit)	
	Without Experimentation	With Experimentation	Without Experimentation	With Experimentation
1	92.50 (0.4414)	96.41 (0.8705)	74.31 (2.3479)	89.63 (3.3303)
2	88.84 (0.7209)	95.44 (0.7979)	71.36 (1.8849)	90.33 (2.6501)
3	95.27 (0.2600)	97.14 (0.5713)	80.29 (1.4441)	89.42 (2.7621)
4	97.44 (0.0927)	98.34 (0.3473)	96.04 (0.2302)	97.83 (0.7374)
5	98.74 (0.0660)	98.81 (0.2682)	98.58 (0.1459)	98.77 (0.4377)

Table 4.12 RTO performance in terms of profit when there is a bias of -1500 lb/h in F_b measurement in case 5 (values in the parentheses are the standard deviation of profit)

Scenario	Total transient profit (% of maximum total transient profit)		Steady-state profit (% of maximum steady-state profit)	
	Without Experimentation	With Experimentation	Without Experimentation	With Experimentation
1	97.23 (0.4354)	98.41 (0.8488)	89.95 (2.1779)	96.28 (2.1324)
2	95.07 (1.1431)	97.48 (1.3953)	86.01 (3.2566)	94.46 (3.6572)
3	98.26 (0.1140)	99.02 (0.5225)	91.88 (0.8853)	97.71 (1.3237)
4	99.20 (0.1576)	99.36 (0.3760)	98.54 (0.4547)	99.29 (0.5335)
5	99.66 (0.1439)	99.64 (0.2458)	99.55 (0.2843)	99.70 (0.2624)

Table 4.13 RTO performance in terms of profit when there is a bias of -3500 lb/h in F_b measurement in case 5 (values in the parentheses are the standard deviation of profit)

Scenario	Total transient profit (% of maximum total transient profit)		Steady-state profit (% of maximum steady-state profit)	
	Without Experimentation	With Experimentation	Without Experimentation	With Experimentation
1	96.24 (0.4589)	96.85 (0.8850)	87.49 (2.6188)	91.67 (2.6044)
2	93.66 (0.9285)	96.42 (0.7237)	83.78 (3.1340)	92.41 (1.8737)
3	97.42 (0.2495)	97.63 (0.6515)	89.16 (1.6742)	94.03 (1.5624)
4	98.56 (0.2303)	98.46 (0.5555)	97.60 (0.5539)	98.21 (0.6823)
5	99.30 (0.1130)	98.84 (0.6163)	99.13 (0.2185)	98.76 (0.8719)

Table 4.14 RTO performance for Scenario 1 when there are biases in F_b measurement in case 5 (values in the parentheses are the standard deviation of profit)

Bias in F_b measurement (lb/h)	**Steady-state profit without experimentation** (% of maximum steady-state profit)	**Steady-state profit with experimentation** (% of maximum steady-state profit)
No bias (base case)	90.49 (1.5639)	98.49 (1.2840)
-1500	89.95 (2.1779)	96.28 (2.1324)
1500	86.13 (1.9034)	97.80 (1.6090)
-3500	87.49 (2.6188)	91.67 (2.6044)
3500	74.31 (2.3479)	89.63 (3.3303)

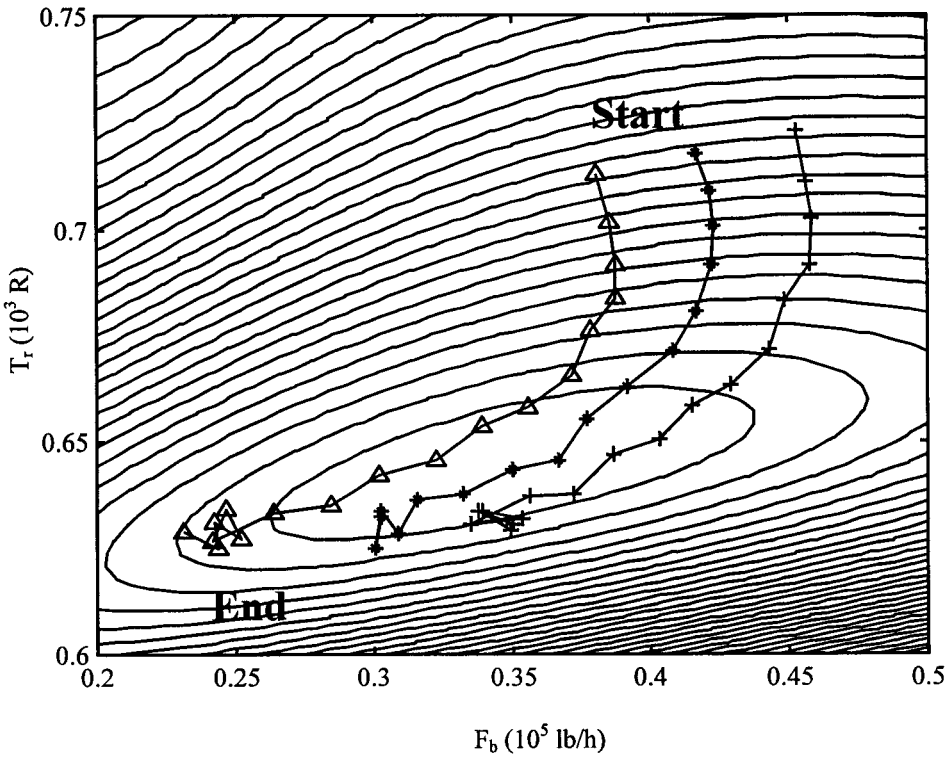

Figure 4.7 The trajectory of the actual process variables for different bias in the F_b measurement for Scenario 1 without experimentation (* : No bias; + : -3500 lb/h; Δ : +3500 lb/h)

measurement. Therefore, frequent calibration of the flow sensor is required to eliminate the possibility of performance degradation due to measurement bias.

4.5 Conclusions

The performance of the RTO system relies on accurate estimation of the parameters to reduce the model mismatch. Information content in the data sets is crucial to have accurate estimation of the parameters. In this chapter, the experimental design technology is integrated with RTO system to improve the estimation of the key parameters by performing plant experiments

The expected profit approach for designing plant experiments for RTO applications has been introduced in this chapter. Since plant experiments are expensive to perform, designing plant experiments based on profit is beneficial. The experiments are designed to trade off the profit loss before and during experimentation and the profit gains after experimentation by reducing the offset and variability. This approach offers an advantage over classical experimental design approaches because prior specification of the experimental window for performing experiments is not required. Large plant movement and many experiments are automatically penalized by the profit loss term in the objective function for experimental design.

The proposed RTO system with experimentation has been successfully applied to the Williams-Otto reactor system. Various disturbance scenarios for different situations in plant operation were simulated. An improvement in profit was observed when plant experiments were performed. These experiments improved the information content of the data sets for updating additional parameters to reduce the model mismatch. Experiments designed by the expected profit approach were located close to the model optimum or along the direction of ridge of the profit contours to reduce the cost of experimentation.

Simulated case study results showed that the disturbance sizes could affect the improvement gained in RTO performance through experimental design, but the RTO performance was not sensitive to disturbance dynamics. Therefore, the designers have to consider the sizes of the disturbances on profit when considering whether the cost of implementing this experimental design approach is justified.

Error due to measurement bias could substantially degrade the RTO performance. The Williams-Otto reactor case study results showed that updating the adjustable parameters may not totally remove the mismatch due to sensor bias even though designed experiments could improve the operating profit. Updating the frequency factors and activation energy could correct the mismatch from the bias in temperature measurement. However, bias in flow measurement could not be totally corrected by updating those parameters. Frequent calibration of the flow sensor is required to avoid RTO performance degradation due to bias.

The experimental design was implemented in a simple example for illustration purpose in this chapter. This example does not represent the typical industrial operations optimization problem. Application of the expected profit experimental design in RTO systems in a simulated industrial boiler case study will be illustrated in the next chapter.

5. MODEL STRUCTURE SELECTION IN BOILER CASE STUDY

5.1 Introduction

Model selection is a key step in the successful application of an RTO system. A good model representing the plant closely is always advantageous. A rigorous fundamental model, which is accurate over a wide range of operation, is sometimes too complex for online optimization. An empirical model is simpler in structure and hence easier to optimize, but it is accurate in a small region. In this chapter, an industrial boiler system is used to study the crucial factors in deciding the model structure to be used in RTO systems. Boilers are commonly used in chemical plants for supplying steam for heat and power generation, and opportunity exists for optimizing the load allocation to different boilers to minimize the energy cost. Three different approaches for boiler network optimization are compared in this case study: 1) model-free direct search method, 2) empirical efficiency curve model, and 3) fundamental model.

Model-free direct search methods [e.g., Bamberger and Isermann, 1978; Bozenhardt, 1986; Garcia and Morari, 1981] track the optimum based on plant data without using a detailed fundamental model. These methods require estimation of the plant performance from the plant data. The direction which improves the plant performance is estimated, and the plant is moved along that direction. The direct search methods have been applied to simulated continuous stirred tank reactors [e.g, Garcia and Morari, 1981; McFarlane and Bacon, 1989], but application of these methods in an industrial boiler system has not been reported.

Optimization of steam allocation using a simplified model using a second order polynomial to relate the boiler efficiency and steam load has been reported [Green and ai-Shaikh, 1980; Koninckx, 1988]. Updating the efficiency curve model requires multiple

data sets at different steam load, and periodic design of plant experiments. The experimental design strategies developed in the previous chapter are demonstrated in an industrial boiler system in this chapter.

Rigorous fundamental models have been developed for boiler simulation and optimization. In a boiler, heat transfer takes place in the air preheater, economizer, riser and superheater. The models developed by Bertrand (1986), Chien et al. (1958), de Mello (1991) and Nicholson (1964) assume that convection is the only mode of heat transfer in the heat exchangers in the boiler. In the latest design of boilers, riser tubes are placed inside the furnace to receive radiation from the flame. Radiation heat transfer is included in the model developed by Dieck-Assad (1990), and Kwan and Anderson (1970). All these models calculate the flame temperature from the heating value of fuel. In this chapter, a more realistic model is developed to include the combustion of fuel components with oxygen for studying the RTO performance in the presence of fuel composition disturbance, which has not been investigated in the previous work.

The boiler model developed in this case study is based on the #9 boiler in Dofasco, Inc. Some modifications have been made for this simulated case study. Two additional controllers are implemented to control the superheated steam temperature and oxygen concentration in the flue gas for safe and smooth operation [Dukelow, 1991]. The heat transfer area is reduced because the original boiler has too large heat transfer area in recovering the heat from the flue gas which could cause acid condensation due to low flue gas temperature. Boilers with different performance are simulated by changing the heat transfer area for this case study.

This chapter begins by presenting the summary of the fundamental model developed for boiler simulation. A simplified fundamental model and an empirical efficiency curve model for RTO application are then discussed. The strategies for using three different modelling alternatives in the RTO system for steam allocation are then

presented. This chapter is concluded by the discussions of the case study results to compare the RTO performances using different models for various disturbances in demand, fuel composition and heat exchanger fouling.

5.2 Fundamental Boiler Model

The configuration of the boiler used in this simulated case study is shown in Figure 5.1. Water is preheated by the flue gas in the economizer. The preheated water mixes with the steam/water mixture in the steam drum. Water flows from the steam drum to the mud drum and water header at the bottom of the boiler in the downcomers by gravity. Water boils in the generating and riser tubes which receive heat from the flue gas and the flame. The steam/water mixture flows upwards to the steam drum in the generating and riser tubes by natural circulation resulting from a decrease in density when water boils. Saturated steam leaving the steam drum is superheated in the superheater to the desired steam temperature. The superheated steam flows to the steam header which supplies steam to different users.

High temperature gas for heating is generated by combustion of fuel with air. Air is preheated by the saturated steam in the steam coil and by the flue gas in the air preheaters. Combustion takes place in the furnace. The flame radiates heat to the riser tubes for boiling the water. Hot flue gas superheats the steam in the superheater, and boils the water in the generating tubes. Further heat recovery from the flue gas is achieved by heating the water in the economizer and air in the air preheaters before discharging the flue gas to the stack.

Controllers are implemented to achieve safe and smooth operation and to protect the equipment. The steam header pressure is controlled by the fuel flow rate, and the oxygen concentration in the flue gas is controlled by the air flow rate to ensure the boiler is operated safely. Flue gas temperature is controlled by adjusting the amount of saturated

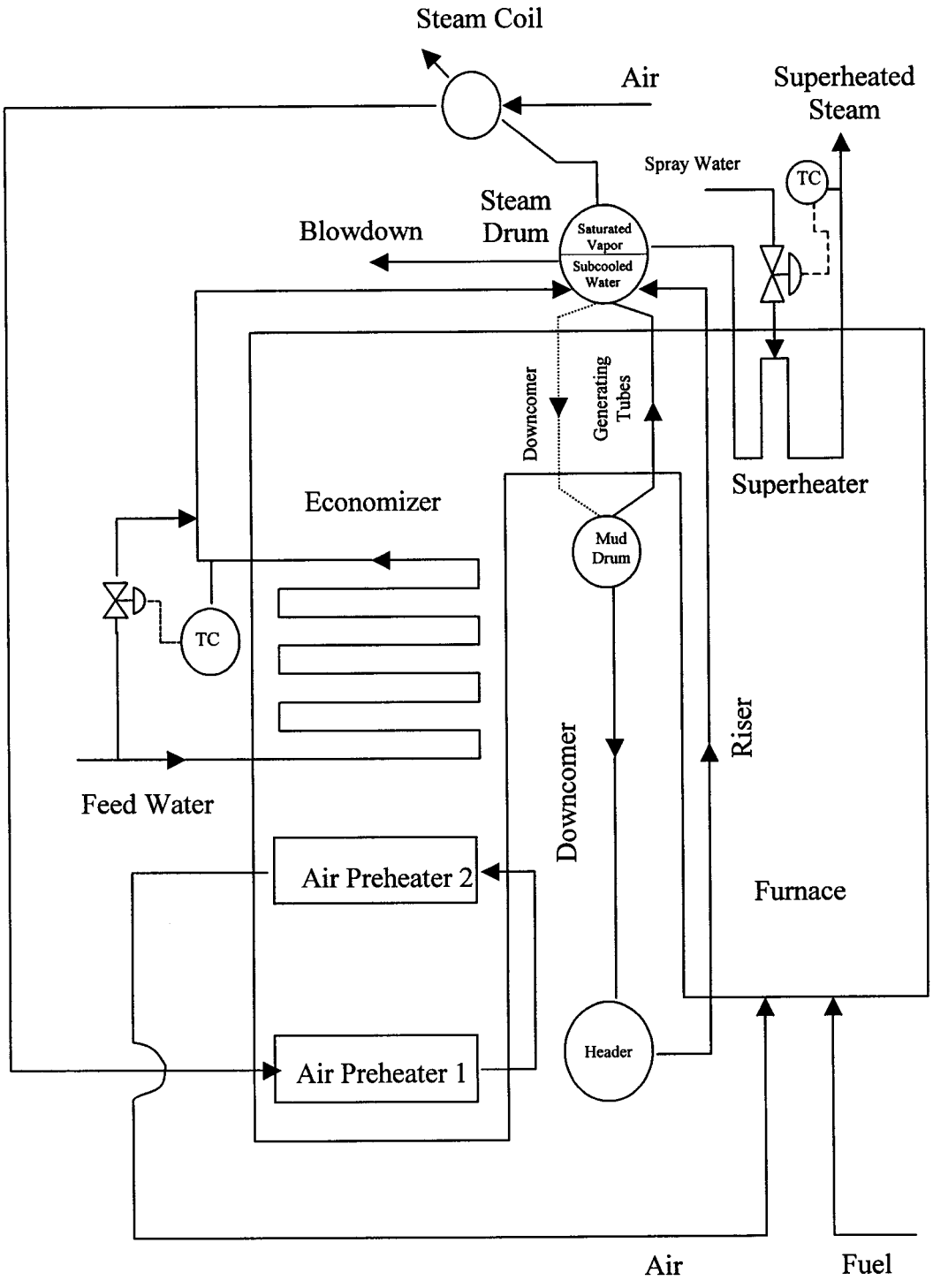

Figure 5.1 Configuration of Dofasco's boiler

steam flowing from the steam drum to steam coil to heat up the incoming air. The setpoint for the flue gas temperature controller is determined by the flue gas dew point. A setpoint higher than the flue gas dew point is required to avoid condensation of water vapor in the flue gas with dissolved sulfur dioxide. This acidic condensate can corrode the equipment. The temperature of water leaving the economizer is also controlled by adjusting the amount of water bypassing the economizer to avoid boiling of water before entering the steam drum.

The systems for modelling heat transfer are shown in Figure 5.2. In Dofasco's boilers, two types of gaseous fuel are combusted for steam generation, namely the blast furnace gas and coke oven gas. The hot gas generated by combustion of fuel heat up the water to produce steam in different heat exchangers represented by the boxes in Figure 5.2. The details of the mathematical modelling of the boiler are discussed in Appendix D. The summary of the model development is presented in Table 5.1. English units are used in all the variables, that is, flow rate in lb/h or scfh (standard cubic feet per hour), temperature in F, energy in btu and pressure in psia, to be consistent with the practice at Dofasco.

Comparisons of the model predictions and measurements taken from the plant are reported in Appendix D. The model predictions match the values of the measured variables closely. There are some discrepancies in the temperature and oxygen concentration in the flue gas. These discrepancies are caused by non-uniform temperature and concentration profiles in the boundary layers which are not taken into account in the model. The sensors measure the local values of the process variables. These measured values are not the same as the "average" values predicted from the model assuming well-mixed zones in the heat exchangers.

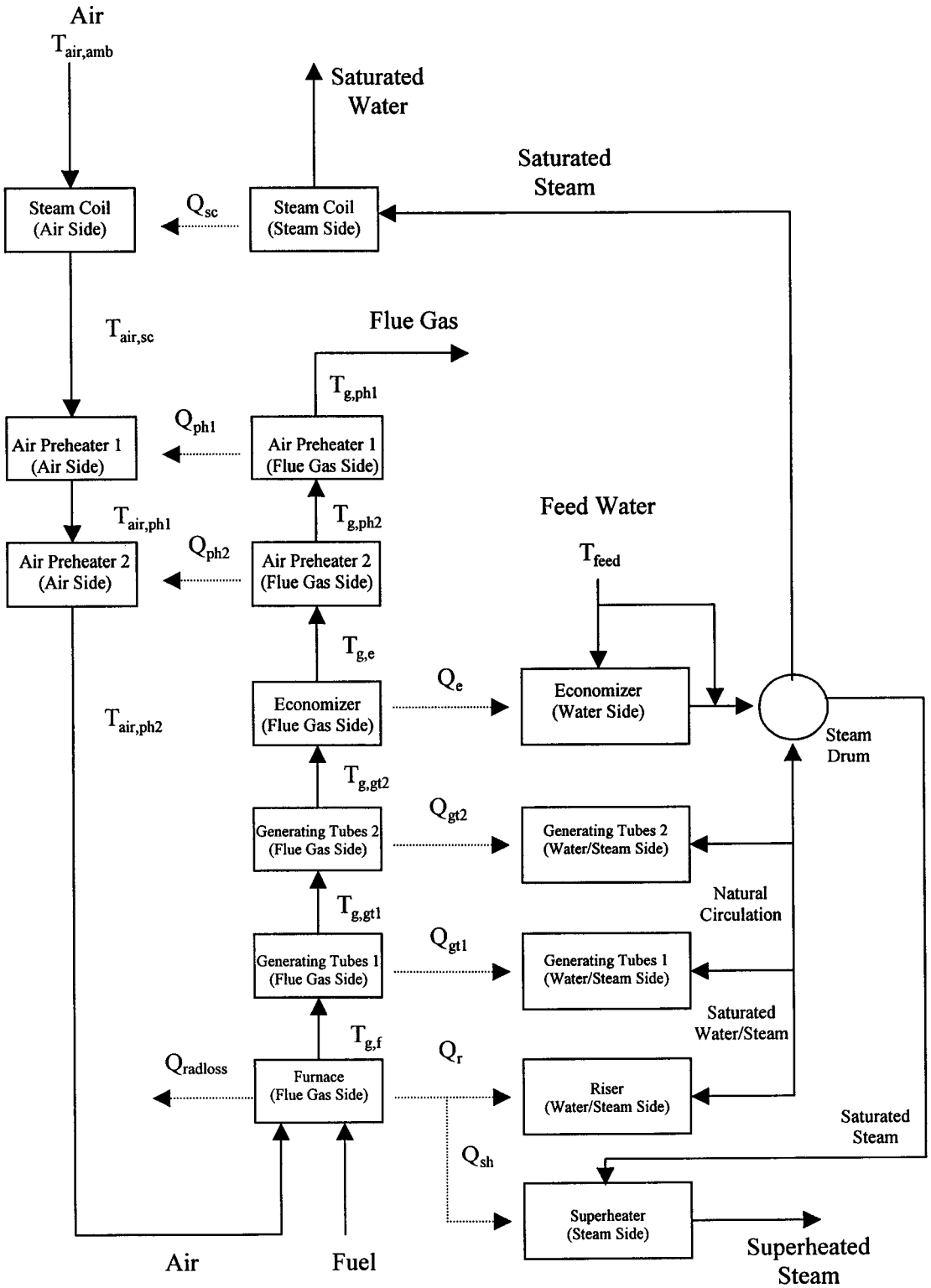

Figure 5.2 Systems for heat transfer modelling

Table 5.1 Summary of model development for the boiler

System	Approaches in Modelling
Steam/Water	• Material and energy balances • Thermodynamic and transport properties derived by fitting with temperature and pressure using polynomials
Flue gas	• Complete combustion in the furnace • Uniform gas temperature in the furnace • 2 zones in generating tubes and air preheater • p_e zones in economizer where p_e is the number of passes of economizer tubes • Thermodynamic and transport properties derived by fitting with temperature and pressure using polynomials
Heat transfer	• Heat exchangers modelled by a series of lumped heat exchangers • Negligible thermal resistance in the tube walls of heat exchangers • Heat transfer coefficients estimated from the empirical correlation $Nu = cRe^mPr^n$ [Holman, 1992; Jana, 1986]
Fluid flow	• Pressure changes due to friction and exit loss, change in elevation and evaporation • Incompressible flow

The model developed for this case study is limited to normal operation. Any abnormal operations such as startup and shutdown are not considered in this model and the case study in this chapter.

5.3 Models for the RTO System

In this case study, a simplified fundamental model and an empirical efficiency curve model are used in the model-based RTO system for boiler network optimization. This section presents these two models used in the RTO system. The simplified fundamental model is presented first and followed by the presentation of the empirical

efficiency curve model with a discussion of different methods for estimating the boiler efficiency from the measurements.

5.3.1 Simplified Fundamental Model

RTO model is never perfect. Mismatch is introduced by making typical simplifications in heat exchanger modelling. The simplified fundamental model used in the RTO system is developed by making assumptions on the relative importance of the thermal resistances of heat transfer at the steam/water side and flue gas side. A simplified log mean temperature model is used for modelling the heat exchangers.

Two air preheaters are lumped to simplify the heat transfer equations described in Appendix D. A log mean temperature difference model is used to model the lumped air preheater with air temperature of $T_{air,sc}$ at the inlet and $T_{air,ph}$ at the outlet, and flue gas temperature of $T_{g,e}$ at the inlet and $T_{g,ph}$ at the outlet. The heat transfer equation is given in the following equation,

$$Q_{ph} = (UA)_{ph} \Delta T_{LM,ph} \tag{5.1}$$

where $\Delta T_{LM,ph}$ is the log mean temperature difference across the air preheater which is defined as follows.

$$\Delta T_{LM,ph} = \frac{(T_{g,e} - T_{air,ph}) - (T_{g,ph} - T_{air,sc})}{\ln \frac{T_{g,e} - T_{air,ph}}{T_{g,ph} - T_{air,sc}}} \tag{5.2}$$

The overall heat transfer coefficient, $(UA)_{ph}$, can be calculated by summing the resistances of heat transfer at the air side, $(hA)_{out,ph}$, and flue gas, $(hA)_{in,ph}$, assuming that the thermal resistance of tube walls is negligible.

$$\frac{1}{(UA)_{ph}} = \frac{1}{(hA)_{in,ph}} + \frac{1}{(hA)_{out,ph}} \tag{5.3}$$

The heat transfer coefficients at the air and flue gas sides are related to the air and flue gas flow rates denoted by W_{air} and W_{flue}, respectively, by the following equations,

$$(hA)_{in,ph} = a_{in,ph} W_{flue}^{\ b_{in,ph}} \tag{5.4}$$

$$(hA)_{out,ph} = a_{out,ph} W_{air}^{\ b_{out,ph}} \tag{5.5}$$

where a and b are the candidate parameters for updating.

The simplified economizer model can be similarly developed based on log mean temperature difference. The heat transfer equations are given in (5.6) and (5.7),

$$Q_e = (UA)_e \Delta T_{LM,e} \tag{5.6}$$

$$\Delta T_{LM,e} = \frac{(T_{g,gt} - T_e) - (T_{g,e} - T_{Feed})}{\ln \frac{T_{g,gt} - T_e}{T_{g,e} - T_{Feed}}} \tag{5.7}$$

where $T_{g,gt}$ and $T_{g,e}$ are the flue gas temperature entering and leaving the economizer, T_{Feed} and T_e are the temperature of water entering and leaving the economizer, Q_e is the heat transfer, and $(UA)_e$ is the overall heat transfer coefficient. The overall heat transfer coefficient is approximately equal to the flue gas side heat transfer coefficient as the heat transfer in flue gas side is limiting, and therefore,

$$(UA)_e = a_e W_{flue}^{\ b_e} \tag{5.8}$$

The modelling equations for the generating tubes can be derived by lumping two cross-flow heat exchangers into a single cross-flow heat exchanger. Since the temperature of the steam/water mixture in the generating tubes is assumed to be uniform, the log mean temperature driving force can be simplified further as shown in (5.9),

$$Q_{gt} = (UA)_{gt}\left(\frac{T_{g,f} + T_{g,gt}}{2} - T_{gt}\right) \tag{5.9}$$

where $T_{g,f}$ and $T_{g,gt}$ are the flue gas temperature entering and leaving the generating tubes, T_{gt} is the temperature of saturated steam/water mixture in the generating tubes, and Q_{gt} and $(UA)_{gt}$ are the heat transfer and overall heat transfer coefficient, respectively. The overall heat transfer coefficient can be calculated from the flue gas flow rate using the following equation, as the resistance of heat transfer is dominant at the flue gas side.

$$(UA)_{gt} = a_{gt} W_{flue}^{\ b_{gt}} \tag{5.10}$$

The model for heat transfer in the riser tubes can be simplified by neglecting the convective heat transfer at the flue gas side, as radiation heat transfer is the dominant mode of heat transfer. Therefore, the modelling equations for the riser tubes are given as follow,

$$Q_r = (UA)_{out,r}(T_{g,f} - T_{w,r}) \tag{5.11}$$

$$(UA)_{out,r} = h_{out,r,rad}\varepsilon A_r \tag{5.12}$$

where $T_{g,f}$ is the gas temperature in the furnace, $T_{w,r}$ is the wall temperature of the riser tubes, and $h_{out,r,rad}$ is the radiative heat transfer coefficient which can be estimated using the same method as in the detailed model.

Each pass in the superheater tubes is modelled as a lumped heat exchanger. The overall heat transfer coefficient is estimated from the flue gas flow rate as heat transfer in flue gas side is limiting. Therefore, the modelling equations are simplified as follows,

$$Q_{sh}(j) = (UA)_{sh}\left(T_{g,f} - \frac{T_{sh}(j-1) + T_{sh}(j)}{2}\right) \qquad j = 1, 2, 3, 4 \tag{5.13}$$

$$(UA)_{sh} = a_{sh} W_{flue}^{\ b_{sh}} \tag{5.14}$$

where $T_{sh}(j)$ is the temperature of steam in j^{th} pass superheater tubes.

5.3.2 Empirical Efficiency Curve Model

Boiler network optimization using an empirical efficiency curve model is a common practice in industrial applications. Each boiler has its own efficiency curve as a function of steam load. There are various factors affecting the boiler efficiency [Dukelow, 1985; Dukelow, 1991; Payne, 1985]. One of them is the design of the boiler. Boilers with auxiliary heat recovery heat exchangers have a higher efficiency. Operating variables, such as air/fuel ratio, flue gas temperature, blowdown flow rate and heating value of fuel, can also have a significant effect on the boiler efficiency. During boiler operation, soot builds up on the tube wall of the heat exchangers and lowers the boiler efficiency.

Commonly used methods for estimating the boiler efficiency are input-output method and input-loss method [Dukelow, 1985; Dukelow, 1991; Payne, 1985]. These methods are the standard boiler efficiency calculation recommended by ASME, and the procedure for the calculation using the ASME standard form can be found in Dukelow (1991) and Payne (1985). In input-output method, efficiency is estimated directly from the heat added to the feed water and energy input to the boiler from the combustion of fuel. Heat absorbed by feed water can be calculated from the flow rates of steam and

blowdown, and the enthalpies of steam, feed water and blowdown determined from the corresponding temperature measurements. Energy input to the boiler is calculated from the fuel flow rate and heating value. Boiler efficiency is simply equal to the ratio of the calculated heat added to incoming water and the energy input to the boiler from fuel. In input-loss method, individual losses expressed as a percentage of total energy input are first calculated and totalized, and the boiler efficiency is obtained by subtracting the total losses by 100 %. Various losses include sensible heat losses in dry flue gas and water vapor in combustion air and fuel, latent heat losses from water in fuel and water formed by combustion of hydrogen, heat loss from unburned fuel and radiation loss. These losses are estimated from the temperature and flow measurements. Although input-output method is easy to understand, boiler efficiency estimated by input-output method is very sensitive to inaccuracies in the measurements, and input-loss method is often preferred as it is more reliable [Green and ai-Shalkh, 1980].

The efficiency curve as a function of steam load depends on the boiler design and operating conditions. Often, the shape of the efficiency curve has a maximum when the steam load is varied. At high steam load, more energy is required to produce superheated steam. Although the high flue gas velocity increases the heat transfer coefficients, the flue gas temperature exiting the boiler increases. This increased loss to the environment results in a lower efficiency. Towards low boiler capacity, excess air has to be increased to generate turbulent mixing of fuel and air [Dukelow, 1991]. Part of the heat is wasted in heating the excess air. In additional, radiation loss is more important towards low steam load. Therefore, boiler efficiency decreases when the steam load is decreased. Boiler efficiency curve without a maximum is not uncommon with the shape of the efficiency curve monotonic increasing or decreasing.

Typically, a boiler efficiency curve as a function of steam load is fitted by a second order polynomial [Green and ai-Shalkh, 1980; Koninckx, 1988]. The optimization problem is given as follows,

$$\text{maximize} \quad \frac{\sum_{j=1}^{N_{boiler}} F_{steam,j}\eta_j}{\sum_{j=1}^{N_{boiler}} F_{steam,j}} \tag{5.15}$$

$$\text{subject to} \quad \eta_j = A_j + B_j F_{steam,j} + C_j F_{steam,j}^2 \quad j = 1, 2, .., N_{boiler}$$

$$D = \sum_{j=1}^{N_{boiler}} F_{steam,j}$$

where η is the boiler efficiency and N_{boiler} is the number of boilers. The parameters in the efficiency curve model, A_j, B_j and C_j, are updated from the measured boiler efficiency and steam flow rate. The optimum steam allocation is determined by solving (5.15) using the updated parameters.

5.4 Boiler Network Case Study Descriptions

This section describes the boiler network and disturbance scenarios for the case study. The boiler network and the steam header pressure control system are discussed first. The efficiency curves for the boilers at the base case operating conditions defined in Appendix D are then described. Finally, various disturbance scenarios are discussed for the evaluation of the RTO performances using different modelling approaches in this case study.

5.4.1 Boiler Network

Different boilers supply steam to a common steam header for distributing the steam to other units of the chemical plant. These boilers can have different performance or efficiency depending on the boiler design and operating conditions. A tremendous

saving in energy cost can be achieved by distributing the demand to different boilers to minimize the energy cost or maximize the overall boiler network efficiency. Typically, the energy cost is about $4/Mbtu. A 0.5 % improvement in boiler efficiency can yield about $120,000/year saving in energy cost for the boiler network in this case study.

The boiler network used in this case study is shown in Figure 5.3. The optimization variables are the steam production rate in each boiler expressed as the percentage or fraction of the steam demand denoted by R in Figure 5.3. Once the ratio, R, is set by the optimizer, the steam header pressure controller will adjust the fuel flow rate to each boiler to generate the corresponding steam production rate.

In this case study, the flow rate of coke oven gas is fixed at 120 kscfh which is the minimum coke oven gas flow rate for the boiler operation. This coke oven gas flow rate corresponds to less than 20 % of the heat duty. Blast furnace gas is adjusted to achieve the desired steam load.

5.4.2 Boiler Efficiency Curves at the Base Case Operating Conditions

The steady-state efficiency curves as a function of steam load for the boilers at the base case operating conditions described in Appendix D are shown in Figure 5.4. The difference in the efficiency curves results from the different boiler designs.

At low steam load, the boilers have similar efficiency. The flue gas flow rate is low and there is sufficient heat transfer area in the economizer and air preheater to recover the heat from the flue gas. The temperature of the flue gas can be kept at the setpoint. The stack losses are similar for different boilers at low steam load, and therefore, they have similar efficiency.

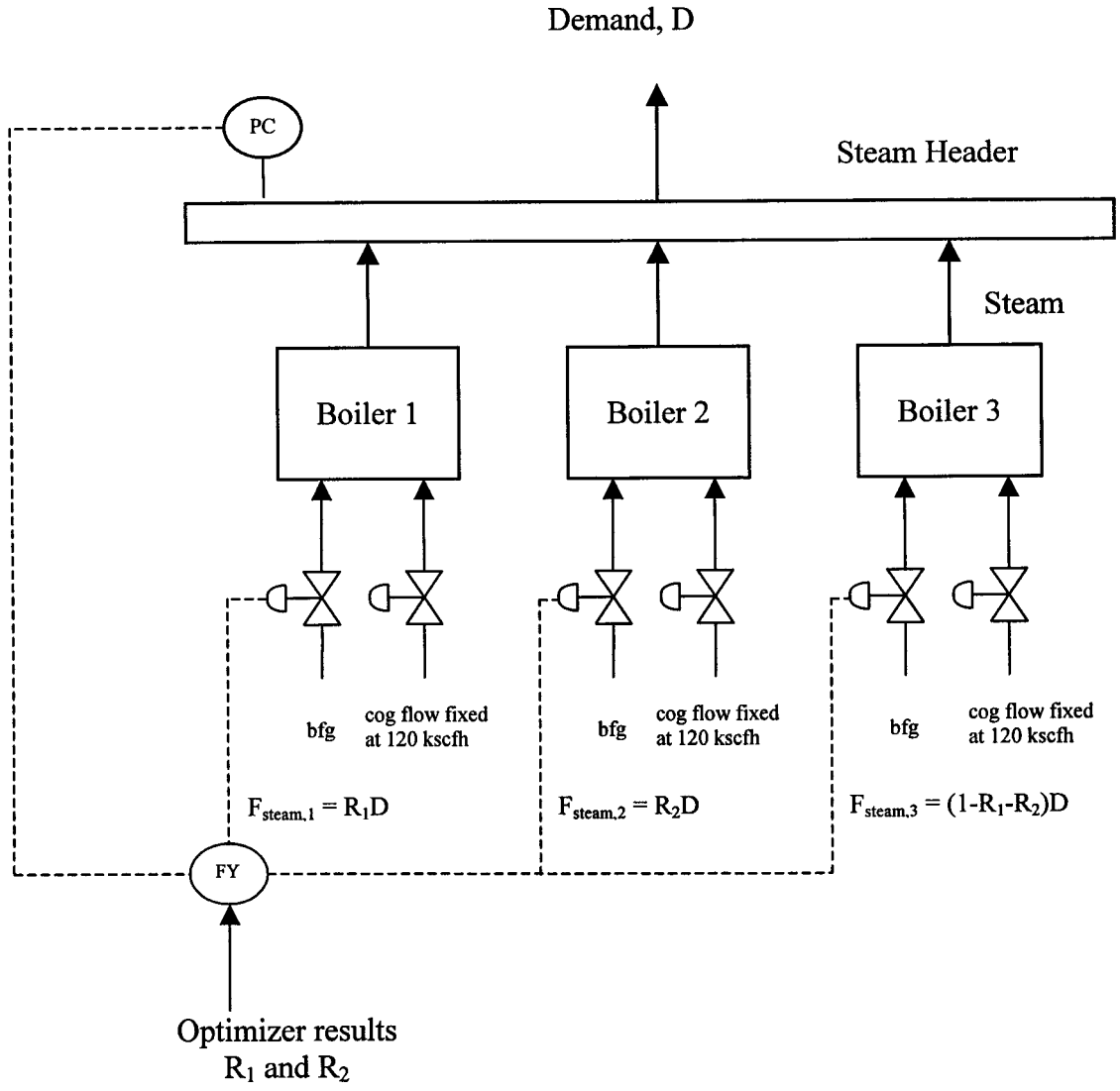

Figure 5.3 Boiler network

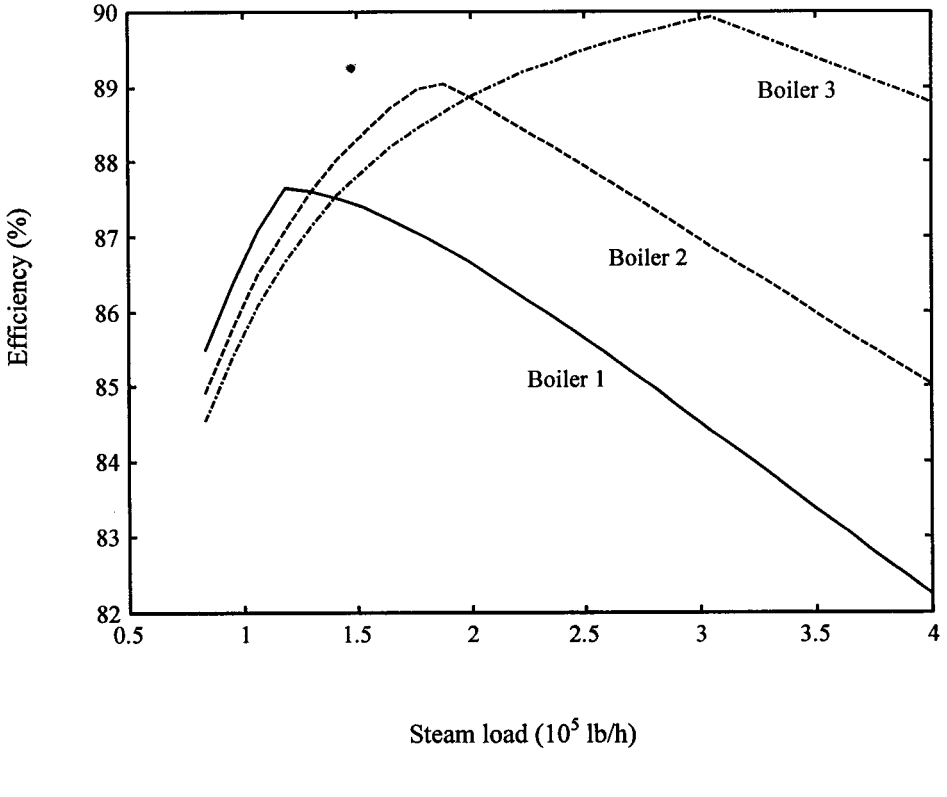

Figure 5.4 Boiler efficiency curve as a function of steam load

Towards high steam load, boilers with more heat recovery area in the economizer and air preheater have higher efficiency. The boiler has to exchange more heat in the riser and superheater for high steam load. Boilers with more heat exchanger area for heat recovery result in lower flue gas temperature and higher boiler efficiency.

There is a maximum in the efficiency curves for the boilers. At low steam load, a higher air/fuel ratio is required to achieve the higher setpoint for oxygen content in the flue gas shown in Appendix D [Dukelow, 1991]. Therefore, efficiency decreases towards low load because of larger sensible heat loss in the flue gas. At high steam load, higher gas temperature is required to exchange more heat in the riser and superheater. Less saturated steam will be taken from the steam drum to control the flue gas temperature at the setpoint. When the valve for manipulating the saturated steam flow is fully closed, the

flue gas setpoint cannot be achieved and the flue gas temperature is increased. The stack loss becomes higher causing a drop in boiler efficiency. The shape of the efficiency curve also depends on the operating conditions. The boiler efficiency can increase or decrease monotonically with steam load when there is a change in the fuel composition which is illustrated in the following section.

5.4.3 Disturbance Scenarios

The disturbances considered in evaluating the RTO performance in this case study include periodic changes in steam demand and fuel composition shown in Figure 5.5 and continuous fouling of heat exchangers. The disturbance frequency in steam demand and fuel composition changes is varied to investigate the capability of the RTO systems in tracking fast and slow disturbances. The size and frequency of the disturbances are summarized in Tables 5.2 and 5.3 for the demand change and fuel composition change in the blast furnace gas in boiler 3, respectively. Fuel composition change occurs in boiler 3 only because opportunity for optimization exists in this case study scenario. This could happen in the plant when different fuels are supplied to different boilers, and there is a change in fuel composition in one of the boilers only. The disturbance frequency is expressed as the number of RTO executions between successive step changes. For demand change, the fuel compositions are fixed at the base case values reported in Appendix D. For the disturbances in fuel composition and heat exchanger fouling, the demand is fixed at 6.5×10^5 lb/h.

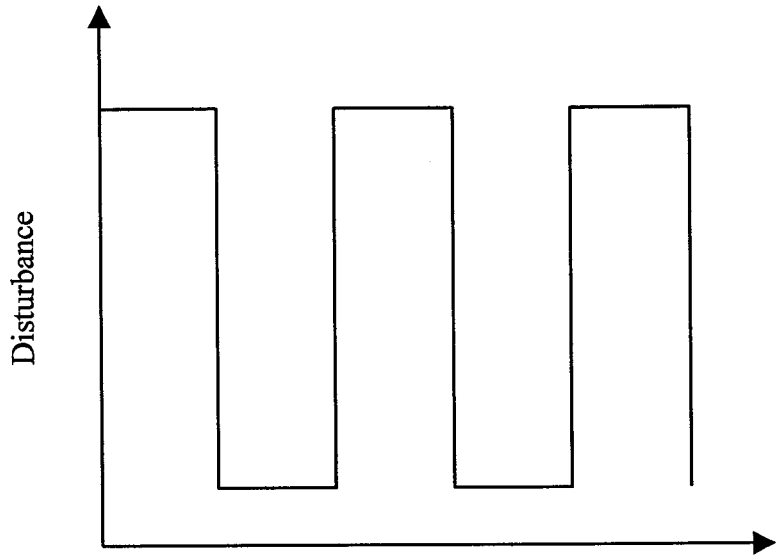

Figure 5.5 Disturbance scenario for demand and fuel composition changes

Disturbance sizes in demand change were designed to cause small and large changes in the optimum steam load in boiler 3. When the steam demand varies between 6.5 and 7.5 × 10^5 lb/h, the optimum steam load in boiler 3 (from 3.2 to 3.6 × 10^5 lb/h) is always in the region in which the efficiency curve has negative slope (Refer to Figure 5.4). On the other hand, when the demand is between 4.5 and 6.5 × 10^5 lb/h, the optimum steam load in boiler 3 (from 1.5 to 3.2 × 10^5 lb/h) varies between the load regions with positive and negative slope.

Table 5.2 Disturbance scenarios for demand change

Demand (10^5 lb/h)		**Disturbance frequency**	**Number of RTO executions simulated**
Minimum	**Maximum**		
4.5	6.5	10	100
4.5	6.5	20	100
4.5	6.5	50	200
6.5	7.5	10	100
6.5	7.5	20	100
6.5	7.5	50	200

Table 5.3 Disturbance scenarios for fuel composition change in the blast furnace gas in boiler 3

Variation in fuel composition				**Disturbance frequency**	**Number of RTO executions simulated**
Steady state 1		Steady state 2			
Volume fraction of CO	Volume fraction of CO_2	Volume fraction of CO	Volume fraction of CO_2		
0.19	0.15	0.09	0.25	10	100
0.19	0.15	0.09	0.25	20	100
0.19	0.15	0.09	0.25	50	200
0.14	0.20	0.27	0.07	10	100
0.14	0.20	0.27	0.07	20	100
0.14	0.20	0.27	0.07	50	200

A disturbance in fuel composition causes a change in the efficiency curve of the boiler. The changes in efficiency curve for the fuel composition disturbances described in Table 5.3 are illustrated in Figures 5.6. As shown in Figure 5.6a, the disturbance in fuel composition can change not only the absolute value of the efficiency but also the location of the maximum efficiency, i.e., the steam load at which the maximum occurs, in the efficiency curve. The fuel composition disturbance shown in Figure 5.6b has a profound change in the shape of the efficiency curve, in which it changes from having a maximum to monotonic increasing. The case studies designed for fuel composition disturbances enable the evaluation of the RTO performances for large changes in the boiler efficiency curve in the boiler being manipulated.

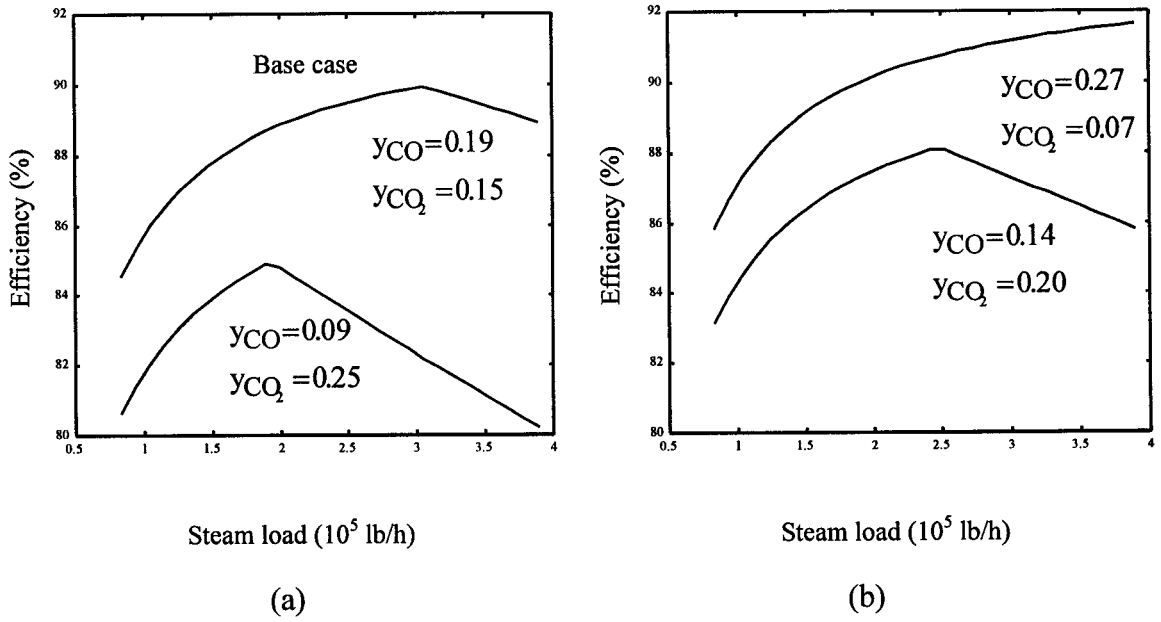

Figure 5.6 Change in the efficiency curve for a disturbance in fuel composition in blast furnace gas in boiler 3

Fouling of heat exchangers is caused by the deposition of soot on the tube walls in the flue gas side of the heat exchangers. The soot layer increases the thermal resistance and reduces the boiler efficiency. Fouling is simulated by a gradual increase in the fouling factors in different heat exchangers in the boiler model. In this case study, it is assumed that the heat exchangers in boiler 3 foul more rapidly compared to the fouling rate in boilers 1 and 2. This behavior would occur when one boiler is coal-fired boiler and the others are gas-fired boilers, and the heat exchangers in coal-fired boiler foul more rapidly. While this is not the case for this plant, it could occur in another plant. The fouling factors in the heat exchangers in boiler 3 increase linearly while the fouling factors in the heat exchangers in boilers 1 and 2 remain constant at 0. The RTO system is simulated for 200 RTO executions and the fouling factors for boiler 3 after 200 RTO executions are reported in Table 5.4. These fouling factors cause a drop of up to 30 % in the overall heat transfer coefficients in the heat exchangers which can be caused by less than 1/8 inch of soot deposited on the tube walls [Dukelow, 1991]. The change in the efficiency curve is shown in Figure 5.7. At low steam load, the efficiency of the fouled boiler is even higher. When the heat transfer coefficients decrease, the gas temperature increases. Therefore, less saturated steam is taken from the steam drum to heat the incoming air in the steam coil for keeping the flue gas temperature at the setpoint. The increase in efficiency is the result of a smaller loss due to less saturated steam taken from the steam drum. At high steam load, the flue gas temperature cannot be controlled at the setpoint at 300 F even though no saturated steam is taken from the steam drum to heat the incoming air in the steam coil. Fouling in the heat exchangers causes the flue gas temperature to increase further resulting in higher stack loss. Therefore, the efficiency at high steam load is decreased after fouling of heat exchangers.

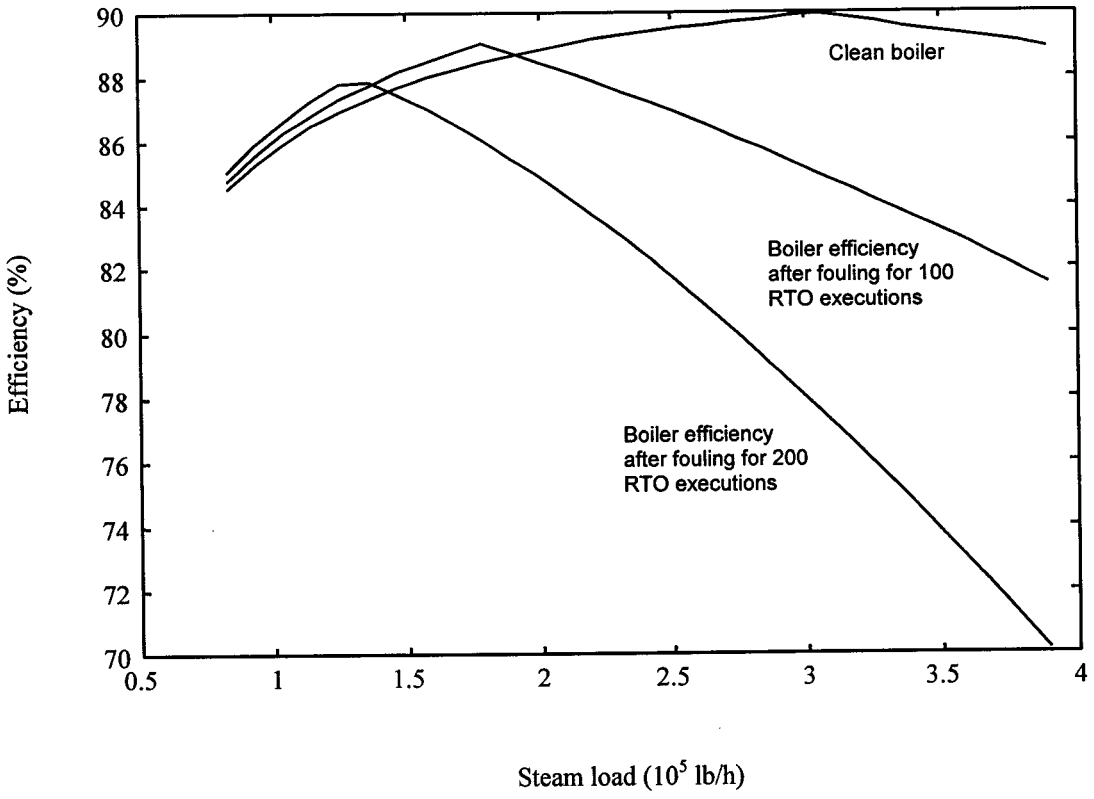

Figure 5.7 Efficiency curves for clean and fouled boiler

Table 5.4 Fouling factors of the heat exchangers in boiler 3

Heat Exchanger	Fouling Factor after 200 RTO executions
Air preheater	0.12
Economizer	0.06
Generating Tubes	0.08
Riser	0.08
Superheater	0.04

5.5 Strategies of the Closed-Loop Optimization of Boiler Network

The strategies of the closed-loop optimization of the boiler network case study using different optimization approaches are presented in this section. The optimization approaches investigated in this case study are the model-free direct search and two model-based methods. In the model-based methods, the RTO system discussed in Chapters 1 and 2 is implemented using two different models: the empirical efficiency curve model and simplified fundamental model described in Section 5.3. These optimization approaches require different sets of measurements taken from the plant for updating. The measurements required for different optimization approaches are shown in Table 5.5. The disturbance scenarios include high and low frequency variations in steam demand and fuel composition and slow decay in the heat transfer coefficients. The results analysis is turned off for better tracking of the fast changing disturbances.

5.5.1 Direct Search Method

A direct search method tracks the changing optimum by using the local derivative of the plant performance estimated from the plant data without using a rigorous model developed from fundamental theories. Therefore, direct search methods require online measurement of the plant performance, which is the boiler network efficiency in this case study. The plant is moved along the direction of improving performance, and the derivative is updated when a new data set is available after the plant movement.

The direct search method using steady-state measurements discussed in Bozenhardt (1986) is implemented for this case study. The plant performance is assumed to be a locally accurate linear function of the optimization variables as shown in (5.16),

$$P(\mathbf{x}) = P_0 + \mathbf{g}^T\mathbf{x} \tag{5.16}$$

Table 5.5 Measurements required for different optimization approaches

Measurement	Unit	Standard deviation of noise	Direct search and efficiency curve model	Fundamental model
Blowdown flow	klb/h	0.15	√	√
Feed water flow	klb/h	5.5		√
Water flow bypassing economizer	klb/h	2.25		√
Superheated steam flow to the header	klb/h	4.5	√	√
Saturated steam flow to the steam coil (two 10:1 flowmeters)	klb/h	0.15 and 0.015	√	√
Oxygen concentration in flue gas	volume %	0.01	√	√
Header pressure	psig	2	√	√
Lower heating value of blast furnace gas	btu/scf	1	√	
Lower heating value of coke oven gas	btu/scf	1	√	
Temperature of ambient air	F	3	√	√
Temperature of air entering east and west burners	F	3		√
Temperature of blast furnace gas	F	3	√	√
Temperature of coke oven gas	F	3	√	√
Temperature of feed water	F	3	√	√
Temperature of flue gas leaving generating tubes	F	3	√	√
Temperature of flue gas leaving economizer	F	3		√
Temperature of flue gas leaving air preheater	F	3		√
Temperature of feed water	F	3		√
Temperature of water leaving economizer	F	3		√
Temperature of superheated steam	F	3	√	√
Temperature of steam in steam drum	F	3	√	√
Volumetric flow rate of blast furnace gas entering east and west burners	kscfh	30	√	√
Volumetric flow rate of air entering east and west burners	kscfh	30		√
Volumetric flow rate of coke oven gas	kscfh	2	√	√

where P is the plant performance and **x** is the vector of optimization variables. P_0 and the elements in the vector **g** are the parameters in the model which are estimated from the plant data. These parameters are estimated by the least squares method [Draper and Smith, 1981] using the most recent data sets. The direction of the vector **g** is the direction of improving the plant performance. The plant is moved along that direction with a fixed step size, α, given in (5.17),

$$\mathbf{x}(N) = \mathbf{x}(N-1) + \alpha \frac{\mathbf{g}}{\|\mathbf{g}\|} \tag{5.17}$$

where N is the RTO execution. The gradient of plant performance, **g**, is normalized so that the change in the optimization variable is independent of the magnitude of the gradient. After the plant movement, the oldest data is removed and the newest data is accepted for the estimation of the parameters in the model in (5.16) for the next RTO execution.

The performance of the direct search method depends on the values of the tuning parameters which are the number of data sets for the estimation of the gradient of plant performance, and the step size for the plant movement. A large number of data sets can reduce the effect of stationary noise but slow down the tracking of the changing optimum. A smaller number of data sets can track the optimum quickly but the RTO system will be more sensitive to noise. The step size should be chosen large enough to have a measurable change in the plant performance but small enough to avoid excessive oscillation around the optimum.

The overall boiler network efficiency, which is to be maximized, is estimated online from the measurements taken from the boilers. The overall boiler network efficiency, η_o, is given in (5.18),

$$\eta_o = \frac{\sum_{i=1}^{N_{boiler}} F_{steam,i}\eta_i}{\sum_{i=1}^{N_{boiler}} F_{steam,i}} \tag{5.18}$$

where η_i is the efficiency of boiler i, and N_{boiler} is the number of boilers. In this case study, the boiler efficiency is estimated by the input-loss method [Dukelow, 1985; Dukelow, 1991; Payne, 1985] from the measurements reported in Table 5.5.

5.5.2 Model-Based Method using the Empirical Efficiency Curve Model

In the empirical efficiency curve model, a second order polynomial for approximating the boiler efficiency as a function of steam load is used for each boiler. The parameters for updating in the RTO system are the coefficients in the polynomials shown in (5.15). The parameters for updating do not have physical meanings. Therefore, the empirical efficiency curve model is accurate locally and cannot be extrapolated for large disturbances. The model is updated by the steam flow measurement and the boiler efficiency in each boiler estimated by the input-loss method using the measurements reported in Table 5.5. The updated model is optimized to determine the optimum steam allocation to the boilers.

Updating the parameters in the second order polynomial in the efficiency curve model requires multiple data sets at different steam loads. The strategy for updating without experimentation involves keeping a record of historical data and checking if the new data set is "different" from the historical data sets based on steam load. If the new data set is inside the data window defined by the historical data sets, it will not be accepted. Otherwise, the new data set is accepted and one data set at the boundary of the old data window is removed as illustrated in Figure 5.8. The model is estimated using the data in the data window and is valid within the operating region inside the data window.

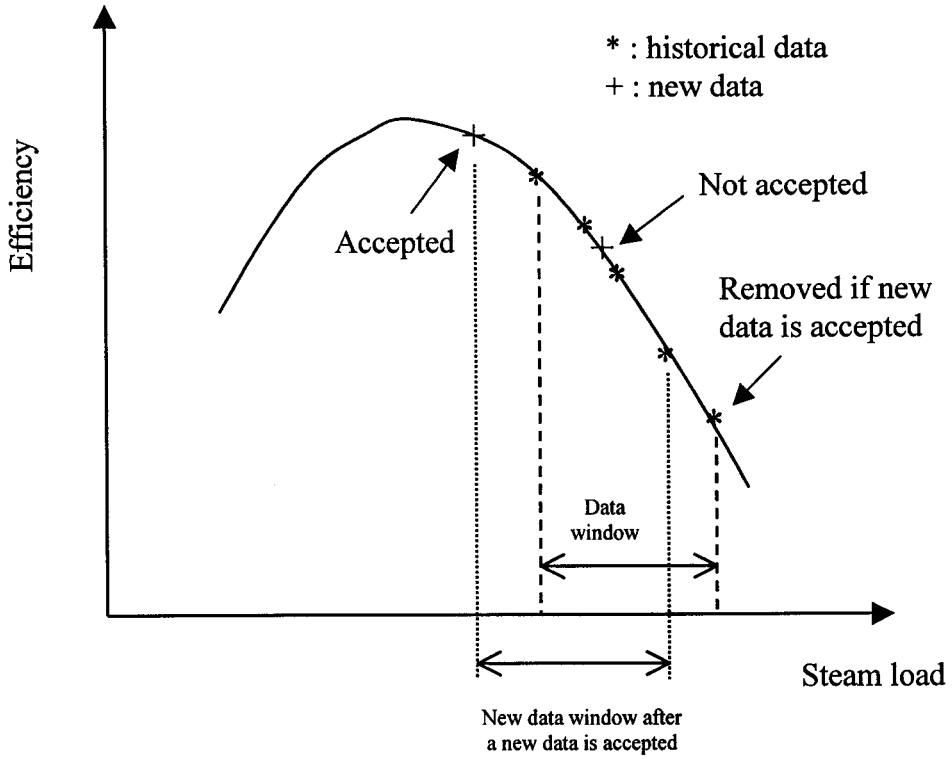

Figure 5.8 Strategy for accepting a new data for updating the efficiency curve model

The model using an updated efficiency curve is optimized subject to a "trust region" in which the approximated model is locally accurate. The trust region is required because the model is valid within the operating region defined by the data window. However, the trust region is defined to be larger than the data window as shown in Figure 5.9 for extrapolation. This extrapolation is required because if the model is optimized subject to the data window in which the model is valid, the optimum cannot be tracked. The model is assumed to be accurate over a small region extended from the region defined by the data window. The size of the trust region is defined by specifying δ which is the tuning parameter in this strategy. When the model optimum is reached, the data window will bracket the optimum.

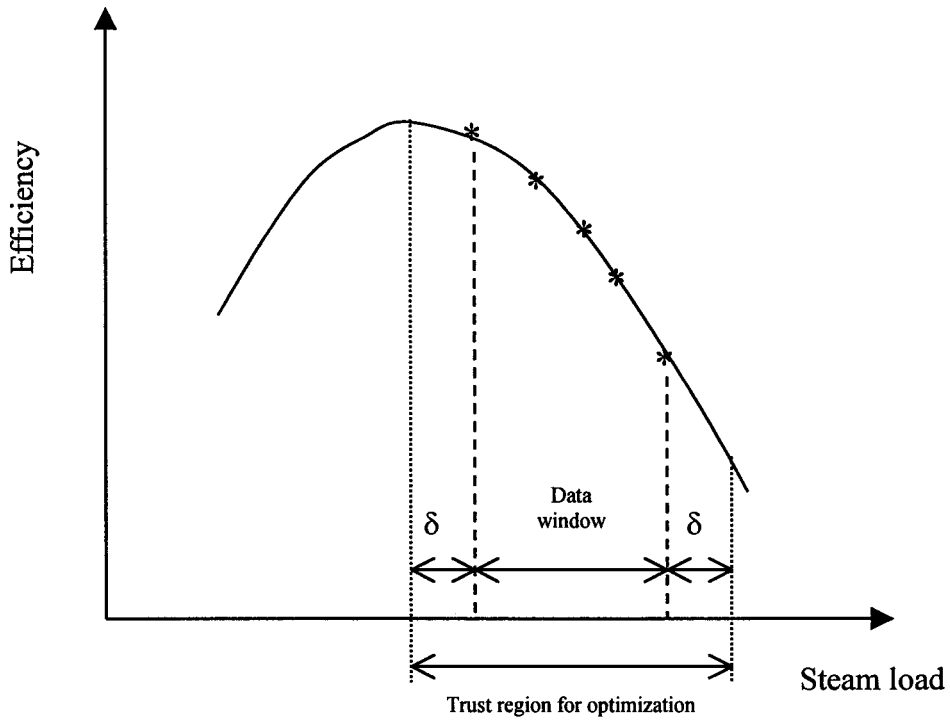

Figure 5.9 Strategy for optimization in the efficiency curve model

Periodic experimentation is required to update the empirical efficiency curve model when disturbances have occurred. As indicated in the previous section, the disturbances in fuel composition and heat exchanger fouling can change the shape of the boiler efficiency curve. Since the shape of the efficiency curve for each boiler is required for optimization, experiments are needed to generate new data sets for updating the parameters in the efficiency curve model after the disturbance has occurred.

Experimental design based on profit discussed in Chapter 4 is implemented to design plant experiments to generate new data sets for updating. This approach requires the knowledge of the occurrence of the disturbances. Process variables can be monitored to detect the presence of the disturbances. After the disturbance has been detected, the RTO system evaluates when to start experimentation and determines the experimental

operating conditions by solving the expected profit experimental design criterion stated in Problem 4.1 in Chapter 4.

A disturbance in fuel composition can be detected by monitoring the fuel flow rates since the disturbance changes the fuel heating value and hence the amount of fuel required to produce the steam. In this case study, it is assumed that *the time of occurrence* of the fuel composition disturbance is perfectly known although the change in average heating value is not known. Furthermore, the disturbance frequency is assumed to be known from the process experience, and the disturbance is modelled as a step disturbance for solving the expected profit experimental design criterion.

Heat exchanger fouling can be monitored by comparing the predicted and measured boiler network efficiency. During heat exchanger fouling, the actual boiler network efficiency deviates from the predicted efficiency as shown in Figure 5.10. When the difference between the predicted and measured network efficiency is larger than a threshold, experiments can be designed to update the efficiency curve of the fouled boiler. Although the boiler efficiency drops continuously for heat exchanger fouling, the disturbance is modelled as a step disturbance for the experimental design. The boilers will be operated for a long period of time (in the order of months) before shutdown for cleaning. The experimental design approach in Chapter 4 to design one set of experiments in such a long horizon can cause a significant loss in boiler efficiency because the experiments are not performed frequently for tracking the changing optimum. Multiple sets of experiments will be designed at the appropriate time if the experimental design is triggered by comparing the difference between the predicted and measured network efficiency with a threshold. The threshold is the tuning parameter for this method. The threshold should be large enough to avoid triggering experimental design too often, and it should be small enough to have frequent experimentation for tracking a changing optimum. The step change is assumed to occur when the deviation between the

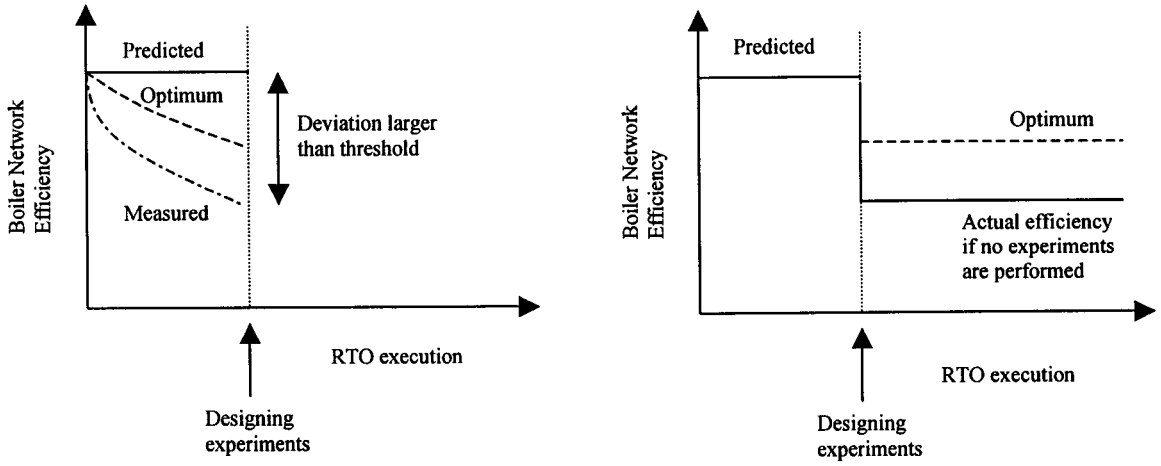

Actual disturbance

Modelled disturbance for the experimental design

Figure 5.10 Actual and modelled disturbance for heat exchanger fouling

predicted and measured efficiency is larger than the threshold which is shown in Figure 5.10.

In this case study, two experiments are designed using the expected profit experimental design approach. When updating the parameters in the second order polynomial in the efficiency curve model, three data sets at different steam load are required. Two experimental data sets and the data set taken from the plant when the disturbance has been detected are sufficient to estimate all the parameters in the efficiency curve model.

The expected profit experimental design criterion in Problem 4.1 is solved after the occurrence of the disturbance has been detected to determine when to start the experiment and the experimental operating conditions. The disturbance is assumed to be a step change, and the offset is assumed to be eliminated after performing plant

experiments. The reduced Hessian of the approximate profit surface is assumed to be equal to the current reduced Hessian estimated in the model-based optimizer.

After experimentation, the model is updated using the experimental data sets and the data set taken just before experimentation. The updated model is then optimized subject to the trust region based on the data sets. When the plant is approaching to the optimum, new data sets are generated for updating in the next RTO execution until the model optimum is reached. Experiments will be designed again when the next disturbance is detected.

5.5.3 Model-Based Method using the Simplified Fundamental Model

A fundamental model is accurate over a wide range of operation and might be able to track the changing optimum even for large disturbances. In this case study, the simplified fundamental model described in Section 5.3 is used in the RTO system. A single data set is used for updating, because experience shows that experimentation is not required for updating in this boiler network case study.

In the fundamental model, the updated parameters have physical meanings. These parameters are the heat transfer coefficients and heating value of fuel. In this case study, it is assumed that the dimensions of the tubes in the heat exchangers are perfectly known. Table 5.6 lists the parameters selected for updating using the data set taken from the plant. The values of the fixed parameters are reported in Table 5.7. The flow dependence of the heat transfer coefficients [Holman, 1992] is derived by assuming

$h_i \propto W^{0.8}$ for fluid flowing inside the pipes

and $h_o \propto W^{0.6}$ for fluid flowing across the pipes

Table 5.6 Adjustable parameters for updating the simplified fundamental model

Parameter	Description
$a_{in,ph}$	Coefficient in the heat transfer correlation for the flue gas side in air preheater in (5.4)
a_e	Coefficient in the overall heat transfer correlation in economizer in (5.8)
a_{gt}	Coefficient in the overall heat transfer correlation in generating tubes in (5.10)
a_{sh}	Coefficient in the overall heat transfer correlation in superheaters in (5.14)
ΔH_{bfg}	Lower heating value of blast furnace gas in btu/scf

Table 5.7 Values of the fixed parameters in the simplified fundamental model

Parameter	Description	Value of the Parameter		
		Boiler 1	Boiler 2	Boiler 3
$a_{out,ph}$	Heat transfer correlation in the air side of air preheater in (5.5)	184.4	250	250
$b_{out,ph}$	Heat transfer correlation in the air side of air preheater in (5.5)	0.6	0.6	0.6
$b_{in,ph}$	Heat transfer correlation in the flue gas side of air preheater in (5.4)	0.8	0.8	0.8
b_e	Overall heat transfer correlation in the economizer in (5.8)	0.6	0.6	0.6
b_{gt}	Overall heat transfer correlation in the generating tubes in (5.10)	0.6	0.6	0.6
b_{sh}	Overall heat transfer correlation in the superheaters in (5.14)	0.6	0.6	0.6
ε	Emissivity of the riser tubes in (5.12)	0.6	0.6	0.6
ΔH_{cog}	Lower heating value of coke oven gas in btu/scf	417.7	417.7	417.7

The parameter, $a_{out,ph}$, is not updated because the heat transfer resistances in the air and flue gas sides in the air preheaters are similar, and both $a_{out,ph}$ and $a_{in,ph}$ cannot be updated with the plant data. The heating value of coke oven gas is calculated from the heating values of the fuel components and the fuel composition at the base case.

Updating the heat transfer coefficients in the heat exchangers require the temperature measurements of the fluids entering and leaving the heat exchangers. Therefore, extra measurements for flow and temperature are required compared to updating the empirical efficiency curve model as reported in Table 5.5. These sensors have actually been installed in Dofasco's boiler for monitoring purpose.

Fuel heating value measurement is not required for the RTO system using the simplified fundamental model as reported in Table 5.5. The lower heating value of coke oven gas is fixed and the lower heating value of blast furnace gas is updated from the measurements taken from the plant for correcting the disturbance in fuel composition.

5.6 Case Study Results and RTO Performance Evaluation

The RTO system with three optimization approaches was applied to the boiler network in Figure 5.3 for the disturbance scenarios discussed in the previous sections. The RTO performances are compared based on actual boiler network efficiency attained by the plant (detailed fundamental model) and the magnitude of change in steam loads, ΔF. The magnitude of the change in steam loads is expressed as the sum of the change in steam loads between successive RTO executions for all the boilers as stated in (5.19),

$$\Delta F = \left(\sum_{i=1}^{N_{boiler}} \left(F_{steam,i}(N) - F_{steam,i}(N-1) \right)^2 \right)^{\frac{1}{2}} \tag{5.19}$$

where $F_{steam,i}$ is the steam load in boiler i, N_{boiler} is the number of boiler and N is the RTO execution. Recall that the ratios of the steam demand are the optimization variables. ΔF is not the variable manipulated by the optimizer. Since ΔF is calculated from the steam loads in the boilers which have the same units and maximum loads, scaling of the variables is not required in (5.19).

The step size for the direct search method and the trust region size for the empirical efficiency curve method have to be specified. The step size for the direct search method was selected to be 0.1 klb/h. In the efficiency curve model, the trust region was defined by expanding the data window by 30 klb/h from the lower and upper steam loads in the data set. No trust region was used in the RTO system using the fundamental model. These tuning values were used in the results presented in Sections 5.6.1 – 5.6.3. The effects of the tuning parameters on the RTO performances are investigated in Section 5.6.4. Five data sets were used for parameter estimation in both the direct search method and model-based method using the efficiency curve model.

The case studies involve several disturbance scenarios at different disturbance frequencies. For each disturbance scenario, the presentation of the results begins with the plots of the boiler network efficiency attained and the histograms of the magnitudes of change in steam loads. Then, tabulations summarizing the results are presented for comparing the RTO performances using different optimization approaches.

5.6.1 Disturbance in Demand

The RTO performances for a periodic disturbance change in steam demand varying between 4.5 and 6.5 $\times$ 10^5 lb/h are shown in Figures 5.11 and 5.12, respectively. Comparison of the RTO performances is reported in Table 5.8.

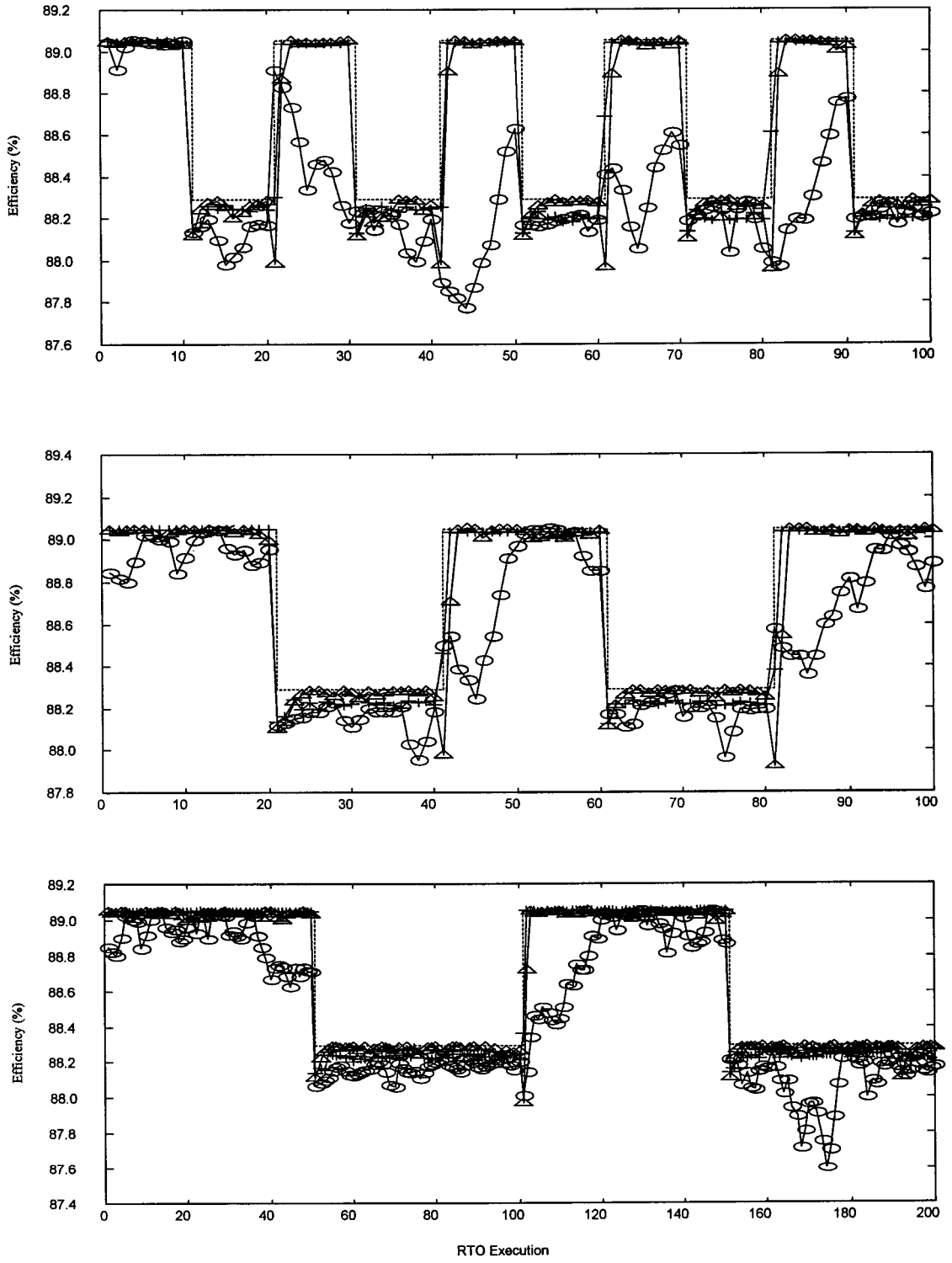

Figure 5.11 Boiler network efficiency attained for a demand change between 4.5 and 6.5 $\times 10^5$ lb/h (o : direct search, + : efficiency curve model, Δ : fundamental model, -- : true optimum)

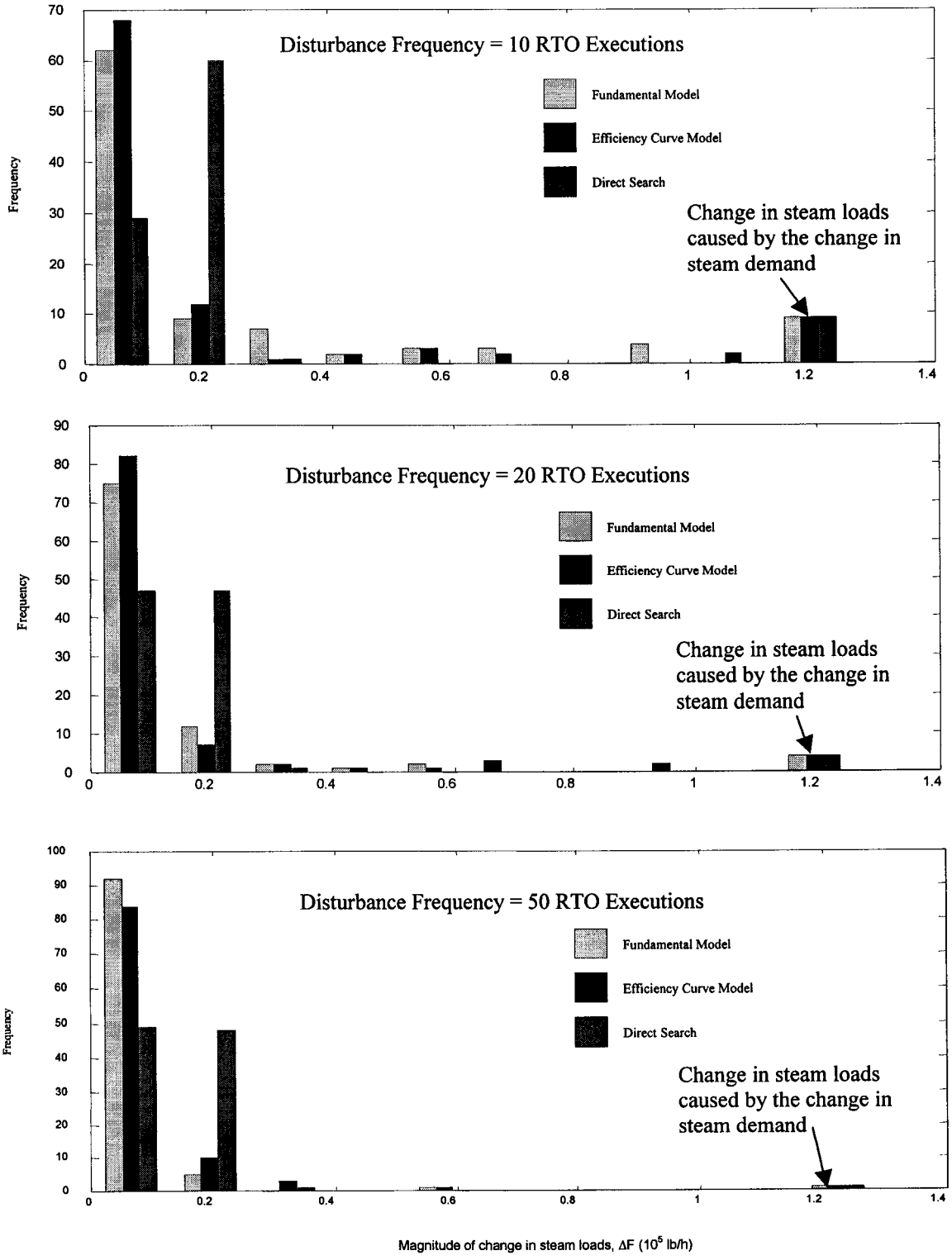

Figure 5.12 Distribution of the magnitude of change in steam loads for demand change between 4.5 and 6.5 × 10^5 lb/h

Table 5.8 Comparison of the RTO performances for a disturbance change in demand between 4.5 and 6.5 × 10^5 lb/h

Modelling Approach	Average efficiency attained (%) for different disturbance frequency			Remarks
	10	20	50	
Direct Search	88.32	88.55	88.45	• Large loss during tracking • Could not track fast disturbance • Lot of intermediate changes in steam loads ($\Delta F < 0.3 \times 10^5$ lb/h)
Efficiency Curve Model	88.60	88.70	88.64	• Could track optimum at different frequencies • Small changes in steam loads ($\Delta F < 0.1 \times 10^5$ lb/h) responding to measurement noise • Occasional large changes in steam loads ($\Delta F = 0.3$ to 1×10^5 lb/h) expanding the data window and trust region for optimization • Occasional large changes in steam loads ($\Delta F = 0.3$ to 1×10^5 lb/h) resulting in better tracking of fast disturbance
Fundamental Model	88.59	88.69	88.64	• Could track optimum at different frequencies • Small changes in steam loads ($\Delta F < 0.1 \times 10^5$ lb/h) responding to measurement noise • Occasional large changes in steam loads ($\Delta F = 0.3$ to 1×10^5 lb/h) resulting in better tracking of fast disturbance
Maximum Average Efficiency*	88.67	88.75	88.67	

* The disturbance caused a 0.76 % change in the optimum network efficiency (varied between 88.29 % and 89.05 %). For the direct search method, there was a difference of 1 % between the efficiency attanined and the optimum efficiency during the transient. Although the average efficiency was close to the maximum attainable average efficiency, the difference during the transient was significant.

The RTO systems using the fundamental model and empirical efficiency curve model tracked the changing optimum better for the disturbance in steam demand at different frequencies. The fundamental model is accurate over a wide range of operation, and the optimum can be reached in a few steps. Therefore, using the fundamental model, the RTO system could track the fast changing optimum responding to fast change in demand. The empirical efficiency curve model requires multiple data sets at different steam load for updating the model. If the data window contains data sets with sufficient variation in steam load, the updated model can predict the boiler efficiency over a wider range of operation, and therefore, the RTO system using the empirical efficiency curve model also performed well for fast disturbance in demand.

The RTO system using the direct search method could not track the changing optimum well, and there was a significant loss in boiler efficiency during tracking. The gradient of profit is estimated from the plant data by fitting a linear model. This linear model is accurate locally, and a small step size is chosen to avoid excessive extrapolation of the locally valid linear model. Sometimes, the optimizer moved the plant in the wrong direction for tracking the optimum immediately after the disturbance change. Since five data sets were used in the simulation, it took five RTO executions to forget all the old data sets after the disturbance change before finding the right direction to improve the boiler network efficiency. Therefore, the direct search method requires more steps to reach the optimum. It is shown in Figure 5.11 that the direct search method could reach the optimum for slow disturbance frequencies. Even though the optimum could be reached, there was a significant loss in boiler efficiency during the transient because the direct search method took longer time to reach the optimum. For fast disturbance, the direct search method could not even reach the optimum causing a large loss in boiler efficiency.

The direct search method tracked the optimum better when the demand was decreased from 6.5×10^5 lb/h to 4.5×10^5 lb/h; in contrast, it took more steps to track the

optimum when the demand was increased from 4.5×10^5 lb/h to 6.5×10^5 lb/h. When the demand is equal to 4.5×10^5 lb/h, the profit contours are relatively flat, and the loss in efficiency due to offset may not be large. However, when the demand is 6.5×10^5 lb/h, the profit contours are steeper and a small offset can cause a significant loss in boiler efficiency. This is illustrated in Table 5.9. When the boiler loads are originally maintained at a ratio corresponding to the optimum allocation at a demand of 6.5×10^5 lb/h, after a change in demand from 6.5×10^5 lb/h to 4.5×10^5 lb/h, the boiler network can still achieve an efficiency of 88.13 %, which is close to the optimum boiler efficiency of 88.29 %. For a demand change from 4.5×10^5 lb/h to 6.5×10^5 lb/h, if the steam loads are maintained at the optimum ratio at the demand of 4.5×10^5 lb/h, there is a 1 % efficiency loss. Therefore, the efficiency loss during transition when the demand was changed 4.5×10^5 lb/h to 6.5×10^5 lb/h was more significant.

Table 5.9 Boiler efficiency as a function of steam allocation

Demand (10^5 lb/h)	**Optimum steam allocation**	**Optimum boiler efficiency (%)**	**Steam allocation**	**Boiler efficiency attained (%)**
4.5	26.1% in boiler 1 40.8% in boiler 2 33.1% in boiler 3	88.29	21.9% in boiler 1 28.8% in boiler 2 49.3% in boiler 3	88.13
6.5	21.9% in boiler 1 28.8% in boiler 2 49.3% in boiler 3	89.05	26.1% in boiler 1 40.8% in boiler 2 33.1% in boiler 3	87.99

The distributions of the magnitudes of change in steam loads, ΔF, are shown in Figure 5.12. The change at a magnitude of 1.2×10^5 lb/h was caused by the step change in the total steam demand, and the changes at other magnitudes resulted from the implementation of the results from the optimizer, which adjusted the ratios of this demand per boiler. In the direct search method, most of the changes in steam loads had

small magnitudes ($\Delta F < 0.3 \times 10^5$ lb/h) because a small step size was chosen to avoid extrapolation of the linear model fitted by the plant data. These small changes slowed down the tracking of the changing optimum. In the model-based approach, occasionally, there were large changes in steam loads ($\Delta F = 0.3$ to 1×10^5 lb/h) which were the optimizer prediction after the disturbance change. These large changes in steam loads enabled the tracking of the fast changing disturbance. There were also a lot of small changes in steam loads ($\Delta F < 0.1 \times 10^5$ lb/h) in the model-based RTO systems. These small changes were caused by the propagation of the measurement noise to the optimizer results because the results analysis was turned off in this case study.

The RTO performances for a periodic disturbance change in demand varying between 6.5 and 7.5×10^5 lb/h are shown in Figures 5.13 and 5.14, and Table 5.10. The results were similar to the disturbance scenario of a demand change varying between 4.5 and 6.5×10^5 lb/h. In this case study scenario, the disturbance size did not cause a large change in the optimum efficiency. The change in the optimum efficiency was only 0.5 %. Although some variability was observed in the efficiency attained using the direct search method, the variability did not cause a significant loss in the efficiency compared to the likely accuracy of the estimated boiler efficiency using the measurements.

Table 5.10 Comparison of the RTO performances for a disturbance change in demand between 6.5 and 7.5×10^5 lb/h

Modelling Approach	**Average efficiency attained (%) for different disturbance frequency (number of RTO executions between successive step changes)**		
	10	20	50
Direct Search	88.72	88.77	88.66
Efficiency Curve Model	88.80	88.85	88.80
Fundamental Model	88.79	88.84	88.79
Maximum Average Efficiency	88.80	88.85	88.81

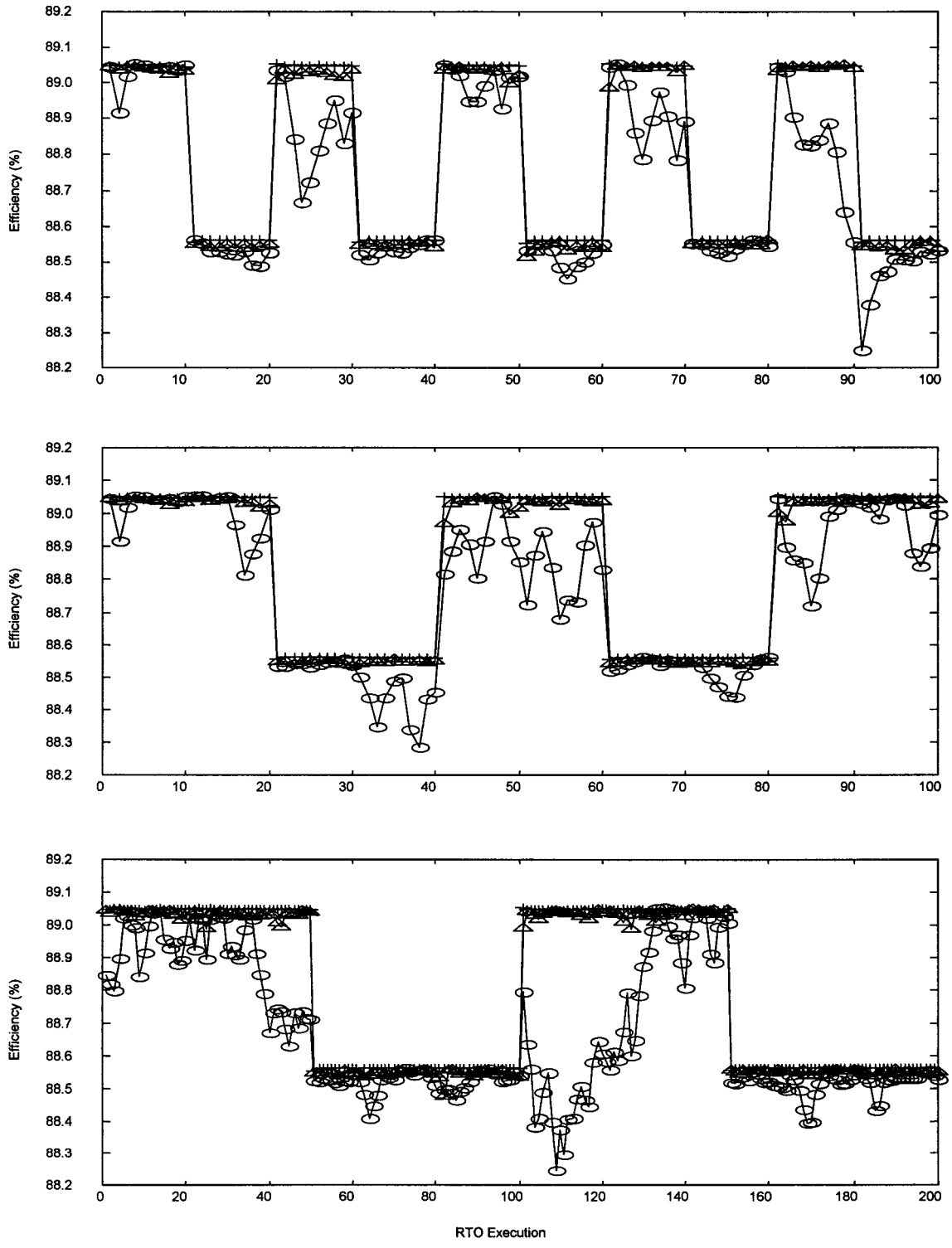

Figure 5.13 Boiler network efficiency attained for a demand change between 6.5 and 7.5 $\times 10^5$ lb/h (o : direct search, + : efficiency curve model, Δ : fundamental model, -- : true optimum)

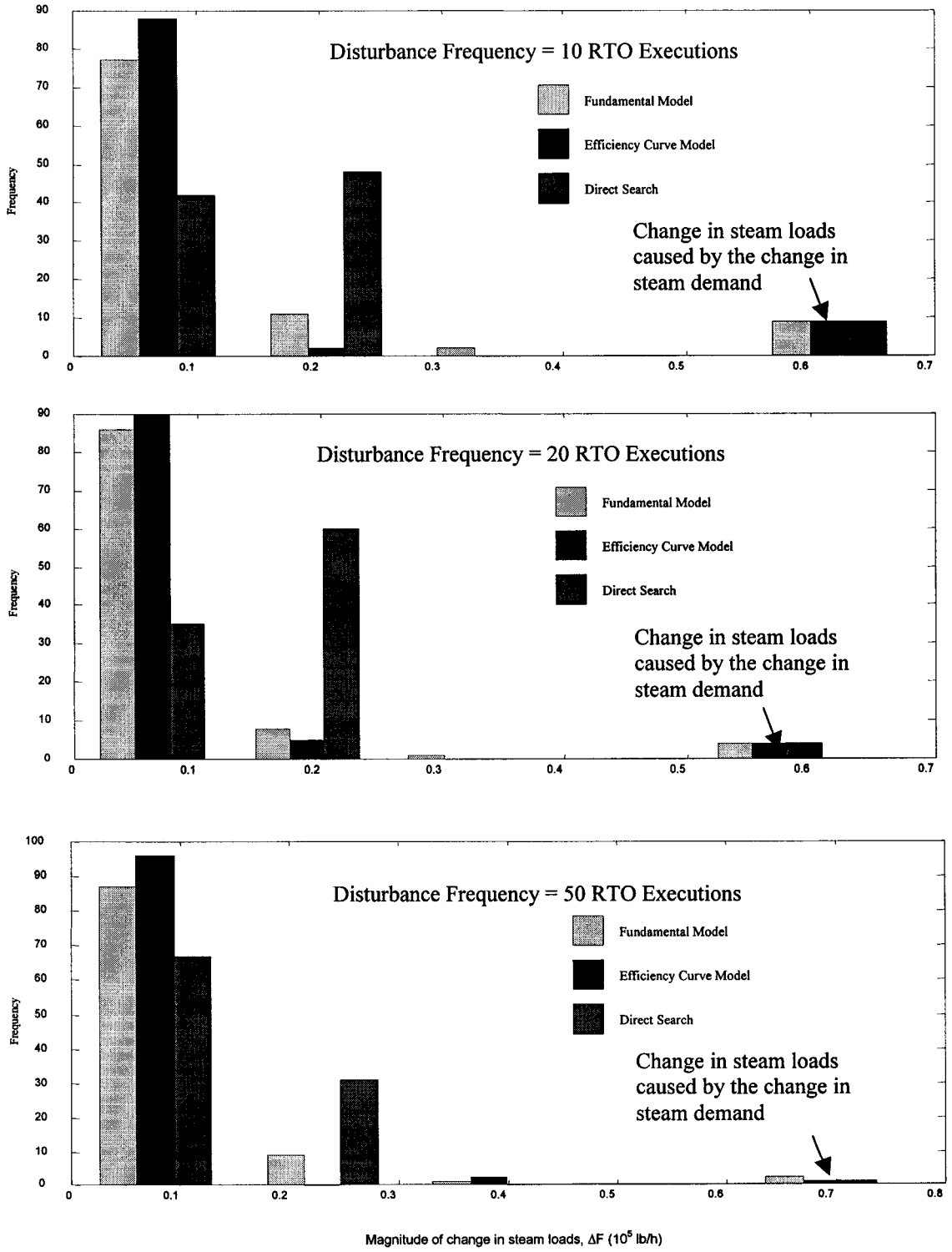

Figure 5.14 Distribution of the magnitude of change in steam loads for demand change between 6.5 and 7.5 × 10^5 lb/h

5.6.2 Disturbance in Fuel Composition

Disturbance in fuel composition can change the heating value and density of the fuel. Therefore, the shape of boiler efficiency curve changes when there is a change in the fuel composition. The RTO system using the fundamental model updates the fuel heating value for correcting the disturbance in fuel composition. When the efficiency curve model is used, experiments are required after the disturbance change to generate new data sets for updating the parameters in the polynomial efficiency model. The direct search method tracks the optimum based on the available plant data for estimating the profit gradient. There is a change in fuel density for a disturbance in fuel composition. In the following case study results, it is assumed that the fuel flow meter measured the volumetric flow rate based on the fuel density at the base case reported in Appendix D, i.e., the orifice meter does not have online density correction. When the fuel composition is not the same as the base case, there is a bias in the measurement of fuel volumetric flow rate, and the mismatch due to this measurement bias is corrected in the model updater.

The RTO performances measured by the boiler network efficiency attained and magnitude of plant movement for a periodic ±10 % change (absolute value) in the CO and CO_2 contents in blast furnace gas (the first three cases in Table 5.3) are shown in Figures 5.15 and 5.16, respectively. In these case study scenarios, the change in the efficiency curve after a disturbance change is shown previously in Figure 5.6a. The efficiency curves always have a maximum in these case study scenarios. Comparison of the RTO performances is reported in Table 5.11.

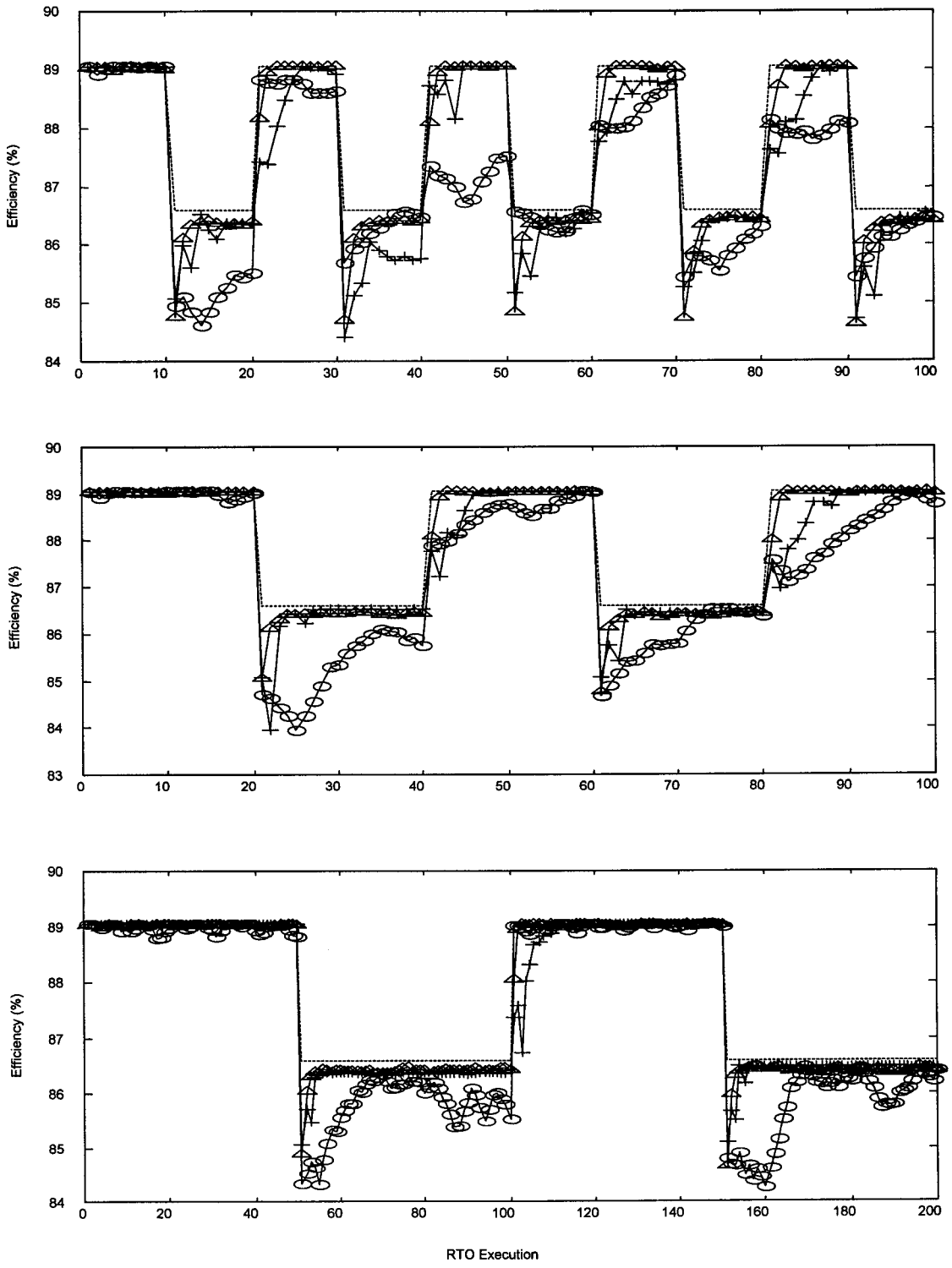

Figure 5.15 Boiler network efficiency attained for a ±10% change in CO and CO_2 contents in blast furnace gas in boiler 3 (o : direct search, + : efficiency curve model, Δ : fundamental model, -- : true optimum)

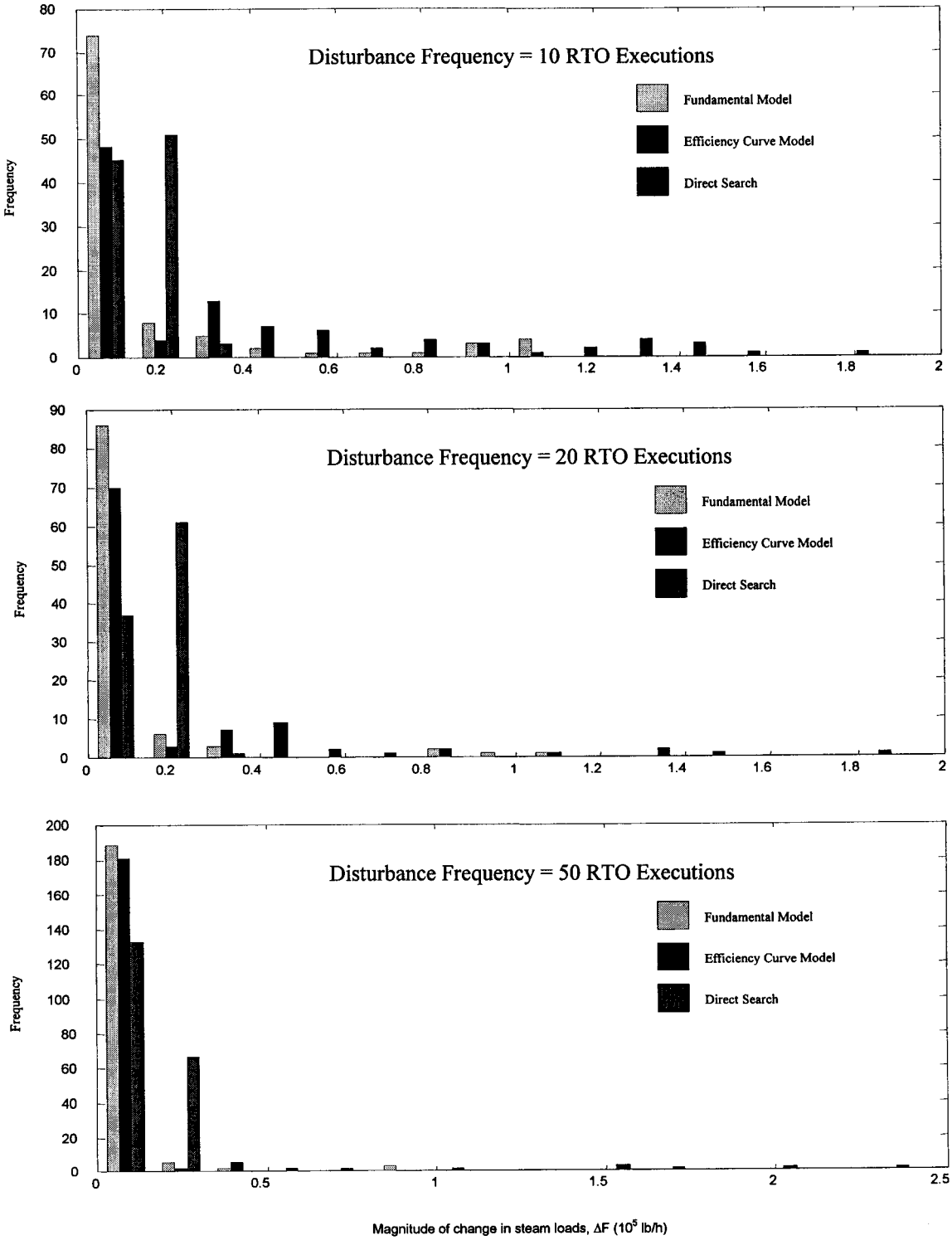

Figure 5.16 Distribution of the magnitude of change in steam loads for a ±10% change in CO and CO_2 contents in blast furnace gas in boiler 3

Table 5.11 Comparison of the RTO performances for a ±10% change in CO and CO_2 contents in blast furnace gas in boiler 3

Modelling Approach	Average efficiency attained (%) for different disturbance frequency			Remarks
	10	20	50	
Direct Search	87.10	87.38	87.34	• Large loss during tracking • Could not track fast disturbance • Lot of small changes in steam loads ($\Delta F < 0.3 \times 10^5$ lb/h) • Heating value measurement required
Efficiency Curve Model	87.34	87.81	87.66	• Large loss during tracking • Could not track fast disturbance • Large changes in steam loads ($\Delta F > 1 \times 10^5$ lb/h) during experimentation • Small changes in steam loads ($\Delta F < 0.1 \times 10^5$ lb/h) responding to measurement noise • Heating value measurement required
Fundamental Model	87.57	87.93	87.70	• Could track optimum at different frequencies • Small changes in steam loads ($\Delta F < 0.1 \times 10^5$ lb/h) responding to measurement noise • Occasional intermediate changes in steam loads ($\Delta F = 0.3$ to 1×10^5 lb/h) for tracking fast disturbance • Heating value updated from all the available flow and temperature measurements
Maximum Average Efficiency*	87.82	88.07	87.82	

* The disturbance caused a 2.46 % change in the maximum network efficiency (varied between 86.59 % and 89.05%). There was a more than 2 % difference between the attained efficiency and maximum network efficiency during tracking for the direct search method and during experimentation for using the empirical efficiency curve model. This difference during tracking was significant.

The RTO system using the fundamental model was able to track the changing optimum responding to the disturbance in fuel composition at different frequencies. The fundamental model, which was accurate over a wide range of operation, was able to predict the boiler performance even if there was a large disturbance change in fuel composition. It took only a few steps to reach the optimum after the disturbance change which is especially advantageous for tracking high frequency disturbances.

The RTO system using the empirical efficiency curve model with experimentation required more steps to reach the optimum compared to the RTO system using the fundamental model. Experiments were performed immediately after the step disturbance change which was determined by solving the expected profit approach in experimental design. During experimentation, there was a loss in boiler network efficiency. The optimum may not be reached immediately after the experimentation because the trust region defined from the data window restricted the plant movement. The efficiency loss during the tracking could be significant for fast disturbance as shown in Figure 5.15.

The direct search method required even more steps to reach the optimum because of the restriction of the plant movement by the step size. The optimum could be reached for slow disturbance but there was a significant loss in efficiency during the transient. When the disturbance frequency was too fast, the RTO performance would be significantly degraded because the direct search method was not able to respond to such a fast disturbance which is illustrated in Figure 5.15.

It is shown in Figure 5.16 that there were significantly larger magnitudes of change in steam loads ($\Delta F > 1 \times 10^5$ lb/h) for the RTO system using the empirical efficiency curve. These large plant movements resulted from the plant perturbation determined by the expected profit experimental design criterion. Relatively small changes in steam loads ($\Delta F < 0.3 \times 10^5$ lb/h) were observed in the direct search method because of the restriction of the plant movement from the chosen step size. In the RTO system using

the fundamental model, small magnitudes of the change in steam loads ($\Delta F < 0.1 \times 10^5$ lb/h) were caused by propagation of measurement noise, and intermediate magnitudes ($\Delta F = 0.4$ to 1×10^5 lb/h) were the results of tracking after the disturbance change.

An online heating value sensor [Goldstein et al., 1999; Sprinkle et al., 1996] was not required for the RTO system using the fundamental model, but it was necessary for the estimation of the boiler efficiency using the empirical efficiency curve model and direct search method. When updating the parameters in the fundamental model, all the available temperature measurements for measuring the flue gas temperature at different locations of the boilers were used for updating the lower heating value of blast furnace gas to correct for the disturbance in fuel composition. Figure 5.17 shows the updated value of the lower heating value of the blast furnace gas for the disturbance frequency of 10 RTO executions. There was a bias between the estimated and the true values of the lower heating value when the CO content was reduced after the disturbance change. This bias was caused by the parametric mismatch between the base case values of fuel composition used in the RTO model and the actual fuel composition after the disturbance change. Thermocouples for temperature measurements are inexpensive and easy to maintain. An online heating value sensor, which can be a chromatograph or calorimeter, is more expensive in terms of fixed and maintenance costs. Using the fundamental model for boiler network optimization offers an advantage of using simple measurements for updating to correct for the fuel composition disturbance.

The RTO performance for a periodic ±13 % change in the CO and CO_2 contents in blast furnace gas (the last three cases in Table 5.3) is shown in Figures 5.18 and 5.19, and Table 5.12. As shown in Figure 5.6b, this disturbance causes a significant change in the shape of efficiency curve in which the efficiency curve can have a maximum or can be monotonic increasing. The results were similar to the disturbance scenario of a periodic ±10 % change in the CO and CO_2 contents in blast furnace gas.

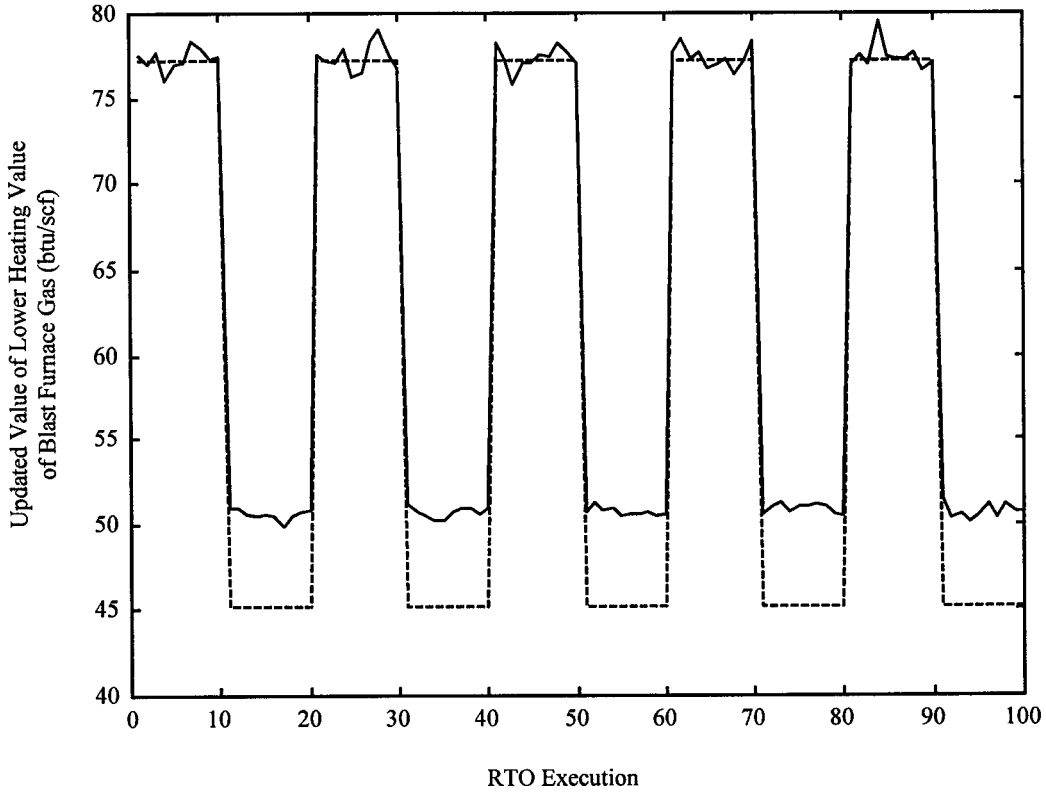

Figure 5.17 Updated values for the lower heating value of blast furnace gas in boiler 3 (dotted line: true value)

Table 5.12 Comparison of the RTO performances for a ±13% change in CO and CO_2 contents in blast furnace gas in boiler 3

Modelling Approach	**Average efficiency attained (%) for different disturbance frequency (number of RTO executions between successive step changes)**		
	10	20	50
Direct Search	88.53	88.45	88.83
Efficiency Curve Model	88.72	88.64	88.93
Fundamental Model	88.88	88.72	88.96
Maximum Average Efficiency	89.01	88.79	89.01

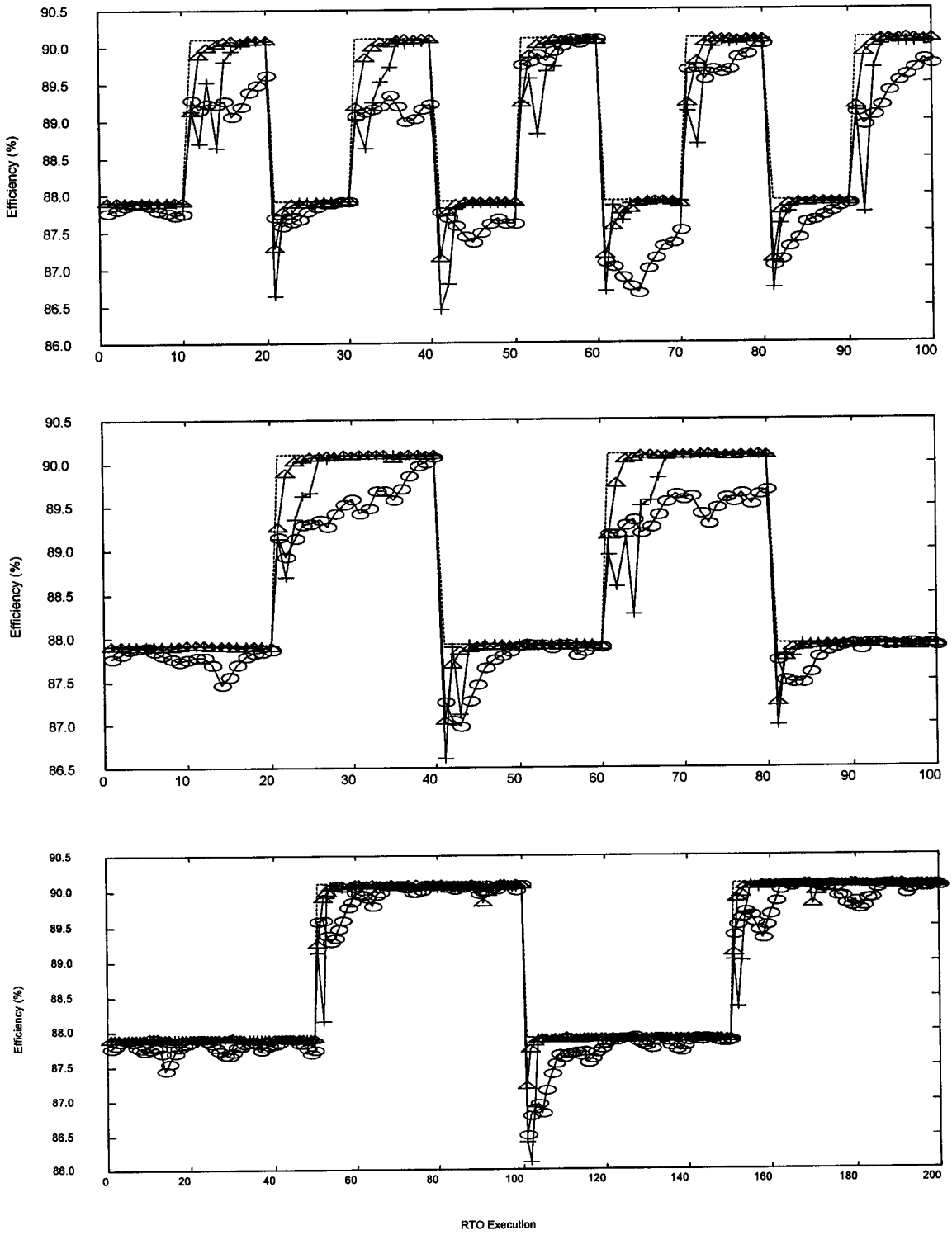

Figure 5.18 Boiler network efficiency attained for a periodic ±13% change in CO and CO_2 contents in blast furnace gas in boiler 3 (o : direct search, + : efficiency curve model, Δ : fundamental model, -- : true optimum)

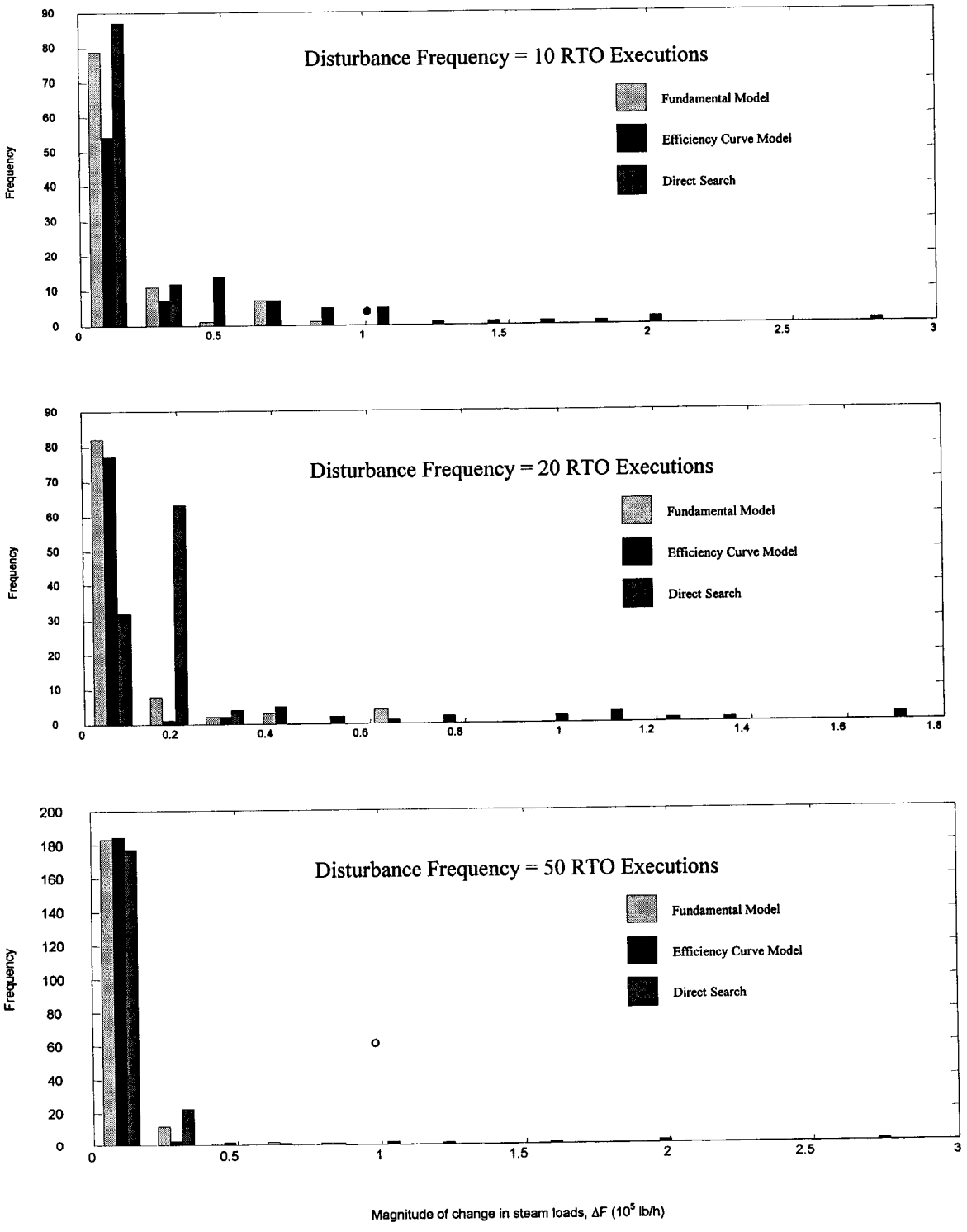

Figure 5.19 Distribution of the magnitude of change in steam loads for a ±13% change in CO and CO_2 contents in blast furnace gas in boiler 3

5.6.3 Disturbance in Heat Exchangers Fouling

The boiler efficiency attained and the magnitudes of change in steam loads for a disturbance in heat exchanger fouling are shown in Figures 5.20 and 5.21, respectively. The average efficiency attained is reported in Table 5.13 with a comparison of different optimization approaches. The threshold for experimentation when using the efficiency curve approach was chosen to be 1 %, so that experiments were performed if the measured network efficiency deviated from the predicted value by 1 %.

The performances of the RTO systems using different modelling approaches were similar for a slow disturbance in heat exchanger fouling. As shown in Figure 5.20, the changing optimum could be tracked closely using different RTO systems. When using the efficiency curve model, there was a periodic drop in boiler network efficiency during plant experimentation for generating new data sets to update the efficiency curves.

The magnitudes of change in steam loads for the RTO system using the direct search method and fundamental model were more gradual, while there were some large changes in steam loads using the efficiency curve model as shown in Figure 5.21. These large plant movements in the RTO system using the efficiency curve model were caused by the plant experimentation. Using the fundamental model, no experimentation was required for tracking the optimum. Since the optimum changed slowly with time, the changes in steam loads responding to the slow disturbance were small.

The performance of the RTO system using the efficiency curve model depended on the selected value for the threshold for triggering experimental design. Figure 5.22 shows the RTO performance with the threshold of 0.75 %. Within the horizon of 200 RTO executions, one more set of experiments was designed compared to the results in Figure 5.20 because a smaller threshold triggered the experimental design more often.

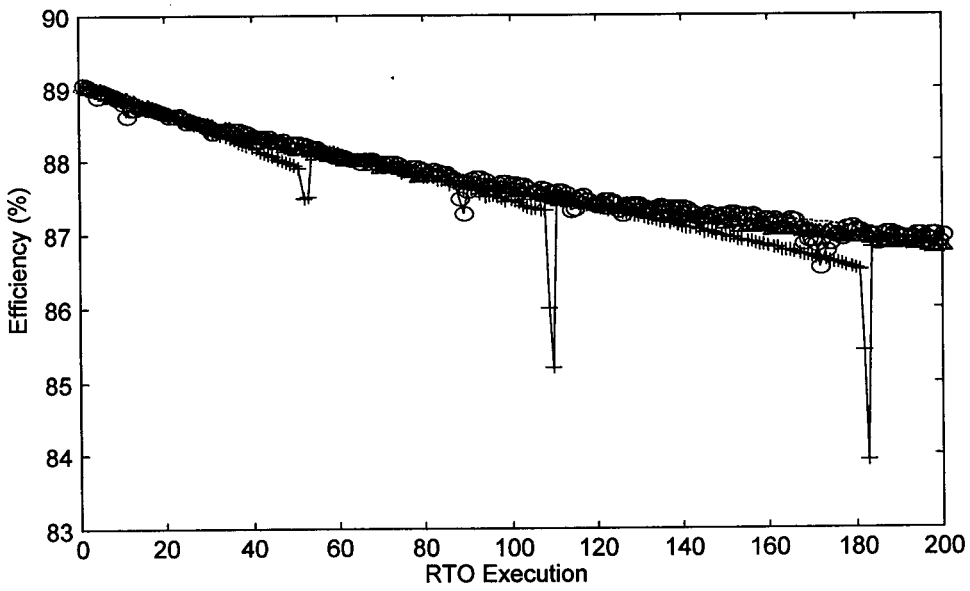

Figure 5.20 Boiler network efficiency attained for a disturbance in heat exchangers fouling in boiler 3 (o : direct search, + : efficiency curve model, Δ : fundamental model, - - : true optimum)

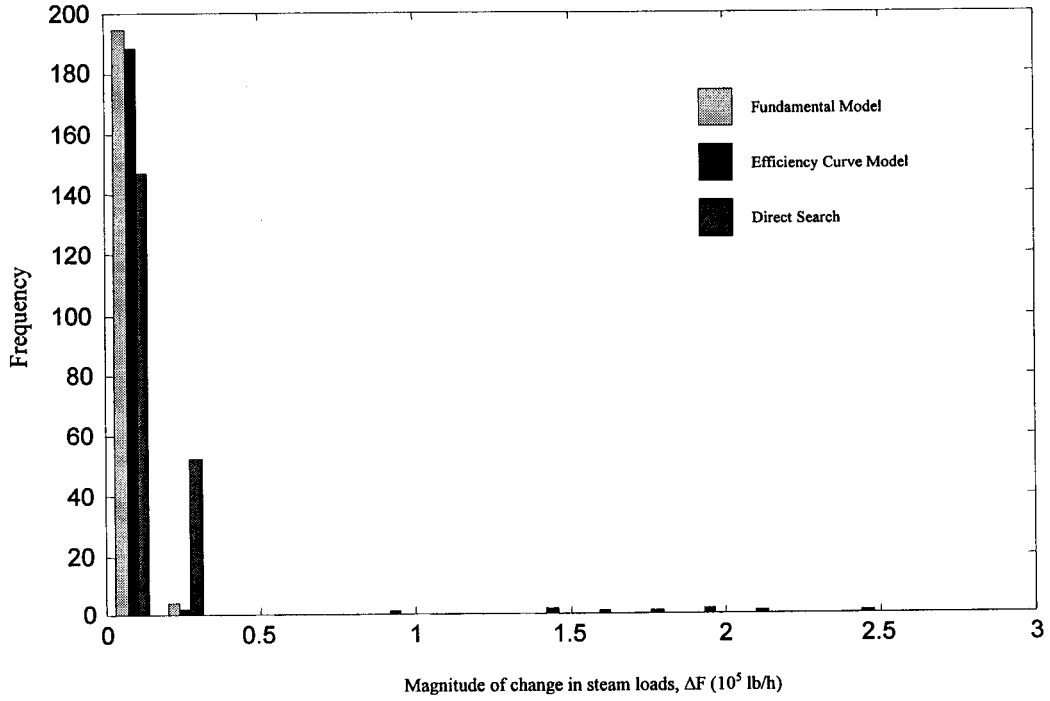

Figure 5.21 Distribution of the magnitude of change in steam loads for a disturbance change in heat exchangers fouling in boiler 3

Table 5.13 Comparison of the RTO performance for a disturbance in heat exchanger fouling

Modelling Approach	Average Efficiency Attained (%)	Remarks
Direct Search	87.74	• Could track the disturbance • Lot of small magnitudes in changes in steam loads ($\Delta F < 0.25 \times 10^5$ lb/h)
Efficiency Curve Model	87.57	• Could track the disturbance • Required experimentation ($\Delta F > 1 \times 10^5$ lb/h)
Fundamental Model	87.70	• Could track the disturbance • Lot of small magnitudes in changes in steam loads ($\Delta F < 0.25 \times 10^5$ lb/h)
Maximum Average Efficiency	87.80	

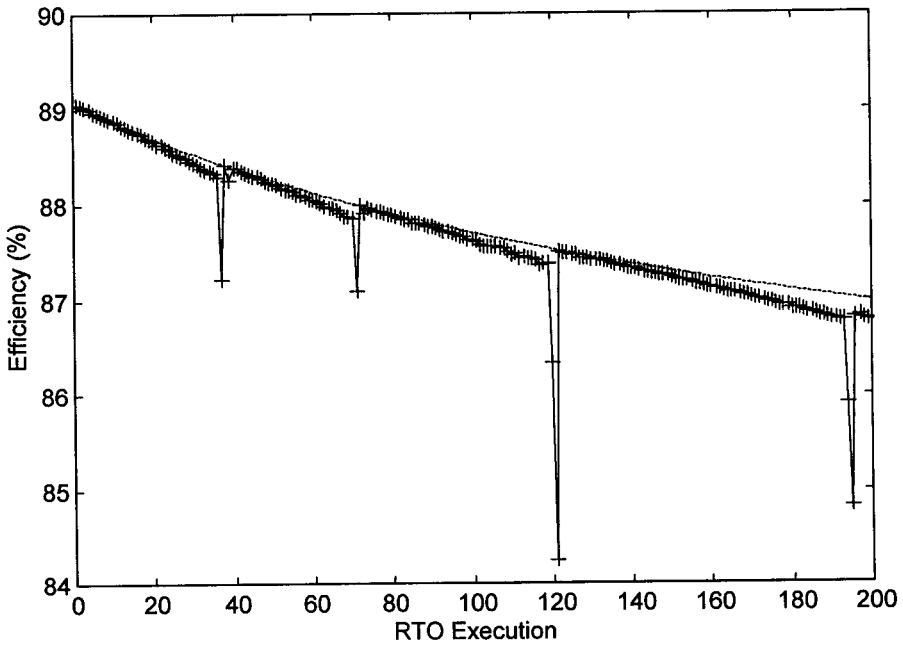

Figure 5.22 The RTO performance for using the empirical efficiency curve model with a threshold of 0.75 % (+ : efficiency curve model, -- : true optimum)

5.6.4 The Effect of Tuning Parameters on the RTO Performances

The performance of the RTO system using direct search method and empirical efficiency curve model depends on the chosen values of the tuning parameters, which are the step size in the direct search method and the trust region size in the efficiency curve model. The effects of the tuning parameters on the RTO performances are investigated in this section. The disturbance scenario considered in this study is the periodic ±10 % change in CO_2 and CO content in the blast furnace gas in boiler 3.

5.6.4.1 The Effect of Step Size on the RTO Performance using the Direct Search Method

The efficiency attained and the magnitude of change in steam loads for the RTO system using the direct search method with different step size are shown in Figures 5.23 and 5.24, respectively. It is shown in Figure 5.24 that the step size determined the magnitude of the plant movements. When the step size was increased, there were more large plant movements. The magnitudes of the plant movement did not have a significant influence on the boiler efficiency attained, as indicated in Figure 5.23 because the contours of the objective function in the boiler network system were flat. Therefore, the boiler efficiency attained was relatively insensitive to the step size.

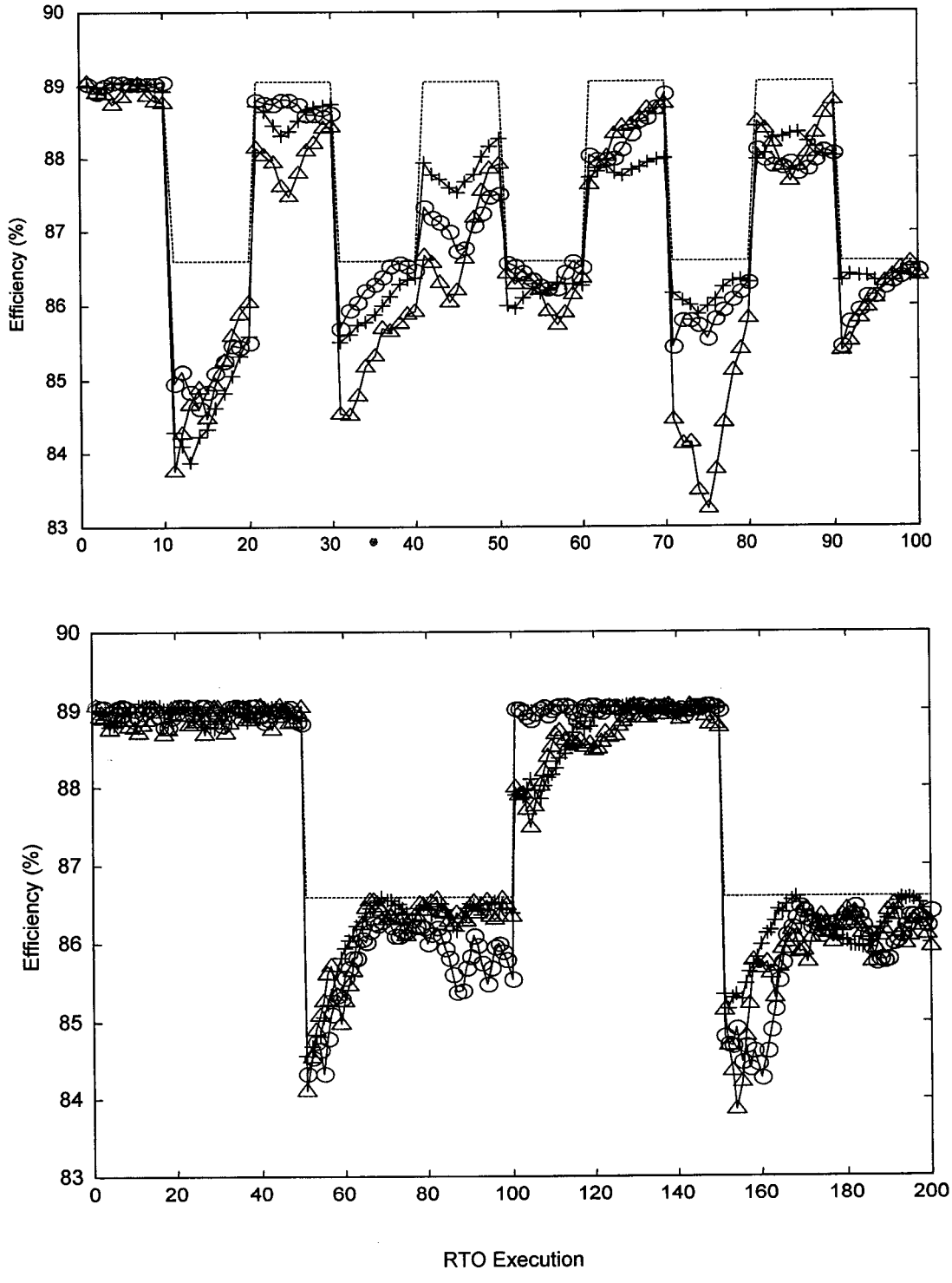

Figure 5.23 Boiler network efficiency attained using the direct search method with different step size for a ±10% change in CO and CO_2 contents in blast furnace gas in boiler 3 (+ : 0.075, o : 0.1, Δ : 0.15, -- : true optimum)

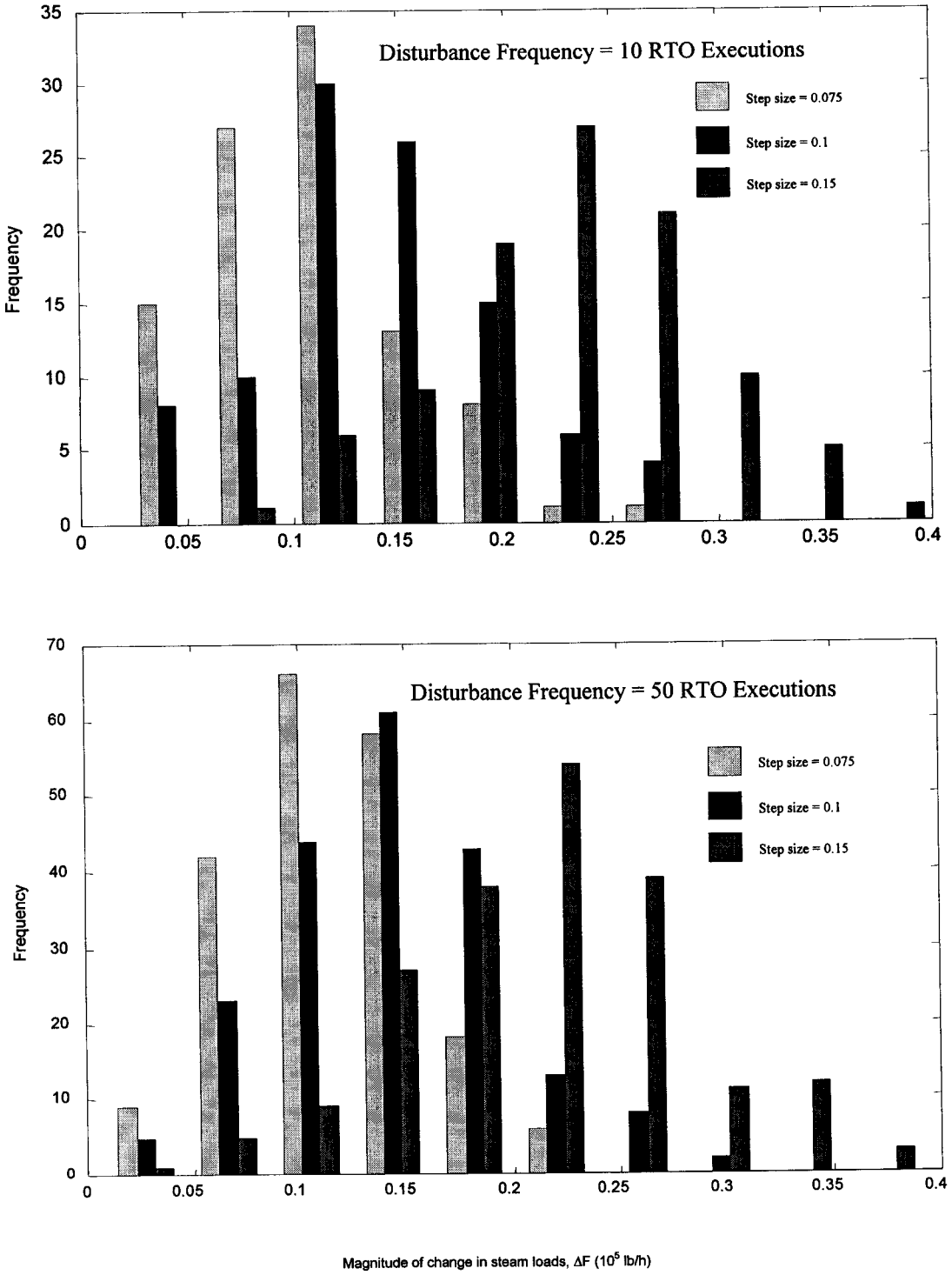

Figure 5.24 Magnitude of change in steam loads using the direct search method with different step size for a ±10% change in CO and CO_2 contents in blast furnace gas in boiler 3

5.6.4.2 The Effect of Trust Region Size on the RTO Performance using the Empirical Efficiency Curve Model

The performance of the RTO system using the efficiency curve model was not greatly influenced by the chosen trust region sizes as shown in Figures 5.25 and 5.26. The trust region size may affect the tracking of the changing optimum because a larger trust region allows for larger plant movement during transition, but the empirical efficiency curve model may not be accurate for such a large trust region. The magnitude of change in steam loads was not influenced by the trust region size as shown in Figure 5.26. The large changes in steam loads shown in Figure 5.26 resulted from plant experimentation. The size of perturbation was designed by the expected profit experimental design criterion which was not determined by the trust region size for optimization.

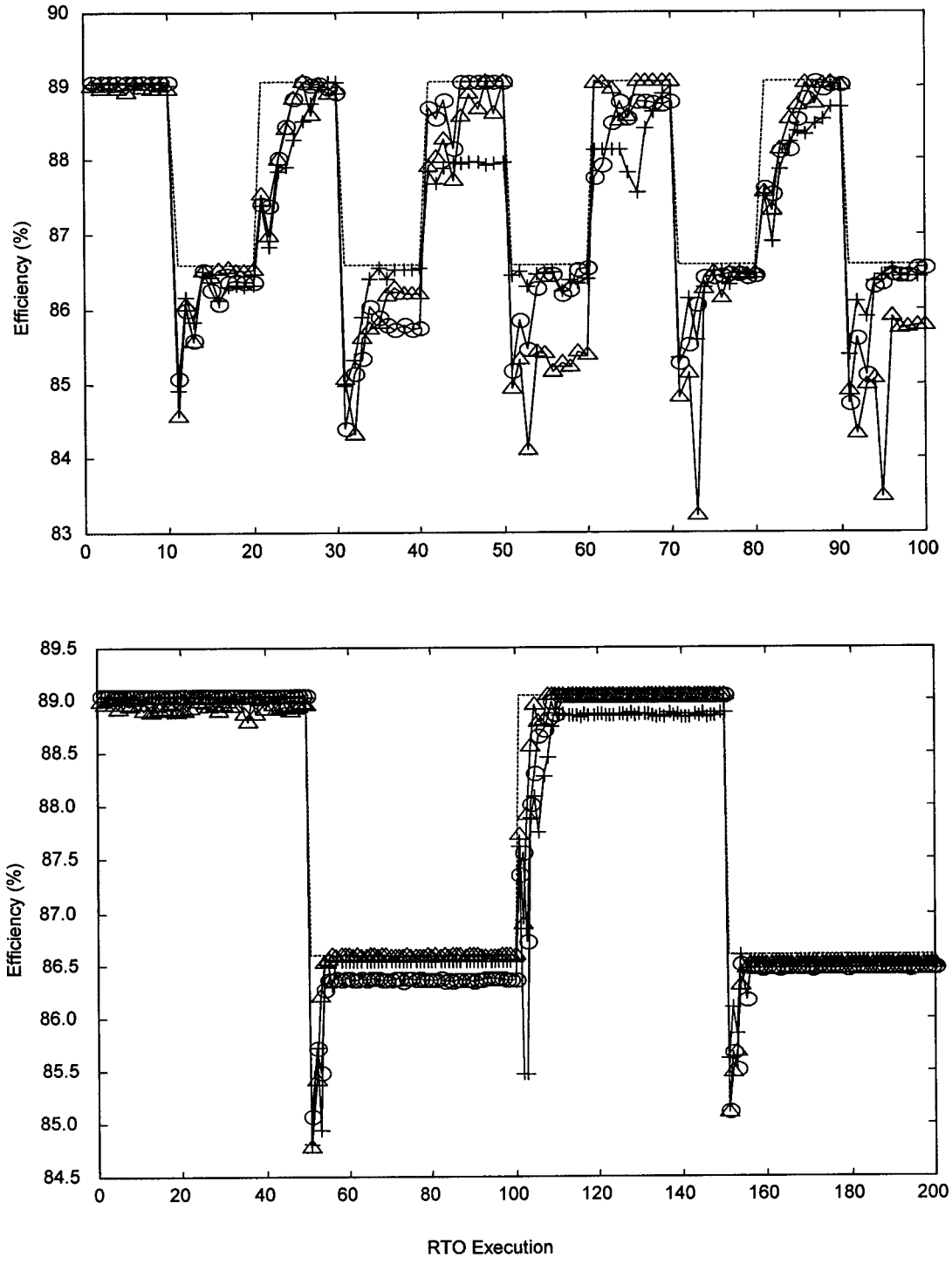

Figure 5.25 Boiler network efficiency attained using the efficiency curve model with different trust region size δ for a ±10% change in CO and CO_2 contents in blast furnace gas in boiler 3 (+ : δ = 20 klb/h, o : δ = 30 klb/h, Δ : δ = 40 klb/h, -- : true optimum)

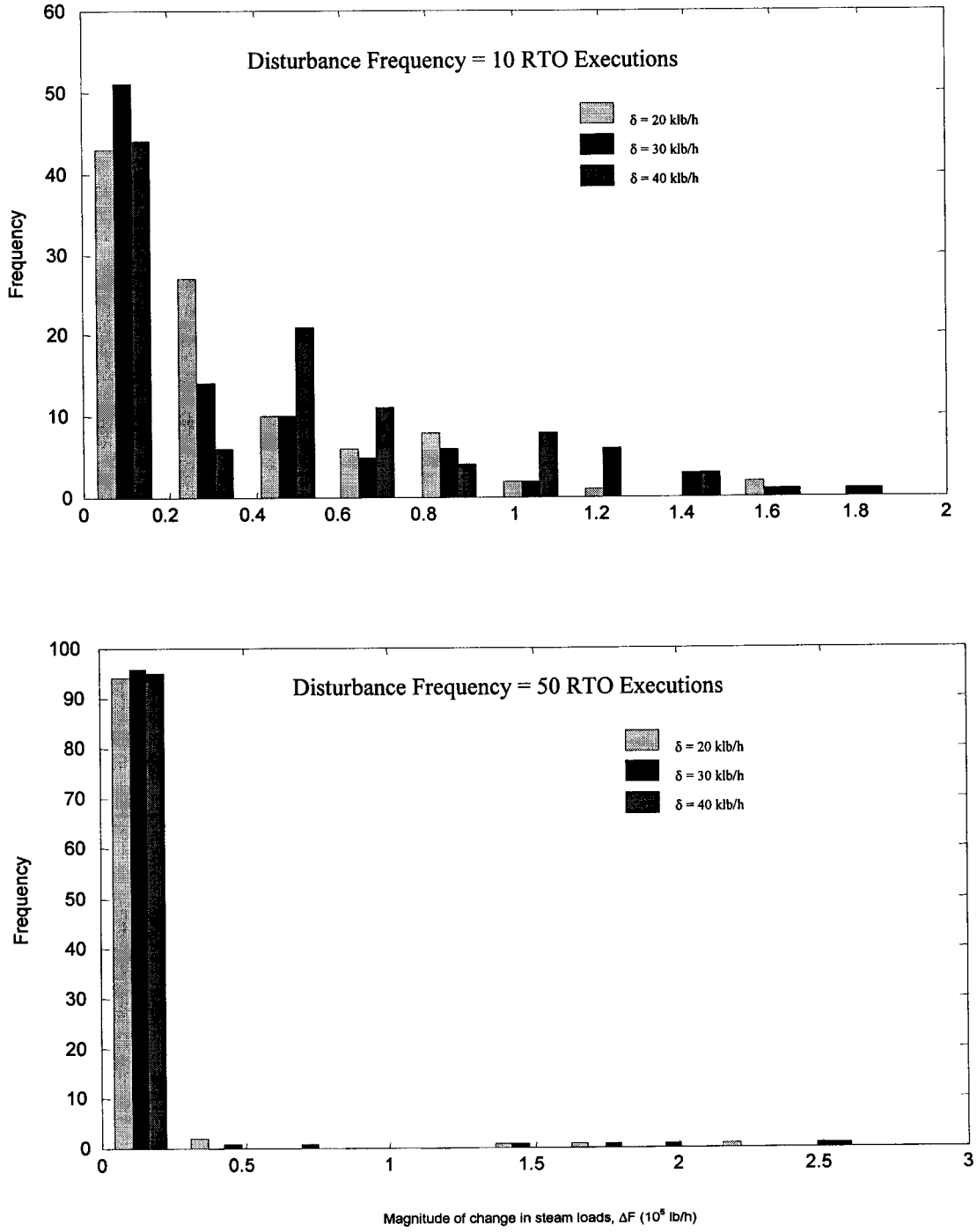

Figure 5.26 Magnitude of change in steam loads using the efficiency curve model with different trust region size for a ±10% change in CO and CO_2 contents in blast furnace gas in boiler 3

5.7 Conclusions

The success in tracking the changing optimum using the RTO system relies on a good model representing the plant accurately in a wide range of operation. This chapter presents the boiler case study to investigate the effect of the model fidelity on the RTO performance. The model-based RTO system and the model-free direct search method were used to compare different approaches in optimizing the boiler network in real time. In the model-based approach, two different models, the simplified fundamental model and empirical efficiency curve, were studied to investigate trading off model complexity and plant experiments.

The simplified fundamental model is accurate in a large range of operation and is able to track the changing optimum for even the most challenging cases, large and fast disturbances. The parameters selected for updating have physical meanings such as the heat transfer coefficients and heating value of fuel. Updating these parameters can correct for the disturbances in heat exchanger fouling and fuel composition. The case study results show that the RTO system using the simplified fundamental model could reach the optimum in a fewer number of steps compared to two other optimization approaches which was beneficial in tracking fast changing optimum responding to high frequency disturbances. Although solving the simplified fundamental model online was computationally more demanding, plant experimentation was not required for updating the disturbances in this boiler case study.

In the empirical efficiency curve model, a second order polynomial for approximating the boiler efficiency as a function of steam load was used for each boiler. The parameters for updating in the empirical model do not have physical meanings. Therefore, the empirical efficiency curve is accurate locally and cannot be extrapolated for large disturbances such as fuel composition change. Plant experimentation was performed to track the changing optimum responding to fuel composition change and

heat exchanger fouling because new data sets were required to update the new efficiency curves after the disturbance change. There was a loss in boiler efficiency during experimentation and tracking. Therefore, this approach was not able to track the fast changing optimum because the efficiency loss during the transient could be significant.

The direct search method tracks the changing optimum by using the local derivative of the plant performance estimated from the plant data. The plant is moved along the direction to improve the performance, and the derivative is updated when a new data set is available after the plant movement. Typically, the direct search method requires a lot of plant movement to estimate the local derivative and takes a larger number of steps to reach the optimum compared to the model-based methods. Case study results show that the direct search method was not able to track fast changing optimum. Although the plant was able to reach the optimum using the direct search method for low frequency disturbances for demand and fuel composition changes, a significant loss in boiler efficiency was observed during the transition because of the small plant movement restricted by the chosen step size. The RTO system using the direct search method was able to track the optimum for the disturbance in heat exchanger fouling because the optimum was changing slowly with time.

An additional advantage of using the simplified fundamental model in optimizing the boiler system is that the online measurement of the fuel heating value is not required. The fuel heating value in the fundamental model can be updated from the available flow and temperature measurements at different locations in the boiler. In the direct search method and efficiency curve model, estimation of individual boiler efficiency is required. The fuel heating value has to be measured online because the energy input to the boiler has to be determined in estimating the boiler efficiency.

Based on the case study results, a fundamental model is always advantageous for this RTO application. However, the cost of model development is also a concern for

practicing engineers, and the empirical efficiency curve model might be a good compromise in some cases. The direct search has poorer performance and high sensor cost, and it is not recommended for RTO application.

6. SUMMARY, CONCLUSIONS AND FUTURE WORK

6.1 Summary and Conclusions

Real-time operations optimization has become increasingly important in determining the best operating policy of a chemical plant to achieve a competitive advantage. The closed-loop real-time optimization (RTO) system relies on model updating as feedback to correct selected model parameters for model errors and disturbances. The capability of an RTO system to track the optimum closely depends on the accuracy of the updated model in representing the plant behavior, and the model accuracy depends on the information content of the plant data set(s) used for parameter estimation. This thesis develops methods for acquiring needed data for parameter updating to improve the RTO performance.

In Chapter 3, a strategy was developed for model updating using multiple data sets to enhance the RTO performance. A moving window with a fixed size is used to keep a record of recent and historical data sets for updating. Prior knowledge of disturbance frequency is incorporated in parameter estimation formulation. Additional parameters can be estimated from multiple data sets to reduce the plant/model mismatch if the data sets have sufficient plant variation or information content. Previous work on updater diagnosis [Miletic and Marlin, 1998a] has been extended to multiple data sets for model updating to identify the information content in the data sets for updating additional parameters. The updating strategy using multiple data sets was implemented on the simulated Williams-Otto reactor case study. The RTO performance was improved by updating additional parameters to correct for modelling errors for various disturbance scenarios. Sufficient plant variation for updating additional parameters could be generated from disturbances or deliberate plant perturbation.

The strategy for designing plant experiments for RTO application when the data sets do not have sufficient information was presented in Chapter 4. Recognizing that plant experimentation is expensive, a new expected profit experimental design criterion has been developed. Experiments are designed by maximizing the overall expected profit over a future horizon. The expected profit experimental design approach finds the best tradeoff between profit loss before and during experimentation and profit gain due to improved model. In this approach, prior specification of experimental window is not required because large plant movement during experimentation is penalized by the cost of experimentation term in the objective function. The expected profit experimental design approach was implemented on the simulated Williams-Otto reactor in Chapter 4 for various disturbance scenarios for different situations in plant operation. Experiments designed by the expected profit approach were located close to the model optimum or along the direction of ridge of the profit contours to reduce the cost of experimentation. The RTO system with experimentation yielded higher profit than achieved by standard RTO system without experimentation.

The effect of model fidelity on RTO performance using the industrial boiler case study was discussed in Chapter 5 which demonstrated the importance of using a rigorous fundamental model. Three optimization approaches were implemented and compared in the boiler network system: 1) model-free direct search method, 2) model-based RTO system using the empirical efficiency curve model with experimentation, and 3) model-based RTO system using the fundamental model without experimentation. The fundamental model was able to represent the boiler accurately over a wide range of operation. The RTO system using the fundamental model took a few steps to reach the optimum, and therefore, could closely track the changing optimum responding to disturbances in demand, fuel composition and heat exchanger fouling without plant experimentation. Using the empirical efficiency curve model, plant experimentation was required to track the changing optimum for the disturbances in fuel composition and heat exchanger fouling. There was a loss in boiler network efficiency during experimentation

which was undesirable for tracking fast disturbances. However, when a fundamental model is not available, the empirical efficiency curve model with experimentation can be a reasonable alternative for boiler network optimization to track low frequency disturbances. The RTO system using the direct search method required more steps to reach the optimum compared to the model-based methods and was not able to track the changing optimum closely because of the significant loss in efficiency during tracking.

The boiler case study in Chapter 5 illustrated that the RTO system using the fundamental model required only simple and inexpensive flow and temperature measurements. Online measurement of the heating value of fuel was required for the empirical efficiency curve model and direct search method for estimating the boiler efficiency online since the heating value of fuel changed with the disturbance in fuel composition. Using the fundamental model, heating value of fuel could be estimated from the flow and temperature measurements to correct for the disturbance in fuel composition.

6.2 Future Work

This thesis emphasizes the importance of good model and data sets for improving the RTO performance and develops the technologies in generating good data sets for model updating. However, there are many questions needed to be answered, and challenges and research opportunities remain.

Multiple data sets for model updating requires extensive computation, and reducing the computation time would be beneficial. Future research is required to reduce the computation time by re-formulating the parameter estimation problem in a recursive approach. The "batch" parameter estimation formulation in Chapter 3 can be expressed in the recursive form by expanding the objective function using the Taylor's series to relate the current estimates of the parameters with their previous estimates and current set of

measurements. The parameters are updated based on the previous estimates and the current data sets to reduce the problem size.

Future work is required for online monitoring of the process to decide whether plant experimentation is needed to improve the RTO performance. The occurrence of the disturbance which is assumed to be known in Chapters 4 and 5 can be detected by process monitoring using multivariate statistical methods. Future research directions also include the selection of the variables for inferring the disturbances and monitoring of the RTO results based on the derivative information from the plant movement and the model to determine if experiments are required to improve the model accuracy.

Various disturbance scenarios have to be investigated in designing plant experiments for RTO systems. The expected profit experimental design approach can be extended to consider different disturbance scenarios in which the disturbance frequency and future horizon for experimental design cannot be defined easily. An example of these disturbance scenarios is the continuous decay in the heat transfer coefficients in the boiler case study. In these disturbance scenarios, multiple sets of experiments will be required, and the expected profit approach has to be modified to design multiple sets of experiments.

The expected profit experimental design approach can be applied to different chemical processes. The boiler case studies investigated in this thesis did not require plant experimentation for tracking the optimum when using the fundamental model. Plant experimentation may be required for other processes even if a fundamental model is used for RTO system. Further research can be done to implement the expected profit experimental design approach to design plant experiments using a fundamental model for the processes in which a fundamental model cannot track the optimum well without experimentation.

NOMENCLATURE

a	= coefficient in the heat transfer correlation
	= parameter in the empirical thermodynamics and transport correlations
a	= vector of measurement adjustments
A	= area
A	= coefficient matrix for a system of linear(ized) equations
A_i	= frequency factor for reaction i
	= parameter in the polynomial efficiency curve model for boiler i
b	= flow dependence heat transfer correlation
	= parameter in the empirical thermodynamics and transport correlations
B	= BFGS approximation for the Hessian matrix
	= coefficient matrix for the basic variables in linear(ized) contraints
B_i	= activation energy for reaction i
	= parameter in the polynomial efficiency curve model for boiler i
c	= parameter in the empirical thermodynamics and transport correlations
C	= design cost
	= parameter in the heat transfer correlations
C_i	= parameter in the polynomial efficiency curve model for boiler i
C_p	= molar heat capacity
CV	= controlled variable
d	= diameter of tubes in heat exchangers
	= parameter in the empirical thermodynamics and transport correlations
d	= search direction
D	= hydraulic diameter
	= steam demand
e	= parameter in the empirical thermodynamics and transport correlations
e	= offset that cannot be reduced by experimentation

$\mathbf{e}_i$	= zero vector except for a 1 in its i^{th} element
EP	= expected profit
f	= friction factor
	= parameter in the empirical thermodynamics and transport correlations
f	= plant model
	= equality constraints
F	= flow rate
g	= gravitational constant
g	= inequality constraints
	= gradient vector
h	= heat transfer coefficient
h	= steady-state material and energy balance equations
H	= enthalpy
H_0	= null hypothesis
H_1	= alternative hypothesis
I	= identity matrix
k	= thermal conductivity
	= k^{th} iteration
k_i	= rate constant for reaction i
K_p	= process gain
L	= Lagrangian
	= length of tubes in heat excahngers
m	= parameter in the heat transfer correlations
M	= total number of RTO execution
MV	= manipulated variable
MW	= molecular weight
n	= dimension of reduced space
	= molar flow rate
	= number of tubes in heat exchangers

N	= number
	= RTO execution
N	= coefficient matrix for the nonbasic variables in linear(ized) constraints
Nu	= Nusselt's number
p	= number of passes in heat exchangers
P	= plant performance
	= pressure
Pr	= Prandlt's number
Q	= heat transfer
Q	= covariance matrix
R	= fouling factor
	= norm of offset
	= setpoint for the fuel ratio controller for boiler network
R	= Cholesky factorization for the reduced Hessian matrix
RADLOSS	= percentage of radiation loss
Re	= Reynold's number
s	= vector of slack variables
S	= scaling matrix
	= coefficient matrix for the superbasic variables in linear(ized) contraints
T	= temperature
T^2	= Hotelling T^2 statistic
U	= overall heat transfer coefficient
U	= orthogonal matrix
UCL	= upper control limit
UD	= updater diagnosis
V	= covariance matrix of the measurements
V_r	= reactor volume
W	= gas flow rate

$\mathbf{x}$	= vector of process variables
	= vector of optimization variables
$\mathbf{x}_m^*$	= model optimum
$\mathbf{x}_{opt}$	= best RTO prediction
$\mathbf{x}_p^*$	= true plant optimum
X_i	= mass fraction of component i
	= steam quality in heat exchanger i
y_i	= volume fraction of component i in fuel
Y	= principal axis along the direction of eigenvector
$\mathbf{Y}$	= basis in the range space
$\mathbf{z}$	= vector of measurements
$\mathbf{Z}$	= basis in the null space

Greek letters

α	= radiation heat transfer coefficient
	= step size
$\boldsymbol{\alpha}$	= vector of fixed parameters
$\boldsymbol{\beta}$	= vector of adjustable parameters
δ	= size of trust region in efficiency curve model
	= step size for numerical differentiation
Δ	= offset that can be reduced by experimentation
ε	= emissivity
ϕ	= direction of offset **e** with reference to the principal axis
η	= coordinate system with reference to the principal axis
η_i	= boiler efficiency for boiler i
λ	= decay rate constant
	= eigenvalue
	= slack variable for controlled variable

$\boldsymbol{\lambda}$ = vector of Lagrange multipliers for equality constraints

$\boldsymbol{\Lambda}$ = diagonal matrix with eigenvalues in the diagonal elements

μ = viscosity

$\boldsymbol{\mu}$ = vector of Lagrange multipliers for inequality constraints

θ = direction of offset Δ with reference to the principal axis

ρ = density

= penalty parameter

σ = slack variable for manipulated variable

σ^2 = element in matrix $\mathbf{Q}$

Subscripts

a = active set of inequality constraints

air = air

amb = ambient air

AE = after experimentation

B = basic variables

bfg = blast furnace gas

boiler = boiler

BE = before experimentation

cog = coke oven gas

comb = combustion

conv = convective heat transfer

d = downcomer

data = data sets in the moving window for model updating

ds = desuperheater

D = dependent variables

= disturbance

DE = during experimentation

e = economizer

econ	= water leaving the mixing point after the economizer in the boiler
expt	= experiments
f	= furnace
flue	= flue gas
Feed	= feed water
FL	= full load
g	= gas
gt	= generating tubes
h	= bottom header
in	= inlet
	= inner diameter
	= inside the tube
I	= independent variables
l	= lower bound
LM	= log mean temperature difference
m	= model
max	= maximum
md	= mud drum
mh	= mud drum to bottom header
min	= minimum
n	= nonbasic variables
o	= before experimentation
	= feed flow
	= outer diameter
out	= outlet
	= outside the tube
p	= plant
ph	= air preheater
r	= riser

rad	= radiation heat transfer
radloss	= radiation loss
ref	= reference
s	= steam
	= superbasic variables
sat	= saturated steam/water
sc	= steam coil
sd	= steam drum
sm	= steam drum to mud drum
sh	= superheated steam
	= superheater
spray	= spray water in desuperheater
steam	= steam produced
sub	= subcooled
u	= upper bound
w	= tube wall
	= water
Y	= basis in the range space
Z	= basis in the null space
Δ	= offset that can be reduced by experimentation

Superscripts

m	= measured
o	= standard condition
u	= unmeasured
‘	= scaled version
*	= optimum

Operators

E	= expectation
∇	= Jacobian
∇_r^2	= reduced Hessian
$\|\bullet\|_2$	= Euclidean norm of $\bullet$
$\|\bullet\|$	= determinant of $\bullet$
Δ	= change
$\lambda(\bullet)$	= eigenvalue of $\bullet$

Conversion Factors

E(btu)	$= 9.47831 \times 10^{-4} \times$ E(J)
F(lb/h)	$= 2.20642 \times$ F(kg/h)
F(scfh)	$= 35.3147 \times$ F(m^3/h) at 15°C and 1 atm
P(psia)	$= 1.45 \times 10^{-5} \times$ P(Pa)
T(R)	$= 1.8 \times$ T(K)
T(F)	$= 1.8 \times$ T(°C) + 32
ρ(lb/ft^3)	$= 0.0624278 \times \rho$(kg/m^3)

REFERENCES

Arora, J. S., Elwakeil, O. A., and Chahande, A. I., "Global Optimization Methods for Engineering Applications: A Review", Structural Optimization, 9, 137-159, 1995.

Bamberger, W., and Isermann, R., "Adaptive On-Line Steady State Optimization of Slow Dynamic Processes", Automatica, 14, 223-230, 1978.

Bard, Y., "Nonlinear Parameter Estimation", Academic Press, New York, 1974.

Bertrand C. R., "A Study on Dynamic Simulation and Control of Steam Systems", MS Thesis, University of Maryland, 1986.

Bozenhardt, H., "Hyperplane: A Case History", Proc. Fifth Annual Control Engineering Conference, May 1986.

Box, G. E. P., "Evolutionary Operation: A Method for Increasing Industrial Productivity", Applied Statistics, 6, 81-101, 1957.

Box, G. E. P., and Draper, N. R., "Evolutionary Operations", John Wiley & Sons, New York, 1969.

Box, M. J., "Improved Parameter Estimation", Technometrics, 12(2), 219-229, 1970.

Brooke, A., Kendrick, D., and Meeraus, A., "GAMS: A User's Guide (Release 2.25)", The World Bank, 1992.

Byrne, R. P., and Bogle, I. D. L., "Global Optimization of Constrained Non-Convex Programs Using Reformation and Interval Analysis", Comp. Chem. Eng., 23, 1341-1350, 1999.

Cervantes, A. M., and Biegler, L. T., "Large-scale DAE Optimization using Simultaneous Nonlinear Programming Formulations", AIChE J., 44(5), 1038-1050, 1998.

Cervantes, A. M., and Biegler, L. T., "A Stable Elemental Decomposition for Dynamic Process Optimization", Journal of Computational and Applied Mathematics, 200, 41-57, 2000.

Chien K. L., Ergin E. I., Ling C., and Lee A., "Dynamic Analysis of a Boiler", Trans. ASME, Vol. 80, 1809-1819, 1958.

Choi, S. H., Ko, J. W., and Manousiouthakis, V., "A Stochastic Approach to Global Optimization of Chemical Processes", Comp. Chem. Eng., 23, 1351-1356, 1999.

Contino, A. V., "Improve Plant Performance Via Statistical Process Control", Chemical Engineering, 95-102, July 1987.

Contreras-Dordelly, J. L, and Marlin, T. E., "Control Design for Increased Profit", Comp. Chem. Eng., 24, 267-272, 2000.

Crowe, C. M., "Reconciliation of Process Flow Rates by Matrix Projection Part II: The Nonlinear Case", AIChE J., 32(4), 616-623, 1986.

Crowe, C. M., Garcia Campos, Y. A., and Hrymak, A. N., "Reconciliation of Process Flow Rates by Matrix Projection Part I: Linear Case", AIChE J., 29(6), 881-888, 1983.

Cuthrell, J. E., and Biegler, L. T., "On the Optimization of Differential-Algebraic Process Systems", AIChE J., 33(8), 1257-1270, 1987.

Cutler, C. R., and Perry, R. T., "Real-Time Optimization with Multivariable Control Is Required to Maximize Profits", Comput. Chem. Eng., 7(5), 643-677, 1983.

Darby, M. L., and White, D. C., "On-Line Optimization of Complex Processes", Chem. Eng. Prog., 51-59, Oct. 1988.

de Mello F. P., "Boiler Models for System Dynamic Performance Studies", IEEE Transactions on Power Systems, Vol. 16, No. 1, 66-74, Feb. 1991.

Dieck-Assad G., "Development of a State Space Boiler Model for Process Optimization", Simulation, 201-213, Oct. 1990.

Draper, N. R., and Smith, H., "Applied Regression Analysis", 2nd Edition, John Wiley & Sons, NY, 1981.

Dukelow, S. G., "Improving Boiler Efficiency", Instrument Society of America, 1985.

Dukelow, S. G., "The Control of Boilers", 2nd Edition, Instrument Society of America, 1991.

Edgar, T. F., Himmelblau, D. M., and Lasdon, L. S., "Optimization of Chemical Processes", 2nd Edition, McGraw-Hill Publishing Company, NY, 2001.

Ferris, M. C., "MATLAB and GAMS: Interfacing Optimization and Visualization Software", Mathematical Programming Technical Report, Department of Computer Sciences, University of Wisconsin, Madison, WI, 1999.

Fiacco, A. V., "Introduction to Sensitivity and Stability Analysis in Nonlinear Programming", Academic Press, NY, 1983.

Fogler, H. S. "Elements of Chemical Reaction Engineering", 2nd Edition, Prentice-Hall: Englewood Cliffs, NJ, 1992.

Forbes, J. F., "Model Structure and Adjustable Parameter Selection for Operations Optimization", Ph.D. Thesis, McMaster University, Hamilton, ON, 1994.

Forbes, J. F., Marlin, T. E., and MacGregor, J. F., "Model Adequacy Requirements for Optimizing Plant Operations", Comp. Chem. Eng., 18(6), 497-510, 1994.

Forbes, J. F., and Marlin, T. E., "Design Cost: A Systematic Approach to Technology Selection for Model-Based Real-Time Optimization Systems", Comp. Chem. Eng., 20(6/7), 717-734, 1996.

Fletcher, R., "Practical Methods of Optimization", John Wiley & Sons, 1987.

Fraleigh, L. M., "Optimal Sensor Selection and Parameter Estimation for Real-Time Optimization", M. Sc. Thesis, University of Alberta, Edmonton, AB., 1999.

Garcia, C. E., and Morari, M., "Optimal Operation of Integrated Processing Systems. Part I: Open-Loop Online Optimizing Contrl", AIChE J., 27(6), 960-968 1981.

Geankoplis, C., "Transport Processes and Unit Operations", 3rd edition, Prentice-Hall, 1992.

Gill, P. E., Murray, W., and Wright, M. H., "Practical Optimization", Academic Press NY, 1981.

Golden, N., Gersh, M., Bien, F., Richtsmeier, S., Gruninger, J., Adler-Golden, S., Griffies, D., Ronnenkamp, C., Householder, D., Krogue, J., and Gould, D., "Real-Time Optical Btu Measurement of Natural Gas at Line Pressure", 4th International Symposium on Fluid Flow Measurement, Denver, Colorado USA, June 27 – 30, 1999.

Green, D., and Al ai-Shaikh, "Evaluating and Improving Efficiency in a Boiler Complex Through Computer Control", JACC, 1980.

Hamer, J. W., and Richenberg, C. R., "On-Line Optimizing Control of a Packed-Bed Immobilized-Cell Reactor", AIChE J., 34(4), 626-632, 1988.

Hardin, M. B., Joshi, A., and Jones, J. D., "Rigorous Crude Unit Optimization", NPRA Computer Conference, 1995.

Health, J. A., Kookos, I. K, and Perkins, J. D., "Process Control Structure Selection Based on Economics", AIChE J., 46(10), 1998-2016, 2000.

Holman, J. P., "Heat Transfer", 7th Edition, McGraw-Hill Publishing Company NY, 1992.

Jang, S. S., Joseph, B., and Mukai, H., "On-Line Optimization of Constrained Multivariable Chemical Processes", AIChE J., 33(1), 26-35, 1987.

Janna, W. S., "Engineering Heat Transfer", PWS Engineering, 1986.

Jewell, D. C., "Practical Issues in the Design of Real-Time Optimization Systems", M. Eng. Thesis, McMaster University, Hamilton, ON., Canada, 1996.

Johnson L. P. M., and Kramer, M. A., "Maximum Likelihood Data Rectification: Steady-State Systems", AIChE J., 41(11), 2415-2426, 1995.

Kage, K., and Joseph, B., "Measurement Selection and Detection of Measurement Bias in the Context of Model Based Control and Optimization", Ind. Eng. Chem. Res., 29, 2037-2044, 1990.

Kassidas, A., Patry, J., Marlin, T. E., "Integrating Process and Controller Models for the Design of Self-Optimizing Control", Comp. Chem. Eng., 24, 2589-2602, 2000.

Keeler, S. E.; Reilly, P. M. "The Design Experiments When There are Errors in All the Variables", Can. J. of Chem. Eng., Vol. 70, 774-779, 1992.

Kim, I. W., Kang, M. S., Park, S., and Edgar, T. F., "Robust Data Reconciliation and Gross Error Detection: The Modified MIMT Using NLP", Comp. Chem. Eng., 21(7), 775-782, 1997.

Kim, I. W., Liebman, M. J., and Edgar, T. F., "Robust Error-In-Variables Estimation Using Nonlinear Programming Techniques", AIChE J., 36(7), 985-993, 1990.

Kim, I. W., Liebman, M. J., and Bell, N. H., "Parameter Estimation for a Laboratory Water-Gas-Shift Reactor Using a Nonlinear Error-In-Variables Method", Comp. Chem. Eng., 15(5), 361-367, 1991.

Koninckx, J., "On-Line Optimization of Chemical Plants Using Steady-State Models", Ph.D. Thesis, University of Maryland, 1988.

Kourti, T., Lee, J., and MacGregor, J. F. "Experiences with Industrial Applications of Projection Methods for Multivariate Statistical Process Control", Comp. Chem. Eng., Vol. 20, S745-S750, 1996

Krishnan, S., Barton, G. W., and Perkins, J. D., "Robust Parameter Estimation in On-Line Optimization – Part I: Methodology and Simulated Case Study", Comp. Chem. Eng., 16(6), 545-562, 1992.

Kwan, H. W., and Anderson J. H., "A Mathematical Model of a 200 MW Boiler", Int. J. Control, Vol. 2, No. 6, 977-998, 1970.

Lee, K. S., and Lee W. K., "On-Line Optimizing Control of a Nonadiabatic Fixed Bed Reactor", AIChE J., 31(4), 667-675, 1985.

Loeblein, C., and Perkins, J. D., "Economic Analysis of Different Structures of On-Line Process Optimization Systems", Comp. Chem. Eng., 22(9), 1257-1269, 1998.

Loeblein, C., and Perkins, J. D., "Structural Design for On-Line Process Optimization: I. Dynamic Economics of MPC", AIChE J., 45(5), 1018-1029, 1999a.

Loeblein, C., and Perkins, J. D., "Structural Design for On-Line Process Optimization: II. Application to a Simulated FCC", AIChE J., 45(5), 1030-1040, 1999b.

Lumley, T., "Personal Communication", 1999.

MacDonald, R. J., and Howat, C. S., "Data Reconciliation and Parameter Estimation in Plant Performance Analysis", AIChE J., 34(1), 1-8, 1988.

Mah, R. S. H., and Tamhane, A. C., "Detection of Gross Errors in Process Data", AIChE J., 28(5), 828-830, 1982.

Marlin, T. E., and Hrymak, A. N., "Real-Time Optimization of Continuous Processes", Fifth International Conference on Chemical Process Control. AIChE Symp., No. 316, 156, 1997.

Marlin, T. E., and Young, M., "Integrating the Effects of Process Controllers with Steady-State, Equation-Based Simulation", Chem. Eng. Comm., 165, 67-87, 1998.

Mathworks, "NAG Foundation Toolbox for Use with MATLAB", The Mathworks Inc., Natick, MA, USA, 1996.

McCaw, T. L., "Two Layer Optimization of a Catalytic Reformer", Master Thesis, Department of Chemical Engineering, McMaster University, Hamilton, ON, Canada, 1995.

McFarlane, R. C., and Bacon, D. W., "Empirical Strategies for Open-Loop On-line Optimization", Can. J. Chem. Eng., 67, 665-677, 1989.

Miletic, I. P., "Results Analysis in Real-Time Optimization", M. Eng. Thesis, McMaster University, Hamilton, ON, Canada, 1995.

Miletic, I. P., and Marlin, T. E., "Results Diagnosis for Real-Time Process Operations Optimizations", Comp. Chem. Eng., 22, S475-S482, 1998a.

Miletic, I. P., and Marlin, T. E., "On-Line Statistical Results Analysis in Real-Time Operations Optimization", Ind. Eng. Chem. Res., 37, 3670-3684, 1998b.

Narasimhan, S., Mah, R. S. H., Tamhane, A. C., Woodward, J. W., and Hale, J. C., "A Composite Statistical Test for Detecting Changes of Steady States", AIChE J., 32(9), 1409-1418, 1986.

Narasimhan, S., and Jordache, C., "Data Reconciliation and Gross Error Detection: An Intelligent Use of Process Data", Gulf Publishing Company, Houston, Texas, 2000.

Narasimhan, S., Kao, C. H., and Mah, R. S. H., "Detecting Changes of Steady States Using the Mathematical Theory of Evidence", 33(11), 1930-1932, 1987.

Narrarway, L. T., and Perkins, J. D., "Selection of Process Control Structure Based on Linear Dynamic Economics", Ind. Eng. Chem. Res., 32, 2681-2692, 1993.

Nicholson, H., "Dynamic Optimization of a Boiler", Proc. IEE, Vol. 111, No. 8, pp. 1479-1499, Aug. 1964.

Payne, F. W., "Efficient Boiler Operations Sourcebook", The Fairmont Press, Inc., 1985.

Pedersen, C. C., Mudt, D. R., Bailey J. K., and Ayala, J. S., "Closed Loop Real Time Optimization of a Hydrocracker Complex", NPRA Computer Conference, 1995.

Pritchard, D. J., and Bacon, D. W., "Prospects For Reducing Correlations Among Parameter Estimates in Kinetic Models", Chem. Eng. Sci., 33, 1539-1543, 1978

Roberts, P. D., "An Algorithm for Steady State System Optimization and Parameter Estimation", Int. J. of Systems Sci., 10(7), 719-734, 1979.

Robertson, D. G., Lee, J. H., and Rawlings, J. B., "A Moving Horizon-Based Approach for Least-Squares Estimation", AIChE J., 42(8), 2209-2224, 1996.

Roffel, B., and Rijnsdorp, J. E., "Dynamics and Control of a Gas-Fired Furnace", Chem. Eng. Sci., 29, 2083-2092, 1974.

Ronholm, L. L. I., "Move Moderation in Real-Time Optimization", M. Eng. Thesis, McMaster University, Hamilton, ON., Canada, 2000.

Smith, J. M., and Van Ness, H. C., "Introduction to Chemical Engineering Thermodynamics", 4th edition, McGraw-Hill Publishing Company, NY, 1987.

Sprinkle, D. R., Chaturvedi, S. K., and Kheireddine, A., "On-Line Measurement of Heat of Gaseous Hydrocarbon Fuel Mixtures", NASA Technical Paper 3572, March 1996.

Sutton, T. L., and MacGregor, J. F., "The Analysis and Design of Binary Vapor-Liquid Equilibrium Experiments Part I: Parameter Estimation and Consistency Tests", Can. J. Chem. Eng., 55, 602-608, 1977a.

Sutton, T. L., and MacGregor, J. F., "The Analysis and Design of Binary Vapor-Liquid Equilibrium Experiments Part II: The Design of Experiments", Can. J. Chem. Eng., 55, 609-613, 1977b.

Tong, H., and Crowe, C. M., "Detection of Gross Errors in Data Reconciliation by Principal Component Analysis", AIChE J., 41(7), 1995.

Tjoa, I. B., and Biegler, L. T., "Simultaneous Strategies for Data Reconciliation and Gross Errors Detection of Nonlinear System", Comp. Chem. Eng., 15(10), 679-690, 1991.

Vasantharajan S., and Biegler, L. T., "Large-Scale Decomposition for Successive Quadratic Programming", Comp. Chem. Eng., 12(11), 1087-1101, 1988.

Vos, B. J.; Grievink, J.; de Jong, P. J.; Verheijen, P. J. T. "A Robust Model-based Approach for On-Line Monitoring of Dynamic Process Performance", AIChE Annual Meeting, Los Angeles, CA., Paper 194d, 1997.

Welty, J. R., Wicks, C. E., and Wilson, R. E., "Fundamentals of Momentum, Heat and Mass Transfer", Wiley, NY, 1984.

White, D. C., "Online Optimization: What, Where and Estimating ROI", Hydrocarbon Processing, 43, June 1997.

Williams, T. J.; Otto, R. E. "A Generalized Chemical Processing Model for the Investigation of Computer Control", A.I.E.E. Trans., 79 (Nov.), 458-473, 1960.

Wolbert, D., Joulia, X., Koehret, B., and Biegler, L. T., "Flowsheet Optimization and Optimal Sensitivity Analysis Using Analytical Derivatives", Comp. Chem. Eng., 18(11/12), 1083-1095, 1994.

Yoon, S., Dasgupta, S., and Mijares, G., "Real Time Optimization System for Hyundai Petrochemical's Olefins Complex", NPRA Computer Conference, 1995.

Zamora, J. M., and Grossmann, I. E., "Continuous Global Optimization of Structured Process Systems Models", Comp. Chem. Eng., 22(12), 1749-1770, 1998.

Zhang, C., "Nonlinear Data Reconciliation and Parameter Estimation for Real-Time Optimization", M. Eng. Thesis, McMaster University, Hamilton, ON, Canada, 1998.

Zhang, Y., and Forbes, J. F., "Extended Design Cost: A Performance Criterion for Real-Time Optimization systems", Comp. Chem. Eng., 24, 1829-1841, 2000.

Zhang, Y., Nadler, D., and Forbes, J. F., "Results Analysis for Trust Constrained Real-Time Optimization", J. of Process Control, 11, 329-341, 2001.

APPENDIX A: OPTIMIZATION ALGORITHMS

Optimization problems in model updater and model-based optimizer in an RTO system can be solved by the existing optimization algorithms [Edgar et al., 2001; Fletcher, 1987; Gill et al., 1981]. Each method has its own advantages and disadvantages. Selection of algorithm for solving an optimization problem should consider the characteristics of the problem, for example, nonlinearity, number of variables, number of equations and degrees of freedom which can affect the performance of the algorithms.

The optimization problem in RTO applications can be formulated as shown in (A.1).

$$\begin{aligned} &\underset{\mathbf{x}}{\text{minimize}} && P(\mathbf{x}) \\ &\text{subject to} && \mathbf{f(x)} = \mathbf{0} \\ & && \mathbf{g(x)} \geq \mathbf{0} \end{aligned} \tag{A.1}$$

The problem can be the parameter estimation in model updating or model-based optimization. In RTO applications, the optimization problem is usually nonlinear with large number of equations and variables. The sequential quadratic programming (SQP) and MINOS are selected for solving the nonlinear optimization problems in this thesis. These two algorithms are briefly discussed in this Appendix.

SQP and MINOS use the local gradient information for searching the optimum. The algorithms terminate when the local optimality conditions are satisfied. For a non-convex problem, there is no guarantee that the converged local optimum is a global optimum. Global optimization algorithms have been developed for searching the global optimum [e.g. Arora et al., 1995; Byrne and Bogle, 1999; Choi et al., 1999; Zamora and

Grossman, 1998]. These global optimization algorithms require extensive computation which are not practical to solve large-scale problems online.

A.1 Sequential Quadratic Programming (SQP)

In SQP, the general nonlinear programming problem in (A.1) is iterated using a second order approximation for the Lagrangian, and first order approximation for the constraints. Therefore, in each major iteration, a quadratic programming (QP) subproblem is solved which determines the search direction to minimize the objective function. A line search is then performed to determine the optimum for the approximate problem. The estimate of the solution is updated for the next major iteration.

The QP subproblem for solving the search direction can be formulated from the KKT conditions of (A.1). For the time being, it is assumed that the correct active set of constraints has been determined from the active set strategy. The active inequality constraints can be treated as equality constraints. The Lagrangian function, L, of (A.1) is therefore given in (A.2)

$$L(\mathbf{x},\boldsymbol{\lambda}) = P(\mathbf{x}) + \boldsymbol{\lambda}^T \mathbf{f}(\mathbf{x}) \tag{A.2}$$

where $\boldsymbol{\lambda}$ is the vector of Lagrange multipliers of the constraints. The first order KKT conditions are given in (A.3).

$$\begin{aligned} \nabla_x L(\mathbf{x},\boldsymbol{\lambda}) &= \nabla_x P(\mathbf{x}) + \nabla_x \mathbf{f}(\mathbf{x})^T \boldsymbol{\lambda} = \mathbf{0} \\ \nabla_\lambda L(\mathbf{x},\boldsymbol{\lambda}) &= \mathbf{f}(\mathbf{x}) = \mathbf{0} \end{aligned} \tag{A.3}$$

The system of nonlinear equations in (A.3) can be solved by Newton's method. At k^{th} major iteration, (A.3) is linearized at the estimated optimum and Lagrange multipliers, $\mathbf{x}^k$ and $\boldsymbol{\lambda}^k$, and the following system of linearized equations is obtained.

$$\begin{bmatrix} \nabla_{xx}^2 L(\mathbf{x}^k, \boldsymbol{\lambda}^k) & \nabla_x \mathbf{f}(\mathbf{x}^k)^T \\ -\nabla_x \mathbf{f}(\mathbf{x}^k) & \mathbf{0} \end{bmatrix} \begin{bmatrix} \Delta \mathbf{x} \\ \Delta \boldsymbol{\lambda} \end{bmatrix} = \begin{bmatrix} -\nabla_x L(\mathbf{x}^k, \boldsymbol{\lambda}^k) \\ \mathbf{f}(\mathbf{x}^k) \end{bmatrix} \tag{A.4}$$

This system of equations is solved for $\Delta \mathbf{x}$ and $\Delta \boldsymbol{\lambda}$. Solution of (A.4) can also be obtained by solving the following QP problem.

$$\begin{aligned} \underset{\mathbf{d}}{\text{minimize}} \quad & \frac{1}{2}\mathbf{d}^T \nabla_{xx}^2 L(\mathbf{x}^k, \boldsymbol{\lambda}^k)\mathbf{d} + \nabla_x P(\mathbf{x}^k)^T \mathbf{d} \\ \text{subject to} \quad & \nabla_x \mathbf{f}(\mathbf{x}^k)\mathbf{d} + \mathbf{f}(\mathbf{x}^k) = \mathbf{0} \end{aligned} \tag{A.5}$$

The search direction, $\mathbf{d}$ (=$\Delta \mathbf{x}$), is determined by solving (A.5) in every major iteration.

In solving (A.5), the first derivatives of the objective function and the constraints, and the Hessian matrix of the Lagrangian function are required. Typically, SQP code uses analytical first derivatives and an approximation of the Hessian matrix of the Lagrangian function for solving (A.5). The Hessian matrix of the Lagrangian can be approximated via the BFGS updating formula without calculating the analytical second derivatives. In addition, the Hessian matrix of the Lagrangian may not be positive definite, and (A.5) may not have a solution. The Hessian matrix approximated by BFGS is always positive definite if the first iterate is positive definite, and a solution for (A.5) is guaranteed.

The QP subproblem in (A.5) can be easily solved by range and null space decomposition [Gill et al., 1981]. Let $\mathbf{Y}$ be a matrix whose columns span the range space of $\nabla_x \mathbf{f}(\mathbf{x}^k)$, and $\mathbf{Z}$ be a matrix whose columns span the set of vectors orthogonal to the rows of $\nabla_x \mathbf{f}(\mathbf{x}^k)$. The search direction, $\mathbf{d}$, can be projected into range and null spaces as shown in (A.6).

$$\mathbf{d} = \mathbf{Y}\mathbf{d}_Y + \mathbf{Z}\mathbf{d}_Z \tag{A.6}$$

Substituting (A.6) into the constraints of (A.5), and noticing that $\nabla_x \mathbf{f}(\mathbf{x}^k)\mathbf{Z} = \mathbf{0}$,

$$\nabla_x \mathbf{f}(\mathbf{x}^k)\mathbf{Y}\mathbf{d}_Y + \mathbf{f}(\mathbf{x}^k) = \mathbf{0} \tag{A.7}$$

If (A.5) has a solution, $\nabla_x \mathbf{f}(\mathbf{x}^k)\mathbf{Y}$ has full rank and $\mathbf{d}_Y$ is uniquely determined by solving (A.7). The search direction projected on the null space, $\mathbf{d}_Z$, can be determined by minimization of the quadratic objective function of (A.5) in the null space, or solving the system of linear equations in shown (A.8)

$$\mathbf{Z}^T\mathbf{B}_k\mathbf{Z}\mathbf{d}_z = -\mathbf{Z}^T\left(\nabla_x P(\mathbf{x}^k)^T + \mathbf{B}_k\mathbf{Y}\mathbf{d}_Y\right) \tag{A.8}$$

where $\mathbf{B}_k$ is the BFGS update for approximating the Hessian matrix of the Lagrangian function. The Lagrange multipliers can be estimated from the following system of linear equations.

$$\mathbf{B}_k\mathbf{d} + \nabla_x P(\mathbf{x}^k) = \nabla_x \mathbf{f}(\mathbf{x}^k)^T\boldsymbol{\lambda}^k \tag{A.9}$$

The QP subproblem in (A.5) can also be solved by the linear complementarity problem [Edgar et al., 2001; Fletcher, 1987]. This method starts with the Lagrangian function of the QP problem. The Kuhn-Tucker conditions of the QP problem are a set of linear equations and a complementary slackness condition. In the linear complementarity problem, LP pivot operations are used to solve the Kuhn-Tucker conditions. The algorithm terminates when the solution is complementary. The tableau for the pivoting method in solving the linear complementary problem is presented in Fletcher (1987).

Once the search direction, **d**, has been determined, the optimizer is moved along that direction to reduce the objective function in the original problem in (A.1). A line search is performed to determine the values of **x** for the next major iteration. The step size, α, is determined by minimizing a suitable merit function that measures the progress toward the optimum solution, $\mathbf{x}^*$, for the problem in (A.1). Different choices of the merit function are possible, for example, the quadratic penalty function, exact penalty function or augmented Lagrangian function [Gill et al., 1981]. The values of **x** at the next major iteration are calculated as follows:

$$\mathbf{x}^{k+1} = \mathbf{x}^k + \alpha \mathbf{d} \tag{A.10}$$

Inequality constraints can be handled by an active set method [Fletcher, 1987; Gill et al., 1981]. A maximum feasible step size along the search direction is first determined and denoted by $\overline{\alpha}$. If $\alpha < \overline{\alpha}$, the working set remains unchanged for the next iteration. If $\alpha = \overline{\alpha}$, the working set must be modified to reflect the fact that a new inequality constraint becomes active. The criteria for selecting the active set are complicated by nonlinear inequality constraints. Typical active set strategy examines the behavior of the constraints or merit function at $\mathbf{x}^k$ to predict which constraints are active [Gill et al., 1981].

A.2 MINOS

MINOS uses the projected augmented Lagrangian algorithm to solve nonlinear constrained optimization problems. The constraints are linearized in each major iteration. The augmented Lagrangian is obtained by adding a quadratic penalty term of the constraints. In the subproblem, the augmented Lagrangian is minimized subject to the linearized constraints and the original linear constraints. The subproblem is solved by reduced gradient method to determine the search direction. A line search along the search

direction is performed to determine the optimum for the subproblem which is the starting point of the next major iteration.

The general nonlinear constrained optimization problem in (A.1) can be formulated as follows:

$$\begin{aligned} \underset{\mathbf{x},\,\mathbf{y}}{\text{minimize}} \quad & P(\mathbf{x}) + \mathbf{c}^T\mathbf{x} + \mathbf{d}^T\mathbf{y} \\ \text{subject to} \quad & \mathbf{l}_1 \le \mathbf{f}(\mathbf{x}) + \mathbf{A}_1\mathbf{y} \le \mathbf{u}_1 \\ & \mathbf{l}_2 \le \mathbf{A}_2\mathbf{x} + \mathbf{A}_3\mathbf{y} \le \mathbf{u}_2 \\ & \mathbf{l} \le \begin{bmatrix} \mathbf{x} \\ \mathbf{y} \end{bmatrix} \le \mathbf{u} \end{aligned} \tag{A.11}$$

In the above formulation, the objective function and the constraints are separated into linear and nonlinear parts. The nonlinear part in the constraints is denoted by **f**. The vector, **y**, contains all the linear variables in the formulation. The upper and lower bounds of the variables are denoted by **l** and **u**, respectively.

The nonlinear part, **f**, in the constraints is linearized in each major iteration at $\mathbf{x}^k$. Therefore, **f**, can be approximated as shown in (A.12).

$$\mathbf{f}(\mathbf{x}) \approx \tilde{\mathbf{f}}(\mathbf{x}) = \mathbf{f}(\mathbf{x}^k) + \nabla_x \mathbf{f}(\mathbf{x}^k)(\mathbf{x} - \mathbf{x}^k) \tag{A.12}$$

The constraints can be written in form of (A.13)

$$\begin{bmatrix} \nabla_x \mathbf{f}(\mathbf{x}^k) & \mathbf{A}_1 \\ \mathbf{A}_2 & \mathbf{A}_3 \end{bmatrix} \begin{bmatrix} \mathbf{x} \\ \mathbf{y} \end{bmatrix} + \begin{bmatrix} \mathbf{I} & \mathbf{0} \\ \mathbf{0} & \mathbf{I} \end{bmatrix} \begin{bmatrix} \mathbf{s}_1 \\ \mathbf{s}_2 \end{bmatrix} = \begin{bmatrix} \nabla_x \mathbf{f}(\mathbf{x}^k)\mathbf{x}^k - \mathbf{f}(\mathbf{x}^k) \\ \mathbf{0} \end{bmatrix} \tag{A.13}$$

where $\mathbf{s}_1$ and $\mathbf{s}_2$ are the slack variables. The constraints can be re-expressed in the following general form:

$$\mathbf{Ax} + \mathbf{Is} = \mathbf{0} \tag{A.14}$$

The objective function to be minimized in the subproblem is the augmented Lagrangian function, and the formulation is shown as follow:

$$\underset{\mathbf{x},\mathbf{y}}{\text{minimize}} \quad P(\mathbf{x}) + \mathbf{c}^T\mathbf{x} + \mathbf{d}^T\mathbf{y} + (\boldsymbol{\lambda}^k)^T(\mathbf{f} - \tilde{\mathbf{f}}) + \frac{1}{2}\rho(\mathbf{f} - \tilde{\mathbf{f}})^T(\mathbf{f} - \tilde{\mathbf{f}}) \tag{A.15}$$

$$\text{subject to} \quad \begin{bmatrix} \nabla_x \mathbf{f}(\mathbf{x}^k) & \mathbf{A}_1 \\ \mathbf{A}_2 & \mathbf{A}_3 \end{bmatrix} \begin{bmatrix} \mathbf{x} \\ \mathbf{y} \end{bmatrix} + \begin{bmatrix} \mathbf{I} & \mathbf{0} \\ \mathbf{0} & \mathbf{I} \end{bmatrix} \begin{bmatrix} \mathbf{s}_1 \\ \mathbf{s}_2 \end{bmatrix} = \begin{bmatrix} \nabla_x \mathbf{f}(\mathbf{x}^k)\mathbf{x}^k - \mathbf{f}(\mathbf{x}^k) \\ \mathbf{0} \end{bmatrix}$$

$$\mathbf{l} \le \begin{bmatrix} \mathbf{x} \\ \mathbf{y} \end{bmatrix} \le \mathbf{u}$$

where $\boldsymbol{\lambda}^k$ is the current estimate of the Lagrange multipliers, and ρ is the penalty parameter. The term involving ρ is the modified quadratic penalty function. The penalty term is included to speed return to the feasible region for a poor initial guess. The penalty parameter is reduced to 0 to have quadratic convergence if the sequence of $\{\mathbf{x}^k, \boldsymbol{\lambda}^k\}$ is converging.

Minimization of the augmented Lagrangian function in (A.15) is solved by reduced gradient method. The variables in the general form of the linearized constraints in (A.14) are partitioned into superbasic variables, $\mathbf{x}_S$, basic variables, $\mathbf{x}_B$, and non-basic variables, $\mathbf{x}_N$. Equation (A.14) can be re-written as shown in (A.16).

$$\mathbf{Bx}_B + \mathbf{Sx}_S + \mathbf{Nx}_N = \mathbf{0} \tag{A.16}$$

At the solution, the basic and superbasic variables will lie between their bounds, while the non-basic variables are equal to one of their bounds. In reduced gradient method, the superbasic variables are free to move to improve the value of the objective function, while satisfying the linear constraints. Therefore, the matrix, **Z**, that determines the reduced space defined by the superbasic variables is given in (A.17)

$$\mathbf{Z} = \begin{bmatrix} -\mathbf{B}^{-1}\mathbf{S} \\ \mathbf{I} \\ \mathbf{0} \end{bmatrix} \tag{A.17}$$

assuming that the basic variables are chosen such that **B** is non-singular.

In the subproblem, the search direction in the space of superbasic variables is solved by quasi-Newton's method. Let P be the objective function of the optimization problem. The search direction in the space of superbasic variables is given in (A.18),

$$\mathbf{R}^{\mathrm{T}}\mathbf{R}\mathbf{d}_s = -\mathbf{Z}^{\mathrm{T}}\nabla \mathrm{P} \tag{A.18}$$

where **R** is the matrix such that $\mathbf{R}^{\mathrm{T}}\mathbf{R}$ approximates the reduced Hessian of the objective function, i.e.

$$\mathbf{R}^{\mathrm{T}}\mathbf{R} \approx \mathbf{Z}^{\mathrm{T}}\nabla^2 \mathrm{P}\mathbf{Z} \tag{A.19}$$

The search direction for all variables can be calculated by the following equation.

$$\mathbf{d} = \mathbf{Z}\mathbf{d}_s \tag{A.20}$$

A line search is performed to improve the values of the objective function along the search direction, **d**. The one dimensional line search problem can be stated as shown in (A.21)

$$\begin{aligned} &\underset{\alpha}{\text{minimize}} && P(\mathbf{x} + \alpha\mathbf{d}) \\ &\text{subject to} && 0 \le \alpha \le \overline{\alpha} \end{aligned} \tag{A.21}$$

where $\overline{\alpha}$ is the maximum step size determined by the bounds of the variables. The estimate of the optimum is updated from the solution of (A.21) for the next major iteration.

A.3 Commercial Codes for Solving the Optimization Problems

The choice of the software for solving the optimization problems in this thesis was based on the availability of standard routines and the relative ease in programming. The Williams-Otto reactor case study was simulated in MATLAB v5.3. The SQP solver in NAG toolbox [Mathworks, 1996] was used to solve the model updating, model-based optimization and experimental design problems. The closed-loop RTO calculation in the boiler case study was performed by interfacing MATLAB and GAMS [Ferris, 1999]. Plant simulation, model updating and model-based optimization were solved by MINOS in GAMS [Brooke et al., 1992], and the experimental design problem was solved by the SQP solver in NAG toolbox in MATLAB v5.3.

APPENDIX B: LINEAR SENSITIVY ANALYSIS IN NONLINAR PROGRAMMING

Linear sensitivity analysis in nonlinear programming studies the behavior of the optimal solution when the parameters are perturbed locally about their nominal values. The sensitivity matrices estimated by linear sensitivity analysis are used to estimate the covariance matrices of the estimated parameters in model updater and the predicted optimum in model-based optimizer. These covariance matrices are required for real-time results analysis and diagnosis. This appendix outlines the procedures in estimating the linear sensitivity matrix for a nonlinear programming problem.

The general optimization problem can be formulated as follows:

$$\begin{aligned} \underset{\mathbf{x}}{\text{minimize}} \quad & P(\mathbf{x},\boldsymbol{\beta}) \\ \text{subject to} \quad & \mathbf{f}(\mathbf{x},\boldsymbol{\beta}) = \mathbf{0} \\ & \mathbf{g}(\mathbf{x},\boldsymbol{\beta}) \geq \mathbf{0} \end{aligned} \tag{B.1}$$

where $\boldsymbol{\beta}$ is the vector of parameters, $\mathbf{x}$ is the vector of optimization variables, $\mathbf{f}$ and $\mathbf{g}$ are the equality and inequality constraints of the model, and P is the objective function. Sensitivity analysis determines how the solution, $\mathbf{x}$, changes when $\boldsymbol{\beta}$ is perturbed.

Sensitivity analysis can be performed by perturbing the first order KKT conditions of (B.1) [Fiacco, 1983; Wolbert et al., 1994]. The Lagrangian of (B.1) is given in (B.2),

$$L(\mathbf{x},\boldsymbol{\lambda},\boldsymbol{\mu},\boldsymbol{\beta}) = P(\mathbf{x},\boldsymbol{\beta}) + \boldsymbol{\lambda}^T\mathbf{f}(\mathbf{x},\boldsymbol{\beta}) - \boldsymbol{\mu}^T\mathbf{g}(\mathbf{x},\boldsymbol{\beta}) \tag{B.2}$$

where $\boldsymbol{\lambda}$ and $\boldsymbol{\mu}$ are the Lagrange multipliers for equality and inequality constraints respectively. At the local optimum, $(\mathbf{x}^*,\boldsymbol{\lambda}^*,\boldsymbol{\mu}^*)$, the following conditions must be satisfied.

$$\begin{aligned}
&\nabla_x L(\mathbf{x}^*,\boldsymbol{\lambda}^*,\boldsymbol{\mu}^*,\boldsymbol{\beta}) = \nabla_x P(\mathbf{x}^*,\boldsymbol{\beta}) + \nabla_x \mathbf{f}(\mathbf{x}^*,\boldsymbol{\beta})^T \boldsymbol{\lambda}^* - \nabla_x \mathbf{g}(\mathbf{x}^*,\boldsymbol{\beta})^T \boldsymbol{\mu}^* = \mathbf{0} \\
&\mathbf{f}(\mathbf{x}^*,\boldsymbol{\beta}) = \mathbf{0} \\
&\mathbf{g}(\mathbf{x}^*,\boldsymbol{\beta}) \geq \mathbf{0} \\
&\mu_i^* g_i(\mathbf{x}^*,\boldsymbol{\beta}) = 0 \\
&\mu_i^* \geq 0
\end{aligned} \tag{B.3}$$

These conditions must hold for an infinitesimal perturbation of $\boldsymbol{\beta}$. Differentiating the conditions in (B.3), assuming that the strict complementary slackness holds, i.e., the active set of inequality constraints remains unchanged in the neighborhood of the nominal parameter value, $\boldsymbol{\beta}$, the following equations are obtained,

$$\begin{aligned}
&d[\nabla_x L(\mathbf{x}^*,\boldsymbol{\lambda}^*,\boldsymbol{\mu}^*,\boldsymbol{\beta})] = \nabla_{xx}{}^2 L^* d\mathbf{x} + \nabla_{\beta x}{}^2 L^* d\boldsymbol{\beta} + \nabla_x \mathbf{f}^{*T} d\boldsymbol{\lambda} - \nabla_x \mathbf{g}^{*T} d\boldsymbol{\mu} = \mathbf{0} \\
&d[\mathbf{f}(\mathbf{x}^*,\boldsymbol{\beta})] = \nabla_x \mathbf{f}^* d\mathbf{x} + \nabla_\beta \mathbf{f}^* d\boldsymbol{\beta} = \mathbf{0} \\
&d[\mathbf{g}_a(\mathbf{x}^*,\boldsymbol{\beta})] = \nabla_x \mathbf{g}_a{}^* d\mathbf{x} + \nabla_\beta \mathbf{g}_a{}^* d\boldsymbol{\beta} = \mathbf{0}
\end{aligned} \tag{B.4}$$

where $\mathbf{g}_a$ represents the active set of inequality constraints. Equation (B.4) can be re-arranged into matrix form as shown in (B.5).

$$\begin{bmatrix} \nabla_{\beta x}{}^2 L^* \\ \nabla_\beta \mathbf{f}^* \\ \nabla_\beta \mathbf{g}_a{}^* \end{bmatrix} = -\begin{bmatrix} \nabla_{xx}{}^2 L^* & \nabla_x \mathbf{f}^{*T} & -\nabla_x \mathbf{g}^{*T} \\ \nabla_x \mathbf{f}^* & \mathbf{0} & \mathbf{0} \\ \nabla_x \mathbf{g}_a{}^* & \mathbf{0} & \mathbf{0} \end{bmatrix} \begin{bmatrix} \nabla_\beta \mathbf{x}^* \\ \nabla_\beta \boldsymbol{\lambda}^* \\ \nabla_\beta \boldsymbol{\mu}^* \end{bmatrix} \tag{B.5}$$

Equation (B.5) can be simplified by performing range and null space decomposition [Vasantharajan and Biegler, 1988]. By augmenting the active inequality constraints, $\mathbf{g_a}$, into the vector $\mathbf{f}$, and the corresponding Lagrange multipliers into the vector $\boldsymbol{\lambda}$, and dropping the superscript * for clarity, the following system of equations can be obtained.

$$\begin{bmatrix} \mathbf{Y}^T\nabla_{\beta x}{}^2\mathrm{L} \\ \mathbf{Z}^T\nabla_{\beta x}{}^2\mathrm{L} \\ \nabla_\beta \mathbf{f} \end{bmatrix} = -\begin{bmatrix} \mathbf{Y}^T\nabla_{xx}{}^2\mathrm{L}\mathbf{Y} & \mathbf{Y}^T\nabla_{xx}{}^2\mathrm{L}\mathbf{Z} & \mathbf{Y}^T\nabla_x \mathbf{f}^T \\ \mathbf{Z}^T\nabla_{xx}{}^2\mathrm{L}\mathbf{Y} & \mathbf{Z}^T\nabla_{xx}{}^2\mathrm{L}\mathbf{Z} & \mathbf{0} \\ \nabla_x \mathbf{f}\mathbf{Y} & \mathbf{0} & \mathbf{0} \end{bmatrix} \begin{bmatrix} \mathbf{Y}^T\nabla_\beta \mathbf{x} \\ \mathbf{Z}^T\nabla_\beta \mathbf{x} \\ \nabla_\beta \boldsymbol{\lambda} \end{bmatrix} \tag{B.6}$$

The choice of $\mathbf{Y}$ and $\mathbf{Z}$ is not unique. A reasonable choice is to partition the variables, $\mathbf{x}$, into independent variables, $\mathbf{x_I}$, and dependent variables, $\mathbf{x_D}$, and $\mathbf{Y}$ and $\mathbf{Z}$ are given in (B.7) and (B.8)

$$\mathbf{Y} = \begin{bmatrix} \left(\dfrac{\mathbf{df}}{\mathbf{dx_I}}\right)^T \left(\dfrac{\mathbf{df}}{\mathbf{dx_D}}\right)^{-1} \\ \mathbf{I} \end{bmatrix} \tag{B.7}$$

$$\mathbf{Z} = \begin{bmatrix} \mathbf{I} \\ -\left(\dfrac{\mathbf{df}}{\mathbf{dx_D}}\right)^{-1} \left(\dfrac{\mathbf{df}}{\mathbf{dx_I}}\right) \end{bmatrix} \tag{B.8}$$

where $\mathbf{I}$ is the identity matrix. With these definitions of $\mathbf{Y}$ and $\mathbf{Z}$, the last two equations in (B.6) can be written as shown in (B.9) and (B.10).

$$\nabla_\beta \mathbf{x_D} = \mathbf{Y}^T\nabla_\beta \mathbf{x} = -(\nabla_x \mathbf{f}\mathbf{Y})^{-1}\nabla_\beta \mathbf{f} \tag{B.9}$$

$$\nabla_\beta \mathbf{x_I} = \mathbf{Z}^T\nabla_\beta \mathbf{x} = -(\mathbf{Z}^T\nabla_{xx}{}^2\mathrm{L}\mathbf{Z})^{-1}[\mathbf{Z}^T\nabla_{\beta x}{}^2\mathrm{L} + \mathbf{Z}^T\nabla_{xx}{}^2\mathrm{L}\mathbf{Y}\nabla_\beta \mathbf{x_D}] \tag{B.10}$$

The sensitivity of the optimum with respect to the parameter perturbation can be obtained from the expressions in (B.9) and (B.10).

$$\nabla_{\beta}\mathbf{x} = \mathbf{Z}\nabla_{\beta}\mathbf{x}_{\mathbf{I}} + \mathbf{Y}\nabla_{\beta}\mathbf{x}_{\mathbf{D}} \tag{B.11}$$

In this thesis, (B.9) to (B.11) are used to calculate the sensitivity matrix of the optimization problem.

Calculation of the sensitivity matrix in (B.10) requires second order derivatives projected onto the null space. In this thesis, the first derivatives are derived analytically. The second derivatives are determined by numerical differentiation. The advantage of range and null space decomposition is that the entire Hessian matrix of the Lagrangian in (B.5) is not required. Numerical differentiation can be done in the reduced space to save the computation time by perturbing all the variables along the directions of the orthonormal columns of **Z** as shown in (B.12) [Wolbert et al., 1994],

$$(\mathbf{e}_i{}^{\mathrm{T}}\mathbf{Z}^{\mathrm{T}}\nabla_{x?}{}^{2}\mathrm{L})^{\mathrm{T}} = \frac{\nabla_{?}\mathrm{L}(\mathbf{x} + \delta\mathbf{Z}\mathbf{e}_i) - \nabla_{?}\mathrm{L}(\mathbf{x})}{\delta} \tag{B.12}$$

where "?" represent $\mathbf{x}$ or $\boldsymbol{\beta}$, $\mathbf{e}_i$ is a zero vector except for a 1 in its i^{th} element, and δ is the step size for numerical differentiation. Equation (B.12) calculates the i^{th} column of the matrix $\mathbf{Z}^{\mathrm{T}}\nabla_{x?}{}^{2}\mathrm{L}$. The required second derivatives in (B.10) can be obtained by post multiplying $\mathbf{Z}^{\mathrm{T}}\nabla_{x?}{}^{2}\mathrm{L}$ from (B.12) by **Y** or **Z**.

APPENDIX C: DERIVATION OF THE EXPECTED PROFIT CRITERION FOR EXPERIMENTAL DESIGN

The formulation of the expected profit experimental design criterion is based on the expected profit derived by Forbes and Marlin (1996). Here, the cost, C, is the expected loss from the maximum possible profit achieved by an RTO system at a given RTO execution. The overall expected profit for a specified future horizon, N_D, for experimental design can be derived by integrating or averaging the design cost over N_D. Experiments are designed by maximizing the overall expected profit. The following sections present the derivation of the overall expected profit (EP in Problem 4.1), which is the objective function for the experimental design problem.

C.1 Definition of Design Cost

The design cost represents the theoretically attainable profit that the RTO system cannot achieve at a particular RTO execution and is defined in the following

$$C = P(\mathbf{x}_p^*) - E[P(\mathbf{x}_m^*)] \tag{C.1}$$

where E is the expectation operator, P is the true plant profit function, and $\mathbf{x}_p^*$ and $\mathbf{x}_m^*$ are the true plant and model optima, respectively. Using a second order Taylor series approximation for the true plant profit, C can be expressed in terms of the true plant optimum, and model optimum and its covariance matrix given in the following

$$C = \left(\mathbf{x}_p^* - \mathbf{x}_m^*\right)^T \left(\frac{1}{2}\nabla_r^2 P\Big|_{x_p^*}\right)\left(\mathbf{x}_p^* - \mathbf{x}_m^*\right) + \frac{1}{2}\nabla_r^2 P\Big|_{x_p^*} \circ \mathbf{Q}_{x_m^*} \tag{C.2}$$

where $$\nabla_r^2 P\Big|_{x_p^*} \circ \mathbf{Q}_{x_m^*} = \sum_{i=1}^{n}\sum_{j=1}^{n} \frac{\partial^2 P}{\partial x_i \partial x_j}\Big|_{x_p^*} \times \sigma_{ij}^2$$

and $\nabla_r^2 P\Big|_{x_p^*}$ is the reduced Hessian of the true plant profit, $\mathbf{Q}_{x_m^*}$ is the variability of $\mathbf{x}_m^*$, σ_{ij}^2 is the ij element in $\mathbf{Q}_{x_m^*}$, and n is the dimension of the reduced space. The first term in the expression is the loss in profit due to offset, and the second term is profit loss due to variability.

C.2 Derivation of Design Cost over the Future Horizon

The total design cost over the future horizon, N_D, can be obtained by summing the design cost at each RTO execution. As shown in Figure 4.1, the horizon N_D can be divided into three periods, before, during and after experimentation. The overall expected profit is the sum of the profit loss terms in these periods which are denoted by $C_{BE}(N)$, $C_{DE}(N)$ and $C_{AE}(N)$, respectively. Using (C.2), the profit loss terms in different periods can be expressed as follows.

$$C_{BE}(N) = \left(\mathbf{x}_p^*(N) - \mathbf{x}_{mo}^*(N)\right)^T \left(\frac{1}{2}\nabla_r^2 P\Big|_{x_p^*(N)}\right)\left(\mathbf{x}_p^*(N) - \mathbf{x}_{mo}^*(N)\right) + \frac{1}{2}\nabla_r^2 P\Big|_{x_p^*(N)} \circ \mathbf{Q}_{x_m^*(N)}$$

$$\text{for } N = 1, 2, \ldots, N_o \qquad \text{(C.3)}$$

$$C_{DE}(N) = \left(\mathbf{x}_p^*(N) - \mathbf{x}_{expt}(N)\right)^T \left(\frac{1}{2}\nabla_r^2 P\Big|_{x_p^*(N)}\right)\left(\mathbf{x}_p^*(N) - \mathbf{x}_{expt}(N)\right)$$

$$\text{for } N = N_o+1, \ldots, N_o + N_{expt} \qquad \text{(C.4)}$$

$$C_{AE}(N) = \left(\mathbf{x}_p^*(N) - \mathbf{x}_m^*(N)\right)^T \left(\frac{1}{2}\nabla_r^2 P\Big|_{\mathbf{x}_p^*(N)}\right)\left(\mathbf{x}_p^*(N) - \mathbf{x}_m^*(N)\right) + \frac{1}{2}\nabla_r^2 P\Big|_{\mathbf{x}_p^*(N)} \circ \mathbf{Q}_{\mathbf{x}_m^*(N)}$$

$$\text{for } N = N_o + N_{expt} + 1, \ldots, N_D \qquad \text{(C.5)}$$

where $\mathbf{x}_{mo}^*$ is the model optimum predicted by the RTO system before experimentation, and $\mathbf{x}_m^*$ is the model optimum predicted after experimentation using the estimated values of the additional parameters updated from experimental operating points, $\mathbf{x}_{expt}$. The overall expected profit, EP, is equal to the summation of the design cost in each period of time as shown in the following.

$$EP = \sum_{N=1}^{N_o} C_{BE}(N) + \sum_{N=N_o+1}^{N_o+N_{expt}} C_{DE}(N) + \sum_{N=N_o+N_{expt}+1}^{N_D} C_{AE}(N) \qquad \text{(C.6)}$$

Equation (C.6) cannot be maximized directly because the true plant optimum and its reduced Hessian matrix, and future model prediction are unknown. Therefore, (C.6) will be modified to estimate the unknown terms.

C.3 Expressing the Design Cost in terms of the Offsets

Offset of the model prediction from the true plant optimum can be separated into two terms, offset that cannot be removed by performing experiments, **e**, and the offset that can be removed by performing experiments, Δ. The term, **e**, is defined as the offset between the true plant optimum and the "best" RTO prediction, when the disturbance is exactly measured. This offset is caused by the inherent mismatch between the RTO model and the true plant. The term, Δ, is the offset between the RTO prediction and the "best" RTO prediction. This section presents the derivation of EP in (C.6) in terms of **e** and Δ.

The terms, $\mathbf{e}$ and Δ, can be expressed in terms of the optima, $\mathbf{x}_p^*$, $\mathbf{x}_{mo}^*$ and $\mathbf{x}_m^*$. If the disturbance is exactly known and the additional parameters can be updated in every RTO execution, theoretically, the best operating policy denoted by $\mathbf{x}_{opt}$ responding to that disturbance can be determined. At any RTO execution, N, the inherent offset, $\mathbf{e}(N)$, is shown as follows.

$$\mathbf{e}(N) = \mathbf{x}_p^*(N) - \mathbf{x}_{opt}(N) \tag{C.7}$$

The offset that can be reduced by experimentation is equal to the offset between $\mathbf{x}_{opt}(N)$ and the RTO predictions, $\mathbf{x}_{mo}^*(N)$ and $\mathbf{x}_m^*(N)$ before and after experimentation, respectively. Therefore, before and during experimentation, the offset that can be reduced by experiments is given by

$$\Delta_o(N) = \mathbf{x}_{opt}(N) - \mathbf{x}_{mo}^*(N) \qquad \text{for } N = 1, 2, \ldots, N_o + N_{expt} \tag{C.8}$$

and after experimentation, the offset is given by

$$\Delta(N) = \mathbf{x}_{opt}(N) - \mathbf{x}_m^*(N) \qquad \text{for } N = N_o + N_{expt}+1, \ldots, N_D \tag{C.9}$$

The design costs before, during and after experimentation can be expressed in terms of the offsets, $\mathbf{e}$, Δ_o, and Δ, by substituting (C.7) – (C.9) into (C.3) – (C.5), which are given as follows:

$$C_{BE}(N) = \left(\Delta_o(N) + \mathbf{e}(N)\right)^T \left(\frac{1}{2}\nabla_r^2 P\Big|_{x_p^*(N)}\right)\left(\Delta_o(N) + \mathbf{e}(N)\right) + \frac{1}{2}\nabla_r^2 P\Big|_{x_p^*(N)} \circ \mathbf{Q}_{x_m^*(N)}$$
$$\text{for } N = 1, 2, \ldots, N_o \tag{C.10}$$

$$C_{DE}(N) =$$

$$\left((\boldsymbol{\Delta}_o(N)+\mathbf{e}(N))+(\mathbf{x}^*_{mo}(N)-\mathbf{x}_{expt}(N))\right)^T\left(\frac{1}{2}\nabla_r{}^2P\Big|_{x^*_p(N)}\right)\left((\boldsymbol{\Delta}_o(N)+\mathbf{e}(N))+(\mathbf{x}^*_{mo}(N)-\mathbf{x}_{expt}(N))\right)$$

$$\text{for } N = N_o+1, \ldots, N_o + N_{expt} \qquad \text{(C.11)}$$

$$C_{AE}(N) = (\boldsymbol{\Delta}(N)+\mathbf{e}(N))^T\left(\frac{1}{2}\nabla_r{}^2P\Big|_{x^*_p(N)}\right)(\boldsymbol{\Delta}(N)+\mathbf{e}(N))+\frac{1}{2}\nabla_r{}^2P\Big|_{x^*_p(N)}\circ\mathbf{Q}_{x^*_m(N)}$$

$$\text{for } N = N_o + N_{expt} +1, \ldots., N_D \qquad \text{(C.12)}$$

Overall expected profit, EP, can be obtained by substituting (C.10) – (C.12) into (C.6). Expanding and rearranging the terms, the following expression for EP can be obtained.

$$\begin{aligned}
EP = &\sum_{N=1}^{N_o}(\boldsymbol{\Delta}_o(N)+\mathbf{e}(N))^T\left(\frac{1}{2}\nabla_r{}^2P\Big|_{x^*_p(N)}\right)(\boldsymbol{\Delta}_o(N)+\mathbf{e}(N))+\\
&\sum_{N=N_o+1}^{N_o+N_{expt}}\Big\{(\mathbf{x}^*_{mo}(N)-\mathbf{x}_{expt}(N))^T\left(\frac{1}{2}\nabla_r{}^2P\Big|_{x^*_p(N)}\right)(\mathbf{x}^*_{mo}(N)-\mathbf{x}_{expt}(N))\\
&\quad+(\boldsymbol{\Delta}_o(N)+\mathbf{e}(N))^T\left(\frac{1}{2}\nabla_r{}^2P\Big|_{x^*_p(N)}\right)(\boldsymbol{\Delta}_o(N)+\mathbf{e}(N))\\
&\quad+2(\mathbf{x}^*_{mo}(N)-\mathbf{x}_{expt}(N))^T\left(\frac{1}{2}\nabla_r{}^2P\Big|_{x^*_p(N)}\right)(\boldsymbol{\Delta}_o(N)+\mathbf{e}(N))\Big\}+\\
&\sum_{N=N_o+N_{expt}+1}^{N_D}(\boldsymbol{\Delta}(N)+\mathbf{e}(N))^T\left(\frac{1}{2}\nabla_r{}^2P\Big|_{x^*_p(N)}\right)(\boldsymbol{\Delta}(N)+\mathbf{e}(N))+\\
&\sum_{N=1}^{N_o}\frac{1}{2}\nabla_r{}^2P\Big|_{x^*_p(N)}\circ\mathbf{Q}_{x^*_{mo}(N)}+\sum_{N=N_o+N_{expt}+1}^{N_D}\frac{1}{2}\nabla_r{}^2P\Big|_{x^*_p(N)}\circ\mathbf{Q}_{x^*_m(N)}
\end{aligned} \qquad \text{(C.13)}$$

In evaluating EP, the offsets, **e**, Δ_o, and Δ, and the reduced Hessian of the plant profit, $\nabla_r^2 P\big|_{x_r^*(N)}$ have to be known. The following sections discuss the assumptions made in simplifying the expression of EP.

C.4 Estimation of the Offsets

The offsets, **e**, Δ_o, and Δ, are unknown, and evaluation of EP in (C.13) requires estimation of these terms. In multivariable processes, these offsets are characterized by their norms as well as the directions. If both norms and directions of the offsets were known exactly, experimental design would not be required, as the true plant optimum would be perfectly known. In estimating the offsets, it is assumed that their norms can be estimated from past historical data but the directions of the current disturbance are unknown. For simplicity, the reduced space with a dimension of two will be considered first, and the expressions for the offsets can be generalized to multidimensional case.

Since the directions of the offsets are unknown, only the average of the overall expected profit in (C.13) with respect to the directions can be estimated. The overall expected profit can be integrated with respect to the directions of the offsets. Only **e**, Δ_o, and Δ are functions of the directions. Therefore, the integrals involving the terms **e**, Δ_o, and Δ in (C.13) are evaluated, and the other terms which do not contain the offsets remain unchanged.

The terms involving the offsets are weighted by $\nabla_r^2 P\big|_{x_r^*(N)}$, and therefore, the directionality of the profit contours has to be considered in averaging the expected profit with respect to the directions of the offsets. The term, $(\Delta+\mathbf{e})^T\left(\frac{1}{2}\nabla_r^2 P\big|_{x_r^*}\right)(\Delta+\mathbf{e})$, can be evaluated easily by transforming the coordinate system with reference to the principal

axes (Y_1 and Y_2) of $\nabla_r^2 P\big|_{x_p^*}$. Since $\nabla_r^2 P\big|_{x_p^*}$ is real and symmetric, there exists an orthogonal matrix, **U**, such that $\nabla_r^2 P\big|_{x_p^*}$ can be diagonalized as stated in the following

$$\Lambda = \mathbf{U}^T \nabla_r^2 P\big|_{x_p^*} \mathbf{U} \tag{C.14}$$

where Λ is a diagonal matrix with diagonal elements equal to the eigenvalues of $\nabla_r^2 P\big|_{x_p^*}$ denoted by $\lambda_i(\nabla_r^2 P\big|_{x_p^*})$, and **U** defines the directions of the principal axes, Y_1 and Y_2. The orthogonal transformations of **e** and Δ to the new set of coordinate system ($\boldsymbol{\eta}_e$ and $\boldsymbol{\eta}_\Delta$) defined by Y_1 and Y_2 are given as follows.

$$\begin{aligned} \boldsymbol{\eta}_e &= \mathbf{U}\mathbf{e} \\ \boldsymbol{\eta}_\Delta &= \mathbf{U}\Delta \end{aligned} \tag{C.15}$$

Therefore, the offset term can be expressed as follow:

$$\begin{aligned} (\Delta+\mathbf{e})^T\left(\frac{1}{2}\nabla_r^2 P\big|_{x_p^*}\right)(\Delta+\mathbf{e}) &= [\mathbf{U}(\boldsymbol{\eta}_\Delta+\boldsymbol{\eta}_e)]^T\left(\frac{1}{2}\nabla_r^2 P\big|_{x_p^*}\right)[\mathbf{U}(\boldsymbol{\eta}_\Delta+\boldsymbol{\eta}_e)] \\ &= (\boldsymbol{\eta}_\Delta+\boldsymbol{\eta}_e)^T\mathbf{U}^T\left(\frac{1}{2}\nabla_r^2 P\big|_{x_p^*}\right)\mathbf{U}(\boldsymbol{\eta}_\Delta+\boldsymbol{\eta}_e) \\ &= \frac{1}{2}(\boldsymbol{\eta}_\Delta+\boldsymbol{\eta}_e)^T\Lambda(\boldsymbol{\eta}_\Delta+\boldsymbol{\eta}_e) \\ &= \frac{1}{2}(\boldsymbol{\eta}_\Delta{}^T\Lambda\boldsymbol{\eta}_\Delta+\boldsymbol{\eta}_e{}^T\Lambda\boldsymbol{\eta}_e)+\boldsymbol{\eta}_\Delta{}^T\Lambda\boldsymbol{\eta}_e \end{aligned} \tag{C.16}$$

The terms, $\boldsymbol{\eta}_\Delta$ and $\boldsymbol{\eta}_e$, can be expressed in terms of their directions with respect to the principal axes, Y_1 and Y_2. It is assumed that Δ and $\mathbf{e}$ make an angle θ and ϕ with the principal axes respectively. Therefore,

$$\boldsymbol{\eta}_\Delta = R_\Delta \begin{bmatrix} \cos\theta \\ \sin\theta \end{bmatrix} \tag{C.17}$$

and

$$\boldsymbol{\eta}_e = R_e \begin{bmatrix} \cos\phi \\ \sin\phi \end{bmatrix} \tag{C.18}$$

where R_Δ and R_e are the Euclidean norms of the offsets, Δ and $\mathbf{e}$, respectively. Substituting (C.17) and (C.18) into (C.16), the following expression can be obtained.

$$(\Delta+\mathbf{e})^T\left(\frac{1}{2}\nabla_r^2 P\Big|_{x_p^*}\right)(\Delta+\mathbf{e}) = \frac{1}{2}\left(R_\Delta{}^2(\lambda_1\cos^2\theta+\lambda_2\sin^2\theta)+R_e{}^2(\lambda_1\cos^2\phi+\lambda_2\sin^2\phi)\right)+ R_\Delta R_e(\cos\theta\cos\phi+\sin\theta\sin\phi) \tag{C.19}$$

where λ_1 and λ_2 are the diagonal elements in Λ which are the eigenvalues of $\nabla_r^2 P\Big|_{x_p^*}$.

The expectation or average of the profit loss due to offset can be derived by averaging (C.19) with respect to the directions of θ and ϕ from 0 to 2π which is stated as follow.

$$E\left[(\Delta+\mathbf{e})^T\left(\frac{1}{2}\nabla_r^2 P\Big|_{x_p^*}\right)(\Delta+\mathbf{e})\right] = \frac{1}{2}\left(R_\Delta{}^2+R_e{}^2\right)\frac{\lambda_1+\lambda_2}{2} \tag{C.20}$$

The expression in (C.20) is the average profit loss due to offset estimated by the "average" eigenvalue of the reduced Hessian matrix of the plant, if only the norm of the offset is known without knowing the direction. This expression can be generalized for n-

dimensional space and the average profit loss due to offset is given in the following expression.

$$E\left[(\Delta+\mathbf{e})^T\left(\frac{1}{2}\nabla_r{}^2P\Big|_{x_p^*}\right)(\Delta+\mathbf{e})\right]=\frac{1}{2}\left(R_\Delta{}^2+R_e{}^2\right)\frac{\sum_{i=1}^{n}\lambda_i}{n} \tag{C.21}$$

The average of the term $(\mathbf{x}_{mo}^* - \mathbf{x}_{expt})^T\left(\frac{1}{2}\nabla_r{}^2P\Big|_{x_p^*(t)}\right)(\Delta_o+\mathbf{e})$ in (C.13) can be evaluated similarly which is equal to zero. Therefore, EP can be expressed in terms of R_Δ, R_{Δ_o} and R_e as shown in the following.

EP =

$$\sum_{N=1}^{N_o}\frac{1}{2}\left(R_{\Delta_o}{}^2(N)+R_e{}^2(N)\right)\frac{\sum_{i=1}^{n}\lambda_i\left(\nabla_r{}^2P\Big|_{x_p^*(N)}\right)}{n}+\sum_{N=N_o+1}^{N_o+N_{expt}}\frac{1}{2}\left(R_{\Delta_o}{}^2(N)+R_e{}^2(N)\right)\frac{\sum_{i=1}^{n}\lambda_i\left(\nabla_r{}^2P\Big|_{x_p^*(N)}\right)}{n}+$$

$$\sum_{N=N_o+N_{expt}+1}^{N_D}\frac{1}{2}\left(R_\Delta{}^2(N)+R_e{}^2(N)\right)\frac{\sum_{i=1}^{n}\lambda_i\left(\nabla_r{}^2P\Big|_{x_p^*(N)}\right)}{n}+$$

$$\sum_{N=N_o+1}^{N_o+N_{expt}}(\mathbf{x}_{mo}^*(N)-\mathbf{x}_{expt}(N))^T\left(\frac{1}{2}\nabla_r{}^2P\Big|_{x_p^*(N)}\right)(\mathbf{x}_{mo}^*(N)-\mathbf{x}_{expt}(N))+$$

$$\sum_{N=1}^{N_o}\frac{1}{2}\nabla_r{}^2P\Big|_{x_p^*(N)}\circ\mathbf{Q}_{x_{mo}^*(N)}+\sum_{N=N_o+N_{expt}+1}^{N_D}\frac{1}{2}\nabla_r{}^2P\Big|_{x_p^*(N)}\circ\mathbf{Q}_{x_m^*(N)} \tag{C.22}$$

Expression of EP in (C.22) contains some unknown terms; the reduced Hessian matrix of the plant, the future model optimum, $\mathbf{x}_{mo}^*(N)$ and its covariance, $\mathbf{Q}_{x_{mo}^*}(N)$. Further assumptions are required to evaluate the expected profit which will be discussed next.

C.5 Further Assumptions in Simplifying EP

Assumptions are made to replace the unknown terms in (C.22) by the known terms to evaluate the expected profit in experimental design. The assumptions are stated as follows:

1. The future model optimum and its covariance matrix are replaced by the current predicted optimum and its covariance matrix during experimental design, that is, $\mathbf{x}^*_{mo}(N) = \mathbf{x}^*_{mo}$, and $\mathbf{Q}_{x^*_{mo}}(N) = \mathbf{Q}_{x^*_{mo}}$.
2. The reduced Hessian matrix of the plant is replaced by the reduced Hessian matrix of the model estimated at the current RTO execution, that is, $\nabla_r^2 P\big|_{x^*_p(N)} = \nabla_r^2 P\big|_{x^*_{mo}}$.

The first assumption is valid if the optimum is changing slowly, which is a good approximation for slow disturbances. The second assumption is the best that can be done because the true plant model is never known. With these assumptions, EP can be expressed in terms of known quantities given as follow.

EP =

$$\sum_{N=1}^{N_o}\frac{1}{2}\left(R_{\Delta_o}{}^2(N)+R_e{}^2(N)\right)\frac{\sum_{i=1}^{n}\lambda_i\left(\nabla_r{}^2P\big|_{x^*_{mo}}\right)}{n}+\sum_{N=N_o+1}^{N_o+N_{expt}}\frac{1}{2}\left(R_{\Delta_o}{}^2(N)+R_e{}^2(N)\right)\frac{\sum_{i=1}^{n}\lambda_i\left(\nabla_r{}^2P\big|_{x^*_{mo}}\right)}{n}+$$

$$\sum_{N=N_o+N_{expt}+1}^{N_D}\frac{1}{2}\left(R_{\Delta}{}^2(N)+R_e{}^2(N)\right)\frac{\sum_{i=1}^{n}\lambda_i\left(\nabla_r{}^2P\big|_{x^*_{mo}}\right)}{n}+$$

$$\sum_{N=N_o+1}^{N_o+N_{expt}}(\mathbf{x}^*_{mo}-\mathbf{x}_{expt}(N))^T\left(\frac{1}{2}\nabla_r{}^2P\Big|_{x^*_{mo}}\right)(\mathbf{x}^*_{mo}-\mathbf{x}_{expt}(N))+$$

$$\sum_{N=1}^{N_o}\frac{1}{2}\nabla_r{}^2P\Big|_{x^*_{mo}}\circ\mathbf{Q}_{x^*_{mo}}+\sum_{N=N_o+N_{expt}+1}^{N_D}\frac{1}{2}\nabla_r{}^2P\Big|_{x^*_{mo}}\circ\mathbf{Q}_{x^*_{m}(N)} \qquad \text{(C.23)}$$

Since R_e cannot be influenced by experimentation, this term can be removed from the objective function. The factor $\frac{1}{2}$ in each term does not affect $\mathbf{x}_{expt}(N)$ and is also removed from the objective function. Therefore, the experimental design problem is shown as follow.

$$\begin{aligned} &\text{maximize} && EP = P_1 + P_2 + P_3 \qquad \text{(C.24)}\\ &N_o,\, N_{expt},\, \mathbf{x}_{expt}(N) && \\ &\text{subject to} && \mathbf{f}(\mathbf{x}_{expt}(N), \boldsymbol{\alpha}, \boldsymbol{\beta}) = \mathbf{0} \quad \text{for } N = N_o+1, \ldots, N_o+N_{expt} \end{aligned}$$

and P_1, P_2 and P_3 are given by

$$P_1 = \sum_{N=1}^{N_o} R_{\Delta_o}{}^2(N) \frac{\sum_{i=1}^{n} \lambda_i \left(\nabla_r{}^2 P \Big|_{x^*_{mo}} \right)}{n} + \sum_{N=N_o+1}^{N_o+N_{expt}} R_{\Delta_o}{}^2(N) \frac{\sum_{i=1}^{n} \lambda_i \left(\nabla_r{}^2 P \Big|_{x^*_{mo}} \right)}{n} +$$

$$\sum_{N=N_o+N_{expt}+1}^{N_D} R_{\Delta}{}^2(N) \frac{\sum_{i=1}^{n} \lambda_i \left(\nabla_r{}^2 P \Big|_{x^*_{mo}} \right)}{n}$$

$$P_2 = \sum_{N=N_o+1}^{N_o+N_{expt}} (\mathbf{x}^*_{\mathbf{mo}} - \mathbf{x}_{\mathbf{expt}}(N))^T \nabla_r{}^2 P \Big|_{x^*_{mo}} (\mathbf{x}^*_{\mathbf{mo}} - \mathbf{x}_{\mathbf{expt}}(N))$$

$$P_3 = \sum_{N=1}^{N_o} \nabla_r{}^2 P \Big|_{x^*_{mo}} \circ \mathbf{Q}_{x^*_{mo}} + \sum_{N=N_o+N_{expt}+1}^{N_D} \nabla_r{}^2 P \Big|_{x^*_{mo}} \circ \mathbf{Q}_{x^*_m(N)}$$

APPENDIX D: BOILER MODEL DEVELOPMENT AND VALIDATION

The boiler modelling equations for plant simulation in Chapter 5 are presented in this appendix. In this appendix, the fundamental model for plant simulation is first presented. Then, the base case operating conditions and the parameters used in the heat transfer correlations for the boiler case study are reported. Finally, the comparisons of the measurements taken from Dofasco and model prediction are discussed.

Modifications were made from Dofasco's boiler to have boilers with different efficiency curves for the case study in Chapter 5. Two additional controllers were implemented to control the superheated steam temperature and oxygen concentration in the flue gas. Heat transfer area was reduced by changing the number of tubes in various heat exchangers without changing the tube arrangements. The model for Dofasco's boiler was first developed in the initial phase of model development. That model was validated based on the measurements taken from the plant and the physical dimensions supplied by Dofasco. Finally, modifications described previously were made to develop the model for the plant for the case study which is described in the following section.

D.1 Fundamental Modelling of Boiler for Plant Simulation

The configuration of the boiler and systems for modelling heat transfer are shown in Figures 5.1 and 5.2, respectively. The modelling approaches are summarized in Table 5.1. The modelling equations include material and energy balances, pressure drop calculations, thermodynamics relationships and heat transfer modelling. The modelling equations for each heat transfer equipment in the boiler are discussed in the following sections.

D.1.1 Steam Coil

Saturated steam is taken from the steam drum to heat the incoming air in the steam coil for controlling the flue gas temperature. The steam coil is modelled by the energy balance equations on the air and steam sides. Saturated steam is totally condensed to saturated water in the steam coil [Lumley, 1999]. Energy supplied by the steam to the incoming air, Q_{sc}, is given by,

$$Q_{sc} = F_{sc}(H_{s,sc} - H_{w,sc}) \tag{D.1}$$

where F_{sc} is the flow rate of saturated steam, and $H_{s,sc}$ and $H_{w,sc}$ are the enthalpies of saturated steam and water, respectively. The energy balance on the air side is given in (D.2),

$$\frac{W_{air}}{MW_{air}} \int_{T_{air,sc}}^{T_{air,amb}} C_{P,air} dT + Q_{sc} = 0 \tag{D.2}$$

where W_{air}, MW_{air} and $C_{p,air}$ are the mass flow rate, molecular weight and molar heat capacity of air.

Thermodynamic properties of saturated steam and water can be determined from the saturated temperature, $T_{s,sc}$, using the following empirical correlations

$$P_{sc} = a_{sat,PT} + b_{sat,PT} T_{s,sc} + c_{sat,PT} T_{s,sc}^{\ 2} \tag{D.3}$$

$$H_{s,sc} = a_{sat,H_sT} + b_{sat,H_sT} T_{s,sc} + c_{sat,H_sT} T_{s,sc}^{\ 2} \tag{D.4}$$

$$H_{w,sc} = a_{sat,H_wT} + b_{sat,H_wT} T_{s,sc} \tag{D.5}$$

where P_{sc} is the saturated pressure at the steam coil, and a, b, and c are the parameters estimated by fitting the thermodynamic data in steam table [Smith and Van Ness, 1987].

Assuming there is a negligible pressure drop along the pipe from the steam drum to steam coil, the steam pressure in the steam coil is the same as the steam drum pressure, P_{sd}, and therefore,

$$P_{sc} = P_{sd} \tag{D.6}$$

D.1.2 Air Preheaters

Air is heated in two air preheaters to recover part of the heat from the flue gas. The air preheaters in Dofacos's boiler are cross-flow heat exchangers in which flue gas is flowing inside the tubes while air is flowing across the tubes. The tubes are modelled as a lumped heat exchanger. The modelling equations are derived from the energy balances on the air and flue gas sides. The tube wall has a very high thermal conductivity and thin thickness. Therefore, the thermal resistance of the tube wall is negligible compared to the thermal resistances at the fluid sides, so that the tube wall is assumed to have a uniform temperature, and energy balance on the tube wall is not required.

The modelling equations at the air side can be derived from the energy balance and heat transfer correlations. The models for predicting the transport properties are obtained by fitting the data from the physical property tables in Welty et al. (1984). Let $T_{air,in}$ and $T_{air,out}$ denote the air temperature entering and leaving the air preheaters, and $T_{w,phj}$ denotes the wall temperature of the tube in air preheater j, the energy balance equation is given in (D.7),

$$\frac{W_{air}}{MW_{air}} \int_{T_{air,out}}^{T_{air,in}} C_{p,air}\, dT + Q_{phj} = 0 \qquad j = 1,2 \tag{D.7}$$

and the heat transfer, Q_{phj}, is equal to the overall heat transfer coefficient, $U_{out,phj}$, at the air side times the area times the temperature driving force as shown in (D.8),

$$Q_{phj} = U_{out,phj}\pi d_{out,phj}L_{phj}n_{phj}\left(T_{w,phj} - \frac{T_{air,in} + T_{air,out}}{2}\right) \qquad j = 1,2 \qquad (D.8)$$

where $d_{out,phj}$, L_{phj} and n_{phj} are the outer diameter, length and number of tubes respectively. In (D.8), the log mean temperature difference is approximated by the temperature difference between the tube wall and the average air temperature. The overall heat transfer coefficient can be determined from the heat transfer coefficient at the air side, h_{out}, and fouling factor, R_{out},

$$\frac{1}{U_{out,phj}} = \frac{1}{h_{out,phj}} + R_{out,phj} \qquad j = 1,2 \qquad (D.9)$$

and h_{out} can be estimated from the following heat transfer correlation [Holman, 1992]

$$Nu = CRe^{m}\,Pr^{\frac{1}{3}} \qquad (D.10a)$$

where Re is the Reynolds number, Pr is the Prandtl number, and the parameters C and m depend on the tube size and arrangement. Therefore, h_{out} can be estimated from (D.10b),

$$h_{out,phj} = \frac{k_{air,phj}}{d_{out,phj}}C_{phj}\left(\frac{d_{out,phj}W_{air}}{A_{phj}\mu_{air,phj}}\right)^{m_{phj}} Pr_{air}^{\,1/3} \qquad j = 1,2 \qquad (D.10b)$$

where k_{air} is the thermal conductivity of air, μ_{air} is the viscosity of air, Pr_{air} is the Prandtl number of air which is approximately equal to 0.7, and A_{phj} is the flow area for the air. Transport properties are estimated from the following empirical correlations,

$$k_{air} = a_{k,air} + b_{k,air}T + c_{k,air}T^{2} \qquad (D.11a)$$

$$\mu_{air} = a_{\mu,air} + b_{\mu,air} T + c_{\mu,air} T^2 \qquad \text{(D.12a)}$$

The physical properties are evaluated at the mean temperature, and therefore,

$$k_{air,phj} = a_{k,air} + b_{k,air} \frac{T_{air,in} + T_{air,out}}{2} + c_{k,air} \left(\frac{T_{air,in} + T_{air,out}}{2} \right)^2 \quad j = 1,2 \qquad \text{(D.11b)}$$

$$\mu_{air,phj} = a_{\mu,air} + b_{\mu,air} \frac{T_{air,in} + T_{air,out}}{2} + c_{\mu,air} \left(\frac{T_{air,in} + T_{air,out}}{2} \right)^2 \quad j = 1,2 \qquad \text{(D.12b)}$$

As shown in Figure 5.2, when j = 1, $T_{air,in} = T_{air,sc}$ and $T_{air,out} = T_{air,ph1}$; when j = 2, $T_{air,in} = T_{air,ph1}$ and $T_{air,out} = T_{air,ph2}$.

Heat transfer at the flue gas side of air preheaters can be modelled similar to that at the air side. The energy balance for the flue gas is given by the following equation,

$$n_{flue} \int_{T_{g,out}}^{T_{g,in}} C_{p,flue} dT - Q_{phj} = 0 \qquad j = 1,2 \qquad \text{(D.13a)}$$

where n_{flue} is the molar flow rate of the flue gas, and T_g is the temperature of the flue gas. Equation (D.13a) can be expressed in terms of the molar flow rate of the combustion products as shown in (D.13b).

$$n_{CO_2} \int_{T_{g,out}}^{T_{g,in}} C_{p,CO_2} dT + n_{O_2} \int_{T_{g,out}}^{T_{g,in}} C_{p,O_2} dT + n_{N_2} \int_{T_{g,out}}^{T_{g,in}} C_{p,N_2} dT + n_{H_2O} \int_{T_{g,out}}^{T_{g,in}} C_{p,H_2O} dT - Q_{phj} = 0 \qquad j = 1,2 \qquad \text{(D.13b)}$$

The heat transfer is modelled as shown in (D.14).

$$Q_{phj} = U_{in,phj}\pi d_{in,phj}L_{phj}n_{phj}\left(\frac{T_{g,in}+T_{g,out}}{2} - T_{w,phj}\right) \qquad j = 1,2 \qquad (D.14)$$

The overall heat transfer coefficient can be estimated using the heat transfer coefficient and fouling factor at the flue gas side shown in (D.15),

$$\frac{1}{U_{in,phj}} = \frac{1}{h_{in,phj}} + R_{in,phj} \qquad j = 1,2 \qquad (D.15)$$

and the heat transfer coefficient at the flue gas side can be estimated using Dittus-Boelter correlation [Holman, 1992],

$$Nu = 0.023Re^{0.8}Pr^{0.4} \qquad (D.16a)$$

or

$$h_{in,phj} = 0.023\frac{k_{flue,phj}}{d_{in,phj}}\left(\frac{4W_{flue}}{\pi n_{phj}d_{in,ph}\mu_{flue,phj}}\right)^{0.8} Pr_{flue}^{0.4} \qquad j = 1,2 \qquad (D.16b)$$

where Pr_{flue} is approximately equal to 0.7. The transport properties of the flue gas are assumed to be equal to the molar average of the transport properties of the individual component in the flue gas. The models predicting the transport properties are developed by fitting the transport data in Welty et al. (1984) with temperature by a second order polynomial. Therefore, the thermal conductivity and viscosity of the flue gas evaluated at the mean temperature are given in the following equations for j = 1,2.

$$k_{CO_2,phj} = a_{k,CO_2} + b_{k,CO_2}\frac{T_{g,in}+T_{g,out}}{2} + c_{k,CO_2}\left(\frac{T_{g,in}+T_{g,out}}{2}\right)^2 \qquad (D.17)$$

$$k_{O_2,phj} = a_{k,O_2} + b_{k,O_2}\frac{T_{g,in}+T_{g,out}}{2} + c_{k,O_2}\left(\frac{T_{g,in}+T_{g,out}}{2}\right)^2 \qquad (D.18)$$

$$k_{N_2,phj} = a_{k,N_2} + b_{k,N_2}\frac{T_{g,in}+T_{g,out}}{2} + c_{k,N_2}\left(\frac{T_{g,in}+T_{g,out}}{2}\right)^2 \quad (D.19)$$

$$k_{H_2O,phj} = a_{k,H_2O} + b_{k,H_2O}\frac{T_{g,in}+T_{g,out}}{2} + c_{k,H_2O}\left(\frac{T_{g,in}+T_{g,out}}{2}\right)^2 \quad (D.20)$$

$$\mu_{CO_2,phj} = a_{\mu,CO_2} + b_{\mu,CO_2}\frac{T_{g,in}+T_{g,out}}{2} + c_{\mu,CO_2}\left(\frac{T_{g,in}+T_{g,out}}{2}\right)^2 \quad (D.21)$$

$$\mu_{O_2,phj} = a_{\mu,O_2} + b_{\mu,O_2}\frac{T_{g,in}+T_{g,out}}{2} + c_{\mu,O_2}\left(\frac{T_{g,in}+T_{g,out}}{2}\right)^2 \quad (D.22)$$

$$\mu_{N_2,phj} = a_{\mu,N_2} + b_{\mu,N_2}\frac{T_{g,in}+T_{g,out}}{2} + c_{\mu,N_2}\left(\frac{T_{g,in}+T_{g,out}}{2}\right)^2 \quad (D.23)$$

$$\mu_{H_2O,phj} = a_{\mu,H_2O} + b_{\mu,H_2O}\frac{T_{g,in}+T_{g,out}}{2} + c_{\mu,H_2O}\left(\frac{T_{g,in}+T_{g,out}}{2}\right)^2 \quad (D.24)$$

$$k_{flue,phj} = \frac{1}{n_{flue}}\left(n_{CO_2}k_{CO_2,phj} + n_{O_2}k_{O_2,phj} + n_{N_2}k_{N_2,phj} + n_{H_2O}k_{H_2O,phj}\right) \quad (D.25)$$

$$\mu_{flue,phj} = \frac{1}{n_{flue}}\left(n_{CO_2}\mu_{CO_2,phj} + n_{O_2}\mu_{O_2,phj} + n_{N_2}\mu_{N_2,phj} + n_{H_2O}\mu_{H_2O,phj}\right) \quad (D.26)$$

When j = 1, $T_{g,in} = T_{g,ph2}$ and $T_{g,out} = T_{g,ph1}$; when j = 2, $T_{g,in} = T_{g,e}$ and $T_{g,out} = T_{g,ph2}$.

D.1.3 Economizer

The economizer in Dofasco's boiler is a multi-pass cross-flow heat exchanger. The structure of the economizer is shown in Figure D.1. There are p_e passes in each economizer tube. Each pass is approximated by a lumped heat exchanger. Flue gas leaving the generating tubes at a temperature of $T_{g,gt2}$ enters the economizer to heat the feed water. The temperature of water leaving the economizer, $T_e(p_e)$, is controlled by adjusting the water flow bypassing the economizer to avoid boiling of water before entering the steam drum.

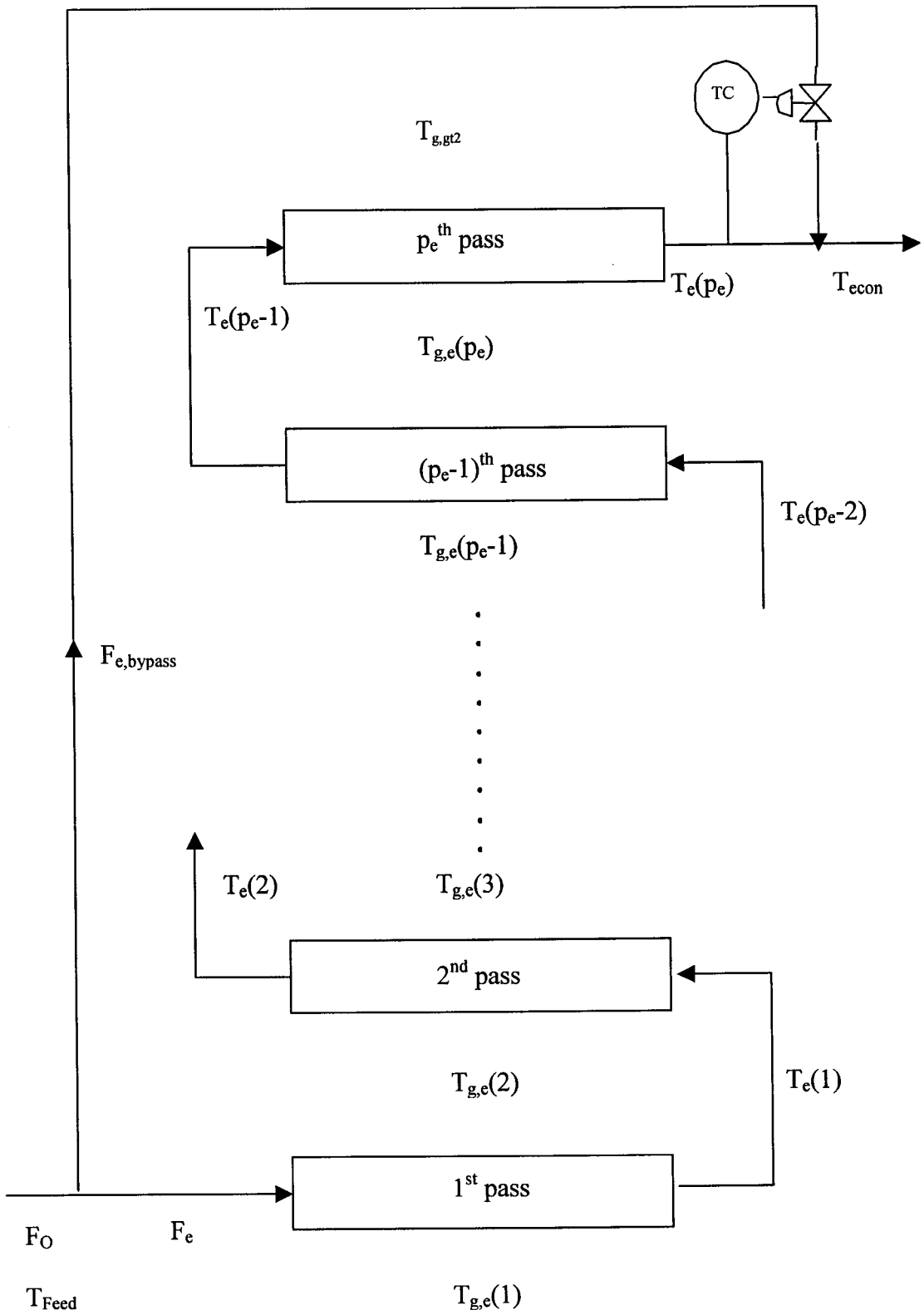

Figure D.1 Structure of economizer tubes

The modelling equations at the water side are developed from the mass and energy balances, and heat transfer correlations. At the splitting point, the mass balance equation is given in (D.27)

$$F_o = F_e + F_{e,bypass} \tag{D.27}$$

where F_o, F_e, and $F_{e,bypass}$ are the feed water flow, flow of water in the economizer and flow of water bypassing the economizer, respectively. The energy balance in each pass of the economizer tubes is given in (D.28), assuming heat capacity of water, $C_{p,water}$, is constant,

$$F_e C_{p,water}(T_e(j-1) - T_e(j)) + Q_e(j) = 0 \qquad j = 1,2, \ldots\ldots p_e \tag{D.28}$$

where $T_e(j)$ is the water temperature leaving j^{th} pass with $T_e(0) = T_{Feed}$. Similar to the heat transfer in air preheater, heat transfer, Q_e, can be calculated by the following equations.

$$Q_e(j) = U_{in,e}\pi d_{in,e} L_e n_e \left(T_{w,e}(j) - \frac{T_e(j-1) + T_e(j)}{2} \right) \quad j = 1,2, \ldots\ldots p_e \tag{D.29}$$

$$\frac{1}{U_{in,e}} = \frac{1}{h_{in,e}} + R_{in,e} \tag{D.30}$$

$$h_{in,e} = 0.023 \frac{k_{water}}{d_{in,e}} \left(\frac{4F_e}{\pi n_e d_{in,e} \mu_{water}} \right)^{0.8} Pr_{water}^{\ 0.4} \tag{D.31}$$

where the transport properties are calculated by the following empirical correlations,

$$k_{water} = a_{k,water} + b_{k,water} T + c_{k,water} T^2 \tag{D.32a}$$

$$\mu_{water} = a_{\mu,water} + \frac{b_{\mu,water}}{T} + \frac{c_{\mu,water}}{T^2} \tag{D.33a}$$

$$Pr_{water} = a_{Pr,water} + \frac{b_{Pr,water}}{T} + \frac{c_{Pr,water}}{T^2} \tag{D.34a}$$

and the parameters in the empirical correlations are determined by fitting the transport data in Welty et al. (1984) with temperature. The transport properties used in (D.31) are evaluated at the mean temperature, and therefore,

$$k_{water} = a_{k,water} + b_{k,water}\frac{T_{Feed} + T_e(p_e)}{2} + c_{k,water}\left(\frac{T_{Feed} + T_e(p_e)}{2}\right)^2 \tag{D.32b}$$

$$\mu_{water} = a_{\mu,water} + \frac{b_{\mu,water}}{\frac{T_{Feed} + T_e(p_e)}{2}} + \frac{c_{\mu,water}}{\left(\frac{T_{Feed} + T_e(p_e)}{2}\right)^2} \tag{D.33b}$$

$$Pr_{water} = a_{Pr,water} + \frac{b_{Pr,water}}{\frac{T_{Feed} + T_e(p_e)}{2}} + \frac{c_{Pr,water}}{\left(\frac{T_{Feed} + T_e(p_e)}{2}\right)^2} \tag{D.34b}$$

Temperature of water leaving the mixing point, T_{econ}, can be determined by the energy balance at the mixing point shown in (D.35).

$$F_o T_{econ} = F_{e,bypass} T_{Feed} + F_e T_e(p_e) \tag{D.35}$$

The enthalpy of water leaving the mixing point can be calculated from T_{econ} shown in (D.36),

$$H_{econ} = H_{ref} + C_{p,water}(T_{econ} - T_{ref}) \tag{D.36}$$

where H_{ref} is the enthalpy of water at the reference temperature, T_{ref}.

The modelling equations at the flue gas side in the economizer can be modelled similar to that at the air side in the preheater. These equations consist of the energy balance equations, heat transfer correlations and evaluation of the transport properties at the mean temperature shown below.

$$n_{CO_2}\int_{T_{g,e}(j)}^{T_{g,e}(j+1)} C_{p,CO_2}\,dT + n_{O_2}\int_{T_{g,e}(j)}^{T_{g,e}(j+1)} C_{p,O_2}\,dT + n_{N_2}\int_{T_{g,e}(j)}^{T_{g,e}(j+1)} C_{p,N_2}\,dT + n_{H_2O}\int_{T_{g,e}(j)}^{T_{g,e}(j+1)} C_{p,H_2O}\,dT - Q_e(j) = 0$$

$$j = 1, 2, \ldots. p_e \qquad \text{(D.37)}$$

$$Q_e(j) = U_{out,e}\pi d_{out,e} L_e n_e\left(\frac{T_{g,e}(j+1) + T_{g,e}(j)}{2} - T_{w,e}(j)\right)$$

$$j = 1, 2, \ldots. p_e \qquad \text{(D.38)}$$

$$\frac{1}{U_{out,e}} = \frac{1}{h_{out,e}} + R_{out,e} \qquad \text{(D.39)}$$

$$h_{out,e} = \frac{k_{flue,e}}{d_{out,e}} C_e\left(\frac{d_{out,e} W_{flue}}{A_e \mu_{flue,e}}\right)^{m_e} Pr_{flue}^{1/3} \qquad \text{(D.40)}$$

$$k_{CO_2,e} = a_{k,CO_2} + b_{k,CO_2}\frac{T_{g,e}(1) + T_{g,gt2}}{2} + c_{k,CO_2}\left(\frac{T_{g,e}(1) + T_{g,gt2}}{2}\right)^2 \qquad \text{(D.41)}$$

$$k_{O_2,e} = a_{k,O_2} + b_{k,O_2}\frac{T_{g,e}(1) + T_{g,gt2}}{2} + c_{k,O_2}\left(\frac{T_{g,e}(1) + T_{g,gt2}}{2}\right)^2 \qquad \text{(D.42)}$$

$$k_{N_2,e} = a_{k,N_2} + b_{k,N_2}\frac{T_{g,e}(1) + T_{g,gt2}}{2} + c_{k,N_2}\left(\frac{T_{g,e}(1) + T_{g,gt2}}{2}\right)^2 \qquad \text{(D.43)}$$

$$k_{H_2O,e} = a_{k,H_2O} + b_{k,H_2O}\frac{T_{g,e}(1) + T_{g,gt2}}{2} + c_{k,H_2O}\left(\frac{T_{g,e}(1) + T_{g,gt2}}{2}\right)^2 \qquad \text{(D.44)}$$

$$\mu_{CO_2,e} = a_{\mu,CO_2} + b_{\mu,CO_2}\frac{T_{g,e}(1)+T_{g,gt2}}{2} + c_{\mu,CO_2}\left(\frac{T_{g,e}(1)+T_{g,gt2}}{2}\right)^2 \quad \text{(D.45)}$$

$$\mu_{O_2,e} = a_{\mu,O_2} + b_{\mu,O_2}\frac{T_{g,e}(1)+T_{g,gt2}}{2} + c_{\mu,O_2}\left(\frac{T_{g,e}(1)+T_{g,gt2}}{2}\right)^2 \quad \text{(D.46)}$$

$$\mu_{N_2,e} = a_{\mu,N_2} + b_{\mu,N_2}\frac{T_{g,e}(1)+T_{g,gt2}}{2} + c_{\mu,N_2}\left(\frac{T_{g,e}(1)+T_{g,gt2}}{2}\right)^2 \quad \text{(D.47)}$$

$$\mu_{H_2O,e} = a_{\mu,H_2O} + b_{\mu,H_2O}\frac{T_{g,e}(1)+T_{g,gt2}}{2} + c_{\mu,H_2O}\left(\frac{T_{g,e}(1)+T_{g,gt2}}{2}\right)^2 \quad \text{(D.48)}$$

$$k_{flue,e} = \frac{1}{n_{flue}}\left(n_{CO_2}k_{CO_2,e} + n_{O_2}k_{O_2,e} + n_{N_2}k_{N_2,e} + n_{H_2O}k_{H_2O,e}\right) \quad \text{(D.49)}$$

$$\mu_{flue,e} = \frac{1}{n_{flue}}\left(n_{CO_2}\mu_{CO_2,e} + n_{O_2}\mu_{O_2,e} + n_{N_2}\mu_{N_2,e} + n_{H_2O}\mu_{H_2O,e}\right) \quad \text{(D.50)}$$

D.1.4 Natural Circulation Loop

Mixture of steam and water circulates inside the natural circulation loops as shown in Figure D.2. The driving force for natural circulation is the change in fluid density when water boils and expands in the generating and riser tubes. Riser tubes receive convection from the gas and radiation from the flame while the generating tubes receive heat from the flue gas through convection.

D.1.4.1 Steam Drum

Steam/water mixture is separated in the steam drum. Most of the saturated steam flows to the superheater for further heating to produce superheated steam. Part of the saturated steam is taken from the steam drum to heat the incoming air for controlling the flue gas temperature. A small amount of water is taken from the steam drum, which is

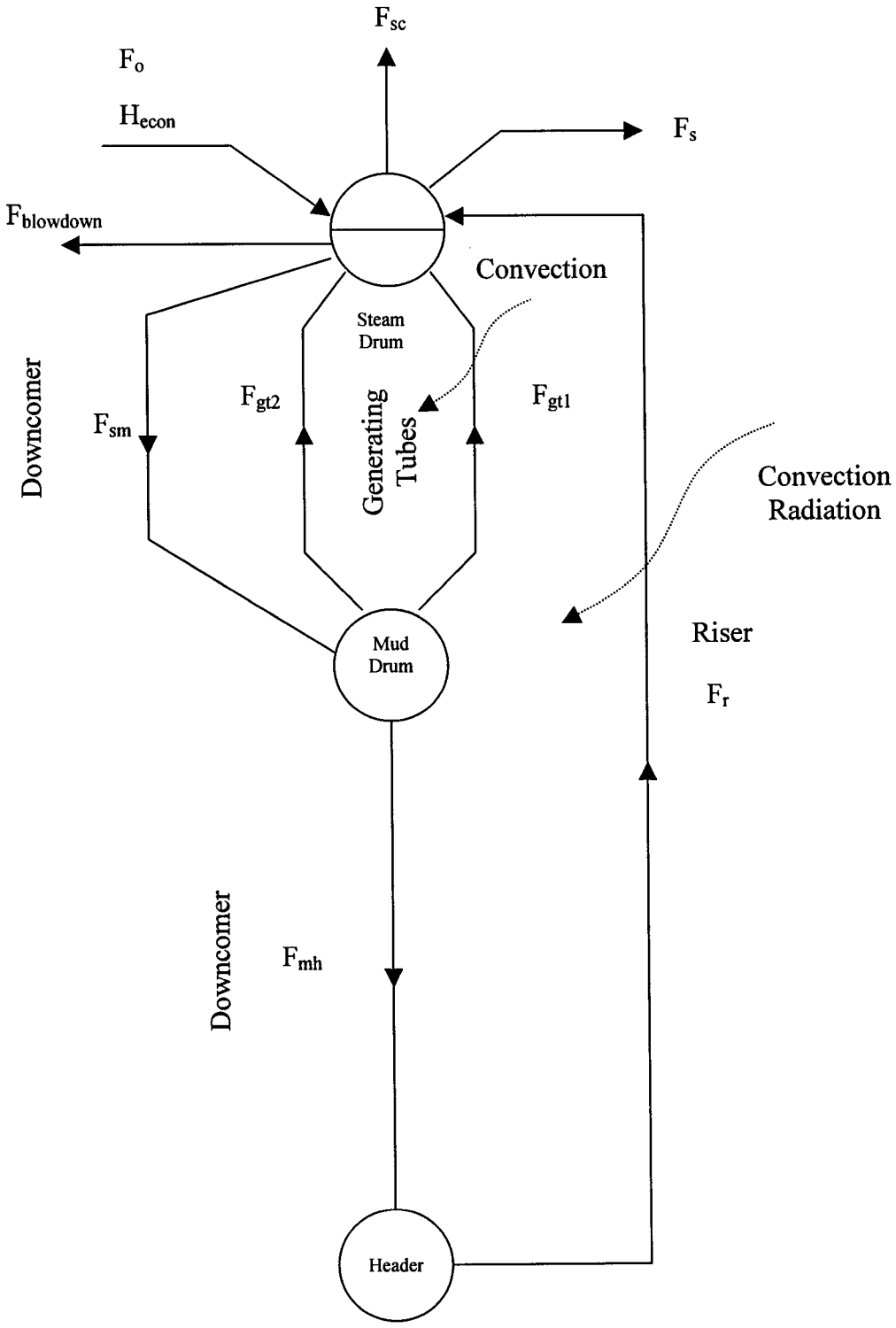

Figure D.2 Natural circulation loops

known as blowdown flow, to remove the chemicals from the boiler water to avoid foaming and priming, and subsequent carryover of chemicals into steam [Dukelow, 1985].

The modelling equations for the steam drum are derived from the mass and energy balances and thermodynamic relationship. The mass balance equations for water and steam in the steam drum are shown in (D.51) and (D.52), respectively,

$$F_o + (1-X_r)F_r + (1-X_{gt1})F_{gt1} + (1-X_{gt2})F_{gt2} - F_{sm} = 0 \tag{D.51}$$

$$X_r F_r + X_{gt1} F_{gt1} + X_{gt2} F_{gt2} - F_{sc} - F_s = 0 \tag{D.52}$$

where X is the steam quality in the steam/water mixture, F_r and F_{gt} are the flow rate of steam/water mixture in the riser and generating tubes respectively, F_{sm} is the flow rate of water from steam drum to mud drum, and F_s is the flow of saturated steam leaving the steam drum. The energy balance for water is given in (D.53),

$$\begin{aligned} &F_o H_{econ} + (1-X_r)F_r H_{w,r} + (1-X_{gt1})F_{gt1} H_{w,gt1} \\ &+ (1-X_{gt2})F_{gt2} H_{w,gt2} - F_{sm} H_{w,sd} = 0 \end{aligned} \tag{D.53}$$

where $H_{w,gt}$ and $H_{w,r}$ are the saturated enthalpies of water in generating and riser tubes respectively, and $H_{w,sd}$ is the enthalpy of subcooled water in the steam drum. These enthalpies and also the densities are related to the pressure and temperature at the steam drum by the following empirical equations.

$$P_{sd} = a_{sat,PT} + b_{sat,PT} T_{s,sd} + c_{sat,PT} T_{s,sd}^{\ 2} \tag{D.54}$$

$$\rho_{s,sd} = a_{sat,\rho_s T} + b_{sat,\rho_s T} T_{s,sd} + c_{sat,\rho_s T} T_{s,sd}^{\ 2} \tag{D.55}$$

$$H_{s,sd} = a_{sat,H_s T} + b_{sat,H_s T} T_{s,sd} + c_{sat,H_s T} T_{s,sd}^{\ 2} \tag{D.56}$$

$$H_{w,sd} = a_{sub,HTP} + b_{sub,HTP}T_{w,sd} + c_{sub,HTP}P_{sd} + d_{sub,HTP}T_{w,sd}^{2} + e_{sub,HTP}P_{sd}^{2} + f_{sub,HTP}T_{w,sd}P_{sd} \quad (D.57)$$

$$\rho_{w,sd} = a_{sub,\rho TP} + b_{sub,\rho TP}T_{w,sd} + c_{sub,\rho TP}P_{sd} + d_{sub,\rho TP}T_{w,sd}^{2} + e_{sub,\rho ub}P_{sd}^{2} + f_{sub,\rho ub}T_{w,sd}P_{sd} \quad (D.58)$$

The parameters in the empirical correlations in (D.54) – (D.58) are estimated by fitting the data in the steam table [Smith and Van Ness, 1987] with temperature and pressure.

D1.4.2 Downcomers

Water flows down by gravity from the steam drum to mud drum, and from the mud drum to bottom header in the downcomers. The downcomers, which are insulated, are located outside the furnace of the boiler and do not receive any heat from the gas. It is therefore assumed that no heat transfer takes place in the downcomers.

The modelling equations are developed from the momentum and mass balances. The momentum balance equation for water flowing from the steam drum to mud drum is given in (D.59) assuming water is incompressible,

$$144(P_{sd} - P_{md}) = \frac{2f_{dl}L_{dl}}{gd_{dl}A_{dl}^{2}}\frac{F_{sm}^{2}}{\rho_{w,sd}} - \rho_{w,sd}L_{dl} + \frac{1.1F_{sm}^{2}}{2g\rho_{w,sd}A_{dl}^{2}} \quad (D.59)$$

where the first term in the RHS is the pressure drop due to friction loss, the second term is the pressure gain due to change in elevation, and the third term is the sum of the entrance and exit loses. The friction factor of the downcomers is f. The flow rate from the steam drum to mud drum, F_{sm}, is related to other flow rates by the mass balance equation in the mud drum,

$$F_{sm} - F_{gt1} - F_{gt2} - F_{mh} = 0 \tag{D.60}$$

where F_{mh} is the flow rate of water from the mud drum to bottom header. Since there is no heat transfer, the enthalpy of water in the steam drum, $H_{w,sd}$, is the same as the enthalpy of water in the mud drum, $H_{w,md}$, and therefore,

$$H_{w,sd} = H_{w,md} \tag{D.61}$$

Similarly, the modelling equations for the downcomers between the mud drum and bottom header can be derived, which are shown in (D.62) – (D.64),

$$144(P_{md} - P_h) = \frac{2f_{d2}L_{d2}}{gd_{d2}A_{d2}^2}\frac{F_{mh}^2}{\rho_{w,sd}} - \rho_{w,sd}L_{d2} + \frac{1.1F_{mh}^2}{2g\rho_{w,sd}A_{d2}^2} \tag{D.62}$$

$$F_{mh} = F_r \tag{D.63}$$

$$H_{w,md} = H_{w,h} \tag{D.64}$$

where F_r is the flow rate of steam/water mixture in riser tubes, and $H_{w,h}$ is the enthalpy of water in the water header at the bottom of the boiler.

D.1.4.3 Generating Tubes

The generating tubes are divided into two cross-flow heat exchangers in parallel as shown in Figure D.2. Each tube is modelled as a lumped heat exchanger, in which water boils when the tubes receive heat from the flue gas. Heat is transferred from the flue gas to the generating tubes by convection.

The modelling equations at the steam/water side are developed from the momentum and energy balances, and heat transfer correlations. The momentum balance equation [Bertrand, 1986; Chien et al., 1958; Nicholson, 1964] is given in (D.65),

$$144(P_{md} - P_{sd}) = \frac{2f_{gt}L_{gt}}{gd_{gt}A_{gt}^{2}}\frac{F_{gtj}^{2}}{\rho_{gtj}} + \rho_{gtj}L_{gt} + \frac{1.1F_{gtj}^{2}}{2g\rho_{gtj}A_{gt}^{2}} + \frac{F_{gtj}^{2}}{gA_{gt}^{2}}\left(\frac{1}{\rho_{gtj}} - \frac{1}{\rho_{w,sd}}\right)$$

$$j = 1,2 \qquad (D.65)$$

where the first term in RHS is the pressure drop due to friction loss, the second term is the pressure loss due to change in elevation, the third term is the sum of the entrance and exit loses, and the forth term is the pressure loss due to evaporation. The density of steam/water mixture in the generating tubes can be calculated from the steam quality, X, and densities of saturated water and steam shown in (D.66).

$$\frac{1}{\rho_{gtj}} = \frac{1-X_{gtj}}{\rho_{w,gtj}} + \frac{X_{gtj}}{\rho_{s,gtj}} \qquad j = 1,2 \qquad (D.66)$$

The energy balance equation is given in (D.67),

$$F_{gtj}(H_{w,md} - H_{gtj}) + Q_{gtj} = 0 \qquad j = 1,2 \qquad (D.67)$$

where the enthalpy of steam/water mixture in generating tubes can be calculated from the steam quality and enthalpies of saturated water and steam shown in (D.68).

$$H_{gtj} = H_{w,gtj}(1-X_{gtj}) + H_{s,gtj}X_{gtj} \qquad j = 1,2 \qquad (D.68)$$

The heat transfer, Q_{gt}, is calculated from the overall heat transfer coefficient and the temperature difference driving force shown in (D.69) and (D.70), assuming the steam/water temperature in the generating tubes is uniform at the saturation temperature,

$$Q_{gtj} = U_{in,gtj}\pi d_{in,gt} L_{gt} n_{gt} (T_{w,gtj} - T_{gtj}) \qquad j = 1,2 \qquad (D.69)$$

$$\frac{1}{U_{in,gtj}} = \frac{1}{h_{in,gtj}} + R_{in,gt} \qquad j = 1,2 \qquad (D.70)$$

The boiling heat transfer coefficient is given in (D.71) [Geankoplis, 1992].

$$h_{in,gtj} = 0.077(T_{w,gtj} - T_{gtj})^3 e^{\frac{P_{gtj}}{225}} \qquad j = 1,2 \qquad (D.71)$$

Thermodynamic properties are related to pressure and temperature by the following empirical equations,

$$P_{gtj} = a_{sat,PT} + b_{sat,PT} T_{gtj} + c_{sat,PT} T_{gtj}^2 \qquad j = 1,2 \qquad (D.72)$$

$$\rho_{s,gtj} = a_{sat,\rho_s T} + b_{sat,\rho_s T} T_{gtj} + c_{sat,\rho_s T} T_{gtj}^2 \qquad j = 1,2 \qquad (D.73)$$

$$\rho_{w,gtj} = a_{sat,\rho_w T} + b_{sat,\rho_w T} T_{gtj} + c_{sat,\rho_w T} T_{gtj}^2 \qquad j = 1,2 \qquad (D.74)$$

$$H_{s,gtj} = a_{sat,H_s T} + b_{sat,H_s T} T_{gtj} + c_{sat,H_s T} T_{gtj}^2 \qquad j = 1,2 \qquad (D.75)$$

$$H_{w,gtj} = a_{sat,H_w T} + b_{sat,H_w T} T_{gtj} \qquad j = 1,2 \qquad (D.76)$$

and the parameters are determined by fitting the thermodynamic data [Smith and Van Ness, 1987] with temperature and pressure. Since the generating tubes are modelled as a lumped system, the saturated pressure inside the generating tubes is assumed to be equal to the steam drum pressure, and therefore,

$$P_{gtj} = P_{sd} \qquad j = 1,2 \qquad \text{(D.77)}$$

The flue gas side in the generating tubes can be modelled similar to the flue gas side in the economizer. The modelling equations, for j = 1 and 2, are shown below

$$n_{CO_2}\int_{T_{g,gt,out}}^{T_{g,gt,in}} C_{p,CO_2}dT + n_{O_2}\int_{T_{g,gt,out}}^{T_{g,gt,in}} C_{p,O_2}dT + n_{N_2}\int_{T_{g,gt,out}}^{T_{g,gt,in}} C_{p,N_2}dT + n_{H_2O}\int_{T_{g,gt,out}}^{T_{g,gt,in}} C_{p,H_2O}dT - Q_{gtj} = 0 \qquad \text{(D.78)}$$

$$Q_{gtj} = U_{out,gtj}\pi d_{out,gt}L_{gt}n_{gt}\left(\frac{T_{g,gt,in}+T_{g,gt,out}}{2} - T_{w,gtj}\right) \qquad \text{(D.79)}$$

$$\frac{1}{U_{out,gtj}} = \frac{1}{h_{out,gtj}} + R_{out,gt} \qquad \text{(D.80)}$$

$$h_{out,gtj} = \frac{k_{flue,gtj}}{d_{out,gt}}C_{gt}\left(\frac{d_{out,gt}W_{flue}}{A_{gt}\mu_{flue,gtj}}\right)^{m_{gt}} Pr_{flue}^{1/3} \qquad \text{(D.81)}$$

$$k_{CO_2,gtj} = a_{k,CO_2} + b_{k,CO_2}\left(\frac{T_{g,gt,in}+T_{g,gt,out}}{2}\right) + c_{k,CO_2}\left(\frac{T_{g,gt,in}+T_{g,gt,out}}{2}\right)^2 \qquad \text{(D.82)}$$

$$k_{O_2,gtj} = a_{k,O_2} + b_{k,O_2}\left(\frac{T_{g,gt,in}+T_{g,gt,out}}{2}\right) + c_{k,O_2}\left(\frac{T_{g,gt,in}+T_{g,gt,out}}{2}\right)^2 \qquad \text{(D.83)}$$

$$k_{N_2,gtj} = a_{k,N_2} + b_{k,N_2}\left(\frac{T_{g,gt,in}+T_{g,gt,out}}{2}\right) + c_{k,N_2}\left(\frac{T_{g,gt,in}+T_{g,gt,out}}{2}\right)^2 \qquad \text{(D.84)}$$

$$k_{H_2O,gtj} = a_{k,H_2O} + b_{k,H_2O}\left(\frac{T_{g,gt,in}+T_{g,gt,out}}{2}\right) + c_{k,H_2O}\left(\frac{T_{g,gt,in}+T_{g,gt,out}}{2}\right)^2 \qquad \text{(D.85)}$$

$$\mu_{CO_2,gtj} = a_{\mu,CO_2} + b_{\mu,CO_2}\left(\frac{T_{g,gt,in} + T_{g,gt,out}}{2}\right) + c_{\mu,CO_2}\left(\frac{T_{g,gt,in} + T_{g,gt,out}}{2}\right)^2 \quad \text{(D.86)}$$

$$\mu_{O_2,gtj} = a_{\mu,O_2} + b_{\mu,O_2}\left(\frac{T_{g,gt,in} + T_{g,gt,out}}{2}\right) + c_{\mu,O_2}\left(\frac{T_{g,gt,in} + T_{g,gt,out}}{2}\right)^2 \quad \text{(D.87)}$$

$$\mu_{N_2,gtj} = a_{\mu,N_2} + b_{\mu,N_2}\left(\frac{T_{g,gt,in} + T_{g,gt,out}}{2}\right) + c_{\mu,N_2}\left(\frac{T_{g,gt,in} + T_{g,gt,out}}{2}\right)^2 \quad \text{(D.88)}$$

$$\mu_{H_2O,gtj} = a_{\mu,H_2O} + b_{\mu,H_2O}\left(\frac{T_{g,gt,in} + T_{g,gt,out}}{2}\right) + c_{\mu,H_2O}\left(\frac{T_{g,gt,in} + T_{g,gt,out}}{2}\right)^2 \quad \text{(D.89)}$$

$$k_{flue,gtj} = \frac{1}{n_{flue}}\left(n_{CO_2}k_{CO_2,gtj} + n_{O_2}k_{O_2,gtj} + n_{N_2}k_{N_2,gtj} + n_{H_2O}k_{H_2O,gtj}\right) \quad \text{(D.90)}$$

$$\mu_{flue,gtj} = \frac{1}{n_{flue}}\left(n_{CO_2}\mu_{CO_2,gtj} + n_{O_2}\mu_{O_2,gtj} + n_{N_2}\mu_{N_2,gtj} + n_{H_2O}\mu_{H_2O,gtj}\right) \quad \text{(D.91)}$$

When j = 1, $T_{g,gt,in} = T_{g,f}$ which is the temperature of flue gas leaving the furnace, and $T_{g,gt,out} = T_{g,gt1}$; when j = 2, $T_{g,gt,in} = T_{g,gt1}$ and $T_{g,gt,out} = T_{g,gt2}$.

D.1.4.4 Riser Tubes

The modelling equations for the steam/water side in riser tubes are similar to that in the generating tubes. The equations are given as follow:

$$144(P_h - P_{sd}) = \frac{2f_r L_r}{gd_r A_r^2}\frac{F_r^2}{\rho_r} + \rho_r L_r + \frac{1.1F_r^2}{2g\rho_r A_r^2} + \frac{F_r^2}{gA_r^2}\left(\frac{1}{\rho_r} - \frac{1}{\rho_{w,sd}}\right) \quad \text{(D.92)}$$

where P_h is the pressure of water at the bottom header.

$$\frac{1}{\rho_r} = \frac{1-X_r}{\rho_{w,r}} + \frac{X_r}{\rho_{s,r}} \tag{D.93}$$

$$F_r(H_{w,h} - H_r) + Q_r = 0 \tag{D.94}$$

$$H_r = H_{w,r}(1-X_r) + H_{s,r}X_r \tag{D.95}$$

$$Q_r = U_{in,r} \times 0.5\pi d_{in,r} L_r n_r (T_{w,r} - T_r) \tag{D.96}$$

A factor of 0.5 is included in (D.96) because only half of the riser tube surface is exposed to the flue gas and the flame, and the other side facing the furnace wall does not receive the heat from the flame and flue gas.

$$\frac{1}{U_{in,r}} = \frac{1}{h_{in,r}} + R_{in,r} \tag{D.97}$$

$$h_{in,r} = 0.077(T_{w,r} - T_r)^3 e^{\frac{P_r}{225}} \tag{D.98}$$

$$P_r = a_{sat,PT} + b_{sat,PT}T_r + c_{sat,PT}T_r^2 \tag{D.99}$$

$$\rho_{s,r} = a_{sat,\rho_s T} + b_{sat,\rho_s T}T_r + c_{sat,\rho_s T}T_r^2 \tag{D.100}$$

$$\rho_{w,r} = a_{sat,\rho_w T} + b_{sat,\rho_w T}T_r + c_{sat,\rho_w T}T_r^2 \tag{D.101}$$

$$H_{s,r} = a_{sat,H_s T} + b_{sat,H_s T}T_r + c_{sat,H_s T}T_r^2 \tag{D.102}$$

$$H_{w,r} = a_{sat,H_w T} + b_{sat,H_w T}T_r \tag{D.103}$$

$$P_r = P_{sd} \tag{D.104}$$

The modelling equations at the flue gas side in the riser tubes are discussed in the section of furnace modelling.

D.1.5 Superheater and Desuperheater

Saturated steam leaving the steam drum receives additional heat from the flue gas in the superheater to produce superheated steam. The superheated steam temperature is controlled by adding spray water in the desuperheater. The structure of the superheater and desuperheater is shown in Figure D.3. There are four passes in each superheater tube. The desuperheater is located between the second and third passes. Each pass in the superheater is modelled as a lumped heat exchanger.

The modelling equations for the steam side in the superheater consists of the momentum and energy balances, heat transfer correlations and empirical correlations for thermodynamic and transport properties. The pressure loss along the superheater tubes is mainly due to frictional loss and change in elevation. An additional exit loss is included when saturated steam is flowing from the steam drum to superheater. The momentum balance equation is, therefore, given in (D.105),

$$144[P_{sh}(j-1) - P_{sh}(j)] = \frac{2f_{sh}L_{sh}}{g_c d_{sh} A_{sh}^2}\frac{F(j)^2}{\rho_{sh}(i)} + k_1\rho_{sh}(i)L_{sh} + k_2\frac{0.55F(j)^2}{2g_c\rho_{sh}(i)A_{sh}^2}$$

$$j = 1, 2, 3, 4 \qquad \text{(D.105)}$$

where $P_{sh}(0) = P_{sd}$,

$F(j) = F_s$ for $j = 1,2$; $F(j) = F_{steam}$ for $j = 3,4$

$k_1 = -1$ for $j = 1,3$; $k_1 = 1$ for $j = 2,4$

$k_2 = 1$ for $j = 1$; $k_2 = 0$ for $j = 2,3,4$

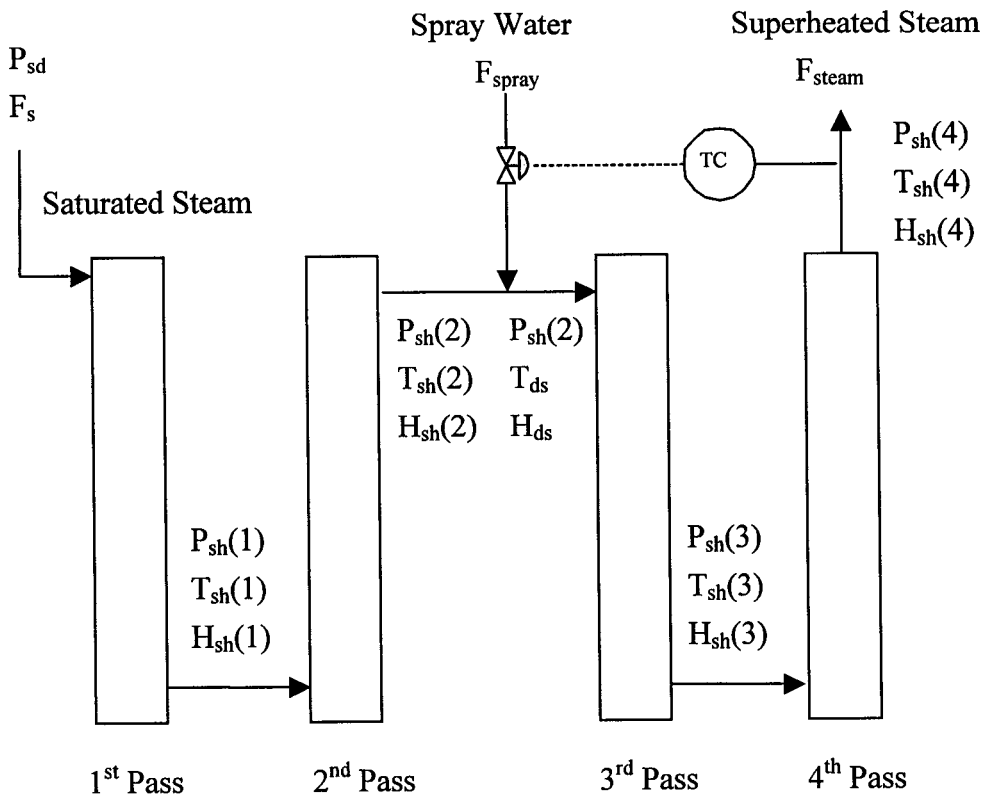

Figure D.3 Structure of superheater and desuperheater

In the RHS, the first term is the frictional loss, the second term is the pressure loss or gain due to change in elevation, and the third term is the exit loss which is present in the momentum balance for the first pass superheater tubes only. The energy balance equation is shown in (D.106)

$$F(j)(H_{sh,in} - H_{sh,out}) + Q_{sh}(j) = 0 \qquad j = 1, 2, 3, 4 \qquad (D.106)$$

where $H_{sh,in}$ and $H_{sh,out}$ are enthalpies of steam entering and leaving the j^{th} pass of superheater which are defined in Table D1. The heat transfer modelling equations, for j = 1, 2, 3 and 4, are shown as follow:

$$Q_{sh}(j) = U_{in,sh}(j)\pi d_{in,sh} L_{sh} n_{sh}\left(T_{w,sh}(j) - \frac{T_{sh,in} + T_{sh,out}}{2}\right) \quad \text{(D.107)}$$

$$\frac{1}{U_{in,sh}(j)} = \frac{1}{h_{in,sh}(j)} + R_{in,sh} \quad \text{(D.108)}$$

$$h_{in,sh}(j) = 0.023\frac{k_{H_2O,sh}(j)}{d_{in,sh}}\left(\frac{4F(j)}{\pi n_{sh} d_{in,sh}\mu_{H_2O,sh}(j)}\right)^{0.8} Pr_{H_2O}{}^{0.4} \quad \text{(D.109)}$$

$$k_{H_2O,sh}(j) = a_{k,H_2O} + b_{k,H_2O}\left(\frac{T_{sh,in} + T_{sh,out}}{2}\right) + c_{k,H_2O}\left(\frac{T_{sh,in} + T_{sh,out}}{2}\right)^2 \quad \text{(D.110)}$$

$$\mu_{H_2O,sh}(j) = a_{\mu,H_2O} + b_{\mu,H_2O}\left(\frac{T_{sh,in} + T_{sh,out}}{2}\right) + c_{\mu,H_2O}\left(\frac{T_{sh,in} + T_{sh,out}}{2}\right)^2 \quad \text{(D.111)}$$

where $T_{sh,in}$ and $T_{sh,out}$ are the temperature of steam entering and leaving j^{th} pass of superheater and are defined in Table D.1

Table D.1 Steam temperature and enthalpy in superheater

j	$T_{sh,in}$	$T_{sh,out}$	$H_{sh,in}$	$H_{sh,out}$
1	$T_{s,sd}$	$T_{sh}(1)$	$H_{s,sd}$	$H_{sh}(1)$
2	$T_{sh}(1)$	$T_{sh}(2)$	$H_{sh}(1)$	$H_{sh}(2)$
3	T_{ds}	$T_{sh}(3)$	H_{ds}	$H_{sh}(3)$
4	$T_{sh}(3)$	$T_{sh}(4)$	$H_{sh}(3)$	$H_{sh}(4)$

$T_{sh}(j)$ and $H_{sh}(j)$ are the steam temperature and enthalpy in the j^{th} pass of superheater, and T_{ds} and H_{ds} are the temperature and enthalpy of steam leaving desuperheater. Thermodynamic properties are estimated from the following empirical correlations,

$$H_{sh}(j) = a_{sh,HPT} + b_{sh,HPT}T_{sh}(j) + c_{sh,HPT}P_{sh}(j) + d_{sh,HPT}T_{sh}(j)^2 + e_{sh,HPT}P_{sh}(j)^2 + f_{sh,HPT}T_{sh}(j)P_{sh}(j) \quad j = 1, 2, 3, 4 \quad \text{(D.112)}$$

$$\frac{P_{sh}(j)}{\rho_{sh}(j)} = a_{sh,P\rho H} + b_{sh,P\rho H} H_{sh}(j) + c_{sh,P\rho H} H_{sh}(j)^2 \qquad j = 1, 2, 3, 4 \qquad \text{(D.113)}$$

and the parameters are determined by fitting the superheated steam properties [Smith and Van Ness, 1987] with temperature and pressure.

The desuperheater is assumed to be a simple mixer. Spray water is mixed with superheated steam to reduce the degree of superheat. The source of spray water is often at the discharge of the boiler feed pump [Dukelow, 1991]. The modelling equations are derived from the mass and energy balances, and thermodynamic relationships. The mass balance equation is shown in (D.114),

$$F_{steam} = F_s + F_{spray} \qquad \text{(D.114)}$$

where F_{spray} is the flow rate of spray water. The energy balance is given in (D.115),

$$F_{steam} H_{ds} = F_s H_{sh}(2) + F_{spray} H_{spray} \qquad \text{(D.115)}$$

where the enthalpy of spray water, H_{spray}, can be calculated from (D.116),

$$H_{spray} = H_{ref} + C_{p,water}(T_{spray} - T_{ref}) \qquad \text{(D.116)}$$

and the enthalpy and density of desuperheated steam can be calculated from the following equations, assuming there is no pressure drop across the desuperheater.

$$\begin{aligned} H_{ds} = {} & a_{sh,HPT} + b_{sh,HPT} T_{ds} + c_{sh,HPT} P_{sh}(2) + \\ & d_{sh,HPT} T_{ds}{}^2 + e_{sh,HPT} P_{sh}(2)^2 + f_{sh,HPT} T_{ds} P_{sh}(2) \end{aligned} \qquad \text{(D.117)}$$

$$\frac{P_{sh}(2)}{\rho_{ds}} = a_{sh,P\rho H} + b_{sh,P\rho H} H_{ds} + c_{sh,P\rho H} H_{ds}^{\ 2} \qquad (D.118)$$

The modelling equations at the flue gas side in the superheater are discussed in the section of furnace modelling.

D.1.6 Furnace

Fuels are combusted in the furnace to generate high temperature gases for heating water and steam. There are two types of fuel used in Dofasco's boiler, the blast furnace gas (bfg) and coke oven gas (cog). Assuming complete combustion, the components in the fuel and the combustion stoichiometry are shown in Table D.2, where y is the mole fraction, W_f is the mass flow rate of fuel and MW_f is the molecular weight of fuel. Therefore, the molar flow rate of fuel and combustion products in the flue gas are given in the following equations,

Table D.2 Combustion stoichiometry

Component	Composition	Oxygen required	CO_2 formed	H_2O formed
CH_4	y_{CH_4}	$\frac{2y_{CH_4}W_f}{MW_f}$	$\frac{y_{CH_4}W_f}{MW_f}$	$\frac{2y_{CH_4}W_f}{MW_f}$
H_2	y_{H_2}	$\frac{y_{H_2}W_f}{2MW_f}$	0	$\frac{y_{H_2}W_f}{MW_f}$
CO	y_{CO}	$\frac{y_{CO}W_f}{2MW_f}$	$\frac{y_{CO}W_f}{MW_f}$	0
CO_2	y_{CO_2}	0	0	0
O_2	y_{O_2}	0	0	0
N_2	y_{N_2}	0	0	0
H_2O	y_{H_2O}	0	0	0

$$n_{cog} = \frac{W_{cog}}{MW_{cog}} \tag{D.119}$$

$$n_{bfg} = \frac{W_{bfg}}{MW_{bfg}} \tag{D.120}$$

$$n_{CO_2} = \left(y_{CH_4} + y_{CO} + y_{CO_2}\right)_{bfg} \frac{W_{bfg}}{MW_{bfg}} + \left(y_{CH_4} + y_{CO} + y_{CO_2}\right)_{cog} \frac{W_{cog}}{MW_{cog}} \tag{D.121}$$

$$n_{H_2O} = \left(2y_{CH_4} + y_{H_2} + y_{H_2O}\right)_{bfg} \frac{W_{bfg}}{MW_{bfg}} + \left(2y_{CH_4} + y_{H_2} + y_{H_2O}\right)_{cog} \frac{W_{cog}}{MW_{cog}} \tag{D.122}$$

$$n_{N_2} = 0.79\frac{W_{air}}{MW_{air}} + y_{N_2,bfg}\frac{W_{bfg}}{MW_{bfg}} + y_{N_2,cog}\frac{W_{cog}}{MW_{cog}} \tag{D.123}$$

$$n_{O_2} = 0.21\frac{W_{air}}{MW_{air}} + y_{O_2,bfg}\frac{W_{bfg}}{MW_{bfg}} + y_{O_2,cog}\frac{W_{cog}}{MW_{cog}} - \left(2y_{CH_4} + \frac{1}{2}y_{H_2} + \frac{1}{2}y_{CO}\right)_{bfg}\frac{W_{bfg}}{MW_{bfg}} - \left(2y_{CH_4} + \frac{1}{2}y_{H_2} + \frac{1}{2}y_{CO}\right)_{cog}\frac{W_{cog}}{MW_{cog}} \tag{D.124}$$

$$n_{flue} = n_{CO_2} + n_{H_2O} + n_{N_2} + n_{O_2} \tag{D.125}$$

and the mass flow rate of flue gas is given by (D.126).

$$W_{flue} = W_{air} + W_{bfg} + W_{cog} \tag{D.126}$$

Oxygen concentration in the flue gas is controlled by manipulating the air flow rate. The setpoint for the percentage of oxygen in the flue gas is a function of steam load

[Dukelow, 1991]. At low steam load, a higher value of oxygen concentration, that is, higher air/fuel ratio, is required to increase the turbulence of the air/fuel mixture. The modelling equation for the oxygen concentration controller is given in the following equation,

$$\frac{n_{O_2}}{n_{flue}} = f(\text{steam load}) \tag{D.127}$$

and the relationship between the percentage of oxygen content in the flue gas as a function of steam load is shown in Figure D.4.

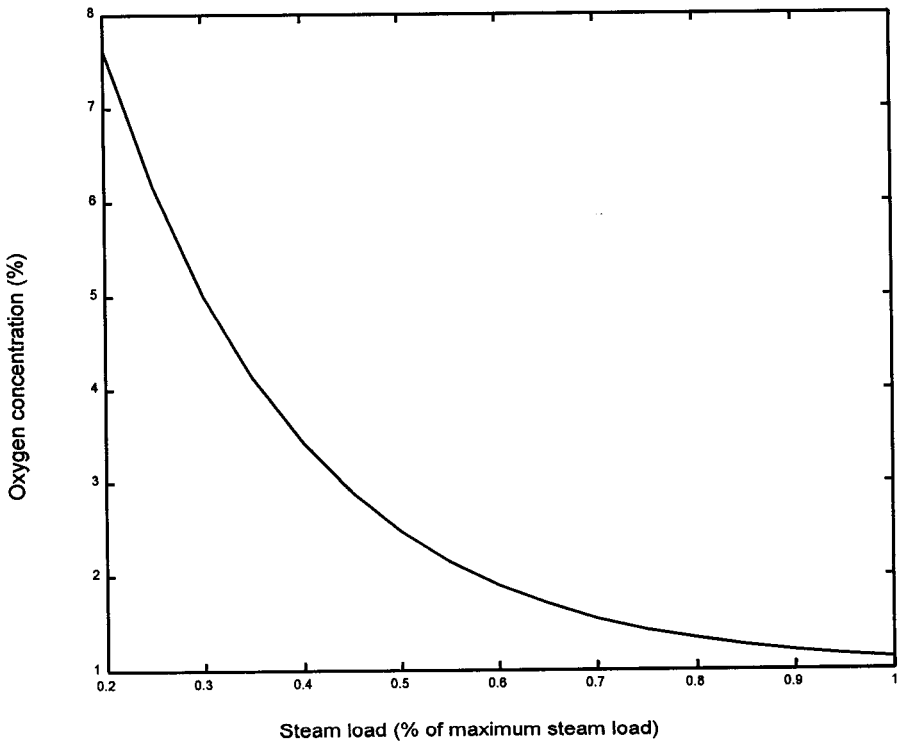

Figure D.4 Setpoint of oxygen controller as a function of steam load [Dukelow, 1991]

The modelling equations for the flue gas in the furnace are derived from the first law of thermodynamics. The systems for modelling the energy balance are shown in Figure D.5. The heat of combustion at standard state generated by combusting W_{bfg} and W_{cog} of blast furnace gas and coke oven gas is given by the following equations.

$$\Delta H^{\circ}_{comb,bfg} = \frac{W_{bfg}}{MW_{bfg}}\left[y_{CH_4}\Delta H^{\circ}_{comb,CH_4} + y_{H_2}\Delta H^{\circ}_{comb,H_2} + y_{CO}\Delta H^{\circ}_{comb,CO}\right]_{bfg} \quad \text{(D.128)}$$

$$\Delta H^{\circ}_{comb,cog} = \frac{W_{cog}}{MW_{cog}}\left[y_{CH_4}\Delta H^{\circ}_{comb,CH_4} + y_{H_2}\Delta H^{\circ}_{comb,H_2} + y_{CO}\Delta H^{\circ}_{comb,CO}\right]_{cog} \quad \text{(D.129)}$$

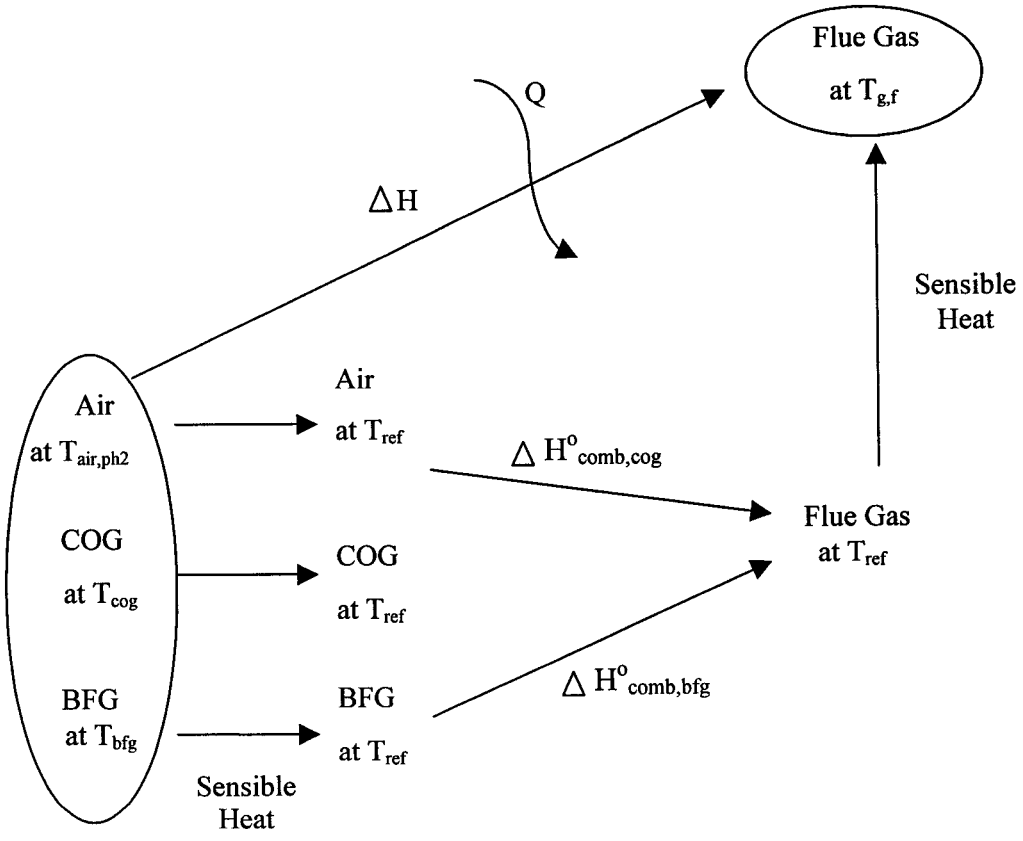

Figure D.5 Systems for modelling the energy balance in the furnace

From the first law of thermodynamics,

$$\Delta H = Q \tag{D.130a}$$

where Q is the total heat added to the system given in the following equation.

$$Q = -Q_r - \sum_{j=1}^{4} Q_{sh}(j) - Q_{radloss} \tag{D.130b}$$

$Q_{radloss}$ is the heat loss due to radiation. The enthalpy change, ΔH, can be calculated from Hess's law and is given in the following equation, assuming the furnace flue gas temperature is uniform,

$$\begin{aligned}\Delta H = {} & n_{air}\int_{T_{air,ph2}}^{T_{ref}} C_{p,air}\,dT + n_{cog}\int_{T_{cog}}^{T_{ref}} C_{p,cog}\,dT + n_{bfg}\int_{T_{bfg}}^{T_{ref}} C_{p,bfg}\,dT \\ & + n_{flue}\int_{T_{ref}}^{T_{g,f}} C_{p,flue}\,dT + \Delta H^{o}_{comb,cog} + \Delta H^{o}_{comb,bfg}\end{aligned} \tag{D.130c}$$

Substituting (D.130b) and (D.130c) in (D.130a) and expressing the heat capacity of flue gas in term of heat capacities of the components in the flue gas, the energy balance equation can be re-expressed as shown in (D.130d),

$$\begin{aligned}& \frac{W_{air}}{MW_{air}}\int_{T_{air,ph2}}^{T_{ref}} C_{p,air}\,dT + n_{cog}\int_{T_{cog}}^{T_{ref}} C_{p,cog}\,dT + n_{bfg}\int_{T_{bfg}}^{T_{ref}} C_{p,bfg}\,dT \\ & + n_{CO_2}\int_{T_{ref}}^{T_{g,f}} C_{p,CO_2}\,dT + n_{H_2O}\int_{T_{ref}}^{T_{g,f}} C_{p,H_2O}\,dT + n_{N_2}\int_{T_{ref}}^{T_{g,f}} C_{p,N_2}\,dT \\ & + n_{O_2}\int_{T_{ref}}^{T_{g,f}} C_{p,O_2}\,dT + \Delta H^{O}_{comb,cog} + \Delta H^{O}_{comb,bfg} + Q_r + \sum_{j=1}^{4} Q_{sh}(j) + Q_{radloss} = 0\end{aligned} \tag{D.130d}$$

The transport properties of the flue gas in the furnace can be calculated from the furnace temperature using the following correlations.

$$k_{CO_2,f} = a_{k,CO_2} + b_{k,CO_2} T_{g,f} + c_{k,CO_2} T_{g,f}^{\ 2} \tag{D.131}$$

$$k_{O_2,f} = a_{k,O_2} + b_{k,O_2} T_{g,f} + c_{k,O_2} T_{g,f}^{\ 2} \tag{D.132}$$

$$k_{N_2,f} = a_{k,N_2} + b_{k,N_2} T_{g,f} + c_{k,N_2} T_{g,f}^{\ 2} \tag{D.133}$$

$$k_{H_2O,f} = a_{k,H_2O} + b_{k,H_2O} T_{g,f} + c_{k,H_2O} T_{g,f}^{\ 2} \tag{D.134}$$

$$\mu_{CO_2,f} = a_{\mu,CO_2} + b_{\mu,CO_2} T_{g,f} + c_{\mu,CO_2} T_{g,f}^{\ 2} \tag{D.135}$$

$$\mu_{O_2,f} = a_{\mu,O_2} + b_{\mu,O_2} T_{g,f} + c_{\mu,O_2} T_{g,f}^{\ 2} \tag{D.136}$$

$$\mu_{N_2,f} = a_{\mu,N_2} + b_{\mu,N_2} T_{g,f} + c_{\mu,N_2} T_{g,f}^{\ 2} \tag{D.137}$$

$$\mu_{H_2O,f} = a_{\mu,H_2O} + b_{\mu,H_2O} T_{g,f} + c_{\mu,H_2O} T_{g,f}^{\ 2} \tag{D.138}$$

$$k_{flue,f} = \frac{1}{n_{flue}} \left(n_{CO_2} k_{CO_2,f} + n_{O_2} k_{O_2,f} + n_{N_2} k_{N_2,f} + n_{H_2O} k_{H_2O,f} \right) \tag{D.139}$$

$$\mu_{flue,f} = \frac{1}{n_{flue}} \left(n_{CO_2} \mu_{CO_2,f} + n_{O_2} \mu_{O_2,f} + n_{N_2} \mu_{N_2,f} + n_{H_2O} \mu_{H_2O,f} \right) \tag{D.140}$$

Heat transfer from the flue gas to the riser tubes can be modelled from the convective and radiative heat transfer correlations. Heat transfer to the riser from the flue gas is given by (D.141).

$$Q_r = U_{out,r} \times 0.5\pi d_{out,r} L_r n_r (T_{g,f} - T_{w,r}) \tag{D.141}$$

A factor of 0.5 is included because only half of the riser surface area faces the flame and flue gas, and remaining half of the surface facing the furnace wall does not receive the heat directly from the flame and the flue gas. The overall heat transfer coefficient can be

calculated from the radiative and convective heat transfer coefficients, $h_{out,r,rad}$ and $h_{out,r,conv}$, shown in (D.142),

$$\frac{1}{U_{out,r}} = \frac{1}{h_{out,r,rad}\varepsilon + h_{out,r,conv}} + R_{out,r} \tag{D.142}$$

where ε is the emissivity of the riser tubes. The radiative heat transfer coefficient can be estimated from the following correlation [Roffel and Rijnsdorp, 1974],

$$h_{out,r,rad} = \frac{1800}{5.6783(T_{g,f} - T_{w,r})}\left\{\alpha_{H_2O}\left[\left(\frac{\frac{1}{1.8}(T_{g,f} - 32) + 273.15}{100}\right)^{3.4} - \left(\frac{\frac{1}{1.8}(T_{w,r} - 32) + 273.15}{100}\right)^{3.4}\right]\right.$$

$$\left. + \alpha_{CO_2}\left[\left(\frac{\frac{1}{1.8}(T_{g,f} - 32) + 273.15}{100}\right)^{4} - \left(\frac{\frac{1}{1.8}(T_{w,r} - 32) + 273.15}{100}\right)^{4}\right]\right\} \tag{D.143}$$

where α_{H_2O} and α_{CO_2} are the radiative heat transfer coefficients for radiation emitted by water vapor and carbon dioxide respectively. The convective heat transfer coefficient can be estimated by assuming the flow of flue gas inside the furnace is turbulent, and therefore, using Dittus-Boelter correlation,

$$h_{out,r,conv} = 0.023\frac{k_{flue,f}}{D_f}\left(\frac{D_f W_{flue}}{\mu_{flue,f} A_f}\right)^{0.8} Pr_{flue}^{\ 0.4} \tag{D.144}$$

where D_f is the hydraulic diameter of the furnace which is defined as four times flow area divided by perimeter for a non-circular duct.

Heat transfer from the flue gas to the superheater tubes can be modelled similar to modelling the flue gas side in the riser tubes, except that the dominant mode of heat transfer from the flue gas to the superheater tubes is convection, because the superheater tubes do not directly "see" the flame. Therefore, the modelling equations are given in the following equations.

$$Q_{sh}(j) = U_{out,sh}(j)\pi d_{out,sh} L_{sh} n_{sh}\left(T_{g,f} - T_{w,sh}(j)\right) \qquad j = 1, 2, 3, 4 \qquad \text{(D.145)}$$

$$\frac{1}{U_{out,sh}(j)} = \frac{1}{h_{out,sh}(j)} + R_{out,sh} \qquad j = 1, 2, 3, 4 \qquad \text{(D.146)}$$

$$h_{out,sh}(j) = \frac{k_{flue,f}}{d_{out,sh}} C_{sh}(j)\left(\frac{d_{out,sh} W_{flue}}{A_{sh}(j)\mu_{flue,f}}\right)^{m_{sh}(j)} Pr_{flue}^{1/3} \qquad j = 1, 2, 3, 4 \qquad \text{(D.147)}$$

Radiation loss can be estimated from the ASME standard. Percentage of radiation loss, RADLOSS, at different steam load can be expressed as shown in the following equation,

$$RADLOSS = \frac{RADLOSS_{FL}}{\frac{F_{steam}}{F_{steam,FL}}} \qquad \text{(D.148)}$$

where FL denotes the full load condition. Percentage of radiation loss in full load as a function of boiler rating can be obtained from the ASME standard [Dukelow, 1991]. Heat loss due to radiation can be estimated from the gross heat input as shown in (D.149).

$$Q_{radloss} = RADLOSS \times \text{gross heat input} \qquad \text{(D.149)}$$

D.1.7 Controllers

Many controllers are implemented to ensure a safe and smooth operation of the boiler. Most of the manipulated variables do not saturate, and the controlled variables are equal to their setpoints. Typical examples of those controlled variables are the level in the steam drum, steam header pressure and feed water flow. However, some controlled variables may not be equal to their setpoints because of the saturation of the manipulated variables. The modelling equations for the steady-state behavior of the controlled system have to be included in the boiler model.

Steady-state model of the controllers are included for the superheated steam temperature controller, flue gas temperature controller and temperature controller for water temperature leaving economizer because saturation of the manipulated variables may occur for those control loops. The model of the controller for steady-state simulation is discussed in Marlin and Young (1997). The modelling equations are shown below,

$$-2K_p(SP-CV)-\lambda_{max}+\lambda_{min}=0 \tag{D.150}$$

$$MV_{max}-MV-\sigma_{max}{}^2=0 \tag{D.151}$$

$$MV-MV_{min}-\sigma_{min}{}^2=0 \tag{D.152}$$

$$\lambda_{max}\sigma_{max}=0 \tag{D.153}$$

$$\lambda_{min}\sigma_{min}=0 \tag{D.154}$$

where K_p is the process gain, SP is the setpoint, CV is the controlled variable, MV is the manipulated variable with the lower and upper limits, MV_{min} and MV_{max}, respectively, and λ and σ are the slack variables. Equations (D.150) to (D.154) are applied to the three controllers described above. When the valve for manipulating the water flow rate bypassing the economizer is fully open, half of the feed water bypasses the economizer.

An additional inequality constraint in (D.155) is required for modelling the valve saturation for controlling the water temperature leaving economizer.

$$F_{e,bypass} \leq 0.5F_o \tag{D.155}$$

D.2 Boiler Design and Base Case Operating Conditions

Boilers with different efficiency curves supplying steam to a common steam header can be obtained from changing the boiler configuration and physical dimensions. Tables D.3a and D.3b report the physical dimensions in feet of different boilers for the simulation. The last column in Tables D.3a and D.3b reports the physical dimensions of Dofasco's boiler, which are not used in the case study in Chapter 5. These boilers have different economizer and air preheater areas for recovering the heat from the flue gas. In addition, numbers of generating tubes are also different. These result in different boiler performances with different efficiency curves.

The values of the parameters in the heat transfer correlations can be obtained from the tube size and arrangements [Holman, 1992; Janna, 1986]. The parameter values used for the boiler simulation are reported in Table D4.

The base case operating point is defined by the external variables such as fuel composition, temperatures of air, fuel and feed water, blowdown flow, and the setpoints of the controllers. Tables D.5 – D.7 summarize the values of the external variables and the controller setpoints at the base case operation which are the same for all the boilers.

Table D.3a Physical dimensions of the boilers

Description	**Physical Dimension**			
	Boiler 1	Boiler 2	Boiler 3	Dofasco's boiler
		Economizer		
Inner diameter	0.1416	0.1416	0.1416	0.1416
Outer diameter	0.1667	0.1667	0.1667	0.1667
Tube length	30.44	30.44	30.44	30.44
Number of tubes	48	48	48	48
Number of passes	4	6	12	28
		Air Preheater		
Inner diameter	0.1723	0.1723	0.1723	0.1723
Outer diameter	0.1979	0.1979	0.1979	0.1979
Tube length	5	10	10	10
Number of tubes	3393	3393	3393	3393
Number of passes	2	2	2	2
		Generating Tubes		
Inner diameter	0.1616	0.1616	0.1616	0.1616
Outer diameter	0.1979	0.1979	0.1979	0.1979
Tube length	23	23	23	23
Number of tubes	1584	1584	1872	1872
		Riser Tubes		
Inner diameter	0.1936	0.1936	0.1936	0.1936
Outer diameter	0.2396	0.2396	0.2396	0.2396
Tube length	74	74	74	74
Number of tubes	258	258	258	258

Table D.3b Physical dimensions of the boilers

Description	**Physical Dimension**			
	Boiler 1	Boiler 2	Boiler 3	Dofasco's Boiler
	Downcomer from Steam Drum to Mud Drum			
Inner diameter	1	1	1	1
Tube length	25	25	25	25
Number of tubes	4	4	4	4
	Downcomer from Mud Drum to Bottom Header			
Inner diameter	1	1	1	1
Tube length	49	49	49	49
Number of tubes	3	3	3	3
	Superheater			
Inner diameter	0.1250	0.1250	0.1250	0.1250
Outer diameter	0.1583	0.1583	0.1583	0.1583
Tube length	21	21	21	21
Number of tubes	60	60	60	60
Number of passes	4	4	4	4
	Furnace			
Length	21.29	21.29	21.29	21.29
Width	23.5	23.5	23.5	23.5

Table D.4 Values of the parameters in the heat transfer correlations for plant simulation

Parameter	Value of the Parameter		
	Boiler 1	Boiler 2	Boiler 3
	Economizer (Equation D40)		
C_e	0.4034	0.4034	0.4034
m_e	0.584	0.584	0.584
	Air Preheaters (Equation D10b)		
C_{ph}	0.3932	0.3932	0.3932
m_{ph}	0.592	0.592	0.592
	Generating Tubes (Equation D81)		
C_{gt}	0.2825	0.2825	0.2825
m_{gt}	0.62	0.62	0.62
	Superheaters (Equation D147)		
C_{sh1}	0.2251	0.2251	0.2251
m_{sh1}	0.632	0.632	0.632
C_{sh2}	0.2251	0.2251	0.2251
m_{sh2}	0.632	0.632	0.632
C_{sh3}	0.2251	0.2251	0.2251
m_{sh3}	0.632	0.632	0.632
C_{sh4}	0.2585	0.2585	0.2585
m_{sh4}	0.608	0.608	0.608
	Riser (Equation D142)		
ε	0.7	0.7	0.7

Table D.5 Base case fuel composition

Component	Volume Fraction	
	Blast Furnace Gas	Coke Oven Gas
Methane	0.283	0
Hydrogen	0.535	0.06
Carbon monoxide	0.0488	0.19
Carbon dioxide	0.0136	0.15
Oxygen	0.0071	0
Nitrogen	0.0681	0.54
Water vapor	0.0444	0.06

Table D.6 Base case external variables

Variable	Value
Ambient air temperature (F)	60
Blast furnace gas temperature (F)	60
Coke oven gas temperature (F)	60
Feed water temperature (F)	240
Blowdown flow (klb/h)	5

Table D.7 Setpoints of the controllers

Controller	Setpoint
Steam header pressure (psig)	270
Superheated steam temperature (F)	550
Water temperature leaving economizer (F)	370
Flue gas temperature leaving air preheater (F)	300
Coke oven gas flow rate (kscfh)	120

D.3 Model Validation

A detailed fundamental model based on the boiler configuration from Dofasco was developed and validated before adding the extra controllers and changing the heat transfer area for the boiler case study in Chapter 5. This model was simulated using the measured external variables from the plant and physical dimensions reported in Tables D.3a and D.3b supplied by Dofasco. The model predictions were compared with the plant measurements.

Operating data supplied by Dofasco was used to validate the model. Table D.8 shows the independent variables used for the boiler simulation from the model developed, and the measured values of those variables taken from the plant. The measured values, the base case fuel composition reported in Table D.5, the parameters in the heat transfer correlations in Table D.4 and the dimensions of the #9 boiler in Dofasco reported in Table D.3 were used to simulate the boiler system. The model predictions are reported in Table D.9 and compared with the measurements taken from the plant.

Table D.8 Measured independent variables for model validation

Independent Variable	Data Set 1	Data Set 2
Header Pressure (psig)	270	270
Ambient Air Temperature (F)	106.66	108.25
Blast Furnace Gas Temperature (F)	60	60
Coke Oven Gas Temperature (F)	84	84
Water Temperature Leaving Economizer (F)	378.4	364.75
Feed Water Temperature (F)	242.28	245.23
Steam Flow to Steam Coil (lb/h)	7799.3	7533.7
Volumetric Flow Rate of Blast Furnace Gas (scfh)	3767500	1998610
Volumetric Flow Rate of Coke Oven Gas (scfh)	121190	215980
Volumetric Flow Rate of Air (scfh)	3332304	3041280

Table D.9 Comparison of measured values of the dependent variables and model prediction

Dependent Variable	Data Set 1		Data Set 2	
	Measurements	Model Prediction	Measurements	Model Prediction
Superheated steam Temperature (F)	574.05	572.3	576.5	581
Temperature of air entering the burners (F)	333.99 (West) 318.22 (East)	314	319.82(West) 298.59 (East)	289.4
Flue gas temperature leaving generating tubes (F)	585	558.5	538.52	506.7
Flue gas temperature leaving economizer (F)	350.65	328.6	336.05	309.3
Flue gas temperature leaving air preheater (F)	281.15	287.3	261.77	267.8
Feed water flow (lb/h)	318900	293900	240000	213200
Steam flow (lb/h)	301220	286100	226840	205700
Oxygen concentration in flue gas (%)	3.493	1.84	5.556	4.15
Steam drum pressure (psig)	288.92	290.01	293.62	280.51
Steam drum temperature (F)	416 – 420.02 (different sensor locations)	419.9	416.42-421.25 (different sensor locations)	417.2

The model predictions match reasonably well with the measurements. The discrepancies in the flue gas temperatures leaving generating tubes and economizer may be caused by the assumption of uniform gas temperature in the model. The thermocouples measured the temperature of the gas in the middle of the duct which had the highest value because of the boundary layer developed in the duct. Temperatures of air entering the east and west burners were supposed to be very similar. Different values measured from the plant could be due to the bias in the measurements.

Predicted oxygen concentration was lowered than the measured value. In modelling the combustion process, the concentrations of different components in the flue gas are assumed to be uniform. The discrepancies may be caused by the spatial variation of the concentrations of the components. In addition, the combustion is assumed to be complete in the model. Local incomplete combustion may be present in the furnace. The flue gas may contain carbon monoxide which is not included in the model. Other possible reasons for the discrepancies may be air leakage, poor mixing of fuel and air and errors in fuel compositions and flow rate measurements.